Government of **Western Australia**
Department of **Mines and Petroleum**

RECORD 2010/21

THREE AND A HALF BILLION YEARS OF LIFE ON EARTH: A TRANSECT BACK INTO DEEP TIME

by
MJ Van Kranendonk


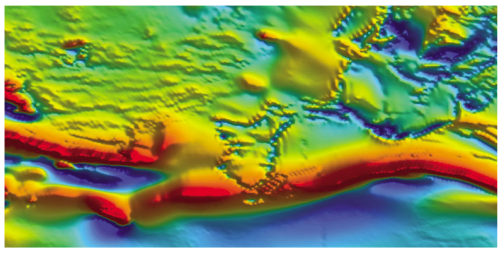


Geological Survey of Western Australia

Government of **Western Australia**
Department of **Mines and Petroleum**

Record 2010/21

THREE AND A HALF BILLION YEARS OF LIFE ON EARTH: A TRANSECT BACK INTO DEEP TIME

by
MJ Van Kranendonk[1]

with a contribution from
M Barley[2]

[1] **Geological Survey of Western Australia, 100 Plain Street, East Perth WA, 6004, Australia**
[2] **School of Earth and Environment, The University of Western Australia, 35 Stirling Highway, Crawley WA, 6009 Australia**

Perth 2010

Geological Survey of Western Australia

MINISTER FOR MINES AND PETROLEUM
Hon. Norman Moore MLC

DIRECTOR GENERAL, DEPARTMENT OF MINES AND PETROLEUM
Richard Sellers

ACTING EXECUTIVE DIRECTOR, GEOLOGICAL SURVEY OF WESTERN AUSTRALIA
Rick Rogerson

REFERENCE
The recommended reference for this publication is:
Van Kranendonk, MJ 2010, Three and a half billion years of life on Earth: a transect back into deep time: Geological Survey of Western Australia, Record 2010/21, 93p.

National Library of Australia Card Number and ISBN 978-1-74168-315-8 (PDF); 978-1-74168-330-1 (Printed)

Grid references in this publication refer to the Geocentric Datum of Australia 1994 (GDA94). Locations mentioned in the text are referenced using Map Grid Australia (MGA) coordinates, Zones 50 and 51. All locations are quoted to at least the nearest 100 m.

Published 2010 by Geological Survey of Western Australia
This Record is published in digital format (PDF) and is available online at <http://www.dmp.wa.gov.au/GSWApublications>.
Laser-printed copies can be ordered from the Information Centre for the cost of printing and binding.

Further details of geological publications and maps produced by the Geological Survey of Western Australia are available from:
Information Centre
Department of Mines and Petroleum
100 Plain Street
EAST PERTH, WESTERN AUSTRALIA 6004
Telephone: +61 8 9222 3459 Facsimile: +61 8 9222 3444
www.dmp.wa.gov.au/GSWApublications

Contents

Figures

Three and a half billion years of life on Earth: a transect back into deep time

by

MJ Van Kranendonk[1]

With a contribution from Mark Barley[2]

Abstract

This field trip for the Fifth International Archean Symposium in Perth presents a transect across Western Australia through three and a half billion years of Earth history, tracing the evolution of life back into deep time. The trip commences in Shark Bay to view the living stromatolites in Hamelin Pool and become familiar with the types of structures formed by living microbial communities within a shallow marine environment. From there, we will drive north and jump back 1.8 billion years (Ga), to an exposure of wonderfully diverse stromatolitic dolostone at Duck Creek. At this locality we will also be able to discuss the seawater chemistry, as gleaned from a transitional section that passes from shallow to deep marine sedimentary rocks and back again, including iron formation. From Duck Creek, we will travel further inland to view a transitional section from c. 2.45 Ga banded iron-formation at the top of the Hamersley Group into glacial sedimentary rocks of the Turee Creek Group (<2.45 Ga, >2.21 Ga) where we will discuss the possible influences of changing tectonics versus changing climate on sediment composition, and also the possibility of using this site as a global stratotype section and point (GSSP) for the Archean–Proterozoic boundary.

Heading east, a visit to Karijini National Park will include a walking day to investigate depositional features of the c. 2.5 Ga Hamersley Group, including banded iron-formation (Brockman Iron Formation), shales, tuffs, carbonates, and horizons deposited from a meteorite impact event. Heading north, we will pass downsection into the Fortescue Group and investigate stromatolitic carbonates of the c. 2.72 Ga Tumbiana Formation deposited in a lacustrine setting, and other lithologies of the group.

From the Fortescue Group, we will drive to the town of Marble Bar and into the Pilbara Supergroup of the basement granite–greenstone terrain, visit the eponymous chert on the Coongan River, and walk to the Schopf locality on Chinaman Creek where we will critically evaluate the geological setting of the controversial microfossils described from this well-known site.

Finally, we will drive into North Pole, to visit Earth's oldest fossils at the Trendall locality (3.35 Ga) and in the Dresser Formation (3.48 Ga), comparing all that we have seen in the better preserved, younger rocks with the structures preserved in these much older rocks. Geological settings and biogenicity arguments will be debated on the outcrops, followed by a discussion on future research projects to better constrain the early history of life on Earth.

KEYWORDS: Archean, Proterozoic, stromatolites, Pilbara Supergroup, Mount Bruce Supergroup, Wyloo Group

Introduction

This fieldtrip will follow a transect across Western Australia, taking the participant back into deep time to explore the evolution of life. The trip will commence with the living stromatolites at Shark Bay and end up 800 km away, and 3.5 billion years later, at Earth's oldest fossils in the East Pilbara (Fig. 1).

From Shark Bay, the trip will pass progressively down stratigraphic section through four major volcano-sedimentary groups, commencing in the Wyloo Group (1.8 – 2.2 Ga) and then passing into the Turee Creek Group (c. 2.4 Ga), the Hamersley Group (2.45 – 2.63 Ga) and the Fortescue Group (2.63 – 2.78 Ga; Fig. 2). After this, the trip will concentrate on the lower part of the unconformably underlying Pilbara Supergroup of the Paleo- to Mesoarchean Pilbara Craton, which was deposited from 3.52 – 3.17 Ga and contains abundant and diverse evidence for early life.

[1] Geological Survey of Western Australia, 100 Plain Street, East Perth WA, 6004 Australia. E-mail: martin.vankranendonk@dmp.wa.gov.au

[2] School of Earth and Environment, The University of Western Australia, 35 Stirling Highway. Crawley WA, 6009 Australia.

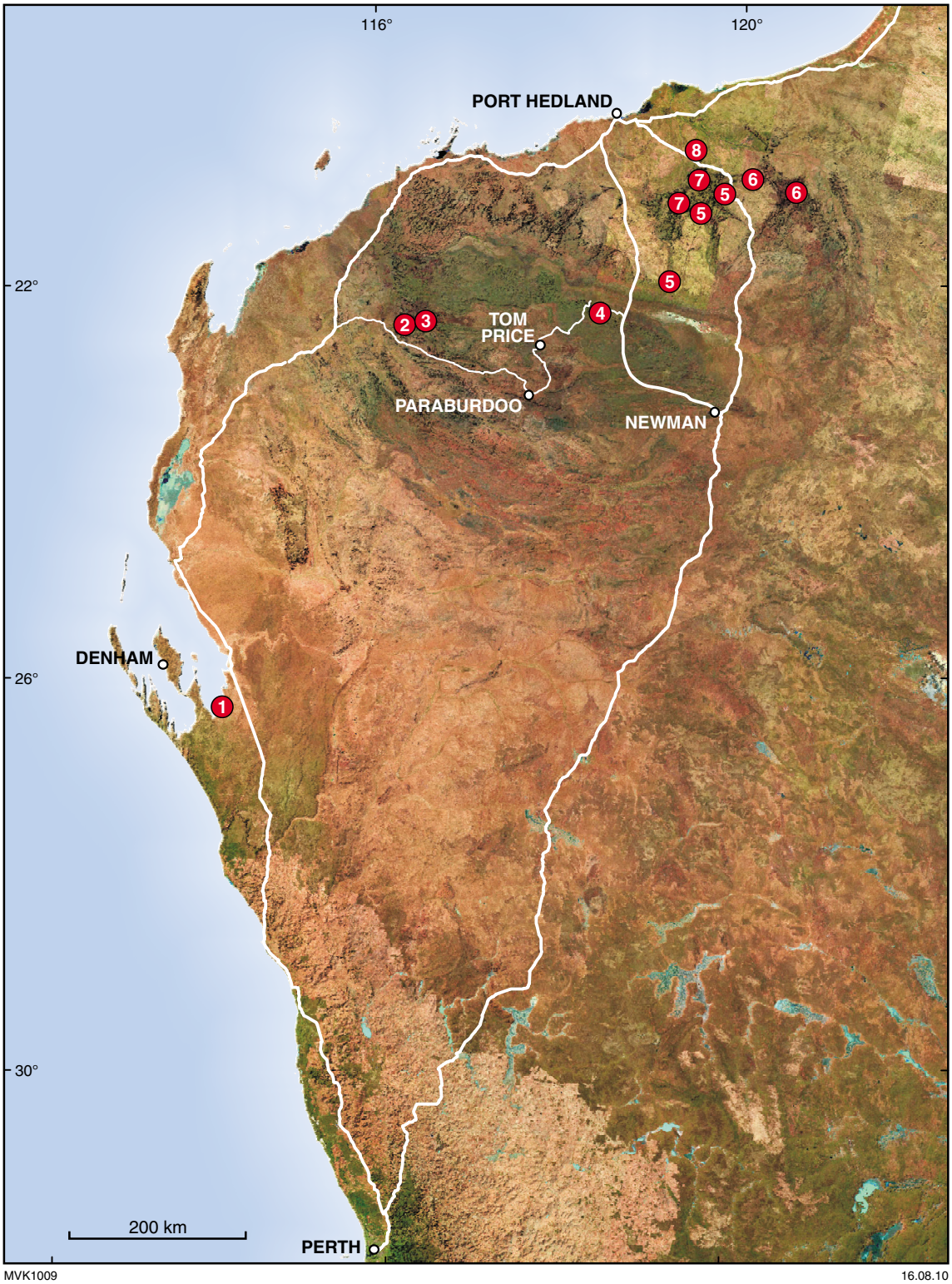

Figure 1. Satellite view of Western Australia, showing field excursion route and localities, numbered by day of the trip (1–8).

Figure 2. Stratigraphic column of the Neoarchean to Paleoproterozoic rocks of Western Australia visited on this excursion.

Wyloo Group (2.2–1.79 Ga)

The Wyloo Group of the Ashburton Basin consists of low-grade sedimentary and volcanic rocks with a thickness of about 12 km (Thorne, 1990; Thorne and Seymour, 1991). The group has been divided into unconformity-bound upper and lower parts, the lower part resting unconformably on the Hamersley Basin (Fig. 2), and the upper part unconformably overlain by younger sequences of the Blair Basin, or the Bresnahan, Edmund, and Collier basins (Cawood and Tyler, 2004).

Lower Wyloo Group

The lower part of the Wyloo Group consists of the basal Beasley River Quartzite (max. 360 m thick), the conformably overlying Cheela Springs Basalt (max. 2 km thick), and the conformably overlying Wooly Dolomite (max. 325 m thick). This succession lies with marked unconformity on rocks of the Turee Creek and Hamersley groups and is unconformably overlain by the upper part of the Wyloo Group.

The Beasley River Quartzite consists primarily of quartz-rich sandstone with local, well-developed, cross-bedding. The basal Three Corners Conglomerate Member consists of coarse conglomerate with abundant clasts of banded iron-formation (BIF; Fig. 3a), and subordinate mudstone and carbonate (Seymour et al., 1988; Martin et al., 2000). The Nummana Member, a siltstone, sandstone, and cross-bedded quartz-rich sandstone unit that conformably overlies the main part of the Beasley River Quartzite was ascribed by Martin et al. (1998, 2000) to the basal part of the Cheela Springs Basalt, on account of it being interpreted to contain interbedded basalt flows. However, the Nummana Member is here assigned to the top of the Beasley River Quartzite, as inferred basaltic rocks below and within the member are intrusive sills rather than extrusive flows. Significantly, some of the BIF clasts in the Three Corners Conglomerate and Nummana members contain microplaty hematite ore, indicating Fe concentration as a result of oxidizing fluids earlier than c. 2210 Ma (Martin et al., 1998).

The Cheela Springs Basalt consists predominantly of vesicular basalt, doleritic basalt, and rare plagioclase-phyric basalt, as subaerial flows up to 35 m thick (Fig. 3b). Flow tops are irregular and locally draped by clastic detritus. Geochemical studies indicate that the Cheela Springs Basalt may be divided into two parts, with distinct compositions, but derived from the same, subduction-modified source, including an upper part derived through a higher degree of partial melting at shallow crustal levels (Martin and Morris, in press).

The Wooly Dolomite consists of lower shallow-marine dolomites, a middle unit of shelf carbonates, and an upper unit of shallow-marine carbonates, and contains locally abundant stromatolites (Fig. 3c; Seymour et al.,

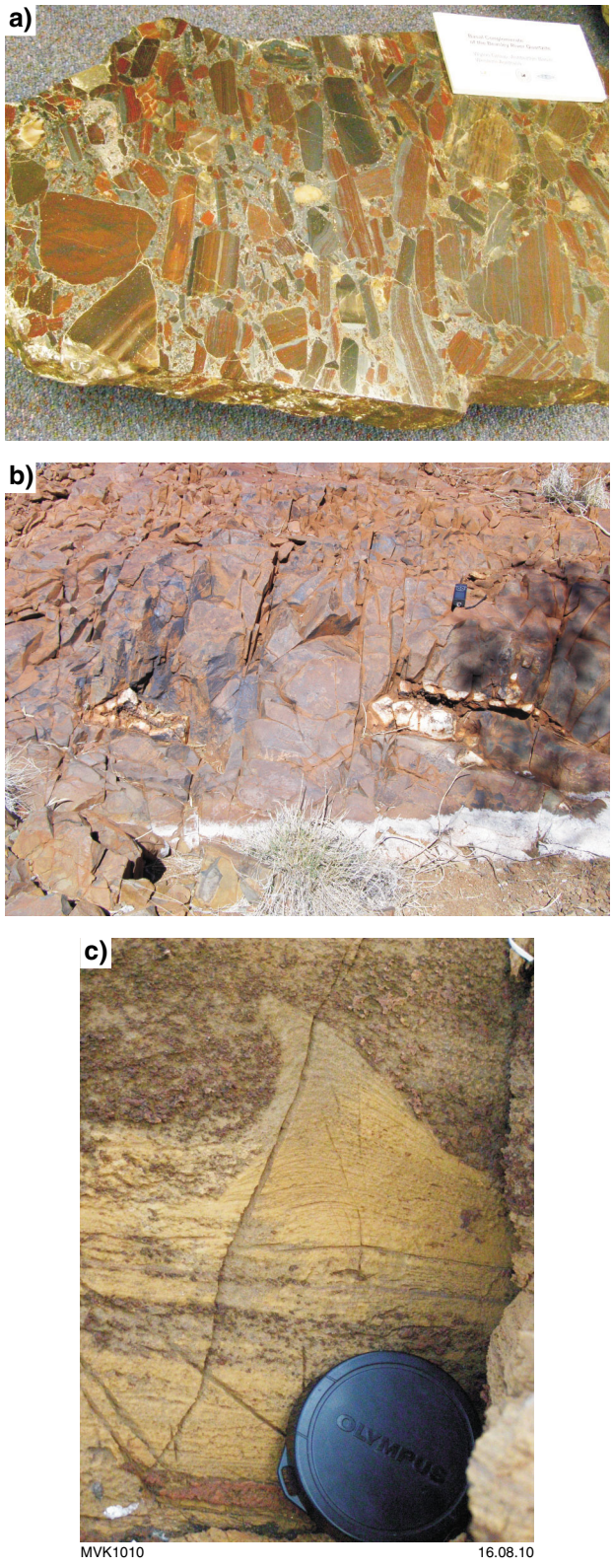

Figure 3. Rocks of the lower Wyloo Group: a) Three Corners Conglomerate Member of the Beasley River Quartzite; b) subaerial tholeiitic basalt of the Cheela Springs Basalt, with large gas cavities; c) coniform stromatolite of the Wooly Dolomite.

1988; Thorne and Seymour, 1991). The formation is lithologically heterogeneous, comprising siliciclastic and carbonate sedimentary rocks with several stromatolitic dolostone intervals that accumulated in shelf-ramp, shelf-platform, and intertidal environments. Sedimentologic logging of several sections across a wide area allowed Müller et al. (2005b) to recognize five depositional sequences with highstand and lowstand cycles. Isotopically heavy carbonate ($\delta^{13}C$ = +6‰) was first reported (Lindsay and Brasier, 2002) from the top of a 60 m thick, slightly sheared succession in the type locality area (Thorne and Seymour, 1991). Müller et al. (2005b) showed that isotopically heavy carbonates with $\delta^{13}C$ values ranging from +4.6‰ to +8.4‰ are restricted to one part of the succession, with other components having $\delta^{13}C_{carbonate}$ values mostly close to 0‰. The isotopically heavy carbonates of the Wooly Dolomite may record the end of the global Lomagundi–Jatuli excursion, at c. 2030 Ma (see Melezhik et al., 2005).

Age constraints for the lower Wyloo Group succession include a 2209 ± 15 Ma date for a tuffaceous lower component of the Cheela Springs Basalt, which is in excellent agreement with two identical dates of 2208 ± 10 Ma from associated subvolcanic dolerite sills emplaced into the underlying rocks of the Beasley River Quartzite and Turee Creek Group (Martin et al., 1998; Müller et al., 2005a). The youngest population of detrital zircons from the Beasley River Quartzite indicate a maximum age of deposition of 2446 ± 6 Ma, although the youngest individual zircon analysis is 2420 ± 18 Ma (Nelson, 2004a). A pumice-bearing tuffaceous siltstone from the base of the Wooly Dolomite returned a date of 2031 ± 6 Ma (Müller et al., 2005a). All of the rocks in the lower Wyloo Group are cut by dolerite dykes emplaced at 2008 ± 16 Ma (Fig. 2; Müller et al., 2005a).

Upper Wyloo Group

The upper part of the Wyloo Group consists of four formations, including, from base to top: the Mount McGrath Formation, the Duck Creek Dolomite, the June Hill Volcanics, and the Ashburton Formation (Fig. 2). The Mount McGrath Formation unconformably overlies folded lower Wyloo Group and older rocks, and comprises ferruginous conglomerate and sandstone, quartz sandstone, siltstone, mudstone, and carbonate, up to a maximum of 900 m thick (Seymour et al., 1988). Deposition of this formation has been interpreted as upward-fining deltaic and shallow-marine cycles composed of channelized conglomerate and siltstone (Thorne and Seymour, 1991).

The Duck Creek Dolomite (**Excursion Localities 2.1–2.3**) is up to 1 km thick and rests conformably on the Mount McGrath Formation, or unconformably on older rocks of the Fortescue and Hamersley groups. It is conformably overlain by the Ashburton Formation, except locally where it grades up into the June Hill Volcanics (Seymour et al., 1988). The formation is commonly stromatolitic and consists of slope, barrier-bar, lagoon, intertidal, and supratidal facies (Grey and Thorne, 1985), together with major developments of subtidal stromatolitic bioherms, mound-and-chanel systems, deeper-water limestones interbedded with dolomitic turbidites, and iron-formations (Wilson et al., 2010), as well as local olistostromes (see below). A characteristic feature of the formation is repeated upward-shallowing sequences, 0.5–4.0 m thick, that may represent transgressive and regressive sedimentation on a barred carbonate shoreline (Grey and Thorne, 1985). Microfossils assigned to the genera *Gunflintia*, *Huroniospora*, and *Eoastrion* have also been discovered in cherty horizons collected from this formation,in addition to larger trichomes comparable to cyanobacteria or sulfur-oxidizing bacteria (Knoll and Barghoorn, 1976; Knoll et al., 1988; Wilson et al., 2010).

The June Hill Volcanics lie across a gradational, interbedded contact with the underlying Duck Creek Dolomite and consist of up to 120 m of mafic lavas (some pillowed), tuffs, and agglomerates, interbedded with felsic volcanics and sedimentary rocks (Seymour et al., 1988). This formation is disconformably overlain by the Ashburton Formation, although stratigraphic and geochronological data indicate that at least part of the Ashburton Formation must also underlie the June Hill Volcanics (see below).

The Ashburton Formation is a thick (5–10 km) succession of dominantly mudstone and immature sandstone, with subordinate conglomerate, BIF, and felsic to mafic volcanics, deposited primarily under deep-water conditions (Seymour et al., 1988).

A number of age constraints show that the Ashburton Basin was deposited rapidly, from 1830–1795 Ma, and deformed and intruded by granites between 1805–1785 Ma during the Capricorn Orogeny, which is interpreted to have arisen through Pilbara–Yilgarn collision (Fig. 2; Krapež and McNaughton, 1999; Hall et al., 2001; Sircombe, 2003; Evans et al., 2003; Cawood and Tyler, 2004; Nelson, 2004d; Martin and Thorne, 2004). Well constrained dates of c. 1795 Ma from the June Hill Volcanics are significantly younger than some dates from along strike in the Ashburton Formation (1830 Ma; e.g. Sircombe, 2003), indicating that the June Hill Volcanics should probably be regarded as a member, or discontinuous formation within the Ashburton Formation (Fig. 2).

The McGrath Trough, Ophthalmian Orogeny, and Capricorn Orogeny

The series of depositional and deformational events that took place in the time between deposition of the ≤2.45 Ga Turee Creek Group and deformation at c. 1.78 Ga at the end of deposition of the upper Wyloo Group (the close of the Capricorn Orogeny) is controversial, and several orogenic events have been suggested (Fig. 2). The oldest deformation event is constrained by its effect on rocks of the Turee Creek Group prior to deposition of the unconformably overlying lower Wyloo Group (Ophthalmian Orogeny of Krapež, 1999). Geochronological evidence in the form of dated hydrothermal alteration minerals suggests that this event took place at 2.43–2.40 Ga (Rasmussen et al., 2005a), consistent with the interpretation of Martin et al. (2000) that the lower Wyloo Group was deposited at c. 2.21 Ga. Müller et al. (2005a), however, suggested that deposition of the lower Wyloo Group did not occur until after

c. 2.03 Ga, based on the age of the Wooly Dolomite, and inferred that the Ophthalmian Orogeny did not take place until c. 2.14 Ga (Panhandle folding event of Taylor et al., 2001). Rasmussen et al. (2005a) identified a hydrothermal mineral growth event at between 2.21 – 2.14 Ga, which they ascribe to northward advancement of the Ophthalmian Orogeny. However, another possibility is that this younger event reflects heat and fluid flow resulting from basin extension associated with eruption of the Cheela Springs Basalt and formation of the lower Wyloo basin. Yet another event at 2.03 – 2.01 Ga was recognized by Krapež (1999) and Müller et al. (2005a), and interpreted as the onset of Capricorn orogenesis. Later Capricorn events were identified at between 1.83 – 1.78 Ga (Krapež and McNaughton, 1999; Sircombe, 2003; Evans et al., 2003).

Horwitz (1982) proposed the McGrath Trough, a post-Hamersley, pre-Ashburton Basin feature that he interpreted as a 'fore-trough', or flexural foreland basin (Powell and Horwitz, 1994; Martin, 1999). Different models suggest that this foreland basin consists either of the Turee Creek Group only (Blake and Barley, 1992; Krapež, 1996), the Turee Creek Group and lower Wyloo Group (including the unconformity at the base of the Beasley River Quartzite; Horwitz, 1982), or the whole of the Turee Creek Group and Wyloo Group (lower and upper) combined (Tyler and Thorne, 1990; Thorne and Seymour, 1991; Myers, 1993). Martin (1999) and Martin et al. (2000) provided paleocurrent data in support of the McGrath Trough, including the Turee Creek Group and lower Wyloo Group, suggesting that both were deposited as a clastic wedge derived from the south *during* orogensis, and thereby accounting for the major unconformity at the base of the lower Wyloo Group. A syn-orogenic deposition for the whole of the McGrath Trough was further supported in this model by the recognition of multiple unconformities and increasing maturity of clastic sedimentary rock compositions upsection (Martin et al., 2000).

Additional evidence in support of a link between deposition of the Turee Creek and lower Wyloo groups and an early period of folding is presented by Martin and Morris (in press). These authors suggested the presence of multiple unconformities within rocks that they assign to the upper Kazput Formation of the Turee Creek Group, but which other authors have ascribed to the lower Wyloo Group (Thorne and Seymour, 1991; see **Excursion locality 3.6**). Martin and Morris (in press) also reiterated that some of the 2210 Ma sills are truncated by an unconformity with overlying lower Wyloo Group sediments, which they use as evidence of folding *during* deposition of the lower Turee Creek Group. However, neither the stratigraphic nor structural arguments put forth by these authors and by Martin et al. (1998) for a major unconformity within the upper part of the Turee Creek Group, nor the arguments in support of an unconformable contact of lower Wyloo Group sediments on 2210 Ma sills, are compelling.

Instead, this guidebook follows a simplified sequence of events that best reflects the broad stratigraphic and structural features of the area, as shown in Figure 2:

1) deposition of the Turee Creek Group, following conformably on from Hamersley Group deposition
2) significant deformation and tilting of Turee Creek Group and older strata during the Ophthalmian Orogeny, at some time between 2.45 – 2.21 Ga, but most likely at 2.43 – 2.40 Ga, as identified by dating of hydrothermal minerals (Rasmussen et al., 2005a). The first hematite-rich ores probably formed during this event (Martin et al., 1998)
3) deposition of the lower Wyloo Group at 2.21 – 2.03 Ga, during extensional basin formation that included eruption of the thick Cheela Springs Basalt and emplacement of associated subvolcanic sills
4) a moderate deformation event, post-dating deposition of the lower Wyloo Group at c. 2.03 Ga, and predating emplacement of c. 2.01 Ga mafic dykes, referred to herein as the Panhandle Orogeny (Müller et al., 2005a)
5) deposition of the upper Wyloo Group at 1.83 – 1.79 Ga, including early passive rift deposits, pre- to syn-collisional volcanics (arc?), and younger, syn-collisional deposits, culminating with the Capricorn Orogeny.

In this sequence of events, the three orogenic events recognized in this area are each separated by a 200–300 Ma period. This strongly suggests that they represent separate and distinct events, unlinked in terms of a broad orogenic framework such as a developing foreland basin; hence, the concept of a McGrath Trough has no relevance except, perhaps, for the upper Wyloo Group.

Turee Creek Group (<2.45, >2.21 Ga)

The Turee Creek Group (Trendall, 1979) conformably overlies the Hamersley Group along the southern margin of the Pilbara Craton, and is in turn unconformably overlain by the lower Wyloo Group. It is the uppermost of the three groups that constitute the Mount Bruce Supergroup (Fortescue, Hamersley, and Turee Creek groups on Fig. 2; Trendall, 1979). The Turee Creek Group varies considerably in thickness along strike, in part due to the downcutting effects of the overlying unconformity, but also as a result of rapid lateral facies variations; it reaches a maximum of 3000 m thick in the central area of its distribution, in the Hardey Syncline (Martin, 1999). The group consists largely of greyish-green siltstone, fine-grained wacke, and fine-grained sandstone, but also contains thin to thick carbonate units and glacially-deposited conglomerates and diamictites (Trendall, 1981; Martin, 1999). Trendall (1979) identified a lower Kungarra Formation, capped by the Meteorite Bore Member of glacial diamictites. Thorne et al. (1995) named the overlying Koolbye and Kazput formations, which consist of 130 m of coarse quartzarenite, siltstone and minor conglomerate, and carbonate, siltstone, sandstone and conglomerate, respectively. Metamorphic grade in the Turee Creek Group does not exceed prehnite–pumpellyite–epidote facies (Smith et al., 1982).

The Meteorite Bore Member is up to 270 m thick at the type locality a short distance northeast of Meteorite Bore, where it consists of diamictite, fine sandstone, and shale

(see **Excursion Locality 3.7**). Diamictites consist of scattered, outsize clasts of a variety of lithologies, up to 80 cm diameter, hosted within fine-grained sandstone to shale. At Meteorite Bore, the matrix is well foliated, and clasts are weakly flattened (Fig. 4a). Throughout the member, the clast population is dominated by porphyritic rhyolite that is petrographically indistinguishable from the underlying c. 2.45 Ga Woongarra Rhyolite of the Hamersley Group, but clasts of sandstone, chloritic siltstone, leucogabbro, carbonate-altered felsic volcaniclastic rock, banded chert, banded iron-formation, dolomite, and oolitic carbonates have also been observed (Martin, 1999). Some larger clasts are decorated with well-developed striae on polished, faceted surfaces (Fig. 4b; Trendall, 1981; Martin, 1999).

The youngest population of detrital zircons from a sample of the Meterorite Bore Member of the Turee Creek Group indicates a maximum depositional age of c. 2420 Ma, with zircon peaks at 2438 Ma and 2468 Ma, and a variety of Archean ages (Takehara et al., 2010).

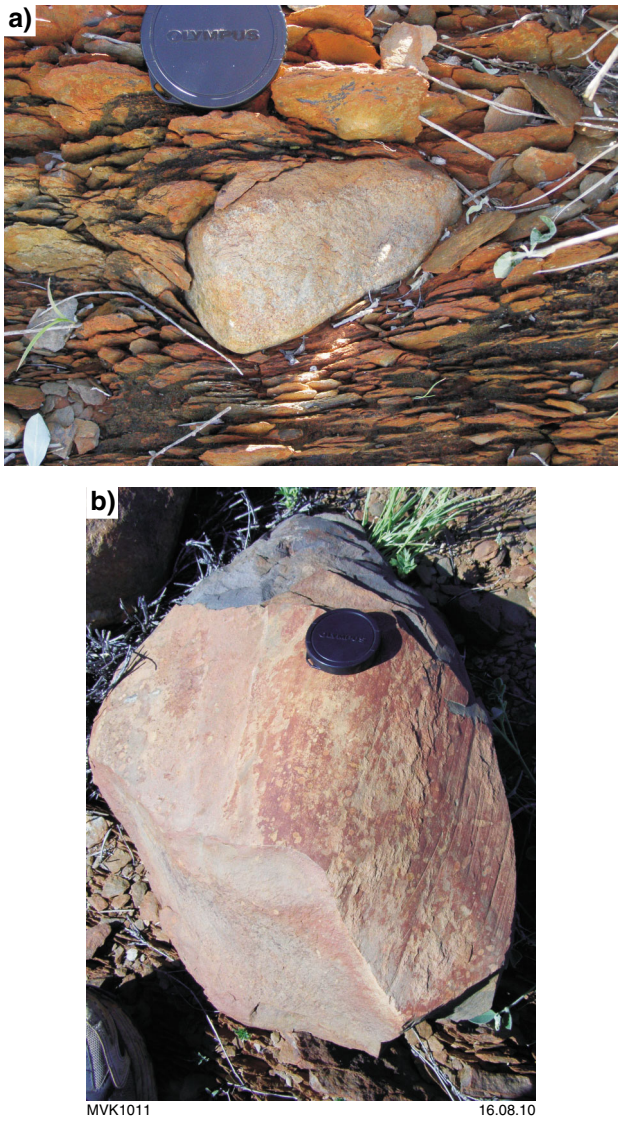

Figure 4. Glacial dropstones of the Meteorite Bore Member (Kungarra Formation, Turee Creek Group), at Meteorite Bore: a) rhyolitic dropstone in foliated siltstone matrix; b) leucogabbro with faceted and striated faces.

Hamersley Group (2.63–2.45 Ga)

The 2.63–2.45 Ga Hamersley Group is the middle of the three groups constituting the Mount Bruce Supergroup (Fig. 2) and reaches a maximum total thickness of 2.5 km (Trendall, 1979). The group consists of thick successions of banded iron-formation interbedded with shale and carbonate, as well as a variety of intrusive and extrusive igneous rocks that account for about 40% of the total thickness of the group (Fig. 5; Trendall, 1990; Barley et al., 1997). The Hamersley Group conformably overlies the Fortsecue Group across a gradational contact (Davy and Hickman, 1988), and is itself conformably overlain by the Turee Creek Group. A large number of precise SHRIMP U–Pb age dates, as well as Pb–Pb carbonate and Re–Os pyrite ages, provide excellent constraints on the depositional history of the basin, including rates of sediment accumulation of between 1 and 225 m/Ma (Trendall et al., 1998, 2004; Woodhead et al., 1998; Pickard, 2002; Anbar et al., 2007).

The Hamersley Group consists of seven distinct units of banded iron-formation (identified as either members or formations) that are interbedded at a large scale with 'shale' and carbonate (Fig. 5). The best known of the iron formations is the Dales Gorge Member of the Brockman Iron Formation, on account of a detailed type section description and isopach map (Trendall and Blockley, 1970). A remarkable feature of the Hamersley Group is the consistent stratigraphy over its entire outcrop area of c. 60 000 km^2, in some instances down to the millimetre scale (Trendall and Blockley, 1970). Another remarkable feature of the iron formations is the chemical homogeneity of each individual unit across the basin (McConchie, 1987). However, each of the iron formations has distinctive characteristics such as layering, mineralogy, and composition, including the Al_2O_3/K_2O ratio and the ratio of ferric to ferrous iron (Trendall and Blockley, 1970).

A characteristic feature of the iron formations is banding, or more properly layering, at scales ranging from millimetre to metre thickness. The layering has been divided into three scale-dependant types: macrobands, mesobands, and microbands (Trendall and Blockley, 1970). Macrobands define major alternations between banded iron-formation (BIF) macrobands and 'shale' (S) macrobands, generally between 1–15 m thick (Figs 5, 6a,b). Mesobands are defined by distinct successions of internally consistent bands of different composition, with average thicknesses of less than 3 cm (Fig. 6c). Mesobands were classified on the basis of the major mineral constituent, including chert, quartz-iron oxide, magnetite, stilpnomelane, carbonate, and riebeckite. Microbands occur typically within chert mesobands only, are generally in the range 0.3–1.7 mm thick, and are defined by the varying content of some iron-bearing mineral within the chert (Fig. 6d).

Generally, banded iron-formation in the Hamersley Group is considered to represent deposition under quiet, deep-

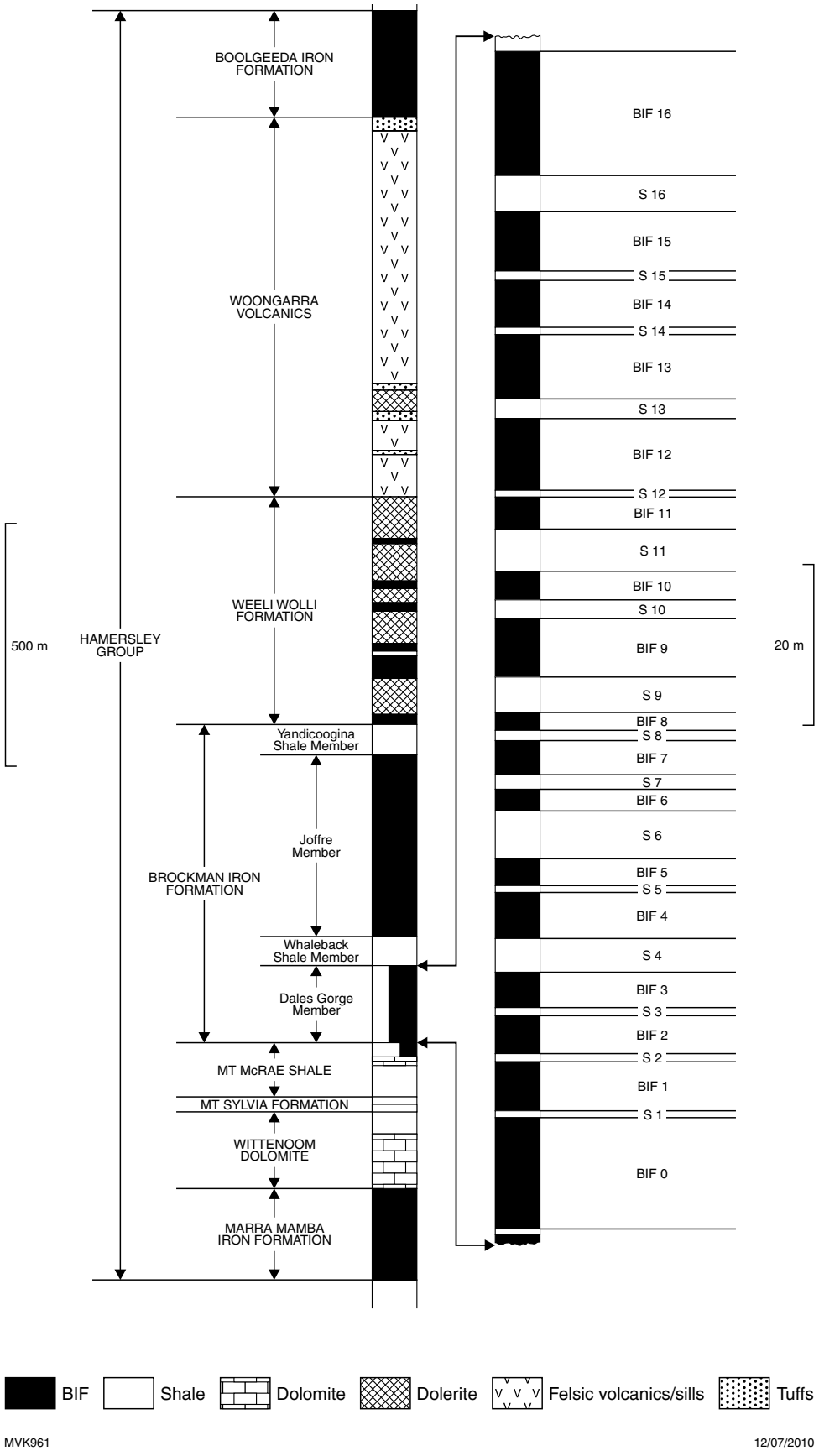

Figure 5. Stratigraphic column of the Hamersley Group, showing major lithologies and the distribution of shale (S) and banded iron-formation (BIF) macrobands in the Dales Gorge Member of the Brockman Iron Formation (modified slightly from Trendall and Blockley, 1970).

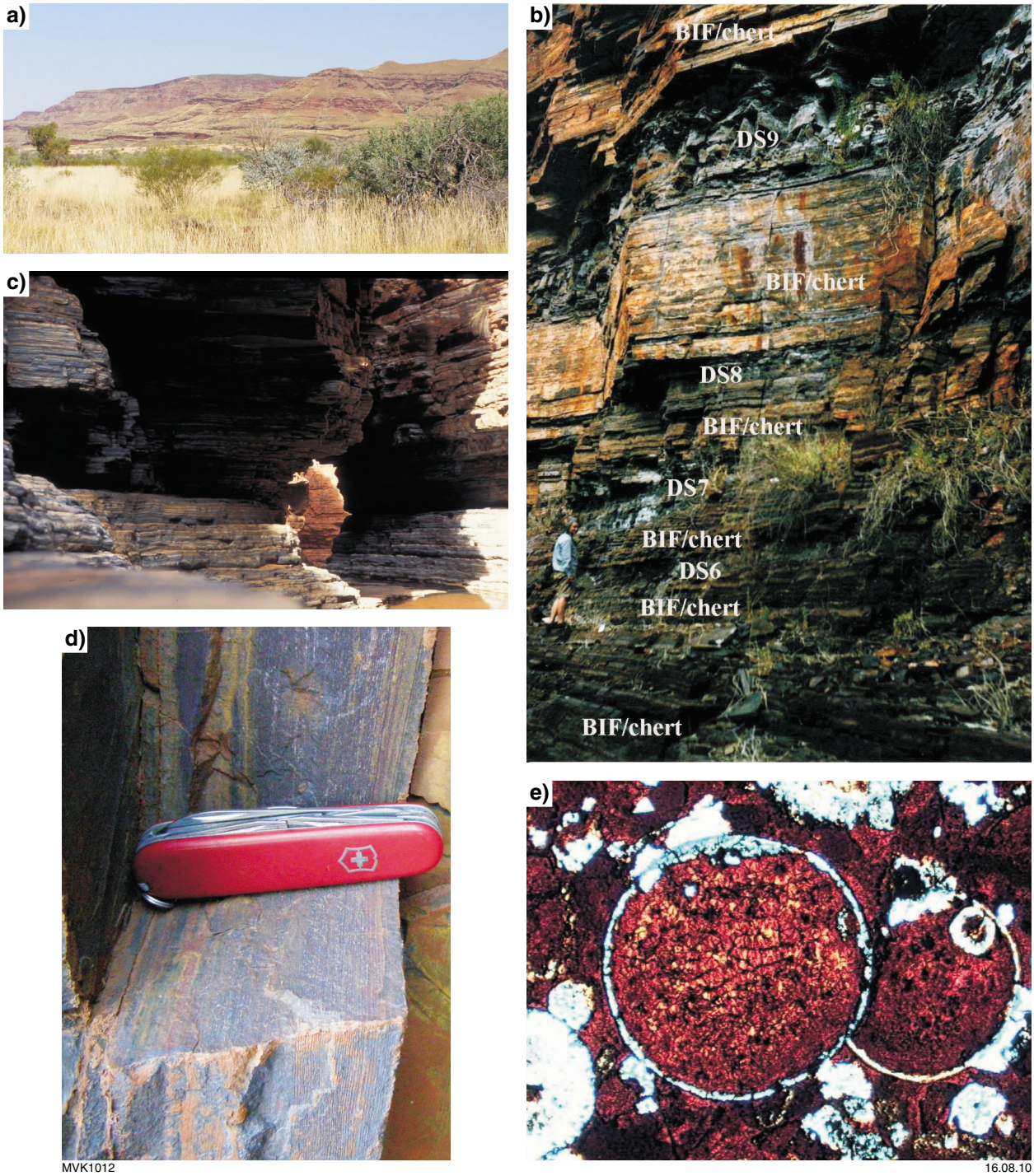

Figure 6. **Outcrop features of the Hamersley Group: a) view looking east-southeast, at bedding in the Hamersley Group from the north side of the Hamersley Range; b) BIF and shale (DS) macrobands of the Dales Gorge Member; c) mesobands in the Dales Gorge Member; d) microbands in the Boolgeeda Iron Formation; e) plane-polarized light thin section view of impact-generated microkrystite from shale macroband 7 of the Dales Gorge Member (width of view 2 mm). Photographs c) and e) courtesy of Dr AY Glikson.**

water conditions, through chemical precipitation from seawater oversaturated in silica and ferrous iron. However, two studies proposed that the iron formation was deposited from distal, episodic density currents (Krapež et al., 2003; Pickard et al., 2004).

The formation of giant iron ore deposits within Hamersley Basin rocks is now known to be the result of post-depositional alteration associated with hydrothermal fluid flow that accompanied tectonothermal events at c. 2.4 and 2.2 Ga (Martin et al., 1998; Rasmussen et al., 2005a). Evidence for such an early age of alteration comes from the discovery of ore-enriched pebbles in unconformably overlying successions, including the c. 2.21 Ga Beasley River Quartzite (Fig. 3a; Martin et al., 1998). These hydrothermal/tectonothermal events concentrated the iron from a background of c. 35–40% in little-altered banded iron-formation, to 60–65% in enriched hematite ores.

'Shale' in formations, members, and macrobands consists of two main, compositionally distinct, rock types. One type is black shale (e.g. much of the Mount McRae Shale), which has relatively high Al_2O_3 (5–11 wt%) and K_2O (1.1–6 wt%), moderate Fe_2O_3 (9–28 wt%) and MgO (2.6–6 wt%), and low CaO (0–1 wt%). The other type is green, stilpnomelane-bearing shale, with high Fe_2O_3 (20–58 wt%), moderate to high CaO (1–8 wt%), and low K_2O (<1 wt%), MgO (0–3 wt%) and Al_2O_3 (generally 0.2–3 wt%, but up to 8.5 wt%). Both shale types have a similar range in SiO_2 of 41–64 wt%. Some previous authors have suggested the green shales are basaltic tuffs, based on the rare occurrence of shard-like textures in thin section (e.g. Pickard, 2002), but their composition is unlike basaltic rocks: they are technically iron formation by virtue of their high iron contents (Trendall and Blockley, 1970; Davy, 1991), they occur over significant and recurrent intervals with BIF and thus are unlikely to represent eruptives, and studies have shown that not all shard-like textures in silicic rocks are the products of volcanic eruptive processes (Allen, 1988). Detailed geochemical analysis has shown that S macrobands are derived at least in part from the same source as BIF macrobands, including weathered mafic–ultramafic crustal material (Pecoits et al., 2009). Thus, following previous workers (Davy, 1991), it is suggested that much of the green 'shale' material in the Hamersley Basin represents a chemical precipitate — a type of siliceous, slightly more magnesian iron formation than normal BIF — derived, at least in part, from intensive chemical weathering of a mafic–ultramafic source.

Another feature of interest within the Hamersley Basin and uppermost Fortescue Group is the occurrence of three impact spherule horizons in rocks deposited from 2.63–2.49 Ga (Fig. 2; Simonson, 1992; Simonson and Hassler, 1997; Woodhead et al., 1998; Hassler and Simonson, 2001; Rasmussen and Koeberl, 2004; Hassler et al., 2005; Rasmussen et al., 2005b). These units have been used to indicate major impact events and to correlate stratigraphy between Australia and South Afric. Features of the deposits include coarse spherules with inward-radiating microcrystallites, microkrystites with offset internal vesicles, quartz grains with sets of planar deformation features, elevated iridium contents, and evidence for impact-associated tsunamis, including local thick deposits of coarse, unsorted chert and carbonate breccia within a matrix of recrystallized carbonate containing scattered spherules (e.g. Carawine Dolomite impact layer; Fig. 6e; see **Excursion Locality 5.7**).

The Hamersley Basin and upper Fortescue Group became famous for hosting molecular fossil evidence of cyanobacteria and the earliest eukaryotes (Brocks et al., 1999, 2003a,b). However, subsequent work has suggested that the molecular biomarkers were actually the result of contamination at some time after peak metamorphism of the rocks at 2.2 Ga (Rasmussen et al., 2008). Nevertheless, independent claims of molecular fossils have been made for Hamersley and upper Fortescue group rocks, including evidence for cyanobacterial aerobiosis (Eigenbrode et al., 2008). Other data, derived through analysis of sulfur and nitrogen isotopes, indicates the presence of sulfate-reducing bacterial activity, as well as both nitrifying and denitrifying microbes, which thrived under at least partly oxidized shallow water conditions (Anbar et al., 2007; Partridge et al., 2008; Garvin et al., 2009). Evidence for bacterial dissimilatory iron reduction (DIR), and coupling of microbial Fe cycling to aerobic methanotrophy or anaerobic oxidation of methane, has also been uncovered from Hamersley Basin rocks (Czaja et al., 2010). Combined, the data show a diverse and highly interactive microbial community in the latest Archean, flourishing under partly oxidized conditions in a generally reducing atmosphere and deep ocean environment.

Fortescue Group (2.78–2.63 Ga)

The 2.78–2.63 Ga Fortescue Group is the oldest and stratigraphically lowest of the three groups that comprise the Mount Bruce Supergroup, and lies with marked erosional unconformity on subdued relict topography of the Pilbara Craton granite–greenstone basement (Fig. 7a). The Fortescue Group reaches a maximum local thickness of >6 km, consisting predominantly of subaerial tholeiitic flood basalts, but also including subordinate pillow basalt and basaltic tuff, felsic volcanic, volcaniclastic, and intrusive rocks, clastic sedimentary rocks (conglomerate to shale), and commonly stromatolitic carbonate (Fig. 7b–d).

The generally accepted stratigraphy of the Fortescue Group is shown in Figure 2, but this varies from north to south, in part due to how mapping was conducted across the area (Trendall, 1990). One possible addition to this scheme has been recently identified in the Marble Bar Sub-basin, in the northern part of the outcrop area of the group (see **Excursion Localities 5.3 and 5.4**). In this area, map, geochronologic, and paleomagnetic data (Van Kranendonk, 2000; Strik, 2004; Van Kranendonk et al., 2006) suggest that a c. 2 km thick unit of gently dipping (25°) to tightly folded (fold limbs to 60°), subaerial tholeiitic basalt (and underlying sandstone and conglomerate) is present unconformably beneath the main, accepted part of the stratigraphy.

Four lines of evidence support this interpretation. First, the underlying rocks are cut by dolerite dykes of the c. 2772 Ma Black Range Dolerite Suite that are dated to

Figure 7. Outcrop features of the Fortescue Group: a) view, looking east-southeast, of the flat-lying unconformity between the Fortescue Group and Pilbara Craton granitic basement at Excursion Locality 5.1; b) ropey pahoehoe lava flowtop of the Mount Roe Basalt; c) metre-high coniform stromatolites and unconformably overlying fluvial gravels, Tumbiana Formation; d) mud-draped rippled pavement, Hardey Formation.

within error of the age of the Mount Roe Basalt (Arndt et al., 1991; Wingate, 1999; Van Kranendonk, 2000, 2004). Second, the underlying rocks are tightly folded, in contrast to the rest of the group (and the dolerite dykes), which is only gently titled. Third, these rocks contain a remnant magnetization that is distinct from the Mount Roe Basalt, whereas unconformably overlying basalts have a similar remnant magnetization as the Mount Roe Basalt. Fourth, the Black Range Dyke is demonstrably coeval with basalts that unconformably overlie the folded, lower rocks (see **Excursion Locality 5.2**). These data suggest that the age of the undated lower basaltic rocks at the base of the Marble Bar Sub-basin is somewhere in the range 2.83 – 2.78 Ga, the product of an event previously unrecorded in the Pilbara.

Flood basalts in the main part of the Fortescue Group were erupted from 2775 to 2715 Ma, in three distinct events at 2775–2756 Ma, c. 2740 Ma, and at 2715 Ma, during periods of continental rifting (Fig. 2; Arndt et al., 1991; Blake, 1993, 2001; Wingate, 1999; Blake et al., 2004). Analysis of the primary, neutral, remnant magnetization from these rocks has resulted in a magnetostratigraphy and defined continental drift rates as fast as, or up to 5 times faster than, any known from the Phanerozoic (Strik et al., 2003; Blake et al., 2004).

Fortescue Group flood basalts are interbedded with sedimentary rocks that were deposited in freshwater settings, at least in part as giant lake systems (Hickman and de Laeter, 1977; Buick, 1992; Bolhar and Van Kranendonk, 2007; Awramik and Buchheim, 2009), although coastal and shallow marine conditions have also been identified for part of the Tumbiana Formation (Sakurai et al., 2005). The Tumbiana Formation contains abundant stromatolites (Walter, 1983; Awramik and Buchheim, 2009), accompanied by sparse, rather poorly preserved, filamentous microfossils (Schopf and Walter, 1983), which

together represent one of the best preserved and most diverse fossil assemblages in the early Earth geological record. In addition to their gross morphology, Tumbiana stromatolites contain abundant microstructural evidence of microbial activity, including erect and radiating filament molds, fine, kerogenous filament remnants, and calcite-infilled open pore space structures that closely resemble gas-filled pockets resulting from bacterial decay. At the nanoscale, even more convincing evidence of microbial activity has been uncovered in the form of organic globule clusters and aragonite nanocrystals within thin layers of the stromatolites, a combination that is remarkably similar to the organo-mineral building blocks of modern stromatolites (Lepot et al., 2008). Detailed analysis of organic matter in Tumbiana stromatolites sampled from fresh drillcore indicate the presence of both organic sulfur-rich material, as encapsulated microbial cells, as well as sulfur-poor material interpreted to represent fossil extracellular polymer substances, or recondensed kerogen (Lepot et al., 2009). The presence of sulfate-reducing bacteria has been inferred from these data. Methanotrophy has also been inferred for Tumbiana stromatolites, based on highly negative $\delta^{13}C_{kerogen}$ values of up to –59‰ (Packer, 1990), as well as for older sandstones of the Hardey Formation (–43 to –55‰; Rasmussen et al., 2009). These highly negative $\delta^{13}C_{kerogen}$ values are some of the most negative recorded in Earth history and represent a late Archean biotic crisis.

Pilbara Craton (3.52–2.83 Ga)

The 3.52–2.83 Ga Pilbara Craton is a nearly circular piece of crust in the northwestern part of Western Australia, the boundaries of which are defined by aeromagnetic and gravity anomalies, and by orogenic belts (Fig. 8). The

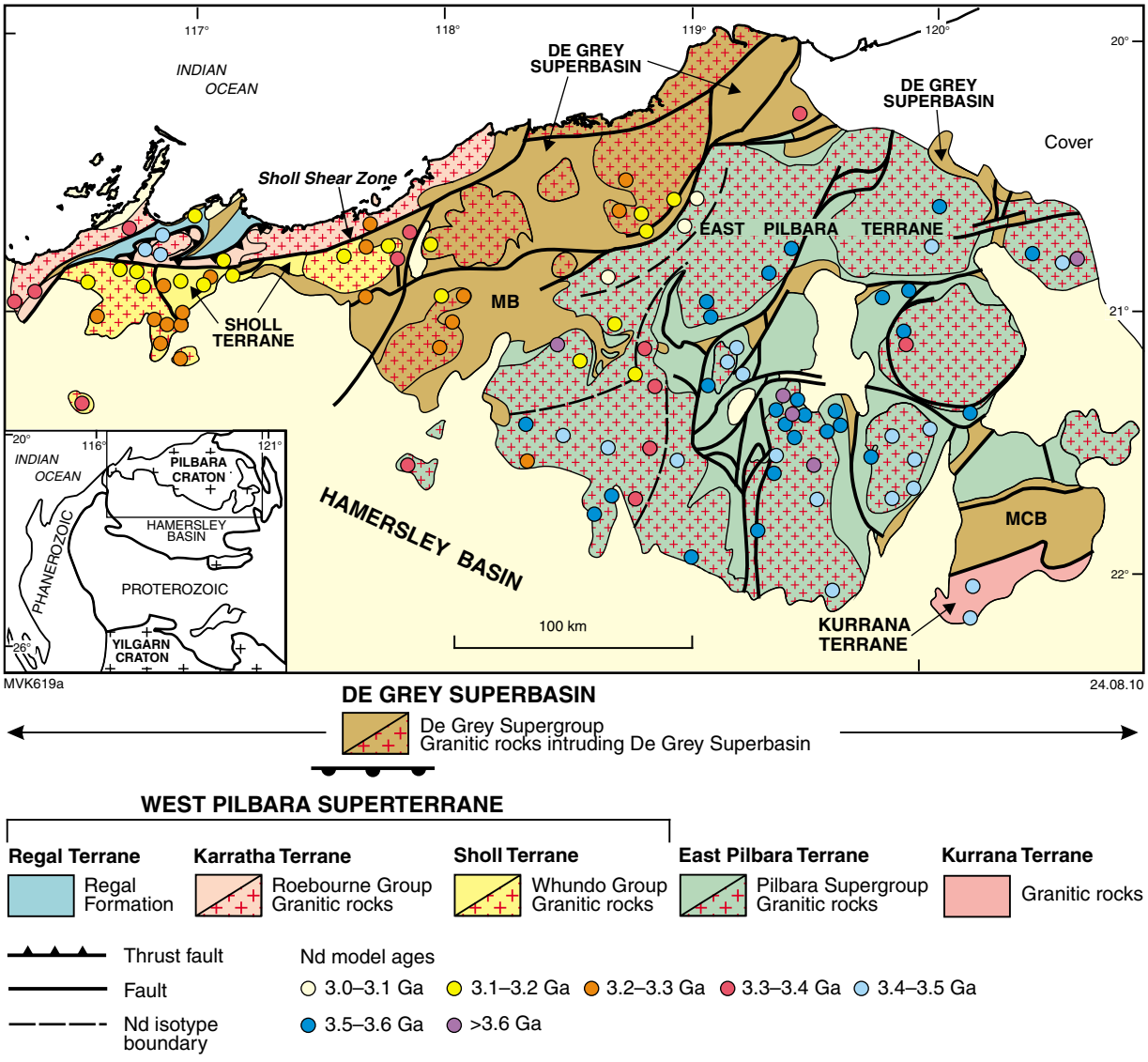

Figure 8. Terrane map of the Pilbara Craton, showing Nd model age data (from Van Kranendonk et al., 2007a): MB = Mallina Basin; MCB = Mosquito Creek Basin.

northern part of the craton is well exposed over an area of 530 km × 230 km, but much of the rest is unconformably overlain by volcanic and sedimentary rocks of the Mount Bruce Supergroup deposited in the Hamersley Basin (inset of Fig. 8; Arndt et al., 1991; Blake et al., 2004; Trendall et al., 2004).

Recent compilations of stratigraphic, geochronological, structural, and isotopic data have been used to divide the granite–greenstone rocks of the northern Pilbara Craton into five terranes and five late-tectonic, dominantly clastic, sedimentary basins (Fig. 8; Van Kranendonk et al., 2002, 2007a,b). Terranes have unique lithostratigraphy, granitic supersuites, structural map patterns, geochemistry, and tectonic histories, as outlined in more detail elsewhere (Hickman, 2004; Smithies et al., 2005a,b; Van Kranendonk et al., 2007a). Terranes include: the 3.53 – 3.17 Ga East Pilbara Terrane (EPT), representing the ancient nucleus of the craton; the ≥3.18 Ga Kurrana Terrane in the southeastern part of the craton, which has EPT-type Sm–Nd model ages and may represent a rifted fragment of this crust; the 3.27 – 3.11 Ga West Pilbara Superterrane (WPS). The WPS is a collage of three distinct terranes: the c. 3.27 Ga Karratha Terrane (KT), which may represent a rifted fragment of the EPT (Hickman, 2004); the c. 3.02 Ga Regal Terrane; the 3.13 – 3.11 Ga Sholl Terrane in the southern part of the WPS, which is juxtaposed against the two northern terranes of the WPS across the crustal-scale, strike-slip Sholl Shear Zone (Fig. 8).

Rocks of the West Pilbara Superterrane, East Pilbara Terrane, and Kurrana Terrane are separated by, and unconformably overlain by, the dominantly clastic sedimentary rocks of the De Grey Supergroup, which were deposited across the whole of the craton between 3.02 and 2.93 Ga (Van Kranendonk et al., 2007a). The supergroup comprises the basal Gorge Creek Group (c. 3.02 Ga), the Whim Creek Group (3.01 Ga), the Croydon Group (2.99 or 2.97 – 2.94 Ga) and the Nullagine Group (≥2.93 Ga). Major depositional basins include the Gorge Creek Basin, which formed across the whole of the craton, the Mallina Basin between the WPS and EPT, and the Mosquito Creek Basin between the EPT and the Kurrana Terrane (Fig. 8).

Rocks of the WPS show lithostratigraphic, geochemical, and structural features that are distinctly different from the EPT. These differences have been used to argue for a change in tectonic style from crust formation processes dominated by mantle plumes prior to 3.2 Ga, to processes dominated by plate tectonics after c. 3.2 Ga (Fig. 9; Smith et al., 1998; Hickman, 2004; Smithies et al., 2005a,b; Van Kranendonk et al., 2004, 2007a,b, 2010). A key element in this model is geologic, isotopic, and geochemical data related to the 3.13 – 3.11 Ga Whundo Group of the Sholl Terrane, which is a fault-bounded, >10 km thick succession of juvenile, bimodal basaltic to felsic volcanic and volcaniclastic rocks that show compelling geochemical evidence of an oceanic arc-like assemblage of rock types. This includes boninites (that have all of the compositional hallmarks of modern boninites), interlayered tholeiitic and calc-alkaline volcanic rocks, Nb-enriched basalts, adakites, and rhyolites (Smithies et al., 2004, 2005a, 2007a,b).

Geology of the East Pilbara Terrane

The East Pilbara Terrane (EPT) is composed of rocks that formed from 3.52 to 3.17 Ga, including volcano-sedimentary rocks (greenstones) of the Pilbara Supergroup as well as voluminous granitic rocks emplaced at discrete intervals from 3.52 to 3.24 Ga (Figs 9, 10; Van Kranendonk et al., 2007a,b). The Pilbara Supergroup is preserved in arcuate greenstone belts that wrap around domical, multiphase granitic complexes (Fig. 8). Periods of deformation and metamorphism accompanied deposition of each of the groups in the Pilbara Supergroup and emplacement of contemporaneous granitic rocks. These events were followed by deposition of unconformably overlying supracrustal rocks (De Grey Supergroup) and intrusion of younger granitic rocks during geological events that affected the whole of the craton between 3.07 and 2.83 Ga (Fig. 9; Van Kranendonk et al., 2007a,b).

Pilbara Supergroup

The generally well-preserved Pilbara Supergroup consists of four demonstrably autochthonous volcano-sedimentary groups deposited between 3.52 and 3.17 Ga (Fig. 10; Van Kranendonk et al., 2007a,b). Detailed geological mapping and extensive SHRIMP geochronology has revealed no stratigraphic repetitions in any of the greenstone belts in the EPT. The maximum *preserved* thickness of the Pilbara Supergroup is c. 22 km. However, contacts of the lower part of the supergroup are everywhere with intrusive granitic rocks and the upper part of each of the groups has been eroded beneath unconformably overlying groups or formations, such that the original thickness of any of the component groups, and the supergroup as a whole, is unknown. Furthermore, there is good evidence from changes in the dip of bedding between groups, and from the nature of the unconformities between groups, that the supergroup was deposited as a laterally accreting succession within developing synclinal basins on the flanks of developing granitic domes, during periods of lithospheric extension (Nijman and de Vris, 2004; Van Kranendonk et al., 2004, 2007b).

The stratigraphically lowest Warrawoona Group is at least 12 km thick and was deposited over 100 Ma as a result of on-going volcanism from 3.53 – 3.43 Ga (Fig. 10; Van Kranendonk et al., 2002, 2007b). The bulk of this succession comprises well-preserved pillow basalt, komatiitic basalt, and komatiite. Lesser felsic volcanic intervals are typically restricted to thin tuffaceous horizons a few tens of metres thick, but dacite-dominated deposits locally reach a few kilometers thick in the Coucal, Duffer, and Panorama formations (locally 8 km thick in the Duffer Formation; Smithies et al., 2007a).

Sedimentary units in the Warrawoona Group include volcaniclastic rocks, quartz-rich sandstone, and carbonates, but mainly consist of grey, white, blue-black, and red layered cherts derived from silicified carbonates and other protoliths (Buick and Barnes, 1984; Van Kranendonk, 2006). An unusual sedimentary unit is the 3470 ± 2 Ma Antarctic Creek Member of the Mount Ada Basalt, which contains thin beds with sand-size grains of altered, quench-textured impact spherules (Lowe and Byerly, 1986; Byerly et al., 2002). Many chert units in the Warrawoona Group,

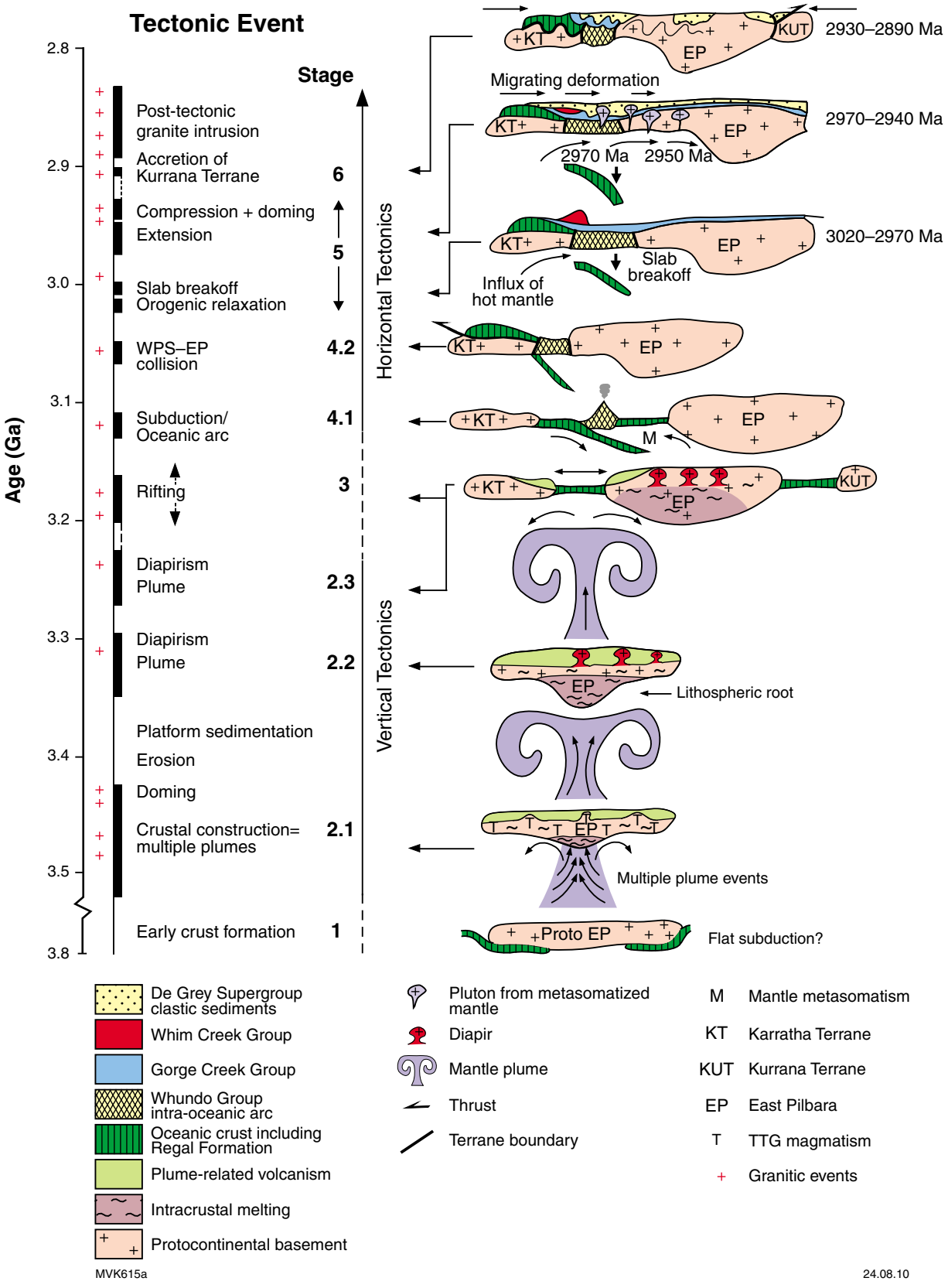

Figure 9. Schematic evolutionary history of the Pilbara Craton (from Van Kranendonk et al., 2007a).

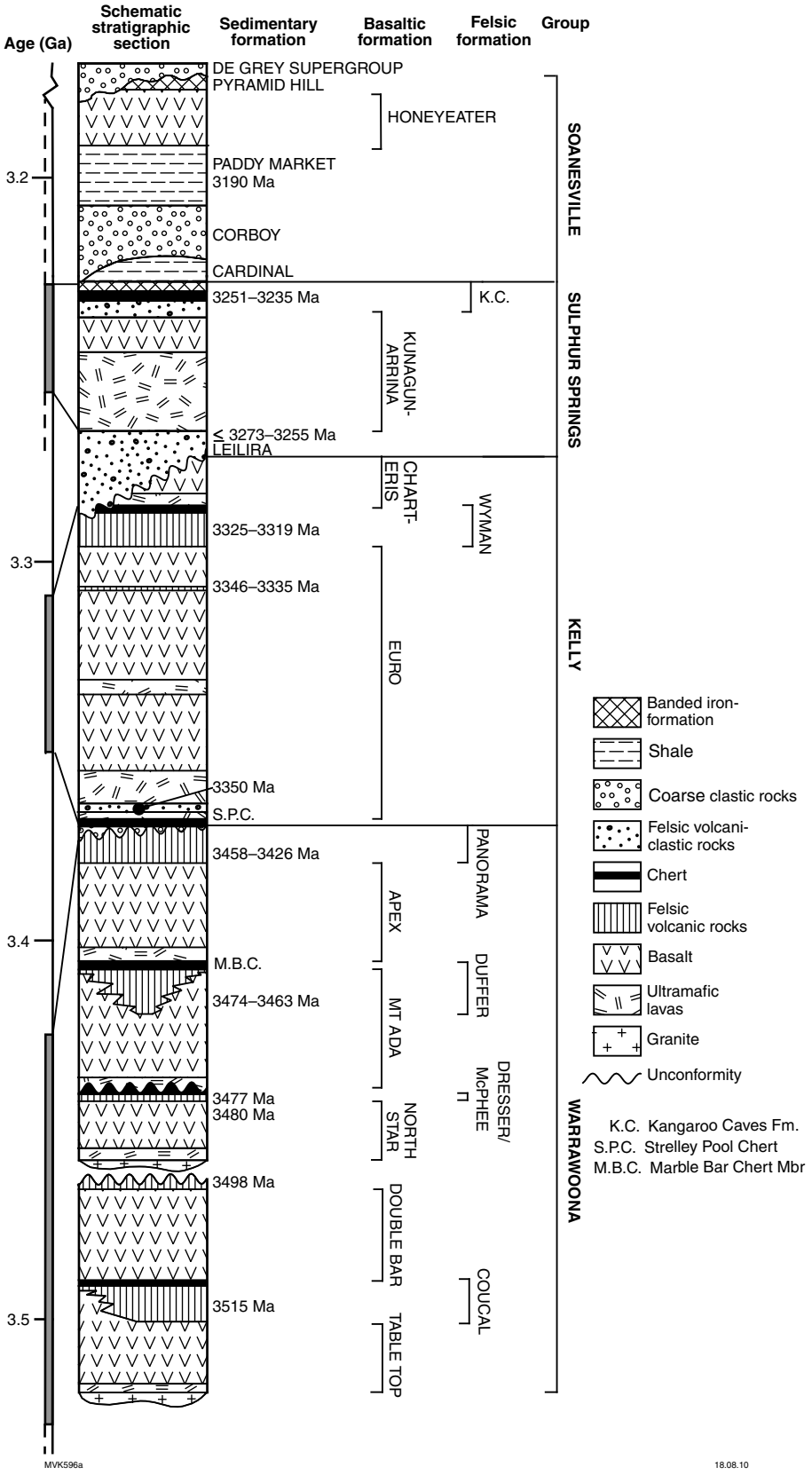

Figure 10. Stratigraphic column of the Pilbara Supergroup.

including the jaspilitic cherts of the c. 3.47 Ga Marble Bar Chert Member of the Duffer Formation, are well layered at a millimetre to centimetre scale, indicating deposition under quiet water, deep marine conditions, consistent with evidence from underlying and overlying pillow basalts. In contrast, the chert–barite unit of the c. 3.49 Ga Dresser Formation in the North Pole Dome shows evidence of deposition under tectonically active conditions, indicated by rapid lateral facies variations, beds of olistostrome breccia, and internal erosional unconformities (Nijman et al., 1998; Van Kranendonk, 2006; Van Kranendonk et al., 2008).

Local preservation of desiccation cracks, and the more widespread occurrence of rippled carbonate sedimentary rocks and stromatolites in this unit, indicate periods of shallow water deposition and subaerial exposure (Lambert et al., 1978; Walter et al., 1980; Groves et al., 1981; Buick and Dunlop, 1990; Van Kranendonk, 2006; Van Kranendonk et al., 2008). Stromatolites are well developed in this unit and vary in morphology, suggesting diverse assemblages of micro-organisms at this early stage in Earth history (Van Kranendonk, 2006, 2010). Whereas earlier studies suggested deposition of the Dresser Formation in a restricted shallow marine basin (Buick and Dunlop, 1990), more detailed recent studies favour deposition within a felsic volcanic caldera affected by syn-depositional growth faults and voluminous hydrothermal circulation (Nijman et al., 1998; Van Kranendonk, 2006; Van Kranendonk et al., 2008).

The stratigraphy of the Warrawoona Group varies across the EPT, but dating confirms stratigraphic correlations across most of the terrane. The thickest (12 km) and most complete section through the group is exposed in the Marble Bar greenstone belt (Hickman, 1983), although the lowermost part of the stratigraphy is excised by intrusive granitic rocks. A distinctive feature of the group in this belt is the great thickness (4 km) of volcaniclastic rocks of the Duffer Formation (Hickman, 1983) and the presence of a voluminous mafic dyke swarm that feeds the Apex Basalt (Van Kranendonk, 2006).

Deposition of the Warrawoona Group was followed by a 75 Ma hiatus in volcanism, during which the terrane was uplifted and eroded under at least locally subaerial conditions (Buick et al., 1995), creating a regional unconformity. Sedimentary rocks of the 30–1000 m thick Strelley Pool Formation (Hickman, 2008) were deposited on the Warrawoona Group during this interval (Van Kranendonk et al., 2007a; Van Kranendonk, 2010). This formation comprises a lower unit of fluviatile to shallow marine conglomerates and quartzite, a middle unit of stromatolitic marine carbonates, and an upper unit of coarse clastic rocks, and was deposited as a carbonate platform on an unconformity that extended across the EPT (Lowe, 1983; Hofmann et al., 1999; Van Kranendonk et al., 2003; Allwood et al., 2006; Van Kranendonk, 2006, 2007).

The conformably overlying Euro Basalt at the base of the Kelly Group consists of a ≤1.5 km thick basal unit of komatiite and up to 5 km of overlying, interbedded komatiitic basalt and tholeiitic basalt that was erupted over c. 25 Ma, from 3.35–3.32 Ga (Fig. 10). This was followed by eruption at c. 3.325 Ga of high-K rhyolites of the Wyman Formation, accompanied by emplacement of genetically related, voluminous monzogranitic plutons. Basaltic volcanism continued with eruption of the conformably overlying, but undated, Charteris Basalt, which is locally 1000 m thick (Hickman, 1984).

The ≤3.27 to 3.23 Ga Sulphur Springs Group was deposited across an unconformity on older greenstones in the western part of the EPT (Van Kranendonk, 2000; Buick et al., 2002). In the type area in the Soanesville greenstone belt, this group is up to 4000 m thick and consists of: basal sandstone and felsic volcaniclastic rocks of the 3.27–3.25 Ga Leilira Formation; up to 2000 m of komatiite to komatiitic basalt of the c. 3.25 Ga Kunagunarrina Formation; and up to 1500 m of andesite–basalt through to rhyolite of the 3.245–3.235 Ga Kangaroo Caves Formation, which is capped by <30 m of silicified epiclastic and siliciclastic rocks (Van Kranendonk, 2000; Buick et al., 2002). Felsic volcanic rocks of the formation thin laterally away from the thickest part of the group and pass into ≤500 m of banded iron-formation (Pincunah Member of the Kangaroo Caves Formation; Van Kranendonk et al., 2007a). The banded iron-formation, along with panels of silicified epiclastic sediments and large blocks of rhyolite, are incorporated within a unit of coarse olistostrome breccia at the top of the formation, over the apex of the Strelley Monzogranite.

The Sulphur Springs Group is intruded by the shallow-level, syn-volcanic Strelley Monzogranite, a K_2O-rich subvolcanic laccolith with rapakivi textures (Brauhart, 1999; Van Kranendonk, 2000, 2006). Heat from this intrusion drove hydrothermal circulation that precipitated volcanogenic massive sulfide (Cu–Zn) deposits (Vearncombe et al., 1998; Huston et al., 2001; Van Kranendonk, 2006). Eruption of the Sulphur Springs Group was coeval with widespread monzogranite plutonism across the northern and western parts of the EPT.

Disconformably overlying the Sulphur Springs Group is the 3.23–3.17 Ga Soanesville Group of clastic sedimentary rocks, basalt, and banded iron-formation (Fig. 10; Buick et al., 2002; Rasmussen et al., 2007; Van Kranendonk et al., 2007a, 2010). This group includes, from base to top: shale of the Cardinal Formation; the Corboy Sandstone; the Paddy Market Formation of shale and siltstone; the 1150 m thick Honeyeater Basalt; and the Pyramid Hill Formation of banded iron-formation and ferruginous shale (Van Kranendonk et al., 2007b). Eruption of the Honeyeater Basalt was accompanied by emplacement of the Daltons Suite of layered mafic–ultramafic sills that range in composition from dunite, through pyroxenite, to dolerite (with local granophyre; Van Kranendonk, 2000). The Soanesville Group lies conformably, or with an onlapping lower contact, on silicified epiclastic rocks of the Sulphur Springs Group (Van Kranendonk, 2000; Buick et al., 2002). Deposition of the lower, clastic components of the group occurred during horst-and-graben style block faulting of the basement, indicating extension (Wilhelmij and Dunlop, 1984), during what is inferred to be a period of rifting of the EPT margins (Van Kranendonk et al., 2010).

There are several significant points to note in regard to the tectonic setting of the Pilbara Supergroup.

- Stratigraphic evidence, confirmed by extensive geochronology and geochemistry, indicates that the Pilbara Supergroup is everywhere a right way up and upward-younging succession. There are no major tectonic duplications, but there are upward changes in geochemistry (Smithies et al., 2005b, 2007a) and demonstrably autochthonous contacts between groups, as well as between formations within groups (Van Kranendonk, 2000; Van Kranendonk et al., 2007b).
- Inherited and detrital zircon, geochemical, and isotopic evidence shows that the Warrawoona Group was extensively contaminated by older felsic crust, and thus was not erupted in either a mid-ocean ridge or intra-oceanic arc setting (Green et al., 2000; Van Kranendonk et al., 2002, 2007).
- The geochemical evidence indicates derivation of the ultramafic and mafic volcanic rocks of the supergroup from mantle plume sources (Smithies et al., 2005b). This includes a component derived from subcontinental mantle lithosphere that became progressively more depleted through time as a result of repeated and voluminous melt extraction events (Smithies et al., 2005b).
- Geochemical evidence also indicates that most felsic volcanic rocks in the Warrawoona Group are the result of fractionation of tholeiitic parental magmas and are not comparable to subduction-generated calc-alkaline volcanic rocks, as previously suggested. Contemporaneous tonalite–trondhjemite–granodiorite (TTG), and a minor volume of TTG-like felsic volcanic rocks, are thought to derive from melting of basalt and older felsic crust at the base of the volcanic pile, rather than from any form of subduction (Smithies et al., 2007a).

Crust formation

The Paleo- to Mesoarchean evolution of the East Pilbara Terrane is thought to arise from three successive mantle plume events, resulting in voluminous outpouring of dominantly basaltic lavas and crustal thickening through magmatic intraplating and underplating (Fig. 9). During plume events, conductive heat from the mantle and from intracrustal magma chambers was augmented by heat from radioactive elements in older granitic rocks, which were buried into the mid crust by the thick eruptive volcanic lid, to result in widespread melting of the granitic lower to middle crust (Sandiford et al., 2004; Van Kranendonk et al., 2004; Bodorkos and Sandiford, 2006). This melting resulted in weakening of the middle crust, which facilitated sinking of newly erupted greenstones, and this in turn drove the partial melts in the middle crust upwards, into the cores of rising domes, where it crystallized to form new granitic intrusions (Fig. 11).

This process was repeated three times, during eruption of the Warrawoona, Kelly, and Sulphur Springs Groups (Hickman and Van Kranendonk, 2004; Van Kranendonk et al., 2004). Each event served to amplify the pre-existing dome-and-keel structure. Evidence from volcanic geochemistry shows that melting events occurred progressively deeper in the lithosphere and mantle through time, and that successive plume events caused ever greater degrees of depletion of the subcontinental lithospheric mantle (Smithies et al., 2005b). This resulted in the depleted mantle becoming more buoyant than surrounding mantle and forming an unsubductable lithospheric keel (Fig. 12; cf. Griffin and O'Reilly, 2007). This is the principal reason for the preservation of the East Pilbara Terrane, leading to subsequent growth of the craton through subduction–accretion of younger material onto this ancient nucleus (Van Kranendonk et al., 2002, 2007a).

Plume magmatism during Warrawoona Group time passed through, and erupted onto, an older sialic basement, forming a sort of hybrid oceanic–continental plateau, in many ways analogous to the Phanerozoic Kerguelen Plateau (cf. Van Kranendonk and Pirajno, 2004; Van Kranendonk et al., 2007b). Periods of shallow-water deposition (Dresser Formation, Panorama Formation) suggest periods of magmatic inflation and crustal uplift, which is common during plume events. However, the presence of thick pillow basalt successions interbedded with the shallow water episodes suggests intervening periods of basin deepening. Evidence in the form of the Salgash Dyke Swarm, and from caldera formation at different times in the Warrawoona Group, suggests that basin deepening was achieved through crustal extension (cf. Nijman and De Vries, 2004; Van Kranendonk, 2006; Van Kranendonk et al., 2008). These dual actions of uplift and extension are interpreted to represent a coupled mechanism, whereby magmatic overthickening caused extension of the overlying crust, achieved by the development of horizontal shear zones in the ductile middle crust (Fig. 12; Van Kranendonk et al., 2007b). Crustal extension facilitated the rise of granitic domes. The radial pattern of lineations around the domes indicates that extension was through pure shear and was equal in all horizontal directions (σ_1 vertical, $\sigma_2 = \sigma_3$). Extension continued after the end of Sulphur Springs Group volcanism, and led to the formation of deep basins filled by a thick, clastic, sedimentary succession (lower part of the Soanesville Group) perched on the EPT, and to whole-lithosphere rifting of the margins of the EPT (Van Kranendonk et al., 2007a, 2010).

Early life in the Pilbara

Many and various claims for Paleoarchean life in the Pilbara Supergroup have been made since Lambert et al. (1978) described stromatolitic edgewise conglomerates from sedimentary rocks of the Warrawoona Group. These claims are based on a variety of geological evidence from rocks at a number of different stratigraphic levels in the Pilbara Supergroup (Fig. 13). This evidence can be divided into the following distinct kinds:

1) c. 3.48 Ga Dresser Formation — diverse stromatolites, putative microfossils, strongly negative $\delta^{13}C$ on carbonaceous material, clasts of kerogenous material in micritic carbonate, sulfur isotopes (Walter et al.,

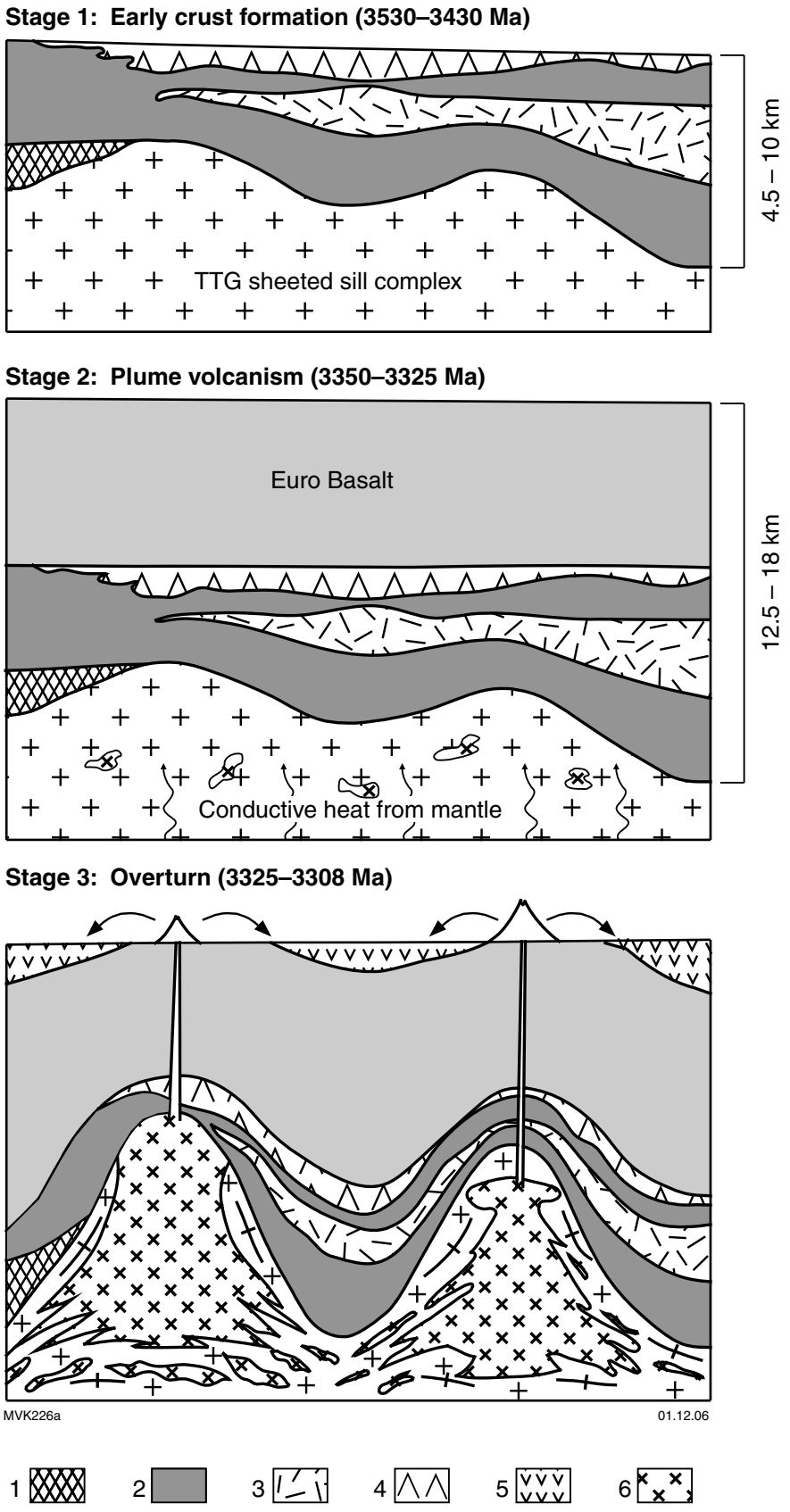

Figure 11. Schematic development of dome-and-keel architecture of the East Pilbara Terrane, Pilbara Craton (from Van Kranendonk et al., 2007a): 1. Coonterunah Subgroup; 2. Warrawoona Group basaltic volcanic rocks; 3. Duffer Formation; 4. Panorama Formation; 5. Wyman Formation; 6. Monzogranite, derived from partial melting of older TTG (tonalite–trondhjemite–granodiorite).

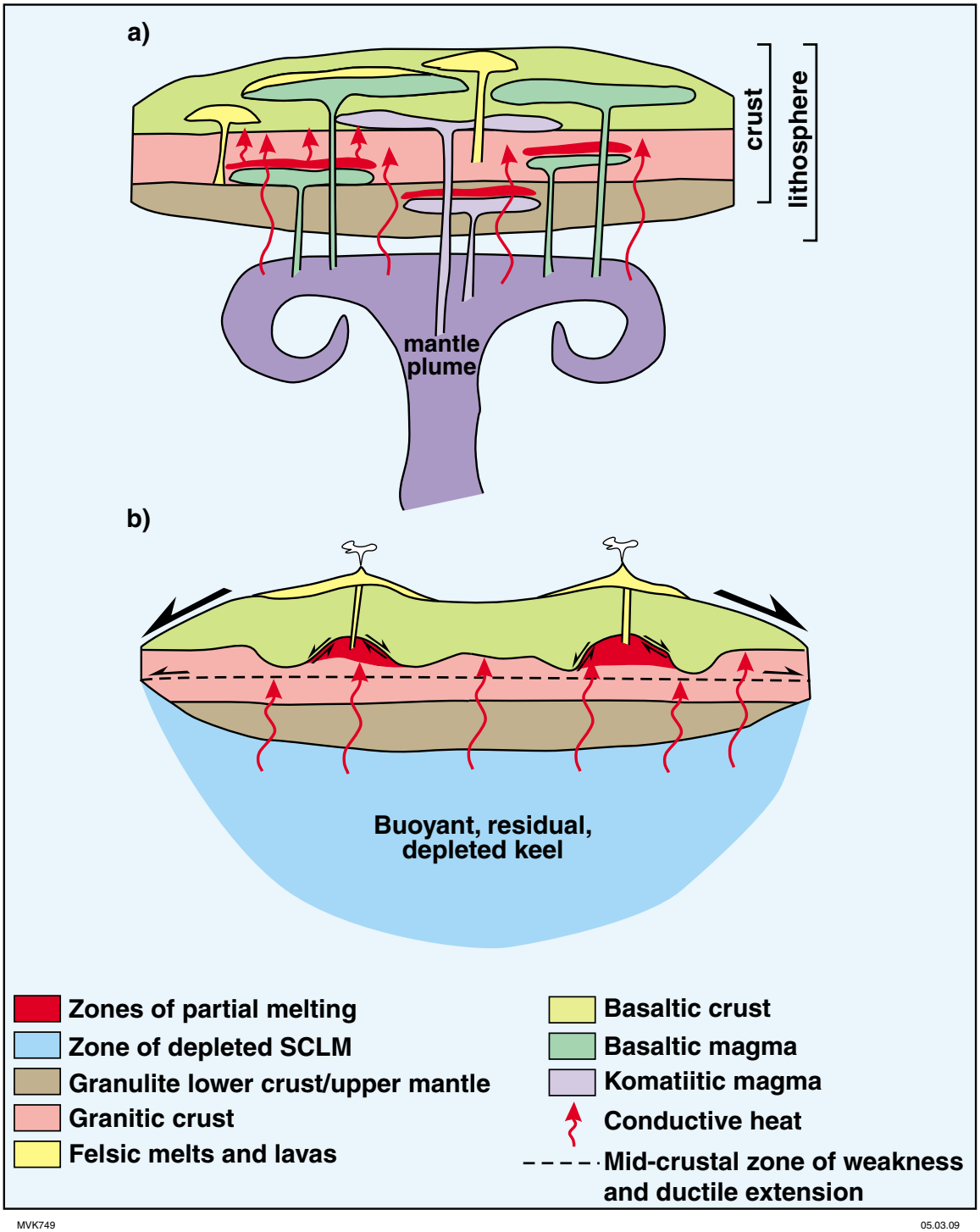

Figure 12. Schematic development of the East Pilbara Terrane, as a result of mantle plume magmatism and internal differentiation (from Van Kranendonk et al., 2007b): SCLM = Sub-continental mantle lithosphere.

1980; Buick and Dunlop, 1990; Ueno et al., 2004; Van Kranendonk, 2006; Philippot et al., 2007; Glikson et al., 2008; Van Kranendonk et al., 2008)

2) c. 3.46 Ga Apex chert — putative microfossils, Laser-Raman spectrography (Schopf, 1993; Schopf et al., 2002, 2007, but see also Brasier et al., 2002, 2005; Garcia-Ruiz et al., 2003)

3) c. 3.40 Ga Strelley Pool Formation — diverse stromatolites, carbon isotope data, and organic geochemistry (Lowe, 1980; Hofmann et al., 1999; Allwood et al., 2006; Van Kranendonk, 2006, 2010; Marshall et al., 2007)

4) c. 3.35 Ga Euro Basalt — ichnofossils in altered basaltic glass (Banerjee et al., 2007; Furnes et al., 2007)

5) c. 3.24 Ga Sulphur Springs Group — putative microfossils in sulfides (Rasmussen, 2000)

6) c. 3.20 Ga Soanesville Group — organic matter, highly negative $\delta^{13}C$ on carbonaceous material, putative microfossils (Duck et al., 2007).

Many claims of biogenicity have been challenged on the basis of either alternative interpretations of the geological data presented in the original claims, or new data gained from more recent research. These include:

1) a non-biogenic interpretation of the macroscopic geometry of stromatolites, wherein previously widely accepted morphological criteria have been re-interpreted as structural or sedimentological artifacts (e.g. Buick et al., 1981; Lowe, 1994; Lindsay et al., 2005)

2) a re-interpretation of microfossils as either more recent contaminants (Neoarchean; Buick, 1984, 1988), or non-biological features resulting from mineral crystallization processes within hydrothermal silica veins (Brasier et al., 2002, 2005; Garcia-Ruiz et al., 2003)

3) an interpretation of fractionated $\delta^{13}C$ carbonaceous material in hydrothermal silica veins as a result of inorganic processes, such as Fischer–Tropsch synthesis (cf. Brasier et al., 2002; McCollum, 2003; Lindsay et al., 2005)

4) different interpretations of highly fractionated $\delta^{34}S$ in microscopic pyrite (Shen et al., 2001; Philippot et al., 2007).

This fieldtrip will expose the participants to all of the major sites where claims for early life have been made, with the objective of providing a common background in which to frame ongoing debate and generate ideas for future research.

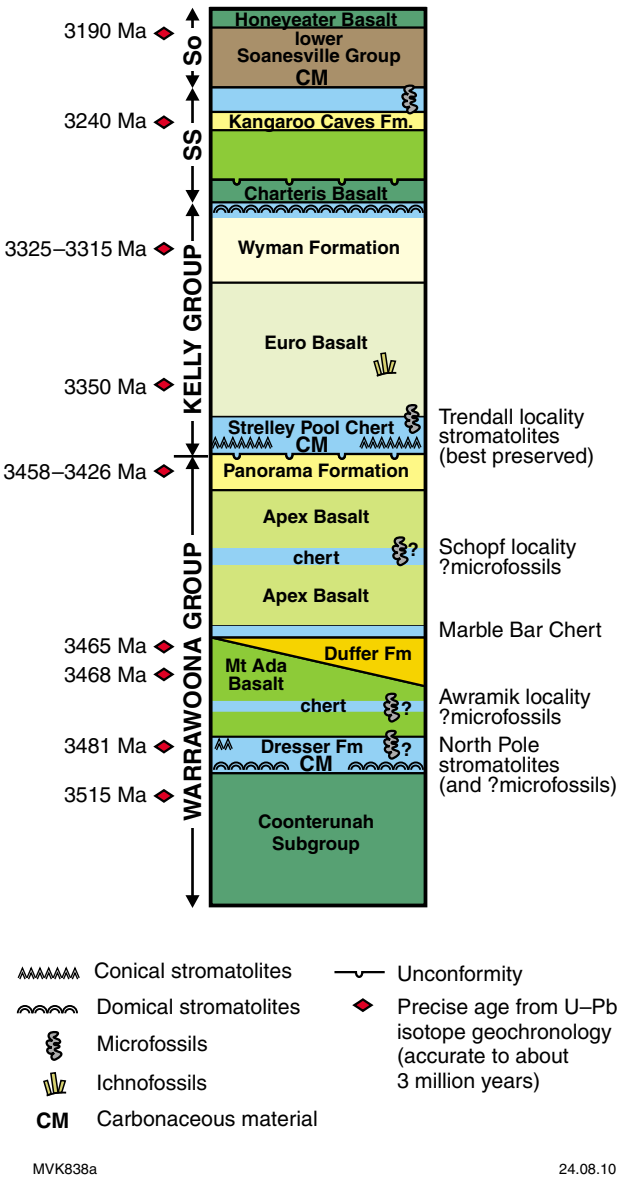

Figure 13. Simplified stratigraphic column of the Pilbara Supergroup, showing kinds of evidence used as claims for early life (from Van Kranendonk, 2010).

Day 1: Shark Bay stromatolites

The fieldtrip starts at the Denham airport. Drive ~8 km west and south into the town of Denham. Here we will have an opportunity for anyone to do some shopping for last minute items and visit the Shark Bay World Heritage Discovery Centre for a group tour. From Denham, drive ~100 km south to the turnoff to the old Telegraph Station and turn left, following the track north into the station parking lot (about 4.5 km). From the vehicles, walk 500 m out to the boardwalk that overlooks the stromatolite reef flanking the shoreline of Hamelin Pool.

OR

continue driving 29 km further east to the Coastal Highway and turn left. Proceed north for 27 km and take the turn to the left onto the track leading to Carbla Homestead. Follow the track for ~9.5 km west to the homestead and then proceed a further 11 km southwest to the coast of Hamelin Pool at Carbla Point. Permission from Carbla station and the Department of Environment and Conservation is needed to visit Carbla Point.

Locality 1.1: Shark Bay stromatolites at Carbla Point (Zone 50J, 222227E 7091994N)

The most abundant and diverse modern stromatolites on Earth line the headlands and embayments for ~100 km along the coast of Hamelin Pool, a shallow (<10 m deep) hypersaline embayment of Shark Bay (Fig. 14). Hamelin Pool measures 55 km long by 27 km wide and is isolated from the open ocean by the Faure Sill, a shallow sheet of sand at the northern edge of the pool, which impedes water circulation and causes an increase in salinity ranging from 55–70‰ throughout the year (Playford, 1990). ,

The Hamelin Pool stromatolites were discovered in 1954 by D Johnstone, PE Playford and RL Chase of West Australian Petroleum Pty Ltd (Logan, 1961; Playford and Cockbain, 1976) and were the first known modern microbial buildups with sizes and shapes analogous to Precambrian stromatolites, which dominate the first 3 billion years of Earth's fossil record (from 3.5–0.5 Ga). The stromatolites at Hamelin Pool are believed to have developed over the last 4000 years as a result of the elevated salinity, which restricts the growth of microbial

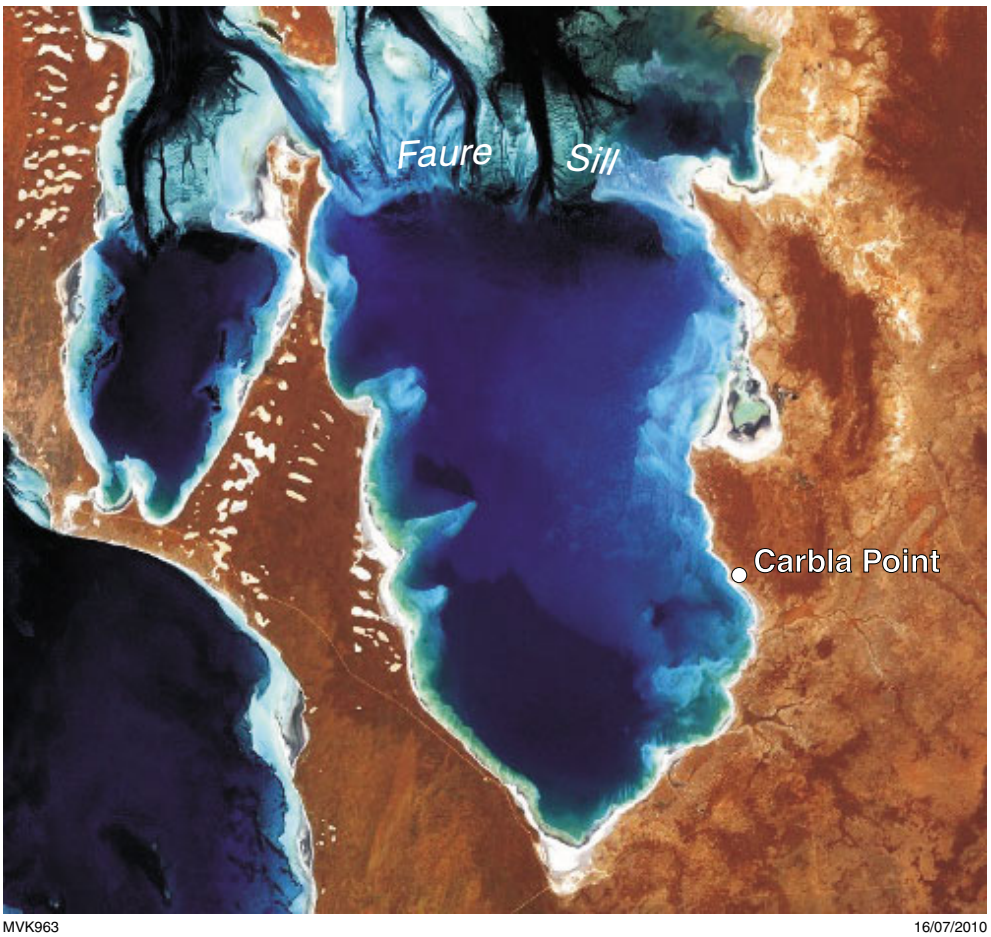

Figure 14. Landsat image of Hamelin Pool, Shark Bay, Western Australia, showing the Faure Sill and location of Carbla Point.

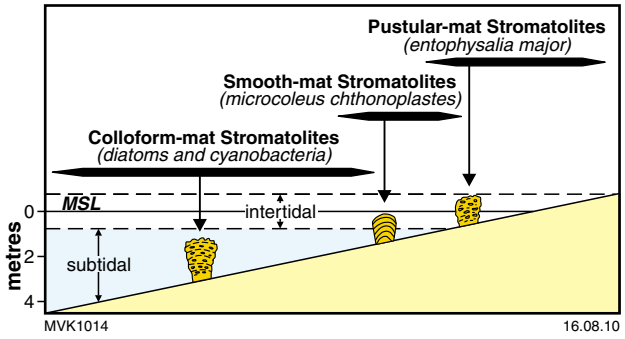

Figure 15. Schematic model of Playford (1990) for growth of Shark Bay stromatolites.

grazers and other organisms that complete for the same ecological niches (Garrett, 1970).

Stromatolites occur from the supratidal zone to water depths of 3–4 m around the margins of Hamelin Pool. Microorganisms construct stromatolites by trapping and binding sediment or precipitating a framework of calcium carbonate. The construction of Shark Bay stromatolites has been widely attributed to three mat types — pustular, smoth, and colliform; each has a characteristic microbial assemblage, the distribution of which is tidally controlled (Fig. 15; Logan et al., 1974; Playford and Cockbain, 1976; Hoffman, 1976; Playford, 1990). Examples of different stromatolites forms are shown in Figure 16.

Pustular mats form large columns and mounds up to 1 m wide and 40 cm high in the upper to middle intertidal zone. These buildups are unlaminated and incorporate sand and silt that accumulates in their irregular surfaces. *Smooth mats* construct smaller, but well laminated stromatolite columns and mounds in the lower intertidal and shallowest subtidal zones. These mats are dominated by filamentous cyanobacteria, which trap and bind sediment. In the

Figure 16. (below) Shark Bay stromatolites: a) typical columnar forms exposed at Carbla Point; b) subtidal forms just off Carbla point; c) extensive microbial mats on the west coast of Hamelin Pool; d) intertidal stromatolites showing dual growth history, with now-dead columnar forms (dark grey) mantled by living stromatolite (light green), at Carbla Point.

MVK1015 16.08.10

subtidal zone, *colliform mats* form elliptical to circular columns and compound masses that vary in size up to 1 m high in water depths of up to 4 m (Logan et al., 1974; Playford, 1990). These include a diverse community including numerous prokaryotic and eukaryotic species. Radiocarbon dating suggests that individual stromatolites have aken about 1000 years to reach their present growth heights of c. 350 mm, but some stromatolites at this locality show evidence of two distinct growth events associated with a drop in sealevel (Fig. 16d; Chivas et al., 1990).

Previous studies suggested that Shark Bay stromatolites form primarily as a result of trapping and binding of sediment by microorganisms (Playford, 1990). However, Reid et al. (2003) determined that microbial precipitation of microcrystalline carbonate is also a fundamental process in these stromatolites, as both framework and cement, particularly in the subtidal zone.

Day 2: Mount Stuart Station and the Duck Creek Dolomite

From Carbla Homestead, head back east to the Coastal Highway (9.5 km) and turn left (north) towards Carnarvon. Drive 171 km to Carnarvon and turn right at the T-junction, heading towards Exmouth, Karratha, and Port Hedland. Continue for 369 km to Nanutarra Roadhouse, where we will stop for lunch. Continue 5 km north along the highway and turn right on the road to Paraburdoo. Drive for 54 km and take the turnoff into Mount Stewart Station on the left. Drive past the homestead and past the shed, heading east. Continue along the track and take the left fork past the second gate. At 23 km from the homestead, turn right (Zone 50K, 429384E 7512743N) and proceed for 8.1 km south to Duck Creek. At the creek, turn left and head upstream for ~1 km to the edge of a pool along the north side of the creek. Exit the vehicle and walk in front of the pool and then for about 100 m along the north face of the outcrop cliff.

You are now on the eastern limb of the Duck Creek Syncline, north of the Wyloo Dome, and south of the Pilbara Craton. The rocks here comprise a succession of Paleoproterozoic to Neoarchean rocks that belong to the Wyloo, Turee Creek, Hamersley, and Fortescue groups, deposited from 2.78 – 1.78 Ga (Fig. 17). The four stops of Day 2 are in the Paleoproterozoic (1.8 Ga) upper Wyloo Group, followed by Day 3 stops within the c. 2.2 Ga lower Wyloo Group (**Excursion Localities 3.1, 3.6**), c. 2.4 Ga Turee Creek Group, and the top of the 2.45 – 2.63 Ga Hamersley Group (**Excursion Localities 3.2 – 3.5**). Together, these localities take us back almost 2.5 billion years to the Archean–Proterozoic boundary.

Locality 2.1: Duck Creek Dolomite stromatolites (Zone 50K, 430045E 7513667N)

The lower part of the c. 1.8 Ga Duck Creek Dolomite at this locality shows a distinctive metre-scale (0.5 – 4 m) striping pattern between light-grey to tan beds with domal to columnar stromatolites, and dark brown beds of slightly more silicified microbial mat (Fig. 18). The section here is rich in stromatolites that display a wide variety of morphologies, from broad, low-amplitude domes, to high-amplitude, narrow columns (Fig. 19a–e), and also a variety of coniform types and abundant, wrinkly, laminated microbial mat (Fig. 19e–g). Particular localities display: broad domical stromatolites, laminated mat, and columnar forms (430021E 7513612N); wrinkly laminated mat with isopachous lamination over weakly coniform stromatolites, showing upward divergence (430017E 7513656N); palisade of coniform stromatolites (430032E 7513681N).

What is significant here, is that it is possible to observe a change in stromatolite morphology with the amount of sediment input. Mats and broad domes formed under periods of low sediment input, whereas high-amplitude columns formed under conditions of greater sediment input.

Also significant here, is a number of morphological features that are very similar to structures observed in the 3.35 Ga Strelley Pool Formation, located further north in the Pilbara Craton. These include palisade columnar forms (Fig. 20a,b), coniform stromatolites with asymmetrical limbs (Fig. 20c,d), and stromatolites with isopachous lamination (Fig. 20e,f).

Locality 2.2: Duck Creek Dolomite olistostrome breccia (Zone 50K, 429723E 7513132N)

Return to the vehicle and head back to the west for ~600 m and stop in front of the cliff face on the north side of the creek.

This upper part of the Duck Creek Dolomite consists of a coarse olistostrome breccia of poorly bedded, angular carbonate blocks, up to several metres long, within a matrix of carbonate sandstone (Fig. 21). This reflects a period of basin deepening resulting from extensional faulting, and immediately preceeds deposition of the deeper-water facies at the next outcrop.

Locality 2.3: Duck Creek Dolomite, basin deepening, and banded iron-formation (Zone 50K, 429841E 7512868N)

Walk ~300 m south to the brown outcrops on the south side of the creek.

This relatively thin (approximately100 m), but spectacular, outcrop shows a gradational transition from carbonates, to banded iron-formation and chert, to shales, and back again, reflecting the effects of basin deepening and rebound on the composition of rocks deposited at this time (Fig. 22). The stratigraphically lower carbonates are planar-bedded dolostones that become progressively more iron-rich upsection and pass through a gradational

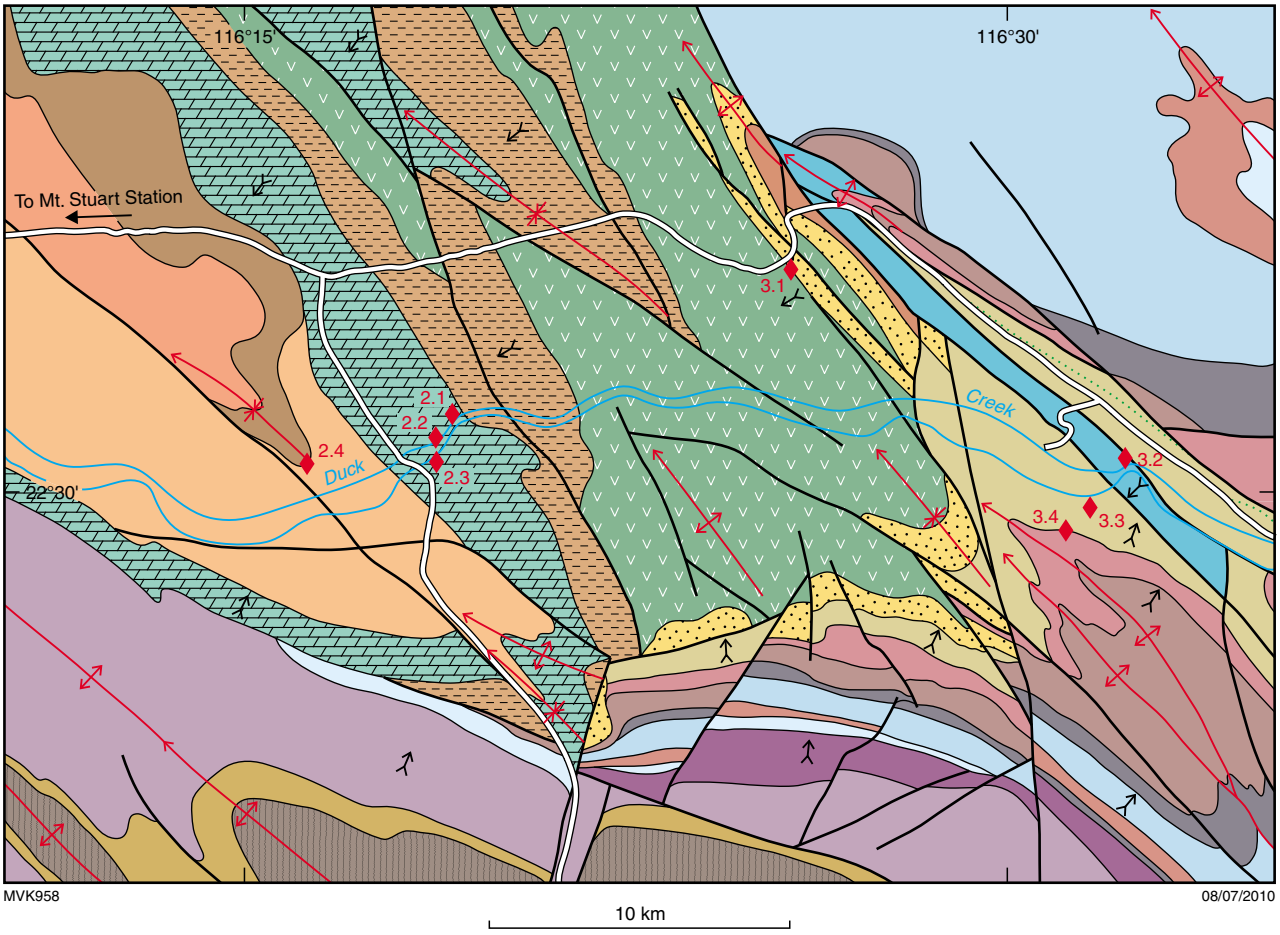

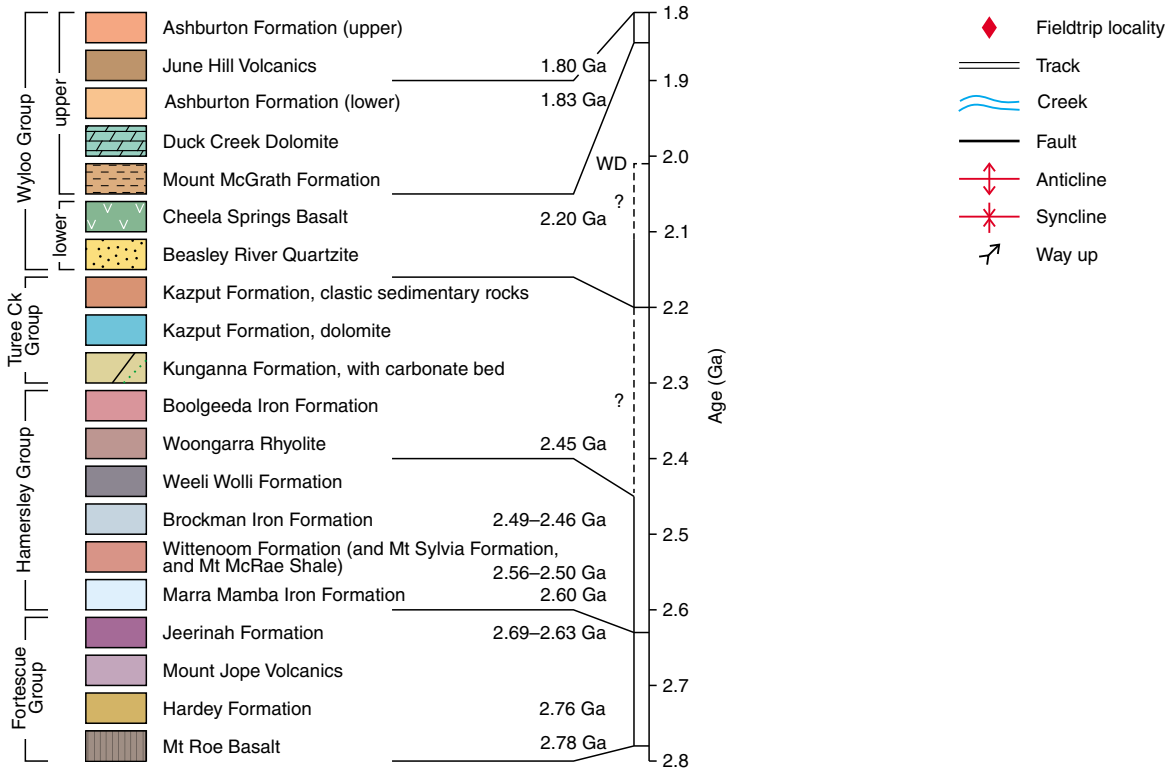

Figure 17. Interpreted solid-geology map of the Duck Creek area, showing field excursion localities.

Figure 18. Photomosaic, looking north, of the eastern half (stratigraphically lower part) of the section through the Duck Creek Dolomite, at Duck Creek (Excursion Locality 2.1).

zone of interbedded carbonate and banded iron-formation into a more concentrated unit of interbedded banded iron-formation, Fe-rich carbonate, and chert (Fig. 23a,b). The iron formation passes upsection to approximately13 m of grey-weathering, carbonate-altered shale, which in turn passes into banded iron-formation interbedded with Fe-rich carbonate and chert, and then Fe-rich carbonate (Fig. 23c) with crudely-laminated stromatolite domes (Fig. 23d).

This succession supports the depositional facies model of Beukes et al. (1990), developed to explain the relationship between Neoarchean carbonates and BIF of the Campbellrand Platform in South Africa (Fig. 24). In this model, the Archean atmosphere and shallow seawater is thought to contain a low level of free oxygen from photosynthesizing cyanobacteria, whereas the deeper oceans are reducing and able to transport Fe^{2+} in solution. Under such conditions, carbonates precipitate in shallow water as a result of microbial activity, whereas BIF precipitates in deeper water at the point where reduced seawater that is rich in dissolved iron mixes with oxygen-bearing shallow seawater to precipitate banded iron-formation. In this section, at Excursion Locality 2.3, it appears that even deeper-water conditions precipitated fully reduced, organic-rich shales.

Locality 2.4: June Hill Volcanics and BIF (Zone 50K, 425445E 7512371N)

Follow the track back to the north side of the creek. Once onto the flat ground, turn off the track to the left and head west-southwest for ~4 km to a prominent hill.

The 1800–1795 Ma June Hill Volcanics (Evans et al., 2003; Wilson et al., 2010) is an important unit, as it provides a maximum age for overlying BIF of the Ashburton Formation, which represents some of the youngest Paleoproterozoic BIFs in the world (prior to their re-emergence in the Neoproterozoic). The Earaheedy Basin, also in Western Australia, is another locality from where such relatively young iron formation, albeit granular, (<1.84 Ga) has been described (Pirajno et al., 2009). These young ages for BIF in Western Australia are in contrast to the hypothesis that the 1.85 Ga Sudbury Impact caused the global disappearance of BIF through stirring of the world's oceans (Slack and Cannon, 2009; Cannon et al., 2010). Rather, it shows that BIFs disappeared gradually from the world's oceans, at different times in different places.

Day 3: Paleoproterozoic successions and the Archean–Proterozoic boundary

Locality 3.1: Numanna Member and Cheela Springs Basalt (Zone 50K, 441395E 7518915N)

Head northeast for 3.1 km back to the track and turn left. Head out along the track for 5.4 km to the main road. At the T-junction (Zone 50K, 425150E 7519157N), turn right and head east for 12.4 km and take the right fork (Zone 50K, 435783E 7522143N). Continue for a further 18.0 km and then continue towards the white quartzite hills, bypassing the turnoff on your right signed to Mount Berry (Zone 50K, 440137E 7519049N). Proceed for a further 1.3 km and park in the shade of the trees in the creek bed. Walk ~200 m due south to the edge of the outcrops on the south side of the creek.

This locality lies at the contact between cross-bedded quartz sandstone of the Numanna Member (Beasley River Quartzite) and conformably overlying vesicular basalts of the c. 2.21 Ga Cheela Springs Basalt. The quartzite is cross-bedded at a metre-scale, with 1–2 cm thick foresets and pebbly sandstone beds with grains to 3 mm diameter (Fig. 25a,b). This is overlain by a thin unit of medium to finely cross-bedded ?fluviatile sandstone (Fig. 25c), which is in turn overlain by weakly amygdaloidal basalt.

The 2209 ± 15 Ma Cheela Springs Basalt is of interest because it is one of several units around the world of the same age that erupted after a c. 200 Ma long period

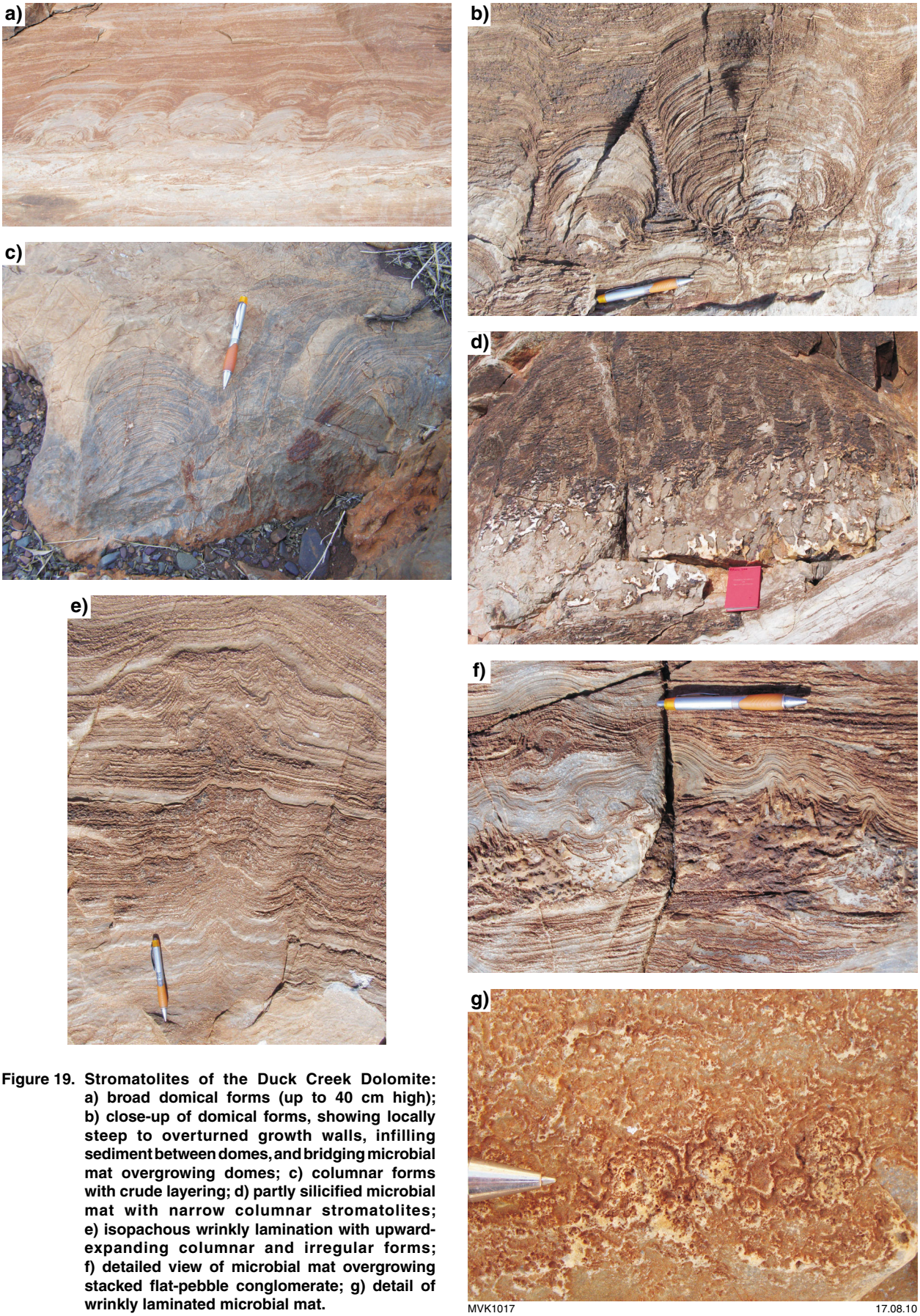

Figure 19. Stromatolites of the Duck Creek Dolomite: a) broad domical forms (up to 40 cm high); b) close-up of domical forms, showing locally steep to overturned growth walls, infilling sediment between domes, and bridging microbial mat overgrowing domes; c) columnar forms with crude layering; d) partly silicified microbial mat with narrow columnar stromatolites; e) isopachous wrinkly lamination with upward-expanding columnar and irregular forms; f) detailed view of microbial mat overgrowing stacked flat-pebble conglomerate; g) detail of wrinkly laminated microbial mat.

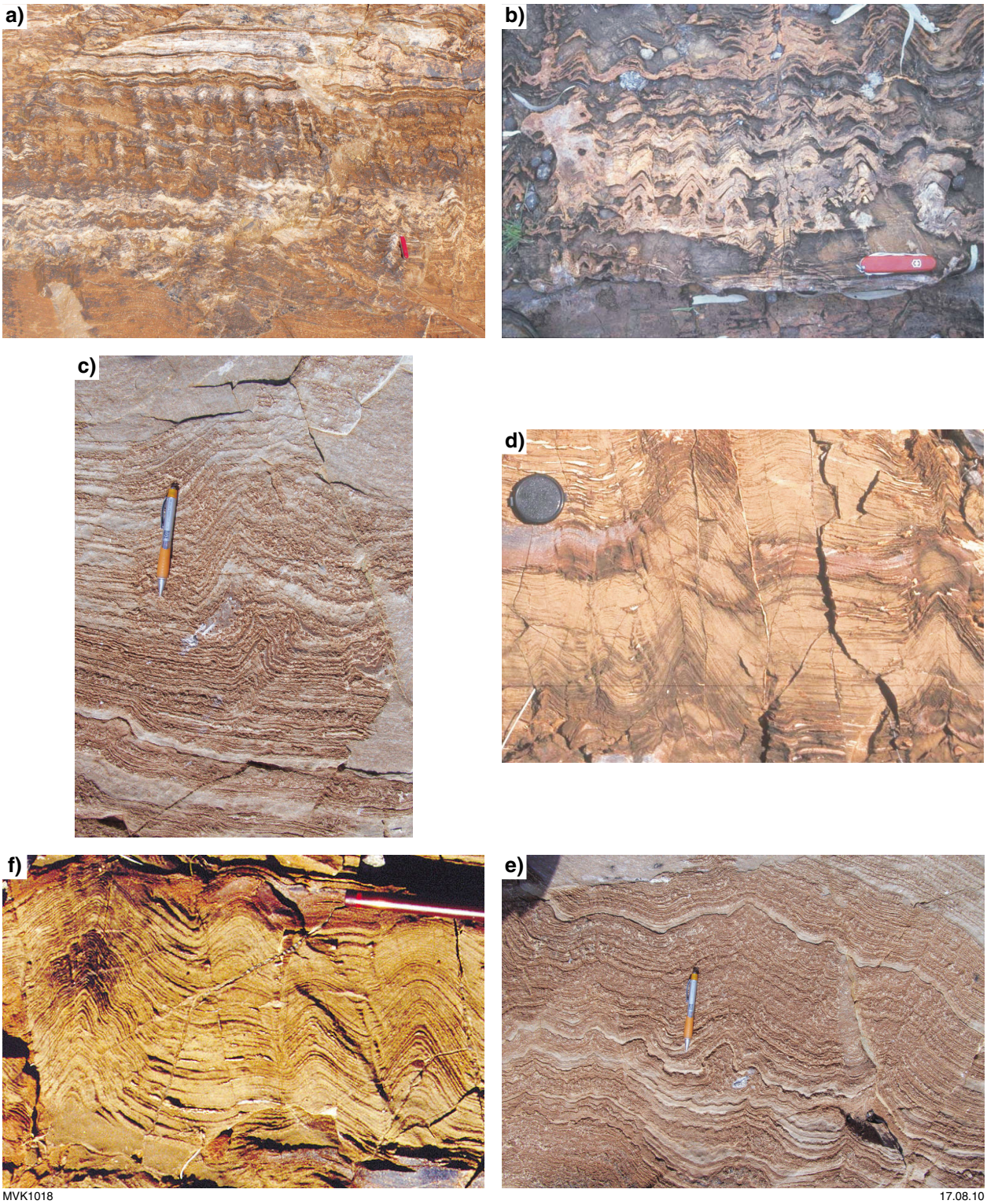

Figure 20. Comparative features of stromatolites from the c. 1.8 Ga Duck Creek Dolomite (a, c, e) and c. 3.35 Ga Strelley Pool Formation (b, d, f): a–b) palisade of vertical, non-branching columnar, conical to domical forms with isopachous lamination; c–d) coniform stromatolite with asymmetrical limbs; e–f) coniform stromatolites with isopachous lamination.

Figure 21. Outcrop photograph of the olistostrome breccia at Excursion Locality 2.2, deposited during the onset of basin deepening. Note the large, angular block of bedded dolostone under and above the camera lenscap, surrounded by a featureless matrix.

of relative geological quiescence, from 2.42 – 2.22 Ga (Condie et al., 2009). Equivalent flood basalts are found in South Africa (2222 ± 12 Ma Hekpoort and Ongeluk lavas; Cornell et al., 1996), North America (extensive 2219 ± 3 Ma to 2210 ± 3 Ma Nipissing diabase intrusions: Corfu and Andrews, 1986; Noble and Lightfoot, 1992), and in China (2199 ± 11 Ma gneisses and 2193 ± 15 Ma gabbros; Zhao et al., 2008; Wang et al., 2010), together with extensive granite–greenstone terrains, such as in West Africa (2229 ± 42 Ma Birimian; Abouchami et al., 1990) and central Brazil (2209 ± 32 Ma Crixás greenstone belt; Jost et al., 2010).

What is interesting to discuss here is the possible relationships between the onset of renewed volcanism at this time and the development of the global Lomagundi–Jatuli excursion of highly positive $\delta^{13}C_{carbonate}$ values (Lindsay and Brasier, 2002; Melezhik et al., 2005). Did volcanism drive disequilibrium in the biosphere to cause the $\delta^{13}C$ excursion, and if so, how? Typically, global volcanism results in warming of the atmosphere as a result of increased volumes of atmospheric CO_2, which in turn leads to increased rates of chemical weathering, drawdown of CO_2 and eventual cooling of the atmosphere, commonly leading to glaciation (e.g. Buggisch et al., 2010). However, in the case of the Paleoproterozoic, there is no evidence for post-2.2 Ga glaciation, but rather a recurrence of BIF after their disappearance from the rock record at about 2.42 Ga. At the same time, there is evidence for a dramatic increase in atmospheric oxygen, with the appearance of widespread evaporitic sulfates and redbeds (e.g. Holland, 1994, 2002). Does this mean that global volcanic activity continued at a high rate well after the 2.2 Ga breakout event, and if so, how might this have affected atmospheric and biosperic conditions? Is tectonic burial of organic carbon really the best way to explain the $\delta^{13}C$ excursion at this time, or could there be other explanations?

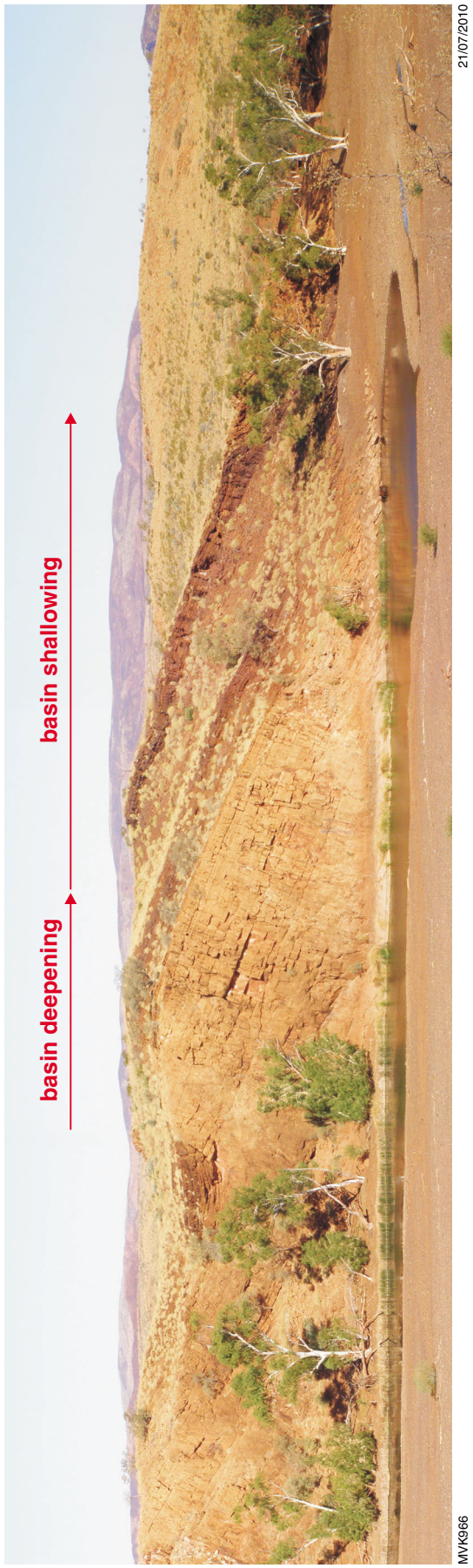

Figure 22. Photomosaic looking south, of the western half (stratigraphically upper part) of the section through the Duck Creek Dolomite at Duck Creek, showing the location of the basin-deepening to basin-shallowing succession at Excursion Locality 2.3.

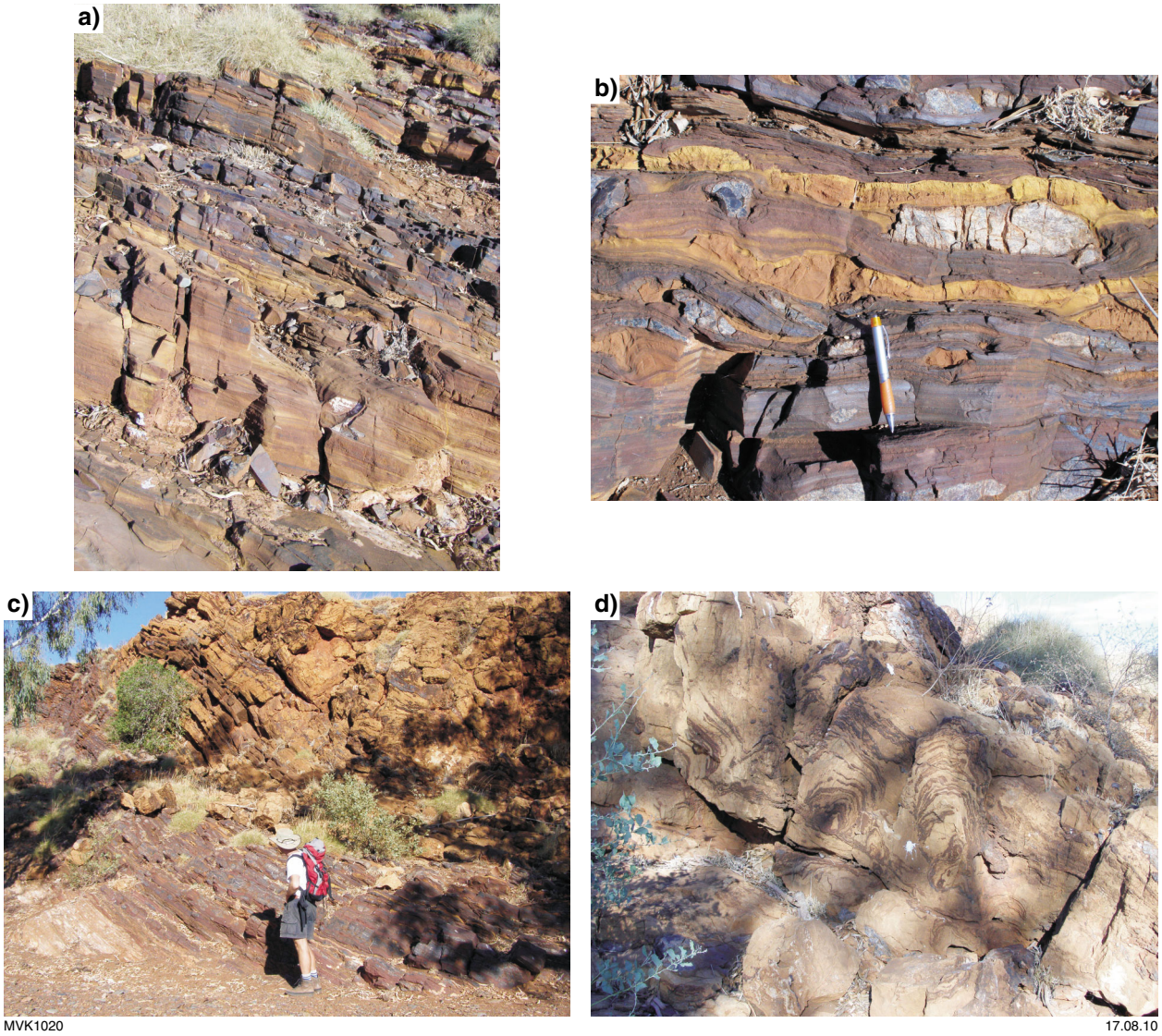

Figure 23. Outcrop photographs of the Duck Creek Dolomite at Excursion Locality 2.3: a) transition into the basin-deepening succession, from Fe-dolomites to banded iron-formation; b) close-up of interbedded banded iron-formation, Fe-carbonate, and chert; c) overview of the basin-shallowing succession, from grey-weathering shale (left, foreground), through banded iron-formation, to Fe-carbonate; d) large domical stromatolites near the top of the basin-shallowing succession.

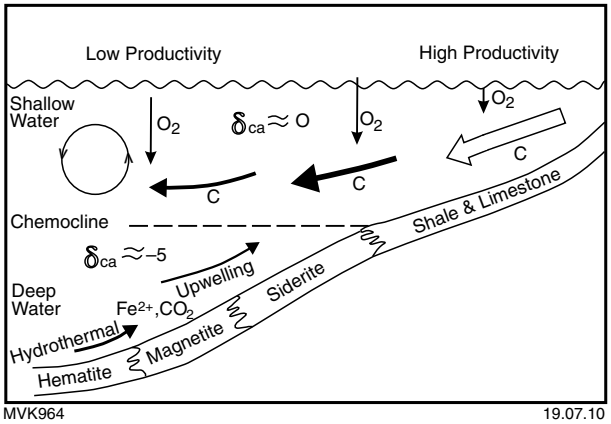

Figure 24. Schematic model showing the depositional relationship between banded iron-formation and carbonate under Archean conditions of a partly oxidized upper water column (from Beukes et al., 1990).

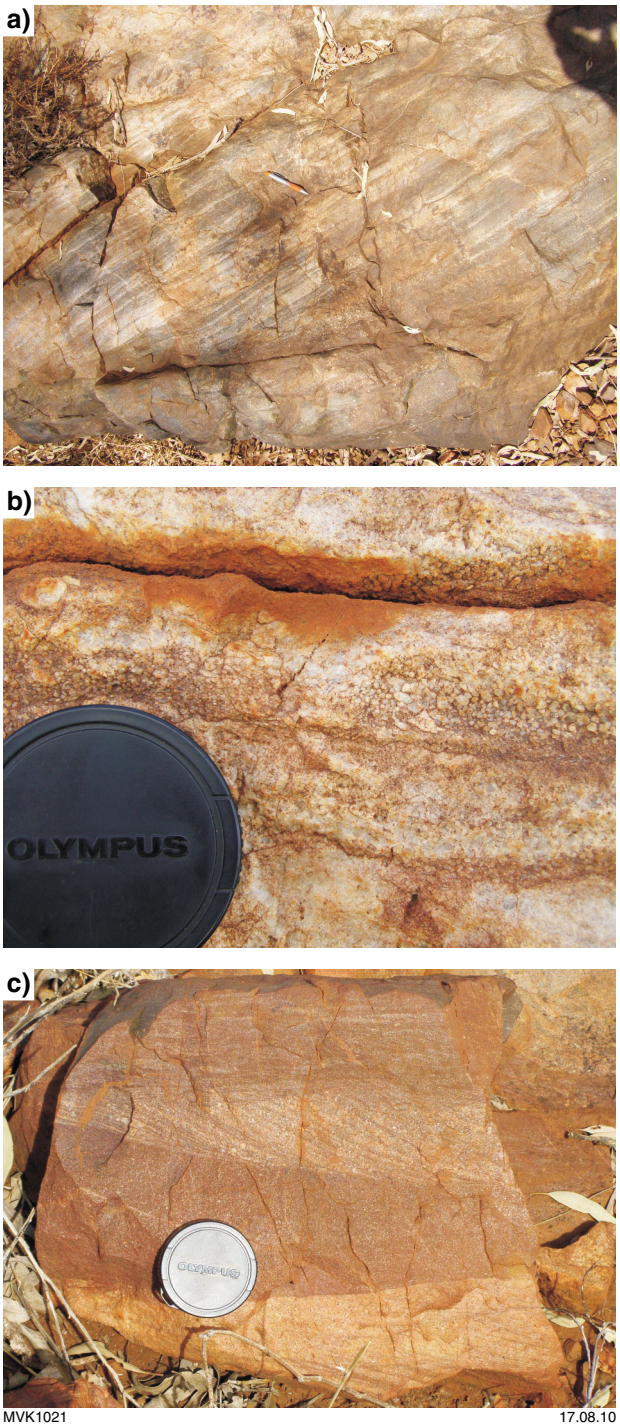

Figure 25. Outcrop photographs of the Beasley River Quartzite at Excursion Locality 3.1: a) large foreset in cross-bedded (?eolian) quartzite; b) close-up view of detrital quartz grains in (?eolian) quartzite; c) finely cross-bedded sandstone, deposited under ?fluviatile conditions.

Locality 3.2: Kazput Formation stromatolitic carbonate (Zone 50K, 452408E 7512538N)

Return to the vehicles. Continue along track for ~15 km to a sharp left turn at Zone 50K, 452159E 7513847N and turn right, off of the track, heading south-southeast for 1.34 km to the edge of a tan-coloured cliff. Park the vehicles. From here, we commence a traverse for 3 km to the next stop. Bring a backpack, hat, and water, as we will be gone from the vehicles for 3–4 hours.

This exposure of stromatolitic dolomite lies within the c. 2.4 Ga Turee Creek Group, and probably belongs to the Kazput Formation. The stromatolitic dolomite at this locality is approximately 360 m thick, but this is probably a minimum, as an interpretation of regional structural geology suggest that both lower and upper contacts are faults (Fig. 17). The dolomite contains a variety of columnar stromatolite forms, including a spectacular, 1 m tall branching form, the branches of which spread out laterally towards the top (Fig. 26a). Further up the hill is a layer of jaspilitic chert (Fig. 26b) — what does this imply for the oxidation state of the atmosphere at this time, or does it only relate to diagenetic alteration of carbonate? Can we tell? Low amplitude domes, straight-walled columns, and extensive microbial mats are also present at various levels in this formation (Fig. 26c–e).

A suite of $\delta^{13}C_{carbonate}$ values obtained from a transect across this unit at this locality vary by about 0.5‰, except for three deeper-water dolomitic sandstones near the upper part of the section that vary to –0.1‰, and a single sample from near the base of the unit at +1.36‰ (Fig. 27). $\delta^{18}O$ values are in the range –10 to –14‰ and show covariation with slight changes in $\delta^{13}C$ values.

Continue traversing up and over the dolomite ridge, keeping your eyes open for variations in stromatolite morphology. Note that the ridge is capped by a ferruginous, Cenozoic regolith duricrust.

Locality 3.3: Turee Creek mudstone (Zone 50K, 451486E 7510824N)

From the western edge of the dolomite ridge, cross Duck Creek heading southwest for 1.65 km, keeping the large hill on your right. Walk up the flank of the hill to the locality coordinates.

The Turee Creek Group here consists of interbedded fine- to medium-grained sandstone and mudstone, with interbedded thin carbonate rocks just a few hundred metres further south (Fig. 28). Dips of bedding are shallow at this location and bedding is transected by a steeply-dipping spaced fracture cleavage that strikes northwest, parallel to the axial plane of regional upright folds in this area.

The mudstones at this locality are brown-weathering green rocks that show very faint evidence of primary bedding on weathered surfaces. Geochemical analysis of these mudstones show that they have compositions similar to, yet still distinct from, the Post-Archean Average Shale (PAAS) of Taylor and McLennan (1985), with negative Eu anomalies, fractionated LREE and elevated HREE, though not quite as eleveated as PAAS (Fig. 29). Significantly, Turee Creek shales are quite distinct from those within the Hamersley Group. What do these differences tell us about the evolution of the continental crust or local sources? What do they reveal about changes in weathering styles between greenhouse (pre-2.4 Ga) and icehouse (post-2.4 Ga) conditions?

Locality 3.4: Boundary ridge (Zone 50K, 450645E 7510111N)

Walk for 1.14 km southwest and pass down over the lip of a small gully.

This small riverbank section exposes the conformable contact between the Boolgeeda Iron Formation, at the very top of the Hamersley Group, and the overlying glacial deposits of the Meteorite Bore Member of the Kunganna Formation, at the very base of the Turee Creek Group (Fig. 30). This marks the only known place in the world where this transition is conformable and well exposed — indeed, you can put your fingernail on the contact (Fig. 31a). For this reason, and because the contrasting rock types in this section represent such a dramatic change from the high pCO_2 (± methane) greenhouse, reducing conditions of early Earth to the cooler, oxidized conditions of more modern Earth, the contact between the two groups here is being considered for the Global Stratotype Section and Point (GSSP) to mark the Archean–Proterozoic boundary in a revised Precambrian timescale.

The section preserved here is dips gently (20°) to the northeast and is little deformed. At the proposed type locality, the section consists of a lowermost unit of grey-black weathering, dark red (magnetite–hematite) banded iron-formation belonging to the very top of the Boolgeeda Iron Formation; more of this unit can be seen along strike to the southeast. Conformably overlying the iron formation is a 15 cm thick transitional unit of chert, consisting of a lower part of jaspilitic chert with thin (<1 mm) bands of iron formation, which grades up to a middle section of jaspilitic chert, which in turn passes up to an upper part of layered grey and jaspilitic chert bands (Fig. 31b,c).

Clastic sedimentary rocks of the Turee Creek Group directly overlie the transitional chert unit across a contact that is characterized by a dimpled surface (Fig. 31d). The basal unit of the Turee Creek Group is green, pyritic mudstone, with sparse dropstones (Fig. 32a). This is overlain by three beds of coarse sandstone, each consisting of angular to subangular quartz clasts in a silty matrix, together with clasts of locally abundant detrital pyrite and outsize clasts (Fig. 32b,c). The topmost sandstone bed 3 is distinctive in that it contains slump structures (Fig. 32d) and overlies diamictite with abundant carbonate clasts in a silty matrix, and a thin (1 cm), but continuous, carbonate bed (Fig. 32e).

Overlying the sandstone beds is a shale unit, also with scattered outsize clasts (Fig. 32f). Lying above this is a unit

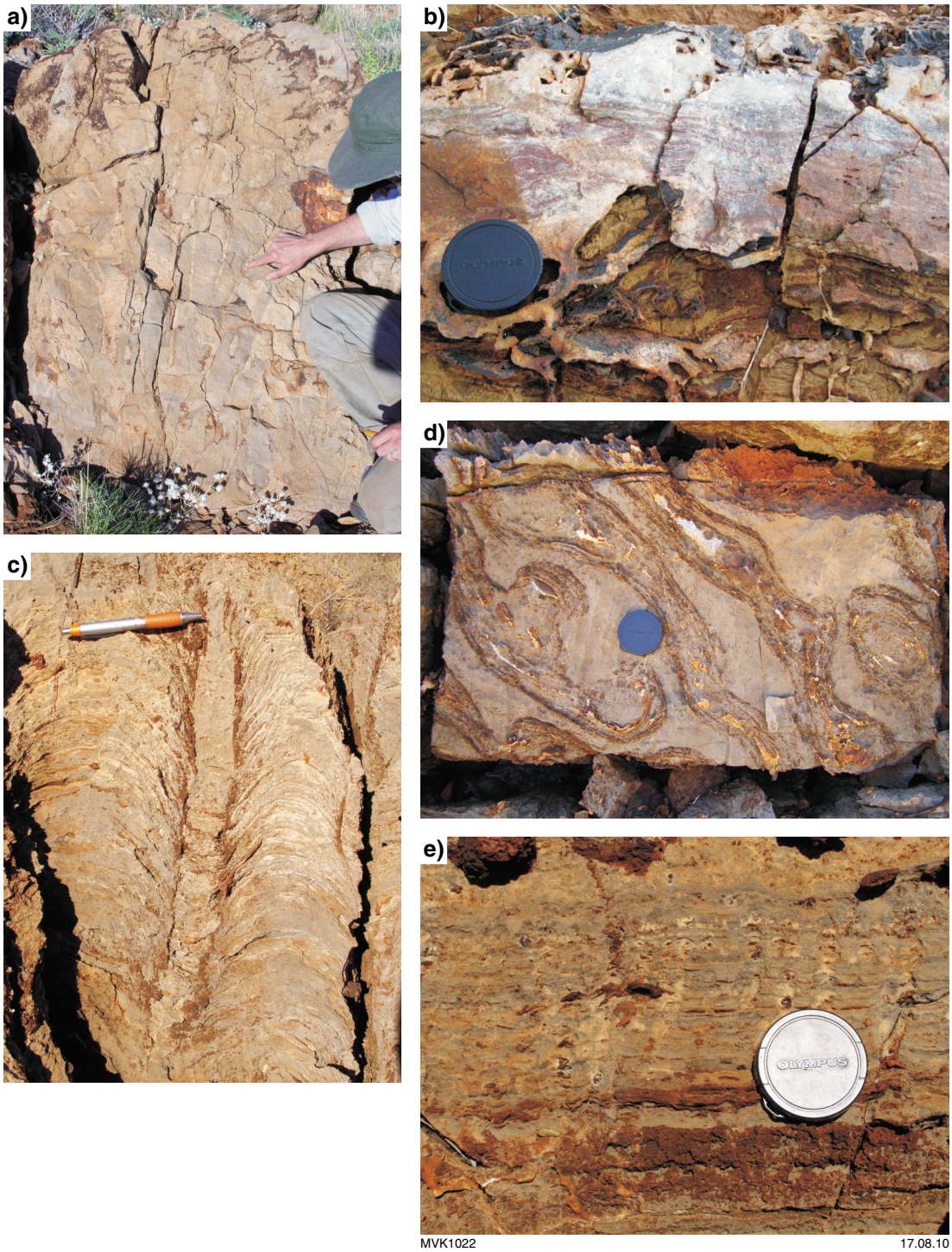

Figure 26. Outcrop photographs of stromatolitic dolomite of the Kazput Formation, Turee Creek Group, at Excursion Locality 3.2: a) metre-high, branching columnar stromatolite — note how the branches extend horizontally near the top; b) layered, jaspilitic chert/quartz in dolostone; c) cross-sectional view through straight-walled columnar stromatolites; d) bedding-plane view of the same columnar stromatolites as c), showing horizontal growth elongation, probably due to flowing water; e) close-up view of wrinkly-laminated microbial mat with small, locally branching, columnar forms.

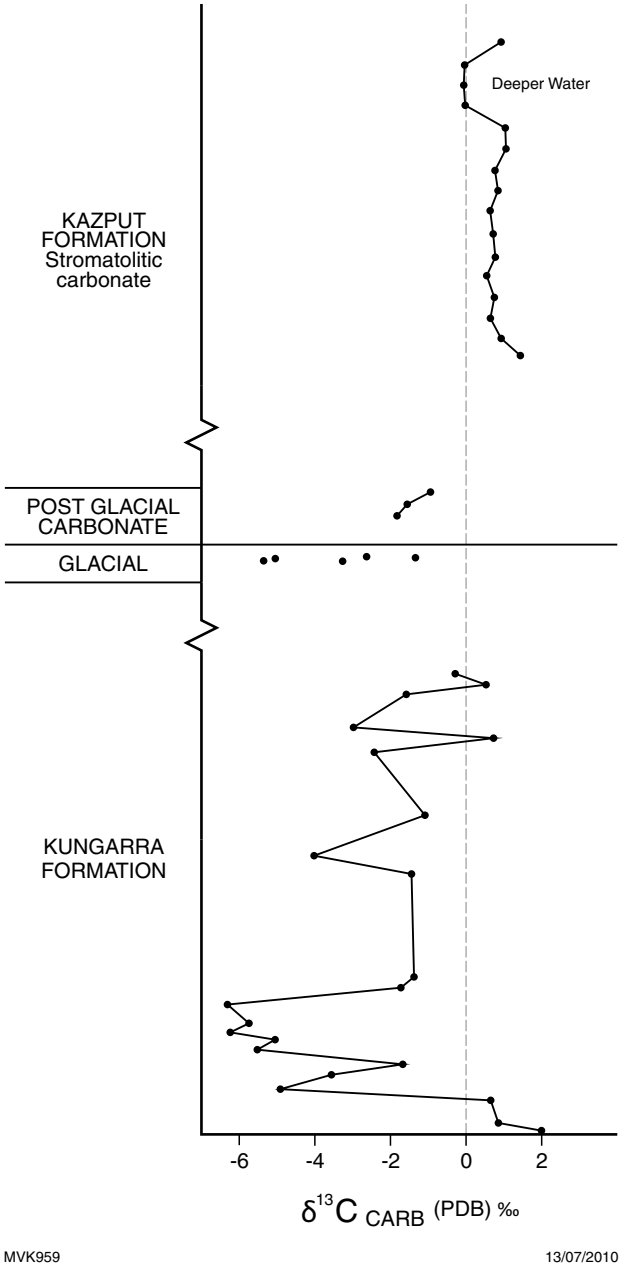

Figure 27. **(left) Plot of $\delta^{13}C_{carbonate}$ values for the Turee Creek Group. Data in lower half from Lindsay and Brasier (2002), adapted into a revised stratigraphy. Unpublished data in upper half provided by K Yamaguchi (written communication). Uppermost data from Excursion Locality 3.2; middle data from Excursion Locality 3.4 and from along strike at Deepdale.**

Figure 28. **(below) Outcrop photographs of the Kungarra Formation, Turee Creek Group, at Excursion Locality 3.3: a) cross-bedded dolarenite; b) bedded mudstone.**

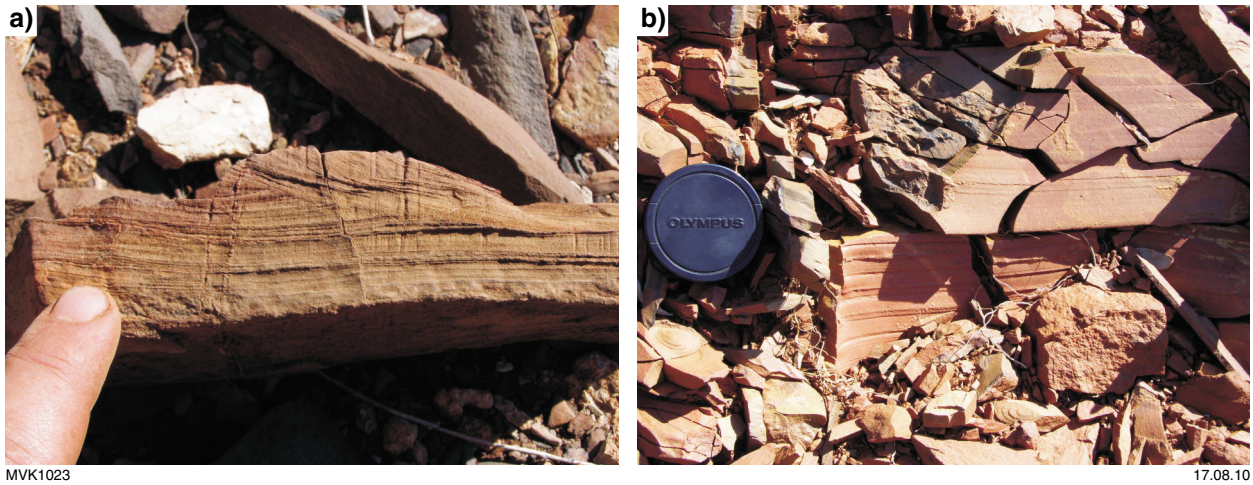

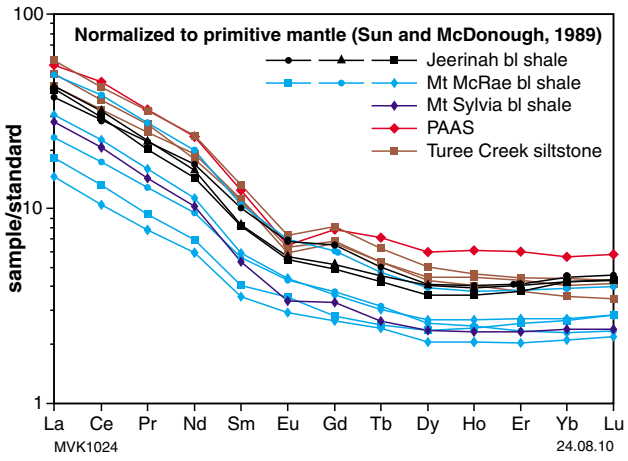

Figure 29. Plot of rare earth elements, normalized to primitive mantle, comparing Turee Creek mudstones with Hamersley Group black shales (Jeerinah, Mount Sylvia, and Mount McRae formations), and the Post-Archean Average Shale (PAAS) composite of Taylor and McLennan (1985).

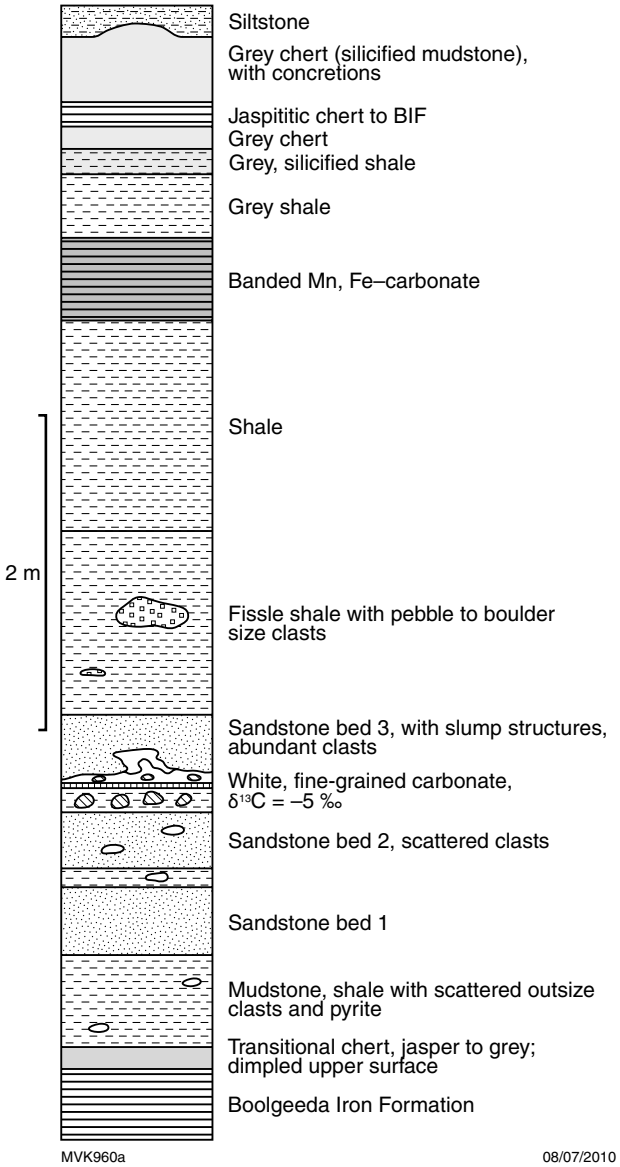

Figure 30. Stratigraphic section for the outcrop at Excursion Locality 3.4 of the Meteorite Bore Member, Kungarra Formation, Turee Creek Group.

of Mn-bearing, banded iron-formation (Fig. 33a). This rock contains 7.4 wt% MnO, 41 wt% SiO_2, 4.4 wt% Al_2O_3, and 39 wt% FeO, with high Ba (475 ppm) and Sr (263 ppm), making this quite an unusual rock composition. REE patterns are similar to those of Turee Creek mudstones and to PAAS, but at lower total concentrations (Fig. 34). Similar Mn-bearing rocks were observed at Deepdale, at the same stratigraphic level.

The Mn-rich BIF unit is overlain by further shales and then by thin units of banded grey chert, jaspilitic chert, and BIF, overlain by siltstone. The topmost surface of the cherty rocks is marked by large concretion structures. Concentric shrinkage rings on the surface of the concretions, and vertical tension gash arrays in cross-section, are evidence that their formation involved shrinkage or contraction (Fig. 33b,c).

Analytical results

Dating

A variety of analytical work has been undertaken on this section in an attempt to better quantify the changes across this boundary. Most important have been attempts to pin down the age range of deposition, but unfortunately, this has proven difficult. Two samples of pyritic mudstone from the lower Turee Creek Group, both here (190575) and at Deepdale 100 km along strike to the northwest (194504), were analysed for Re–Os dating of pyrite. Whereas one fraction appears to lie along a 2450 Ma reference line, it could lie equally well along a 2700 Ma reference line (Fig. 35a,b). A two-point yield line for 190575 and 194594A is 2718 ± 120 Ma, with a high initial ratio of 2.87 ± 0.33, suggests that much of the pyrite is detrital in origin, a feature recognized in thin sections and high-resolution images (Figs 32c, 35c).

Pb–Pb carbonate dating on three samples collected both from this locality (190577), and from Deepdale (194502 = carbonate conglomerate; 194503 = varved carbonate), yielded a poor apparent age of 1983 ± 56 (MSWD = 60), whereas a spread of Pb–Pb results from four subsets of sample 194503 yield a model age of 2078 ± 15 Ma (Fig. 35d; MSWD = 1.9). Neither of these results is near the approximate age of the sample (c. 2.4 Ga), and must therefore reflect the effects of younger hydrothermal events, as previously recognized by Rasmussen et al. (2005a).

Sulfur isotopes

S-isotopic data from samples collected across the sections exposed here and at Deepdale show clear evidence for the effects of mass-independent fractionation right up to the uppermost BIF unit above the glacials. Two samples from sandstone beds 1 and 2 show a very wide spread of $\Delta^{33}S$ (–4 to +12‰), which is interpreted to reflect values

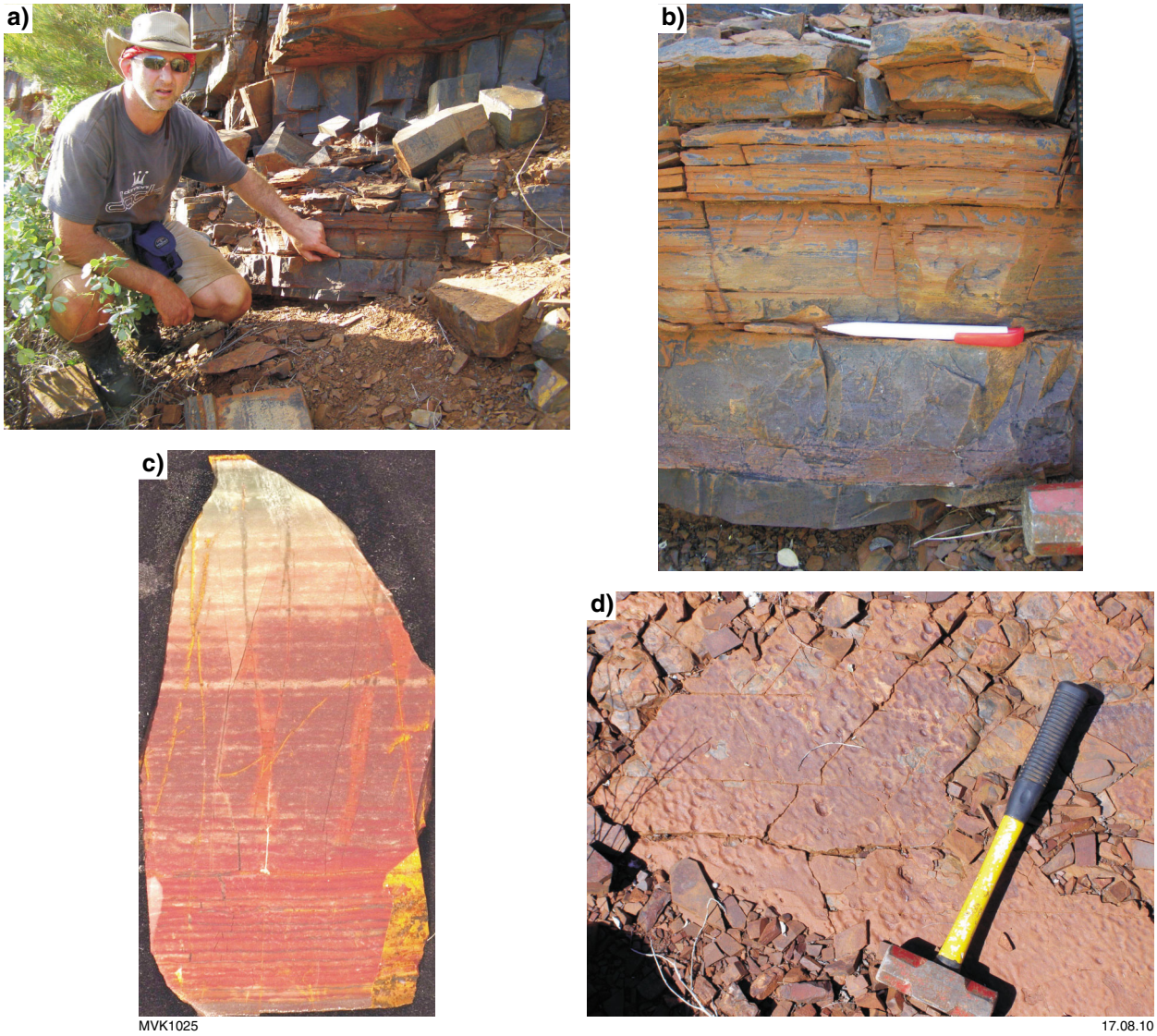

Figure 31. Outcrop photographs of the Boundary Ridge section at Excursion Locality 3.4: a) pointing to the contact between the top of the Hamersley Group and base of the Turee Creek Group, representing a highly favoured candidate for a GSSP locality for the Archean–Proterozoic boundary; b) close-up view of the contact, showing lowermost banded iron-formation (Boolgeeda Iron Formation, at hammer head), conformably overlain by transitional chert unit (under pen) and fissile mudstone of the Turee Creek Group; c) cut section through the transitional chert showing the gradational nature of the change from iron formation at the base (dark red bands) to grey chert at the top, reflecting the gradual decrease in iron content of the world's oceans and possible cooling of the atmosphere; d) dimpled top surface of the transitional chert unit at the top of the Boolgeeda Iron Formation.

inherited from Neoarchean detrital pyrite grains (Fig. 35c). One other interesting feature of the data is apparent from the results from sample 194504, basal pyritic mudstone from Deepdale. The narrow range in $\Delta^{33}S$ values from this sample likely reflects the true extent of mass-independent fractionation (MIF) at this time (e.g. Papineau et al., 2007), whereas the wide range in $\delta^{34}S$ values to highly negative values (–39‰) suggests pyrite formation through in situ microbial sulfate reduction.

Carbon isotopes

The thin carbonate unit from this section, as well as carbonates from Deepdale, have yielded $\delta^{13}C$ values of –3 to –5‰ (Fig. 27), close to the mantle value at 2.4 Ga, signifying a massive imbalance of the global carbon cycle during this glacial event, as also recorded in North American rocks of this age (Bekker et al., 2005). These values also closely match those obtained by Lindsay and Brasier (2002) from the lower Turee Creek Group along strike to the east (–2 to –6‰; Fig. 27), from rocks that lie stratigraphically beneath the Meteorite Bore Member and thus are part of the lower Kungarra Formation, but which Lindsay and Brasier (2002) mistakenly assigned to the Kazput Formation.

Carbonate units 1 m thick from approximately 300 m stratigraphically above the glacial rocks at this locality

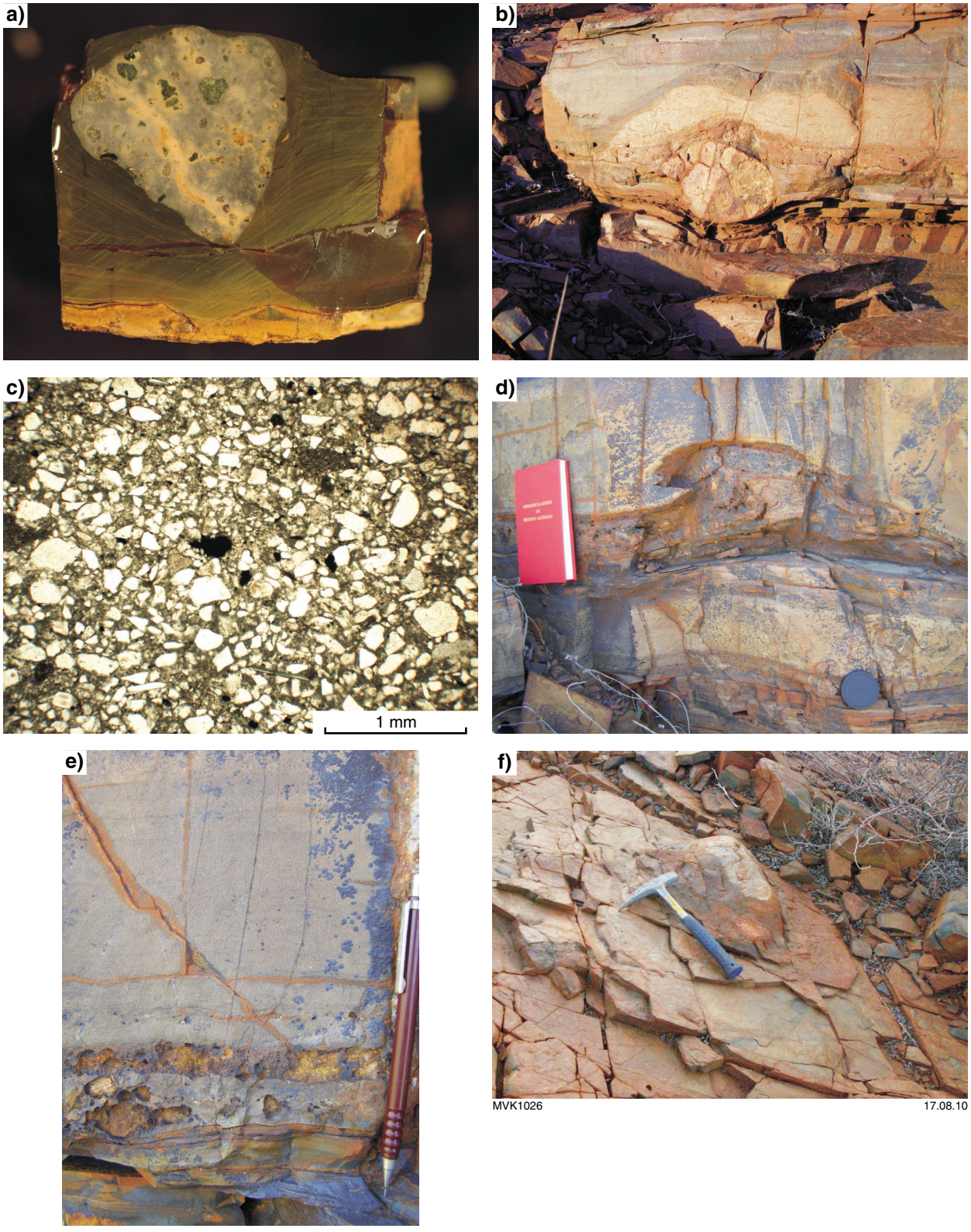

Figure 32. Evidence of glaciation at the Boundary Ridge section: a) cut sample face of porphyritic rhyolite clast in mudstone, from basal mudstones of the Turee Creek Group; b) rounded, outsize clast of porphyritic rhyolite in sandstone bed 2; c) photomicrograph (plane-polarized light) of sandstone bed 1, showing detrital pyrite among angular to subrounded quartz clasts; d) syn-sedimentary slump fold in sandstone bed three; e) close-up of sandstone bed 3, with underlying carbonate bed and carbonate clasts — $\delta^{13}C_{carbonate}$ for these rocks return values of –5‰; f) subrounded boulder of porphyritic rhyolite in shale above the sandstone beds.

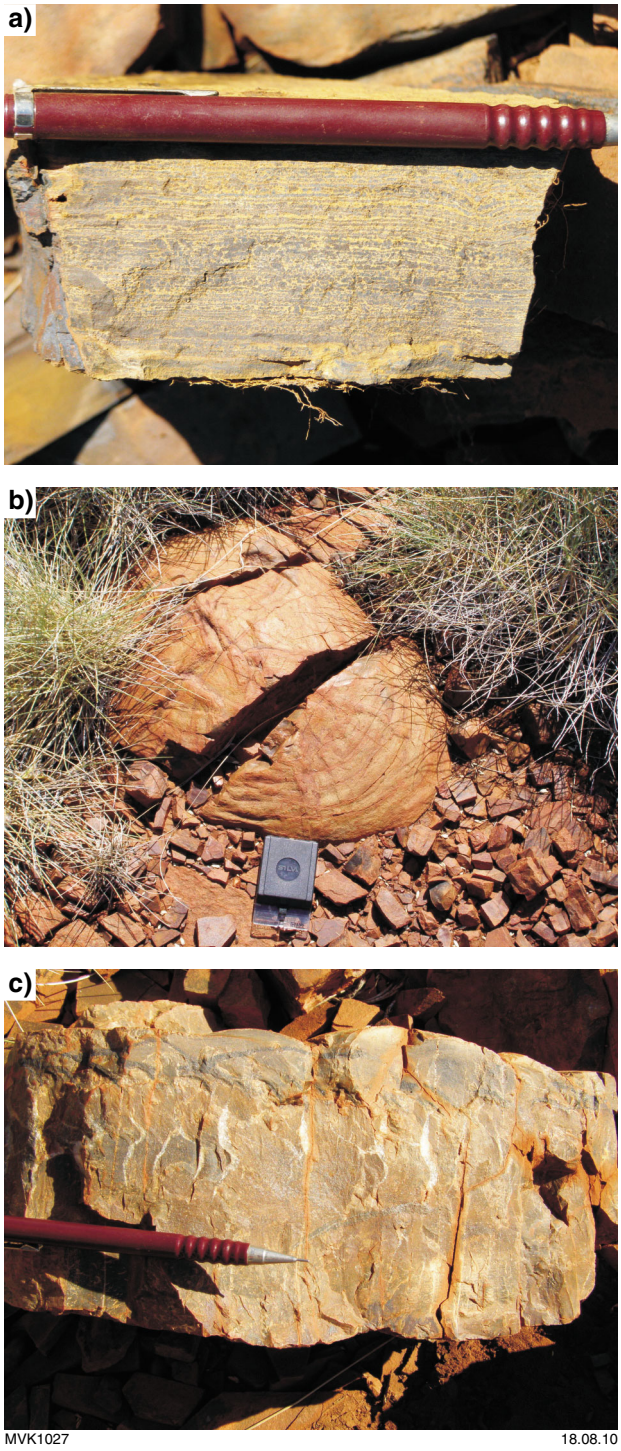

Figure 33. Outcrop photographs of rocks from near the top of the Boundary Ridge section at Excursion Locality 3.4: a) banded Mn-rich iron-formation above the glacial deposits; b) bedding-plane view of large concretion in cherty BIF; c) cross-sectional view through large concretion, showing vertical quartz-filled tension gashes.

yield $\delta^{13}C_{carbonate}$ values of –1.1 to –1.9‰, slightly less depleted than carbonates within the glacial deposits, but more depleted than those from the overying stromatolitic carbonate (+0.5‰) (Fig. 27). These results help confirm that, even though the section here represents a condensed

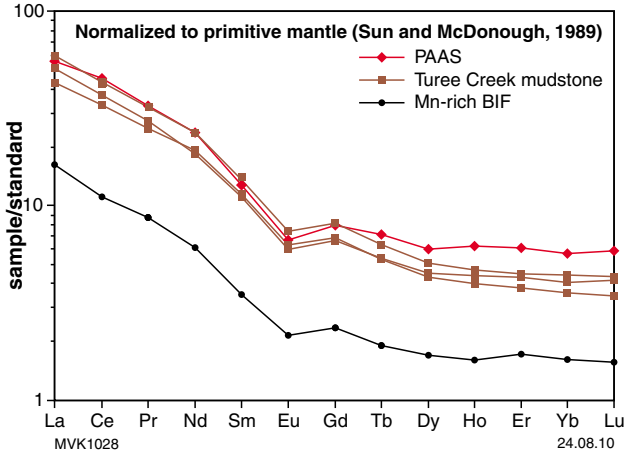

Figure 34. Plot of rare earth elements, normalized to primitive mantle, comparing Turee Creek mudstones (brown) with the banded Mn-rich unit at the Boundary Ridge section (purple), and PAAS (red diamonds).

section, it appears that all of the Kungarra Formation was deposited during glaciation, and that the combined stratigraphy of the Turee Creek Group documents both the decline into, and the recovery of the biosphere after, a global glaciation event at from 2.42 – 2.22 Ga.

Oxygen isotopes

Given the colour change visible across the transitional chert unit at the top of the Boolgeeda Iron Formation, it was thought that it might be possible to measure a change in the temperature of the global oceans as the Earth as it entered the Paleoproterozoic glacial period. However, oxygen isotope data from across the transitional chert unit returned consistent values of –16‰, indicating that the chert is not a primary depositional material, but a homogeneously recrystallized material resulting from low-temperature hydrothermal alteration at c. 2215 Ma (Rasmussen et al., 2005a).

Stratigraphic considerations and tectonics

Martin (1999) and Martin et al. (2000) suggested that the presence of thin BIF units above the glacials warranted inclusion of the glacials within the Boolgeeda Iron Formation. They also suggested that the change in sedimentology from the Hamesley Group to the Turee Creek Group reflected a change in tectonics related to the onset of foreland flexure during development of the McGrath Trough. However, recent dating has shown that the McGrath Trough concept should be abandoned, as explained in the Introduction to this guidebook. Also, the recognition of the banded Mn-rich unit at this site indicates that changes in stratigraphy were controlled by changes in the redox state of the atmosphere and hydrosphere, rather than by tectonics. Thus, it is suggested that the glacial deposits and associated sedimentary rocks containing

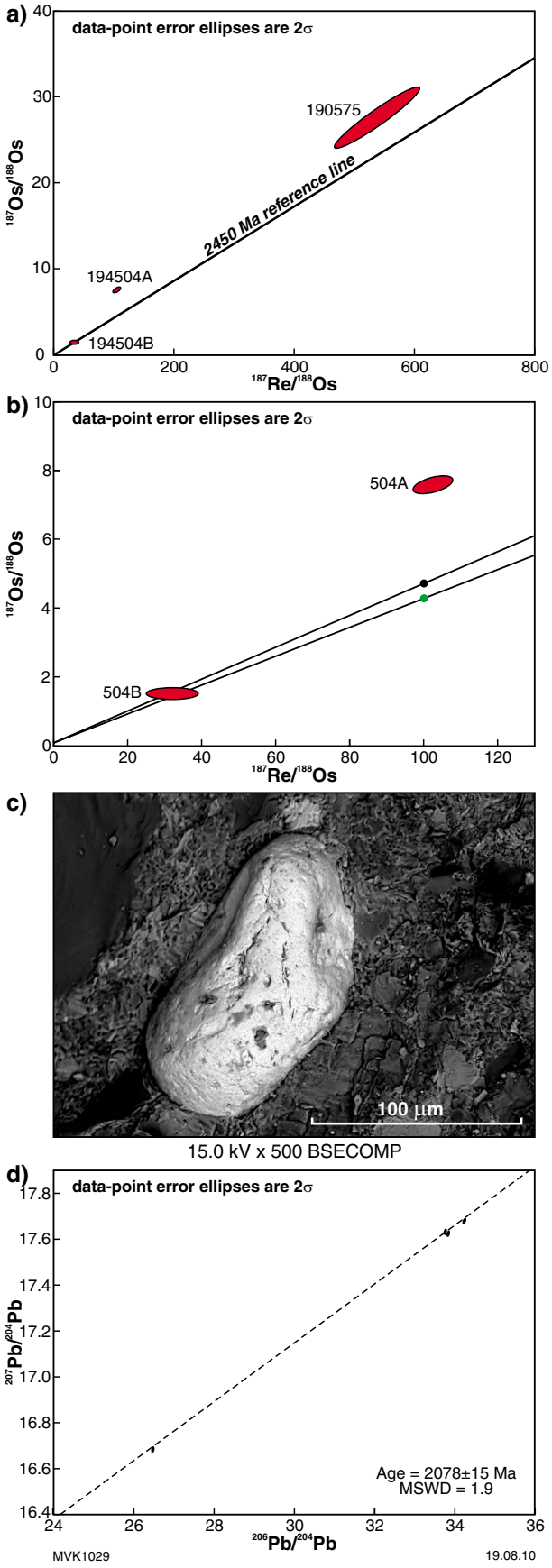

evidence of deposition during global icehouse conditions (i.e. negative $\delta^{13}C_{carbonate}$ values) be assigned to the Turee Creek Group, as originally proposed (Trendall, 1979), to reflect a significant change in Earth conditions. Indeed, analysis of global stratigraphy shows that BIF disappears from the rock record around the world at some time near 2420 Ma, reflecting the onset of worldwide cooling, collapse of a greenhouse (CO_2 and/or CH_4) atmosphere, and rise in O_2 (Fig. 36; Kirschvink et al., 2000; Catling et al., 2001; Pavlov et al., 2001, 2003; Papineau et al., 2007).

Locality 3.5: Woongarra Rhyolite and Boolgeeda Iron Formation at Woongarra Pool (Zone 50K, 510447E 7469491N)

Return to Mount Stuart Station, and exit through the gate onto the sealed road. Turn left, heading east towards Paraburdoo, and continue along the highway for ~140 km, then turn left onto a dirt track at Zone 50K, 518124E 745921N. Follow this track for ~12 km to Woongarra Pool. Park the vehicle and walk north, up the valley, to low exposures on the west side of the creek (Zone 50K, 511028E 7469835N).

From this pont, we will walk back out to the flat plain to the south, through the Woongarra Rhyolite and the overlying Boolgeeda Iron Formation. The Woongarra Rhyolite has been described either as a large intrusive sheet or as an extrusive rhyolitic lava. At this locality, outcrops of rhyolitic breccia exhibit dark-weathering fiamme and rounded to angular clasts of porphyritic rhyolite in a fine-grained, lighter coloured matrix, which certainly give the appearance of an extrusive volcaniclastic rock (Fig. 37a,b).

On the east side of the creek, traverse up over the contact between the Woongarra Rhyolite and Boolgeeda Iron Formation and inspect the contact between these two units (Fig. 37c). Continue upsection, through the Boolgeeda Iron Formation and view the low outcrops of green shale at the base of the saddle (Fig. 37d) on the way back to the car. These green shales, like other green shales in the Hamersley Group, have high iron (42–44 wt% Fe_2O_3), a small amount of Al_2O_3 (2.7 wt%), MgO (1.4–1.7 wt%), and K_2O (1.25 wt%). They also have low CaO and Na_2O, and REE patterns that are distinct from PAAS, with positive relative Eu anomalies, and depleted LREE (Fig. 38).

Figure 35. Geochronological data from basal Turee Creek Group rocks: a) Re–Os data from all samples, plotted against a 2450 Ma reference line; b) Re–Os data for two splits of pyrite from sample 194504 (from Deepdale) plotted against 2450 and 2700 Ma reference lines; c) close-up view of detrital pyrite from Turee Creek Group glacial sediments (courtesy of K Williford, University of Wisconsin); d) Pb–Pb isochron for glacial carbonates (analysis by R Maas, University of Melbourne).

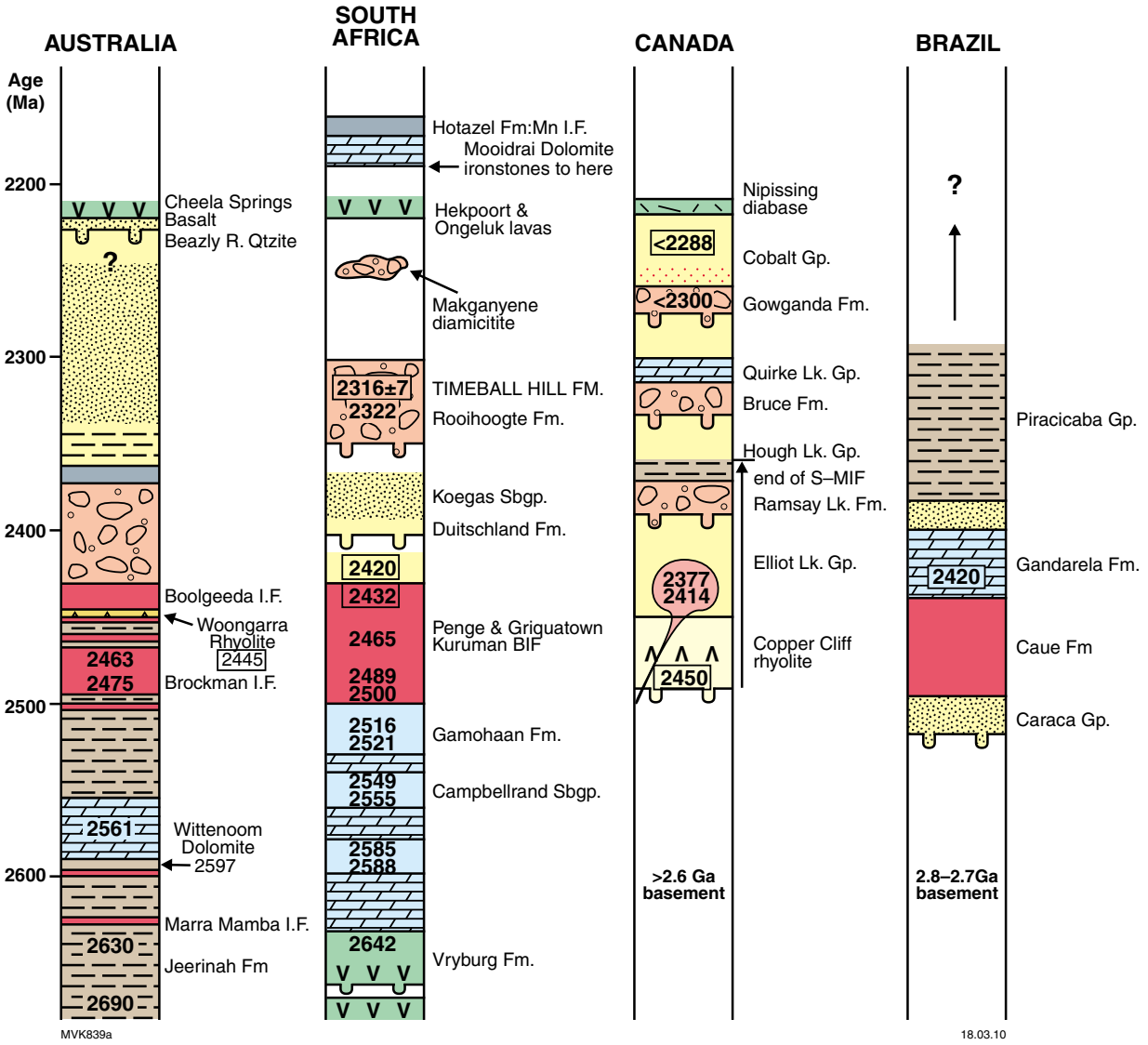

Figure 36. Stratigraphic columns across the Archean–Proterozoic boundary from four places around the world, showing that banded iron-formations disappeared from the rock record prior to 2420 Ma, followed by the deposition of glacial rocks at some time between 2420–2220 Ma.

Locality 3.6: Unconformity at the base of the lower Wyloo Group in the Hardey Syncline (Zone 50K, 507776E, 7467533N)

Return to the vehicle and drive back onto the main track, heading out from Woongarra Pool to the southeast. When out of the river gravel, continue for 100 m and turn right onto a small dirt track that curves to the south. Follow this track for ~1.82 km and stop, looking due west.

The hill in front of you shows the angular unconformity between moderately-dipping rocks of the Turee Creek Group in the lower part of the hill (122°/58°*) and the flat-lying rocks of the Beasley River Quartzite (lower Wyloo Group) forming the upper part of the hill (Fig. 39). Original mapping placed all of the flat-lying rocks into the Beasley River Quartzite (Powell and Horwitz, 1994; Thorne and Tyler, 1996). However, Martin et al. (2000) suggested that a lower, flat-lying package of siltstones and fine-grained sandstones belongs to the Kazput Formation of the Turee Creek Group, as it is cut out along strike by the unconformity at the base of overlying conglomerate and quartzite , which they assign to the Three Corners Conglomerate Member of the Beasley River Quartzite and the main part of the formation, respectively. However, despite the fact that the lower flat-lying package may be cut out by the overlying unit, it is still not clear why it should be placed within the Kazput Formation and not in the lower Wyloo Group.

* Strike and dip of bedding given following the right hand rule, where by strike direction is given along the direction such that the dip is to the right.

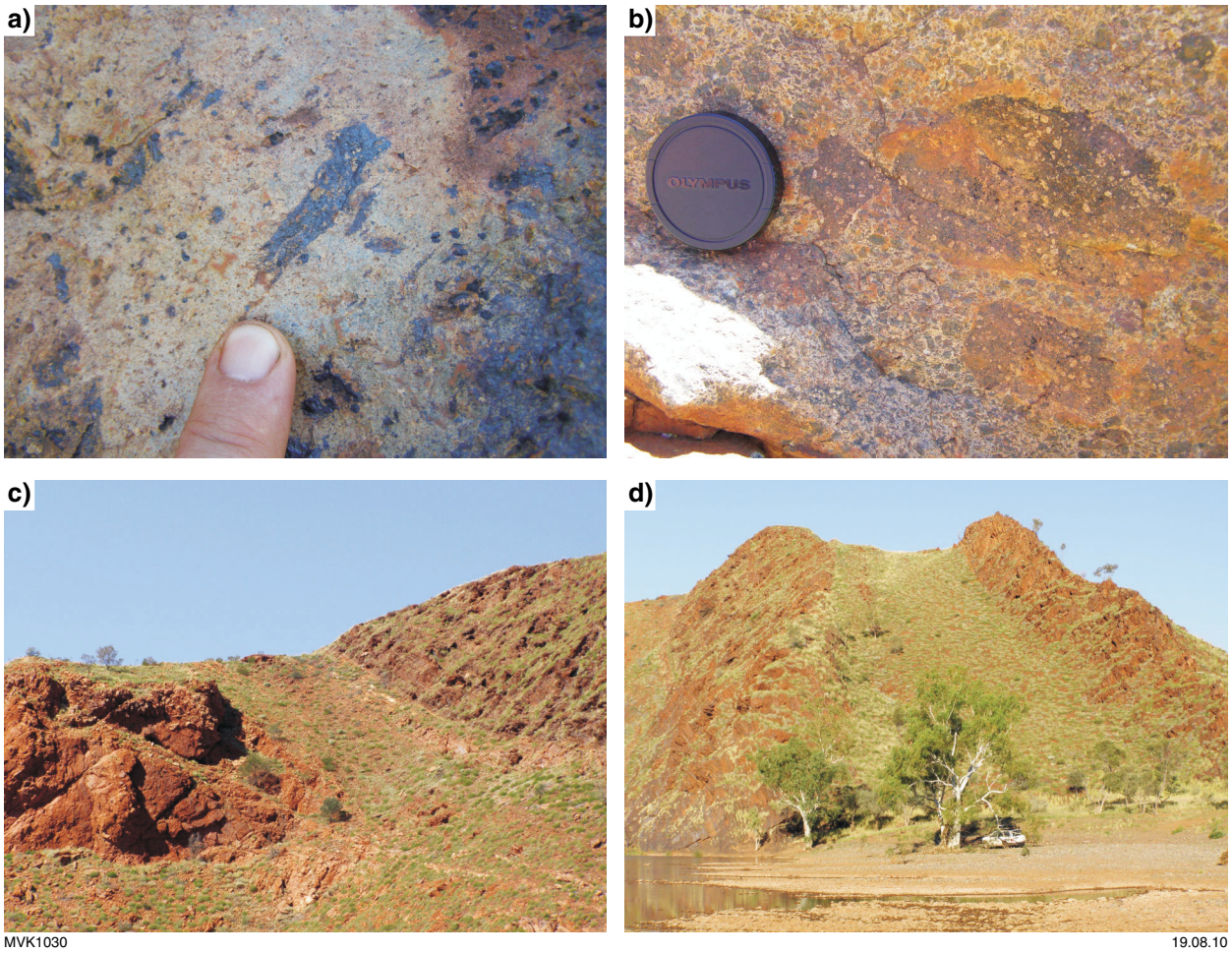

Figure 37. **Outcrop features of the Woongarra Rhyolite and Boolgeeda Iron Formation at Woongarra Pool, Excursion Locality 3.5: a–b) close-up views of volcaniclastic texture in Woongarra Rhyolite, including fiamme (a) and clasts of porphyritic rhyolite in fine-grained rhyolite; c) contact between Woongarra Rhyolite and Boolgeeda Iron Formation; d) outcrop features of the Boolgeeda Iron Formation, consisting of two resistant iron formation ridges, separated by a saddle of poorly exposed green 'shale'.**

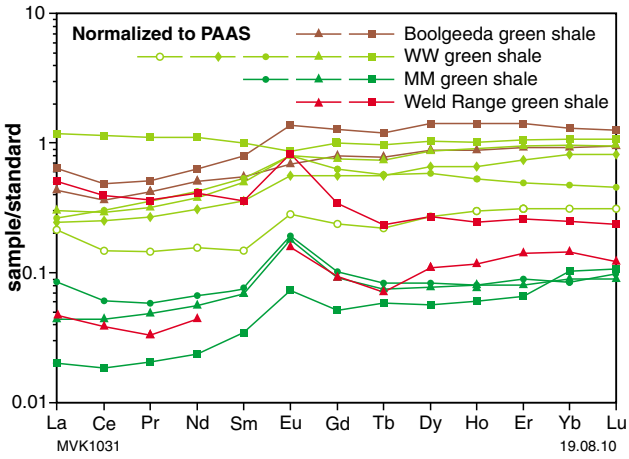

Figure 38. **Plot of rare earth elements, normalized to PAAS, comparing green 'shales' from different formations of the c. 2.63–2.45 Ga Hamersley Group, with green shale from c. 2.75 Ga Weld Range BIFs of the Polelle Group (Murchison Domain, Yilgarn Craton): MM = Marra Mamba Iron Formation; WW = Weeli Wolli Formation; Boolgeeda = Boolgeeda Iron Formation. Note the change in composition up stratigraphic section in the Hamersley Group, and the similarity between Weld Range and Marra Mamba green shales, which both have typical seawater REE profiles.**

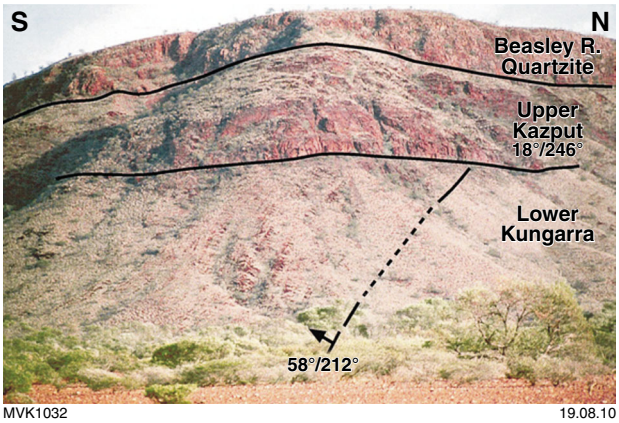

Figure 39. View, looking west, of the unconformity between the Turee Creek Group and lower Wyloo Group (Beasley River Quartzite; see Introduction for discussion). From Martin et al. (2000).

Locality 3.7: The Meteorite Bore Member at Meteorite Bore (Zone 50K, 504990E 7465312N)

Continue driving south and then west along the track for ~7.3 km to a T-junction with a graded dirt track (Zone 50K, 504815E 7464073N). Turn right onto this new track and head north for ~800 m to Meteorite Bore. Pass the bore, keeping it on your left, and cross a small creek, then head northeast through the bush for ~800 m to a low dark-brown outcrop.

This is the type area of the glacigenic Meteorite Bore Member of the Turee Creek Group. The fine-grained sandstones and siltstones at this outcrop contain a penetrative, steeply-dipping cleavage that is parallel to bedding, although bedding is difficult to see at this outcrop. Scattered sparsely throughout the sediments are pebble- to boulder-size, subrounded to subangular clasts, reaching up to 40 cm diameter at the top of the hill. Clasts are predominantly white, porphyritic rhyolite, most likely derived from the underlying, nearby Woongarra Rhyolite. However, a variety of other lithologies have been noted from this locality, including leucogabbro, carbonate-altered felsic volcaniclastic rocks, banded iron-formation, dolomite, granite, and quartz (Martin, 1999). Clasts are commonly faceted and some show striae, indicative of a glacial origin (Fig. 4).

Day 4: Karijini NationalPark

Contributed by ME Barley

Return to Meteorite Bore and follow the main track due south for 4.5 km to a T-junction with the highway (Zone 50K, 504719E 7460328N). Turn left, heading east, and follow the highway for 34 km. Continue past the signed turnoff to Paraburdoo at this point and drive northeast, heading for Tom Price.Continue for a further 70 km, then turn right onto the sealed road and drive southeast to Tom Price. Take a left, then a right, before entering the town proper, following the signs to Karijini National Park. Continue southeast for 10 km, then turn left, heading northeast to the park. Continue along this road for 41 km and turn left into Karijini Park (Zone 50K, 612784E 7503557N). Follow the track into the park for 26 km, past the turnoff to the visitors centre, and continue for a further 10 km to the Oxer lookout over Weano Gorge (Zone 50K, 632298E 7527084N).

Locality 4.1: Oxer Lookout and Weano Gorge; the Joffre Member of the Brockman Iron Formation (Zone 50K, 632687E 7526696N)

The Oxer Lookout provides an excellent view of the Joffre Member banded iron-formation (BIF) (the thickest BIF unit in the Brockman Iron Formation) in the Weano, Joffre, Hancock, and Red Gorges (Fig. 40a). The view into the gorges shows the c. 2.46 Ga Joffre Member with continuous interlayered BIF macrobands and S macrobands (thicker than 50 cm). Details of the style of the laminated chert and iron oxide rich layers of the BIF microbands (less than 2 mm), mesobands (less than 3 cm), and macrobands of the Joffre Member can be observed in outcrops in the Weano Gorge.

Locality 4.2: Joffre Falls; the Joffre Member of the Brockman Iron Formation (Zone 50K, 630624E 7523427N)

Head back out from the Oxer Lookout area, drive 14 km north and turn left towards the Visitor's Centre, driving east. After 3 km, turn left and take the track for 1 km to Joffre Falls.

The Joffre Falls (Fig. 40b) locality exposes key outcrops of banded iron formation of the Joffre Member, with implications for the formation of the BIF. These exposures include bedded chert and iron oxide rich layers. Truncated BIF and bedded chert layers at the falls provide evidence that the BIFs were originally deposited as iron oxide-rich sediments. Diagenetic laminated magnetite layers with listric normal offsets of bedded chert provide evidence of diagenetic processes during early deformation and compaction of the BIF.

Locality 4.3: Kalamina Falls; the Joffre Member of the Brockman Iron Formation (Zone 50K, 644445E 7520401N)

Head back out to the north for ~1 km to a T-junction and turn left, returning east towards the Visitor's Centre. Proceed for 10 km and take the left turn to Kalamina Falls, 6 km further on.

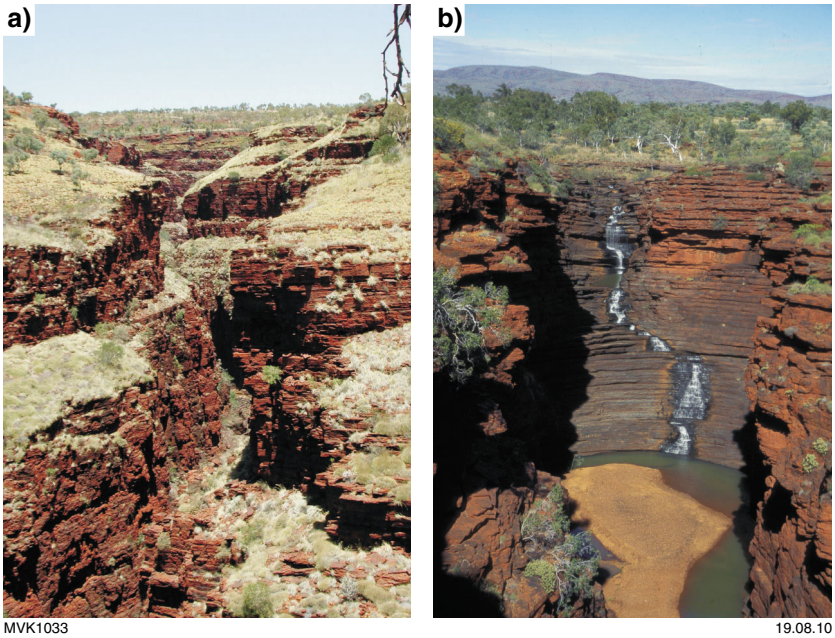

Figure 40. The Hamersley Group in Karijini National Park: a) view from the Oxer Lookout down a gorge cutting through the Dales Gorge Member of the Hamersley Group; b) Joffre Falls.

The Kalamina Falls contain key outcrops of turbiditic sedimentary S macrobands associated with the Joffre Member BIF. These include carbonate and shale sedimentary layers.

Locality 4.4: Dales Gorge; the Dales Gorge Member of the Brockman Iron Formation (Zone 50K, 660227E 7513558N)

Return for 6 km back out along the track and turn left. Head south and then east for 19 km to the Visitor's Centre. Continue east for a further 10 km to Dales Gorge and follow the signs down into the gorge.

Dales Gorge provides excellent outcrops of the 2.5 to 2.46 Ga Dales Gorge Member of the Brockman Iron Formation, which contains 17 BIF macrobands and 16 S macrobands. The lowermost units outcrop near Circular Pool. The first S macroband (S_1) is a carbonate turbidite. There are also outcrops of primary sedimentary and diagenetic compaction structures (chert nodules) in the interlayered BIF bands. From there, walking up Dales Gorge towards Fortescue Falls shows excellent outcrops of several key S macrobands (S_2 and S_6 are also carbonate turbidites). S_4 is an impact layer (and S_7 is a complex unit with a possible impact layer) and the other S macrobands include shales and tuffs and some carbonates. The interlayering of BIF and S macrobands provides evidence for deposition in a deep marine basin with fluctuating sea levels (deeper during BIF deposition, shallower during mainly turbidite S macroband deposition).

Day 5: The Neoarchean Fortescue Group

From the Dales Gorge campground, head 10 km west towards the Visitor's Centre, but turn left before you get there, heading south for 8 km to Karijini Drive. At the T-junction, turn left and head east for 30 km to the great Northern Highway. Turn left and head north for 34 km to the Munjina (Auski) Roadhouse. 300 m before the roadhouse (Zone 50K, 673954E 7523949N), turn right onto a dirt track, heading east-southeast along the foot of the ranges. Follow this road for ~54 km to a junction with the BHP railway. Turn sharp left and follow the tracks west-northwest, then north, for ~69 km. At Zone 50K, 707382E 7564504N), take a small track across the railroad trcks onto the west side and head back south along the tracks for ~900 m and park the vehicle. From here we shall walk up the hill in front of us, to the west, for about 600 m.

Locality 5.1: Tumbiana Formation stromatolites (Zone 50K, 706555E 7563622N)

The hills around us are capped by a subhorizontal unit of dark-brown to black weathering dolomitic rocks of the c. 2.72 Ga Tumbiana Formation, of the Fortescue Group (see Fig. 2 for stratigraphic position). These rocks lie unconformably on the granite–greenstone basement terrane of the Pilbara Craton, which you can see across the railway tracks looking east (see Fig. 7a).

At this locality, and indeed for much of its 400 km strike length, the Tumbiana Formation contains abundant and diverse stromatolites that thrived in very shallow water, lacustrine to lagoonal environments (Buick, 1992; Bolhar and Van Kranendonk, 2007; Awramik and Buchheim, 2009). The very shallow water conditions are evidenced by common desiccation cracks, common layers of flat-pebble conglomerates, and the occurrence of interbedded fluvial deposits (e.g. Fig. 7c). This locality contains some of the largest stromatolites, to 40 cm (Fig. 41a–c), although structures up to 1.5 m high have been observed near the Nullagine River, some 160 km to the east-northeast of this locality (**see Locality 5.8**). However, the stromatolites here (Locality 5.1) are quite distinct in form from their larger Meentheena cousins, with low- to steep-sided laminae and narrow to broad columnar to domical shapes. In places nearby, laminated microbial mats show evidence of formation as tufted mat, akin to textures in living Shark Bay stromatolites (Fig. 41d).

Locality 5.2: The 2772 Ma Black Range Dyke and phreatomagmatic boulder conglomerate (Zone 50K, 763436E 7627340N)

Return to the vehicles, turn around, cross back over the railway and turn left, back onto the main track that runs alongside the railway. Head north along the track for ~50 km until you reach a stopsign and a crossroad (Zone 50K, 696655E 7611804N). Turn right and follow the Hillside Track east for ~73 km to a small outcrop on the left side of the track, in the bed of Coolyia Creek.

The 2772 ± 2 Ma (Wingate, 1999) Black Range Dyke is the largest dyke of the Black Range Dolerite Suite, which was emplaced during eruption of the Mount Roe Basalt at the base of the Fortescue Group (Fig. 42). This locality lies within the core of a narrow zone of unusual boulder conglomerates that extends along strike to the northeast

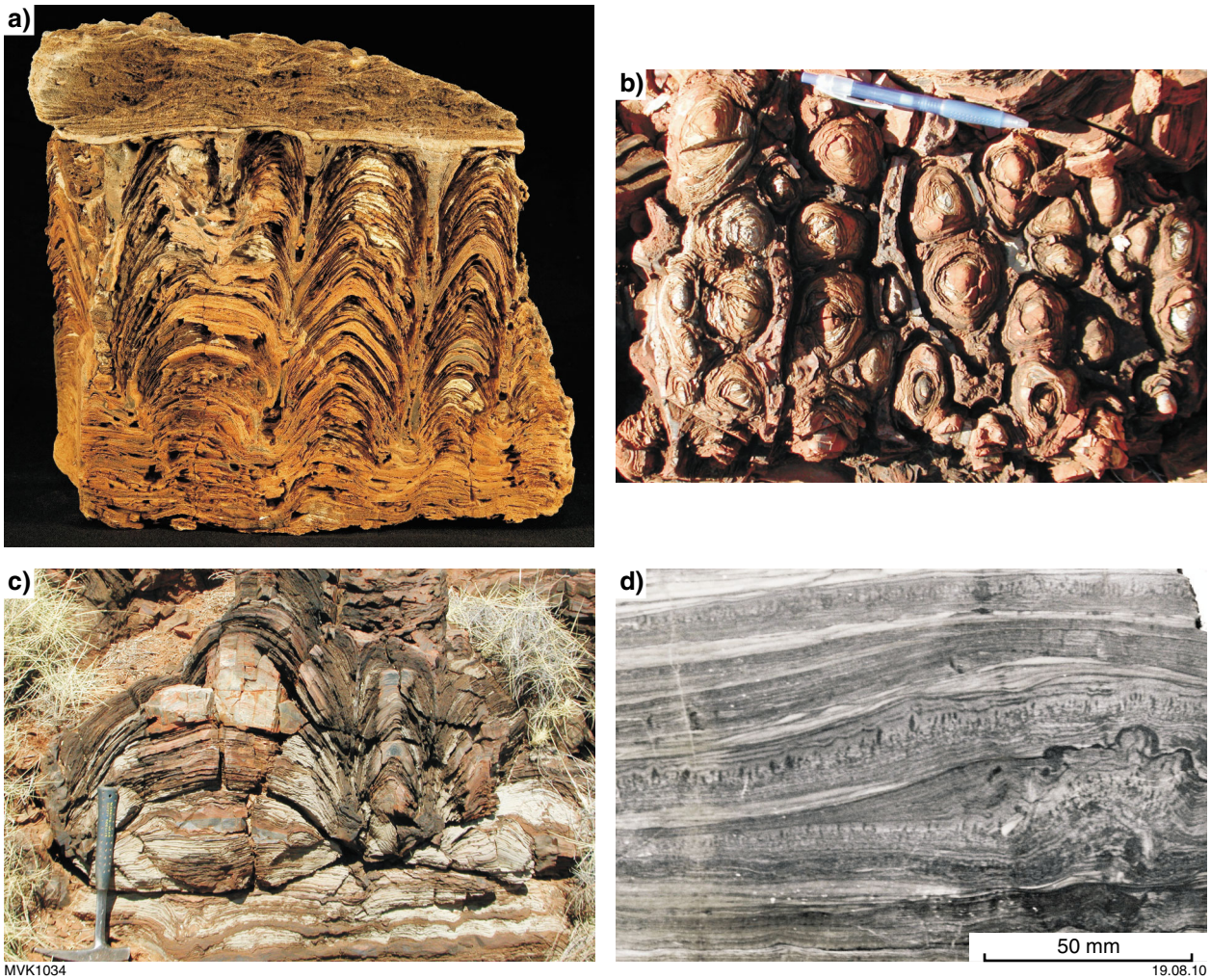

Figure 41. A selection of Tumbiana Formation stromatolites from Excursion Locality 5.1: a) cross-sectional view of round-topped, branching columnar forms truncated by rippled carbonate sandstone; b) bedding-plane view of same stromatolite horizon as a). Note favourable comparison of this with the view of 3.35 Ga stromatolites presented in Figure 79a; c) outcrop view of large, domical form; d) cut face of stromatolitic carbonate, showing tufted filaments.

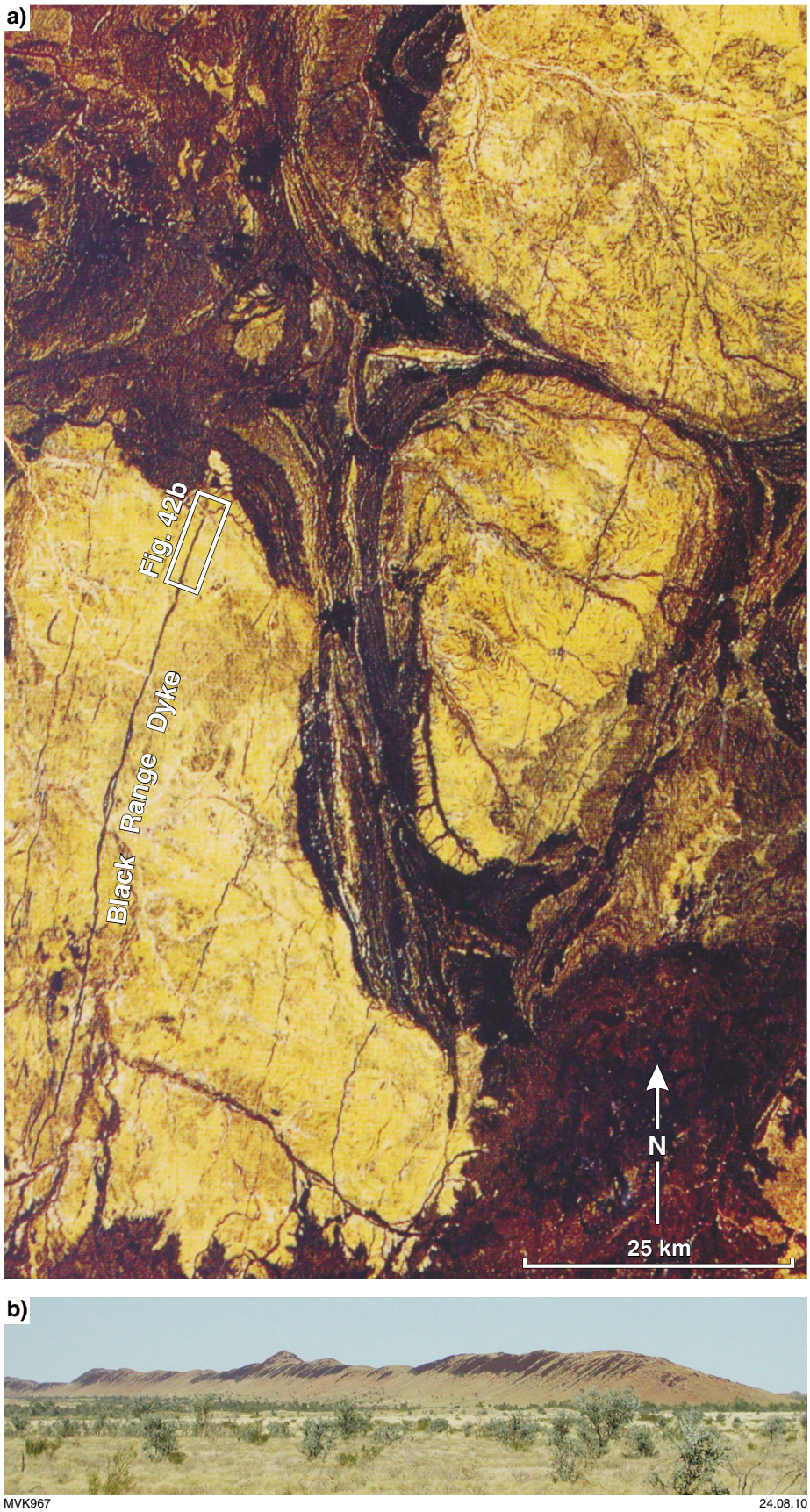

Figure 42. **a) Landsat view of part of the East Pilbara Terrane of the Pilbara Craton, showing granites as yellow ovoids, wrapped by dark greenstones, and cut by dolerite dykes of the c. 2.77 Ga Black Range Dolerite Suite (width of view ~75 km): b) view, looking south, of the northern tip of the Black Range Dyke.**

of the Black Range Dyke for ~5 km, reaching 1 km wide (Fig. 43; Van Kranendonk et al., 2006).

Although superficially resembling normal sedimentary conglomerates, the boulder conglomerates within the narrow zone in front of the Black Range dyke are unusual because they contain:

- no evidence of bedding (Fig. 44a)
- clasts that show increasing angularity with decreasing grain size, opposite to that in conglomerates of sedimentary origin (Fig. 44b)
- well-rounded basaltic pebbles within granitic boulder conglomerates, which would probably not have survived in a sedimentary environment (Fig. 44b)
- biotite-rich granitic clasts with dark alteration rinds (Fig. 44b)
- a matrix that varies from sand-size rock crystal grains to rock flour (Fig. 44c)
- a component of the matrix that consists of chlorite, which shows reaction with, and resorbtion of, granitic clasts, indicatinve of a hot matrix component (Fig. 44d)
- clasts showing evidence of in situ disaggregation, indicative of some sort of intense shaking (Fig. 44e)
- rounded basaltic clasts with chilled rinds (Fig. 44f)
- lateral changes in the composition of the conglomerate, from dominantly granitic clasts in the core of the zone, to hybrid basalt–granite conglomerates near the margins of the zone, and basaltic breccias with sparse granitic clasts at the very edges of the zone, in contact with basaltic lavas (Fig. 44g,h).

These conglomerates show a variety of textures and compositions across strike and have peperitic contacts with remnants of basaltic lava flows, indicating contemporaneity of formation with basalt eruption. Contemporaneity is supported by a U–Pb zircon date of 2767 ± 3 Ma from an intermediate tuffaceous sandstone that flanks the linear zone of conglomerate (Fig. 46; Van Kranendonk et al., 2006).

For these reasons, Van Kranendonk et al. (2006) concluded that the conglomerates were caused by phreatomagmatic brecciation of the granitic country rocks during emplacement of the Black Range Dyke, through one of two ways (Fig. 45a,b). The preferred model (Fig. 45a) has the Black Range Dyke emplaced laterally into a developing fracture, the propagating tip of which was filled by disaggregated country rock, as well as basaltic droplets sourced from the intruding magma. Rounding of the country rock boulders was due to turbulent milling during gas/magma (phreatic) eruptions, which resulted in fine, angular fragments being chipped off, development of matrix rock flour, alteration/resorption of fragments by hot matrix, and in situ clast disaggregation. This type of linear zone may be equivalent to the lunar rilles, which have been interpreted as graben developed over intrusive dykes (Fig. 45c).

Locality 5.3: Basal unconformity of the Fortescue Group in Glen Herring Gorge (Zone 50K, 771233E 7636598N)

Drive further along the track for 15 km and turn right at the sign to Glen Herring Gorge (Zone 50K, 770118E 7638795N). Follow the track almost due south for 2.5 km and take a sharp turn left, downhill (Zone 50K, 770641E 7636465N) into the gorge. Follow the track for 375 m, crossing a small creek near the end, and park on the gravel.

As you walk north from the parking area along the creek bed, you will walk over flows of c. 2.8 Ga vesicular basalt belonging to the basal (unnamed) unit of the Fortescue Group in the Marble Bar Sub-basin (Fig. 46). These smooth, white-weathering rocks have been polished by the flow of the creek and carved into odd shapes. If you look closely at the rocks, you will notice they contain numerous small, white, round to irregular amygdales in fine-grained basalt; these magmatic vesicles are now filled by secondary minerals (quartz, calcite) precipitated out of solution from later circulating fluids. You will also notice red fractures and stains in the rock, which reflect the passage of highly oxidized groundwater through fractures in the rock caused by episodes of more recent faulting.

As you walk further north, down the gorge, notice that the rocks change from smooth-textured basalts to cobble and boulder conglomerate that was deposited under very high-energy conditions on a steep slope — probably conditions that were much the same as those you see around you today. Some of the fragments in the conglomerate are very large and probably derived from episodes of faulting, possibly the same fault that formed this gorge.

Even further north, in the heart of the gorge, the rocks change again. The steep cliff at the sharp bend of the river is part of the 3.32 Ga felsic volcaniclastic Wyman Formation, which forms the basement to the Fortescue Group at this locality.

Locality 5.4: Basal pillow breccia, c. 2775 Ma Mount Roe Basalt (Zone 50K, 771266E 7639443N)

Return back out to the Hillside Track and turn right. Proceed by vehicle for 1.15 km and park by the side of the road.

At this locality, we see orange-weathering sandstones of the ?Bellary Formation, dipping 30°N on the south side of the track. North of the track are some impressive outcrops of the pillow breccia unit that forms the base of the Mount Roe Basalt throughout the Marble Bar Sub-basin. This unit is 100–450 m thick and is conformably overlain by subaerial basalt flows, which suggests that the pillow breccia unit may have been deposited in a lacustrine setting. The pillow breccia contains rare, whole pillows surrounded by hyaloclastite, but much more commonly consists of angular pillow fragments (Fig. 47).

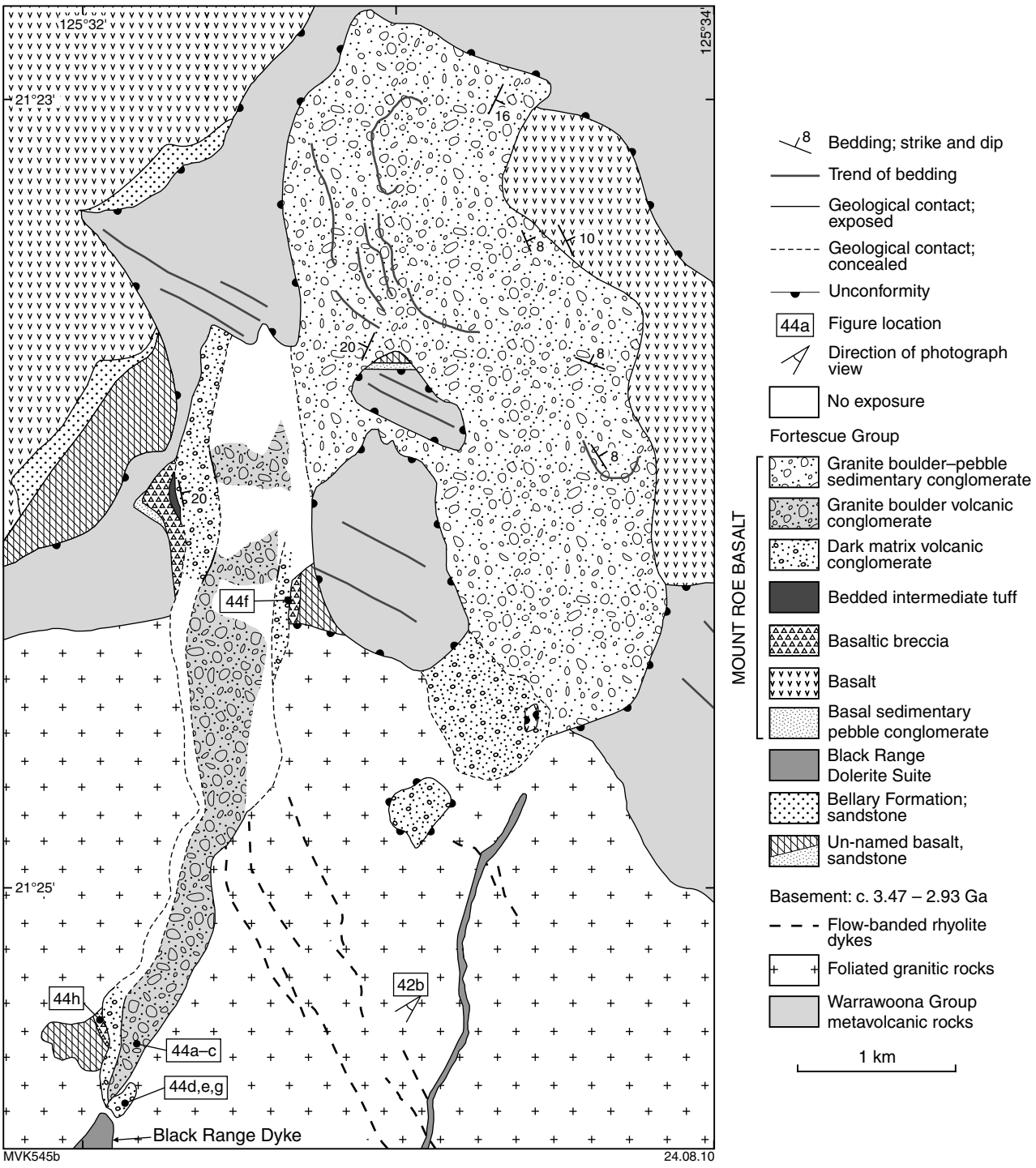

Figure 43. Geological map of the phreatomagmatic breccia dyke immediately along strike to the north of the Black Range Dyke. Excursion locality 5.2 is at the position where Figure 44 is indicated. (Modified from Van Kranendonk et al., 2006.)

Figure 44. (facing page) Outcrop features of the phreatomagmatic breccia dyke at Excursion Locality 5.2: a) river-washed outcrop of well-rounded granitic boulder conglomerate; b) close-up of granitic boulder conglomerate, showing dispersed basaltic clasts and angular nature of finer-grained matrix (top right); c) area of dark rock-flour matrix between granite cobbles; d) photomicrograph (plane-polarized light) showing dissolution of quartz clasts by matrix; e) photomicrograph (plane-polarized light) showing in situ disaggregation of granitic clasts, suggestive of seismic shaking; f) photomicrograph (plane-polarized light) of basaltic droplet with chilled margin defined by inward-radiating plagioclase crystallites; g) dark-coloured breccia along the margin of the phreatomagmatic dyke, consisting predominantly of angular basaltic clasts, but including scattered granitic clasts; h) basaltic breccia at the contact with basaltic lavas on the edge of the phreatomagmatic dyke.

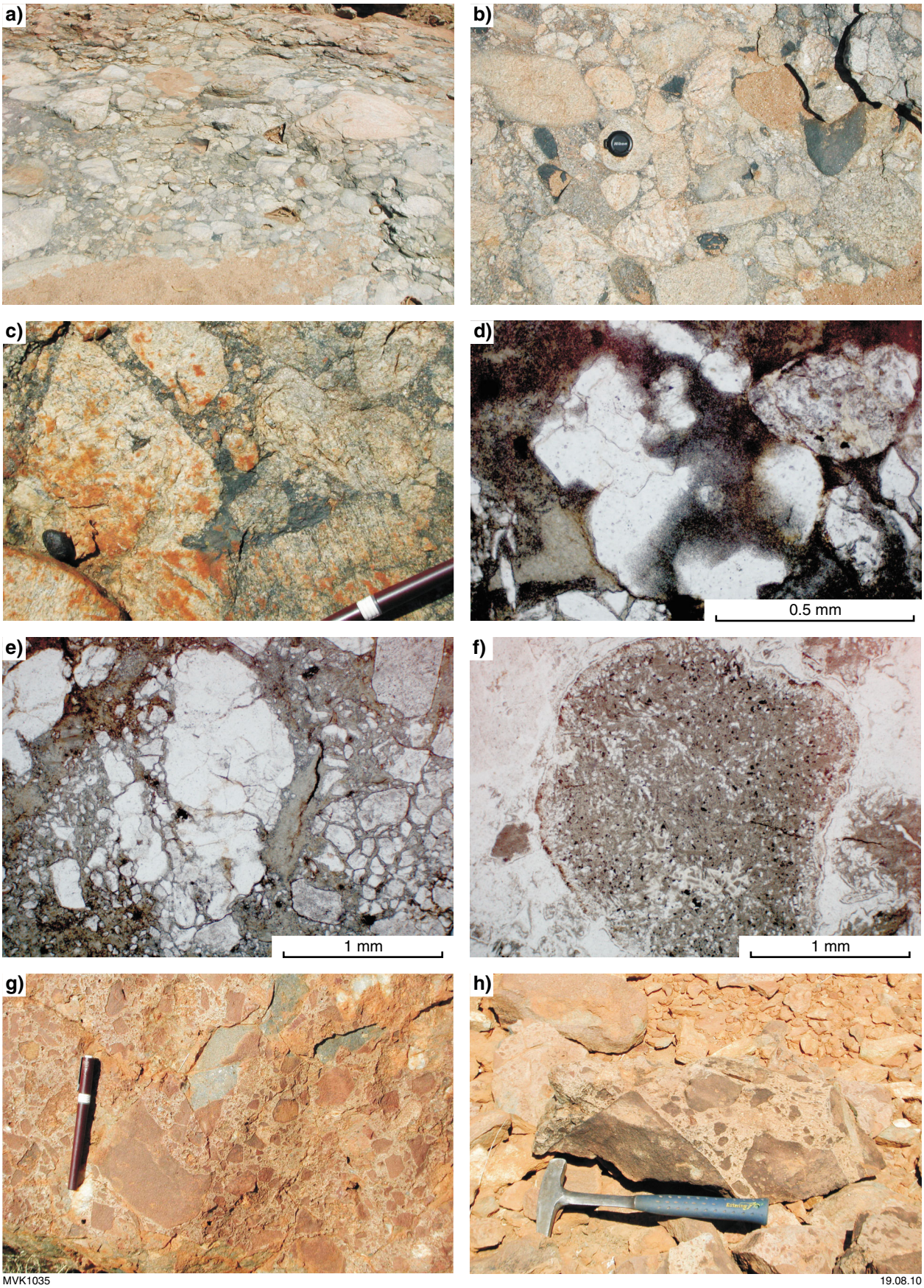
a)
b)
c)
d)
0.5 mm
e)
1 mm
f)
1 mm
g)
h)
MVK1035
19.08.10

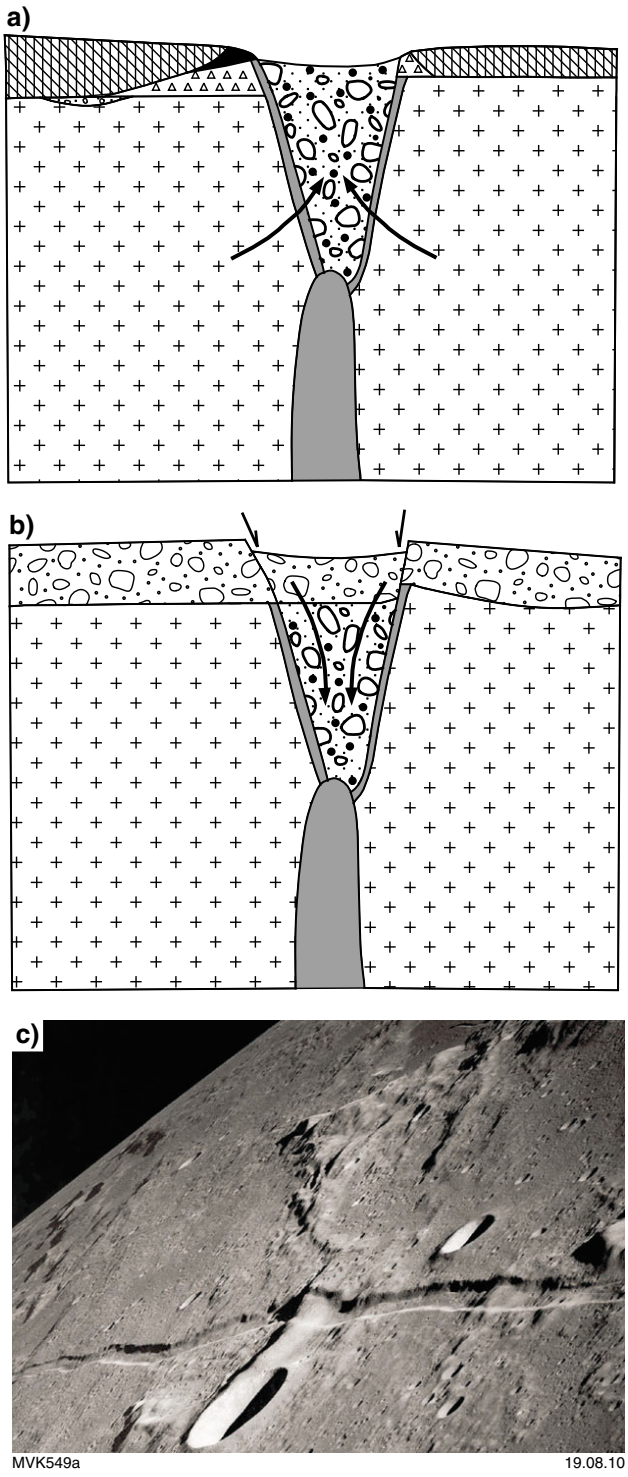

Figure 45. Two possible models of formation of the phreatomagmatic breccia dyke at Excursion Locality 5.2: a) phreatomagmatic brecciation at the propagation tip of the Black Range Dyke in granitic country rocks, through steam-generated milling of country rocks and with the addition of basaltic droplets from the incoming magma; b) phreatomagmatic brecciation at the propagation tip of the Black Range Dyke emplaced beneath a pre-existing sedimentary cover. (From Van Kranendonk et al., 2006.) c) Apollo photo of lunar rille.

Locality 5.5: Rheomorphic ignimbrite, Hardey Formation (Zone 51K, 224716E 7650704N)

Return to the main track and continue on for ~27 km towards Marble Bar. Join the sealed road and then turn right at the T-junction, heading into town. From the Ironclad Hotel, continue east, out of town, towards Port Hedland. After 8.6 km (Zone 50K, 792968E 7657108N), turn right onto the Nullagine–Telfer–Newman Road. After a further 14 km, continue on the Ripon Hills Road, towards Woodie Woodie and Telfer. Continue driving east across the flat Mount Edgar Granitic Complex, and sweep around the big curve in the road and continue to 59.5 km. Stop beside the outcrop on the left hand side of the road.

This spotted, white and black rock here is a rheomorphic ignimbrite of the 2.76 Ga Hardey Formation. During eruption, fragments of dark green volcanic glass were thrown high into the air, together with crystals from the magma chamber deep in the crust, and abundant very fine grained volcanic ash. All of this material fell back down onto the side of the volcano while still hot and fused into the rock you see here. However, as the ash, glass, and magma cooled, it started to flow down the side of the volcano and in the process smeared out the darker glassy fragments and rotated the crystals so that in places it looks like it is a strongly deformed rock (Fig. 48). If you look closely at the texture, you will see that the dark green fragments (lapilli) have ragged and/or cuspate edges, which indicate they were originally hot, glassy fragments erupted from the volcano into the air. The heat from the volcanic eruption slightly metamorphosed the rocks so that the glass has devitrified to a very fine aggregate of crystals and the white, originally volcanic ash, matrix has fused into a finely crystalline rock. This is a good example of how weathering of the rock has actually enhanced its texture; you will notice that fresh broken surfaces are much duller and more homogeneous in colour.

Locality 5.6: Kylena Formation, subaerial basalt flows (Zone 51K, 247442E 7646949N)

Continue along the road to the east for 25.1 km and stop at a large roadside cutting.

This cutting on the north side of the road displays a section through two, almost flat-lying, very thick basalt flows of the c. 2.74 Ga Kylena Formation (Fig. 49a). The lower part of the lower flow contains large gas cavities filled by quartz and calcite in a groundmass of deuterically altered basalt (chlorite–carbonate–titanite; Fig. 49b). The top contact of the lower flow is broadly lobate. About two-thirds of the way up the cutting, the top of the lower flow is highly vesicular and bleached to a pale brown colour. Relict patches of chilled basaltic texture in

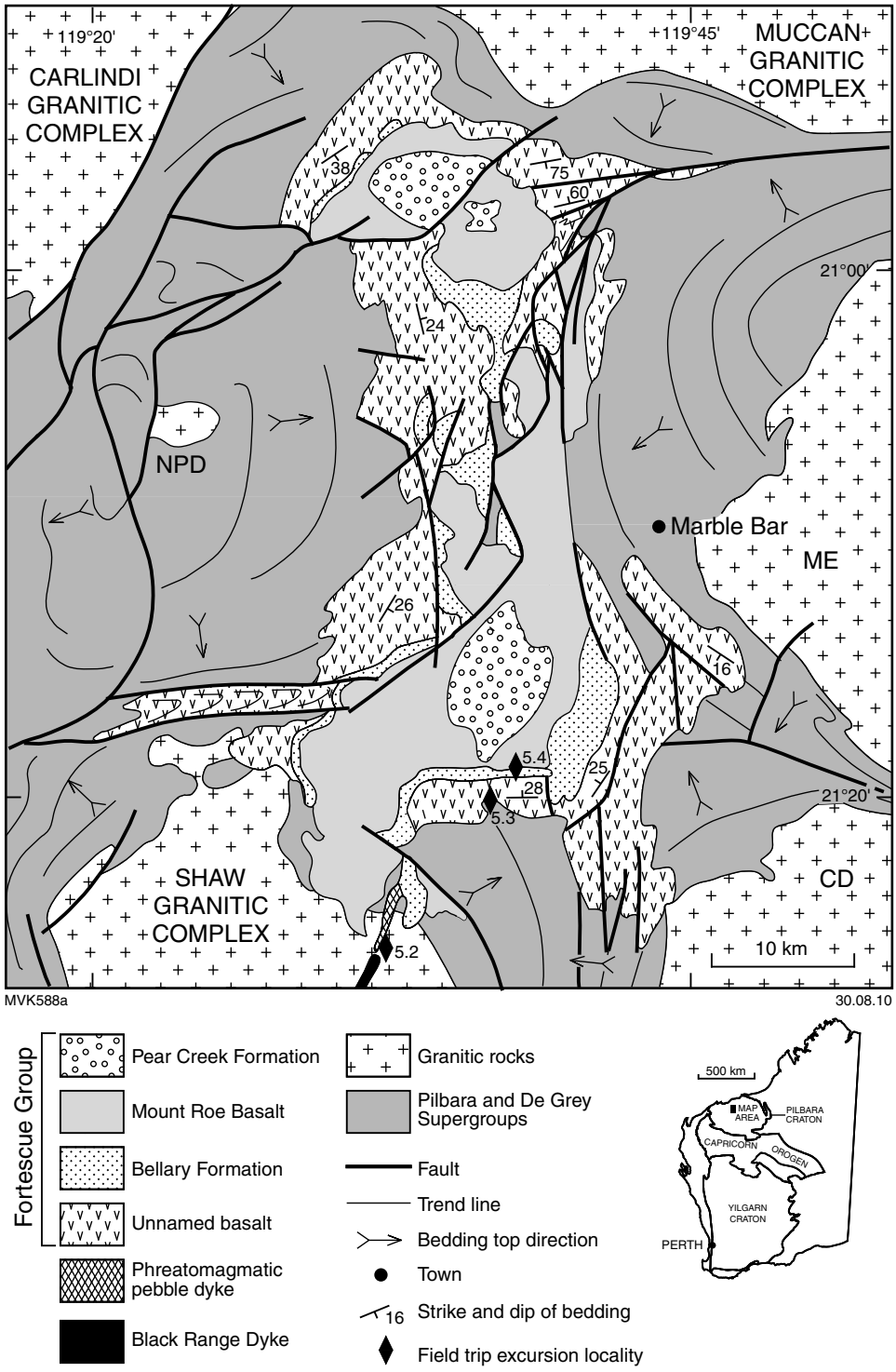

Figure 46. Geological map of the Marble Bar Sub-basin, showing excursion localities.

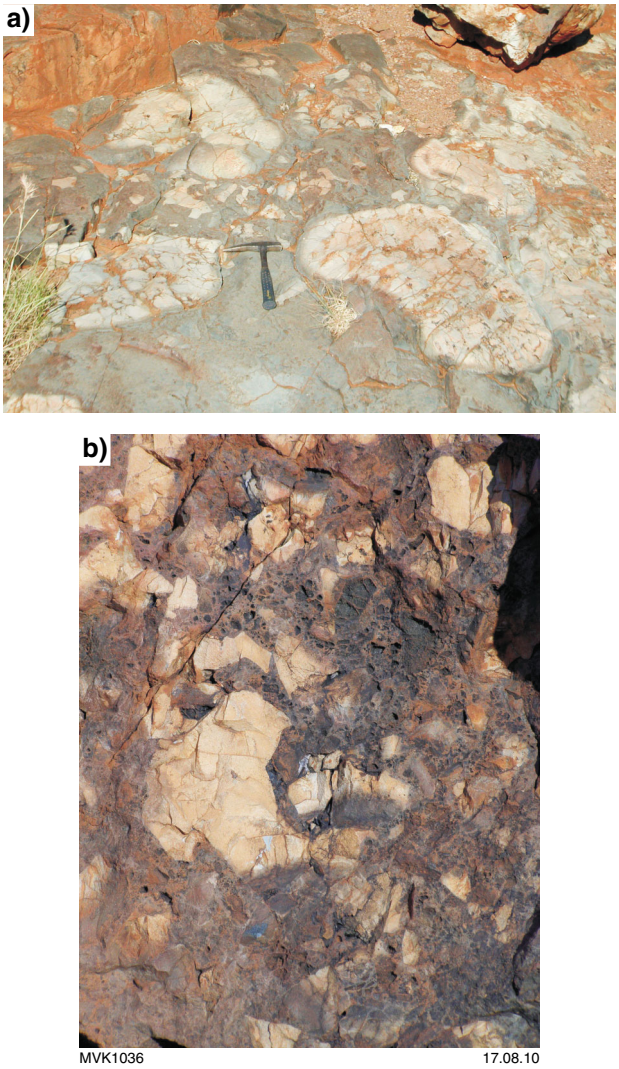

Figure 47. Outcrop features of the Fortescue Group basaltic pillow breccia at Excursion Locality 5.4: a) nearly whole pillows surrounded by hyaloclastite; b) angular brecciated pillow fragments in hyaloclastite.

Figure 48. Rhyolitic rheomorphic ignimbrite, Hardey Formation at Excursion Locality 5.5.

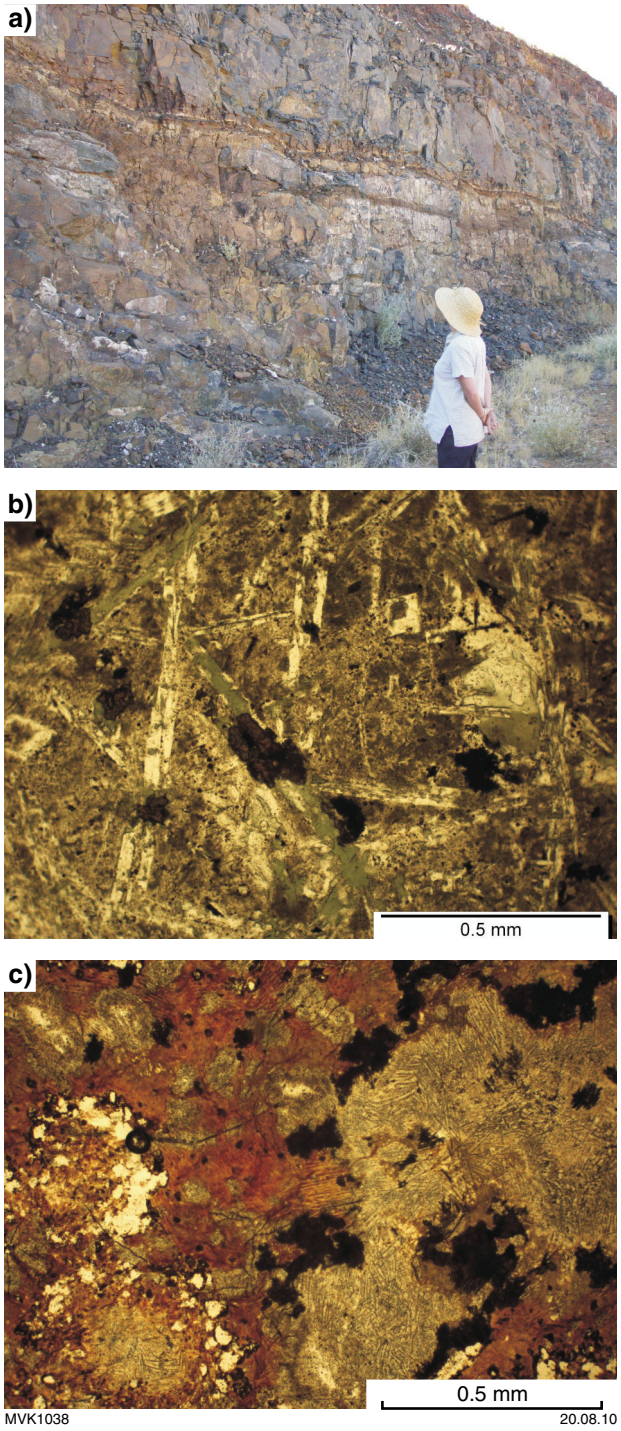

Figure 49. Features of the Kylena basalt at Excursion Locality 5.6: a) roadside cutting through two, thick subaerial flows of the Kylena Formation; b) photomicrograph (plane-polarized light) of Kylena basalt from the middle, dark-green part of the lower flow unit, showing chlorite (light green) and titanite alteration; c) photomicrograph (plane-polarized light) of Kylena basalt from the more highly altered top of the lower flow unit.

this zone is overprinted by patches of very fine-grained, reddish brown alteration and by growth of titanite and small white porphyroblasts of white mica (Fig. 49c). Chemical analyses of this zone show that it has been stripped of iron (Fe), magnesium (Mg), and silica (Si) and enriched in Al_2O_3. Does this alteration reflect ancient weathering processes, and if so, how could we discriminate this from younger hydrothermal or groundwater alteration?

Locality 5.7: Carawine Dolomite impact breccia horizon (Zone 51K, 278885E 7640823N)

Continue driving east for a further 35.2 km and turn left onto a small dirt track heading north (Zone 51K, 279091E 7639997N). Proceed for 600 m and turn left towards the windmill. Park at the windmill. Walk towards the outcropping rocks, up a small, steep-sided gully for about 150 m.

As you walk up the gully, notice the very regular bedding and lack of stromatolites in the Carawine Dolomite here, suggesting deposition in deep-water conditions. Further up the gully, around a sharp bend, the bedded dolomite is overlain by a coarse, unsorted carbonate breccia containing scattered angular clasts of black, white, grey, and red chert and dolomite, up to 30 cm across (Fig. 50a). This highly unusual feature indicates extremely high energy conditions during deposition, something that only happens during major storms (hurricanes), earthquake-generated tsunamis, or the impact of a meteorite.

Minute observation of the carbonate matrix of the rock that this unit has shown that it was deposited as the result of a bolide impact. The key piece of evidence is the observation of beige, 1 mm spheres of altered glass distributed through the unit; you can find these if you search the rocks very carefully (Fig. 50b). The force of the meteorite impact caused a giant tsunami, which broke up some of the underlying, or adjacent, rock and transported it possibly hundreds of kilometres to this location where it became incorporated into the thick bed of limestone. We infer from these pieces of evidence that the whole breccia unit you see here was deposited almost instantaneously. An identical bed in rocks of identical age has been identified in South Africa, and this feature has been used to suggest that the impact may have had a global influence.

The Carawine Dolomite has been correlated with the Wittenoom Dolomite. Jahn and Simonson (1995) and Woodhead et al. (1998) obtained precise Pb–Pb isochrons, of 2541 ± 32 Ma and 2541 +18/–15 Ma, respectively, on carbonates from the Carawine Dolomite and interpreted this as the depositional (early diagenetic) age of the formation. Zircon dating from the Wittenoom Dolomite shows that this formation was deposited at the roughly the same time, at between 2597–2504 Ma (Trendall et al., 2004; Rasmussen et al., 2005). However, petrographic observations from spherule beds within these and bounding formations have been used to suggest that the Carawine spherule layer is the same as the Jeerinah spherule layer, dated at c. 2600 Ma (Hassler et al., 2005). Dating of zircons from a tuff layer just below the Carawine spherule layer yielded a U–Pb age of 2630 ± 6 Ma (Rasmussen et al., 2005), which has been used to confirm a Jeerinah–Carawine correlation, with the previous Pb–Pb carbonate dates regarded as due to a younger recrystallization event. However, the common occurrence of inherited zircons in thin tuffaceous layers suggests that this correlation is not yet 100% confident.

As you drive out from the windmill, there is a wide flat valley on the right. This is a Permian glacial valley, which is strewn with striated and faceted exotic boulders (Fig. 50c,d).

Locality 5.8: Tumbiana Formation stromatolites at Meentheena (Zone 51K, 229656E 7640541N)

Return to the Ripon Hills Road and turn right, heading west back towards Marble Bar. Proceed for ~46 km, then turn left onto a dirt track (236392E 7650525N). Follow the track south for ~5 km to the old buildings and stay right, heading southwest for a further 6.8 km to a turnoff on the left (230025E 7642801N). Follow this track south for ~2.6 km to a gate. Pass through the gate, then drive offtrack, uphill to the northwest, for about 500 m and park the vehicle at the top of the hill on the lip of a small gully (229649E 7640463N).

This outcrop of the Tumbiana Formation is remarkable for the size and diversity of its stromatolites, which reach a height of nearly 1.5 m within an extensive expanse of microbial mat (Fig. 51a). The large stromatolites are broad and domical, but there are all sorts of varities of morphology here, from small columnar forms (Fig. 51b), to asymmetric coniform varieties that compare closely with those seen in the Duck Creek Dolomite (e.g. compare Fig. 51c with 20c).

Return to the track and reverse your route back out to the Ripon Hills Road. Turn left and drive to Marble Bar.

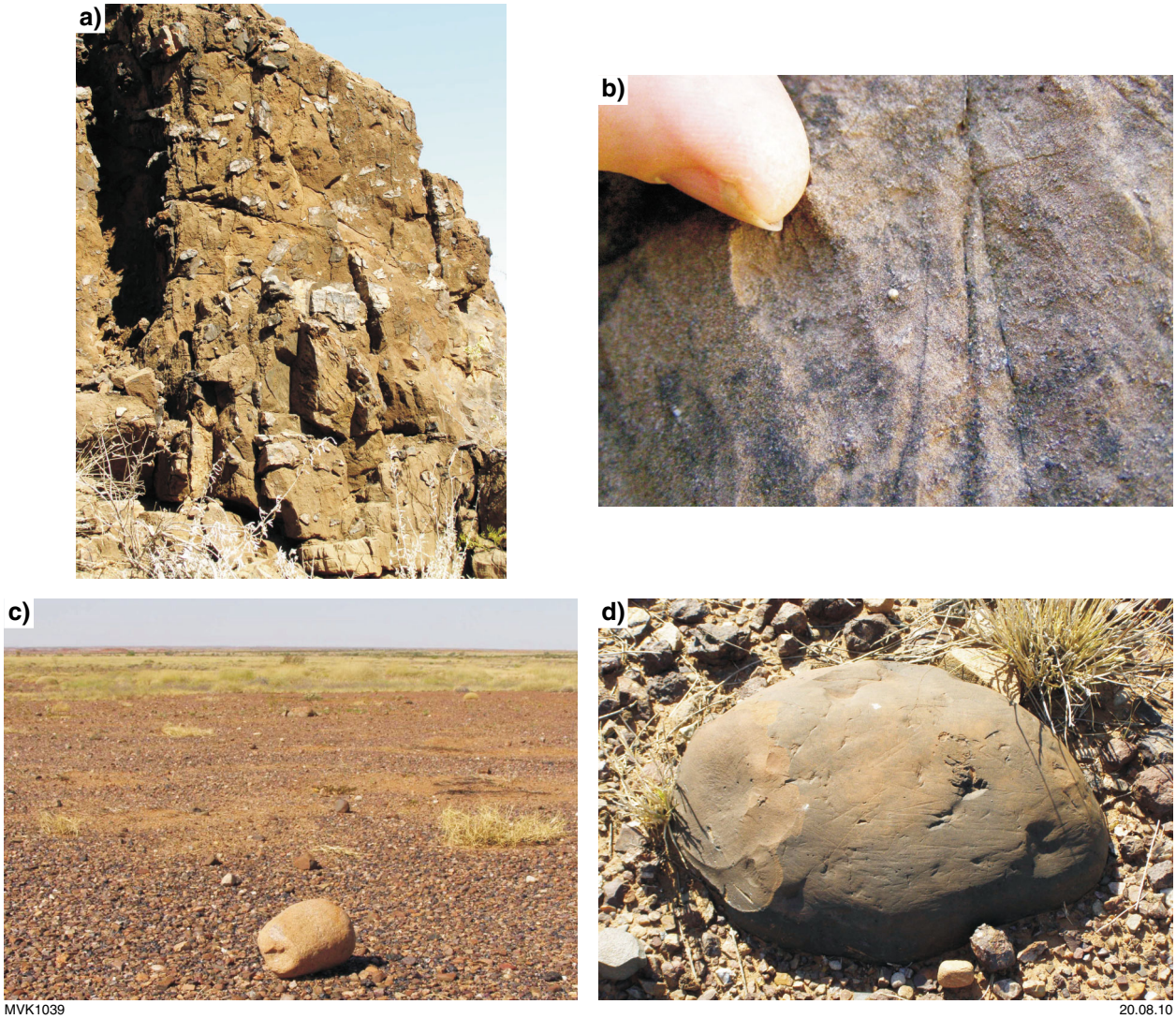

Figure 50. Outcrop features of Excursion Locality 5.7: a) overview of the impact-generated breccia in the Carawine Dolomite, consisting of angular chert fragments in carbonate matrix, overlying bedded carbonate (pale brown at bottom of photograph). Note the weak imbrication of chert clasts; b) close-up view of the carbonate matrix in a), showing impact spherule with K-feldspar altered outer rind; c) view to the east, overlooking the Permian glacial valley strewn with glacially-transported debris, including polished, well-rounded boulders of granite derived from hundreds of kilometres away; d) striated boulder in the Permian glacial valley.

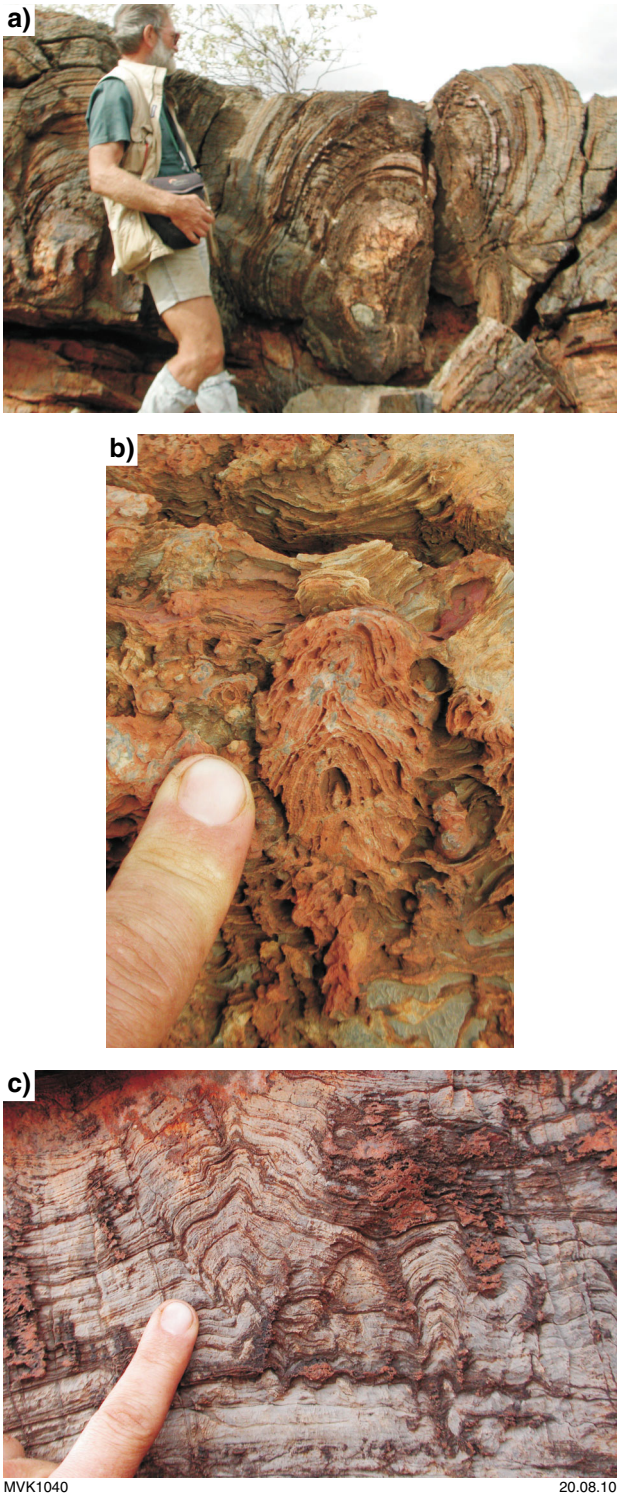

Figure 51. Stromatolites of the Tumbiana Formation at Meentheena: a) giant domical form; b) tiny columnar form; c) asymmetrical conical form, with isopachous lamination (compare with Figures 20c–f).

Day 6: The Paleoarchean Pilbara Supergroup

From the Ironclad Hotel, head west along the main street for 600 m, past the government offices, and turn left at the sign to Marble Bar Pool. Follow the sealed road for 860 m and turn right, following the sealed road towards The Marble Bar. Proceed for 2.1 km and then turn hard right onto a dirt track leading to Chinaman Pool. Follow the track to its furthest point, where it loops back on itself, and park the vehicle (Zone 50K, 781736E 7655642N). From here we will undertake a 1 km long traverse south along the bank of the Coongan River.

Locality 6.1: Traverse across the upper Duffer Formation, including the Marble Bar Chert Member, along the Coongan River (Zone 50K, 781600E 7655400N to 781400E 7654400N)

This traverse along the east bank of the Coongan River starts in felsic agglomerate or volcaniclastic conglomerate (or both) at the upper contact of the Duffer Formation (**Locality 6.1a** on Fig. 52). The rock consists predominantly of coarse, angular to subangular clasts of porphyritic dacite in a fine-grained dacitic matrix, but laso includes scattered, rounded chert fragments (Fig. 53). As you wander over the outcrop, notice crude bedding in some packages that is locally at a distinct angle to bedding in adjacent packages, suggesting large-scale slumping.

Heading upstream to **Locality 6.1b**, we reach the contact between felsic volcaniclastic rocks and the discontinuous unit, about 3 m thick, of centimetre-layered, blue, white, and red chert of the Chinaman Pool Chert Member of the Duffer Formation. These rocks are cut by dolerite sills with sheared margins. The chert dips 80° east-northeast and, as seen from pillow structures in overlying basalt, is overturned.

Continuing upsection, you pass through a unit of pillowed, variolitic komatiitic basalt (**Locality 6.1c**) that has well-preserved textures, including small vesicles around pillow margins, crackle rinds, interpillow hyaloclastite, and way-up structures defined by pillow tops and tails, despite minor to moderate flattening. The pillows are slightly overturned and dips to the east-northeast, but face west. Continuing south, the pillows become increasingly altered, with bleached pillow rinds and gas cavities filled by carbonate and quartz. At the southern end of the platform is a thick, almost undeformed dolerite sill.

Across the parking lot at Marble Bar Pool is the well-known, water-polished outcrop of blue, white, and red layered chert known as 'The Marble Bar' (**Locality 6.1d**; Figs 52, 54, 55). The Marble Bar Chert Member is composed of three distinct colour varieties that are interlayered at a centimetre to decimetre scale: thinly bedded jasper, milky-white chert, and blue-black chert

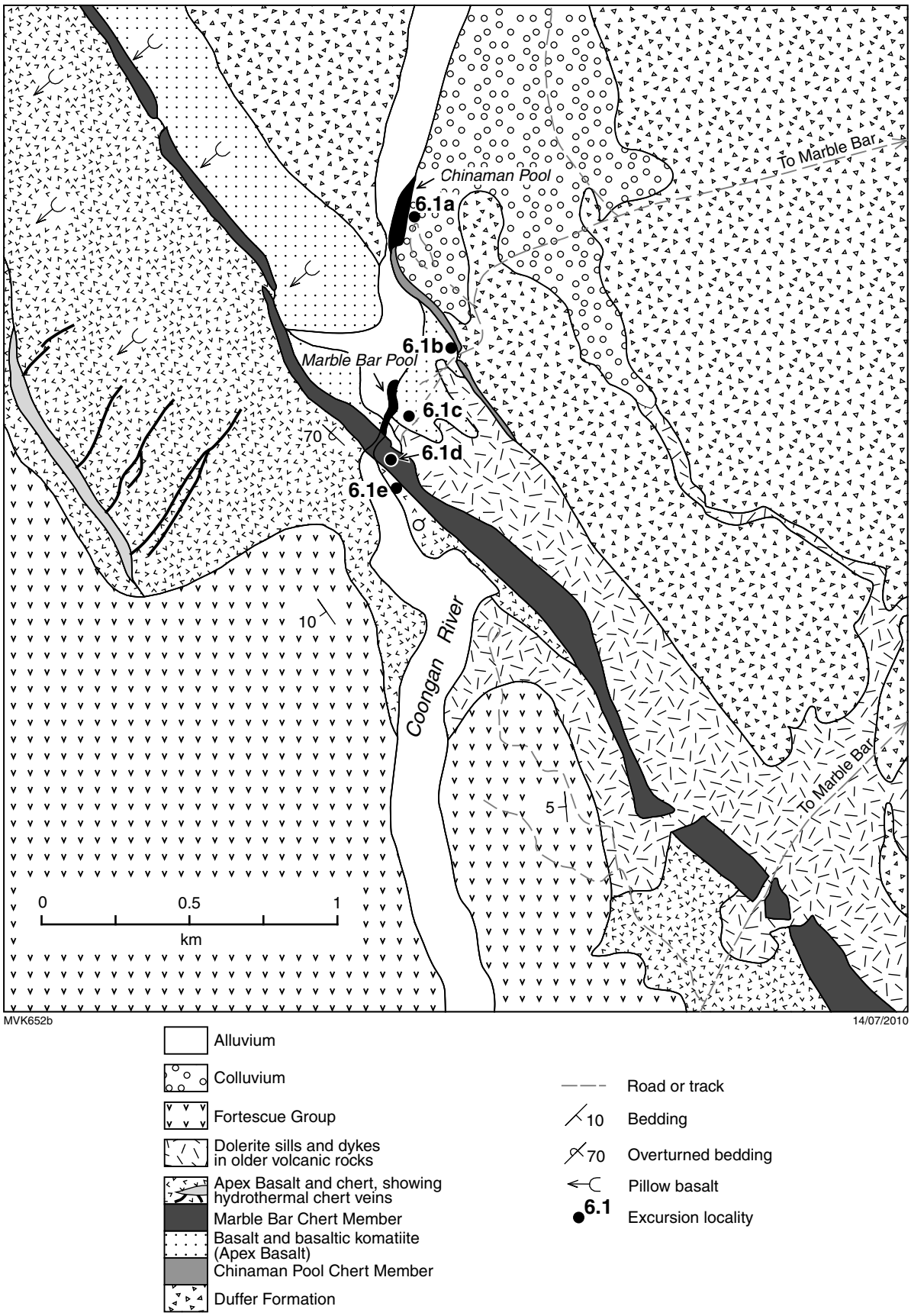

Figure 52. Geological map of the area around Marble Bar and Chinaman pools on the Coongan River, showing excursion localities.


MVK1041 20.08.10

Figure 53. Dacitic volcaniclastic breccia of the Duffer Formation, with rounded clast of jaspilitic chert.

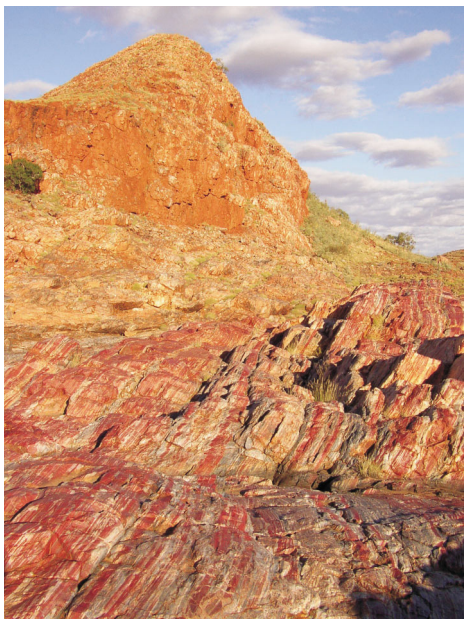
MVK1042 20.08.10

Figure 54. The Marble Bar.

(Fig. 55). At Marble Bar Pool, jasper is only present in the top third of the unit, although along strike where hydrothermal veining is less prevalent, bedded jasper comprises nearly all of the member. The lower parts of the chert at this locality are composed of more massive white and blue-black chert, and all of the chert is transected by veins of white, grey, and black chert. Jasper is bedded at a millimetre scale, defined by slight changes in colour and the degree of faint granularity (Fig. 56a). The fine layering of the jasper indicates deposition under quiet-water conditions, and the presence of pillowed basalts above and below suggests that this was probably in a deep-marine setting.

At the basal contact of the chert, altered massive volcanic rocks are cut by an anastomosing network of weakly folded, massive blue-black chert veins (Fig. 56b). Near the basal contact of the chert, the veins contain numerous fragments of the country rock, many with a jigsaw-fit, consistent with phreatic brecciation during instantaneous, explosive boiling of hydrothermal fluids. Some of these veins extend up into the layered chert as breccia veins (Fig. 56c), some of which become quite large, up to 12.5 m wide.

The white chert forms centimetre-thick layers spaced at irregular intervals through the jasper, but is not bedded (Fig. 56a). Characteristically, the white chert forms lenses in the jasper, often with pinch-and-swell structures, and in many places bedded jasper strikes directly into, and is replaced by, white chert (Fig. 56a), much of which emanates sideways, out from white to grey chert veins (Fig. 56d). In places, the white chert is clearly intrusive into the red jasper chert, but elsewhere represents the product of in situ chemical replacement of the jasper chert (Van Kranendonk, 2006). Bedding-subparallel breccia horizons in the layered white and jasper chert are composed of elongate, angular fragments of white chert within a homogeneous matrix of remobilized, homogeneous jasper or blue-grey chert. Detailed mapping (Fig. 55), shows that these horizons emanate out from discordant chert veins and thus represent the products of silica-saturated fluids emplaced into the chert under high fluid pressures, rather than sedimentary deposits.

The top contact of the chert is in contact with overlying, beautifully preserved pillow basalt of the Apex Basalt (**Locality 6.1e**; Fig. 52). Pillows commonly contain one or more pillow shelves. No chert veins extend up through the chert into the pillow basalt, indicating that deposition of the basalt occurred *after* chert veining.

Locality 6.2: The Schopf microfossil locality in chert of the Apex Basalt (Zone 50K, 780140E 7656013N)

Walk from Marble Bar Pool across the Coongan River, heading west. Round the hill of Marble Bar Chert on your right and continue northwest along the valley for 1.7 km to where a ridge of chert is transected by Chinaman Creek (Zone 50K, 780140E 7656013N).

At this locality (Fig. 57), Schopf (1993) described three-dimensional microfossils, cellularly permineralized in subangular to subrounded siliceous sedimentary clasts, <1 mm to a few mm in diameter, within a siliceous matrix. The host chert was described as containing clasts of other rock types, including possible stromatolites and lithic

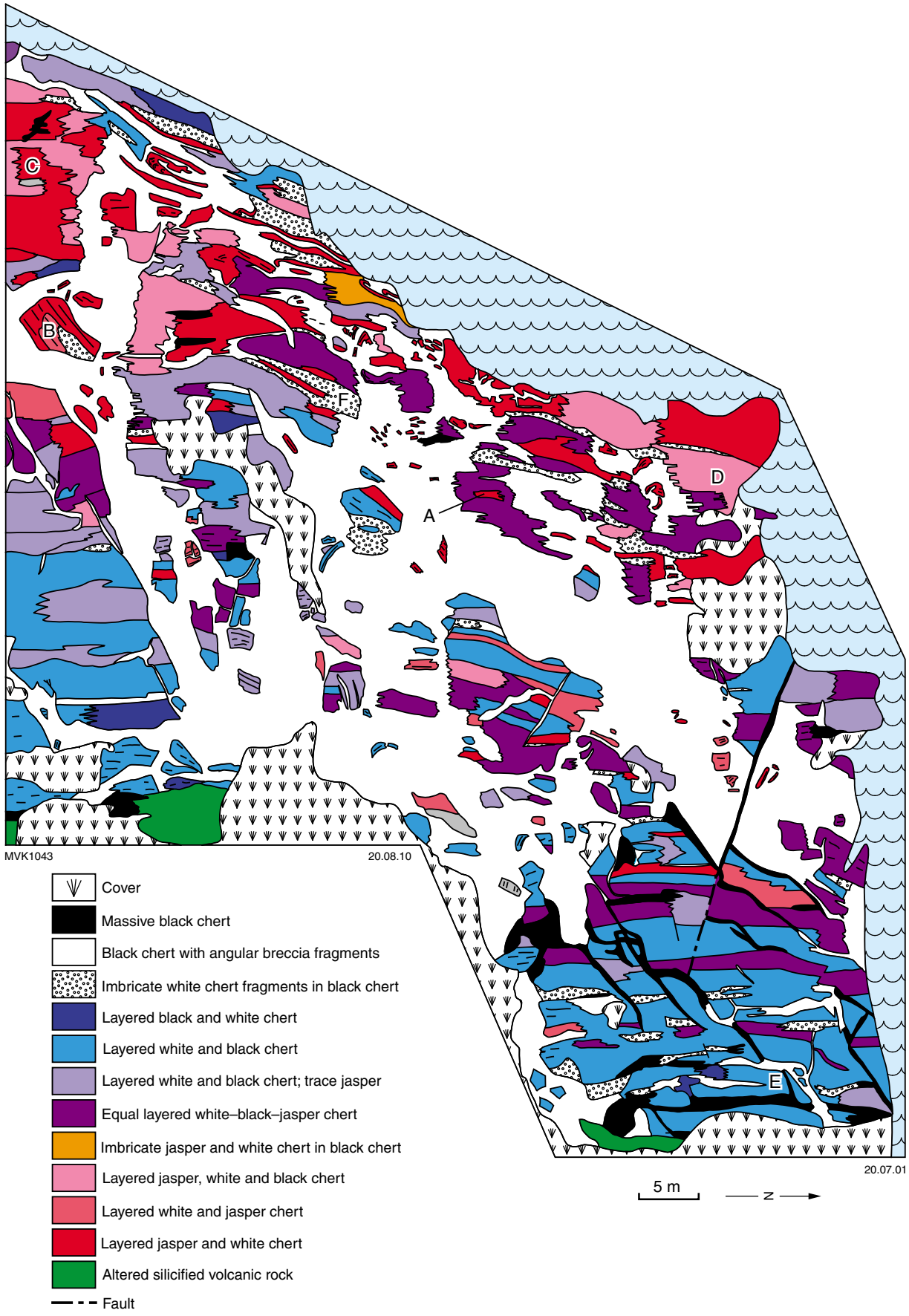

Figure 55. Geological map of the Marble Bar Chert Member on the east bank of Marble Bar Pool, at Excursion Locality 6.1d (from Van Kranendonk, 2006).

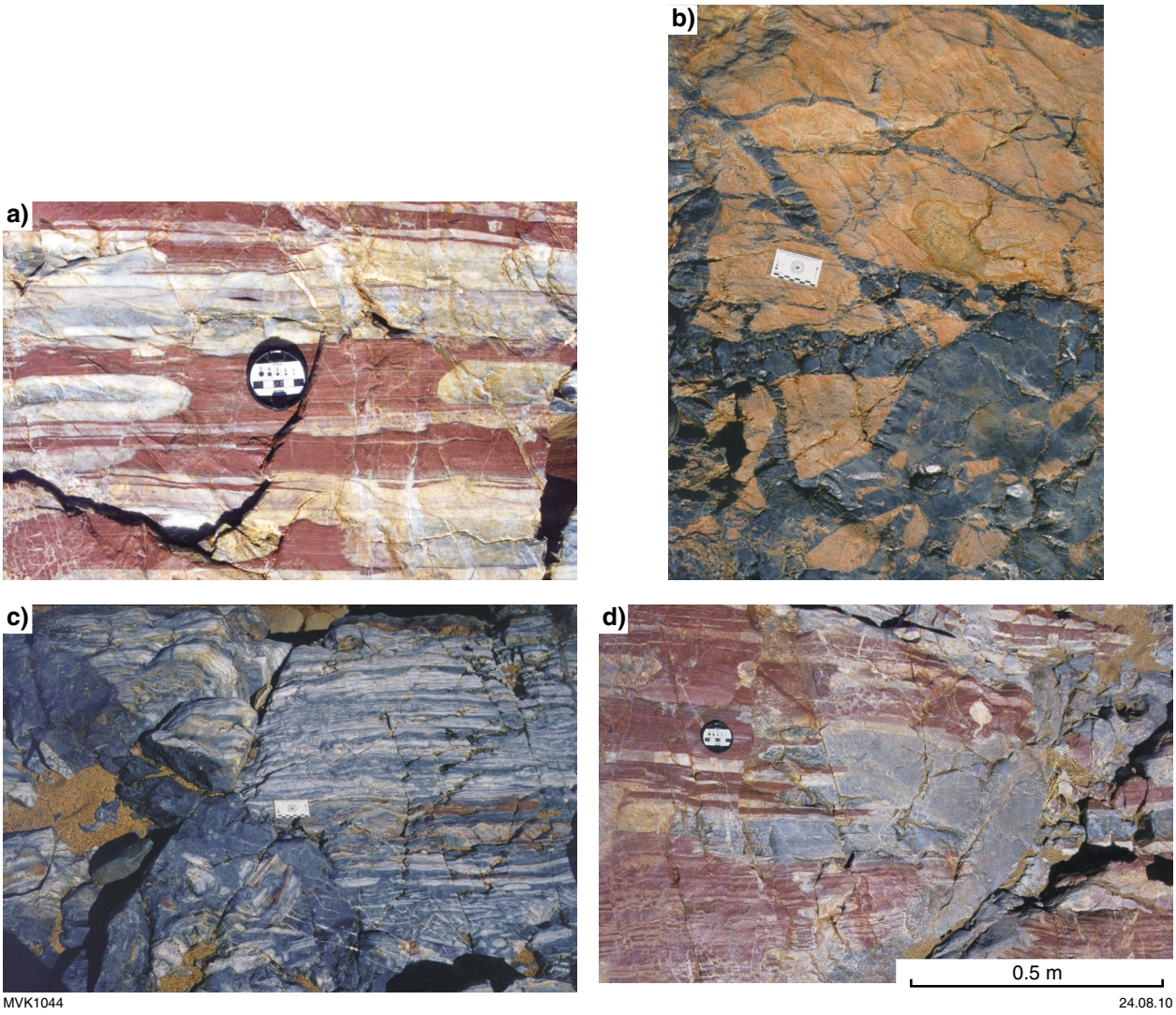

Figure 56. Outcrop features of the Marble Bar Chert Member at Excursion Locality 6.1d: a) bedded jaspilitic chert intruded or replaced by sills of white chert; b) network of black hydrothermal chert veins cutting through and breaking up Duffer Formation host rock immediately beneath the Marble Bar Chert; c) black hydrothermal chert breccia vein cutting through the Marble Bar Chert; d) sills of grey and white chert emanating out from a crosscutting central feeder vein.

clasts. The variety of clasts, combined with observations of bedding and crossbedding in nearby chert exposures, were used to interpret the host rock protolith as silicified clastic sediment.

However, a return visit to the site in 1999 with WJ Schopf and a host of leading early-life experts from around the world, and a photograph of the discovery site, revealed that the sample with putative microfossils came from a hydrothermal chert breccia vein from approximately 25 m *below* the unit of bedded chert at the creek. This threw wide open the question of biogenicity of the reported microfossils (Brasier et al., 2002; Garcia Ruiz et al., 2003). Significantly, the microfossiliferous sample was the only one of several collected from cherts in the local vicinity that contained microfossils, including several collected from the bedded black chert (JW Schopf, 1999, personal comm.).

The bedded chert unit that crosses Chinaman Creek here is the stratigraphically lowest of five bedded chert units within the 3 km thick, pillowed Apex Basalt in the Marble Bar greenstone belt (Fig. 58; Van Kranendonk, 2006). The bedded chert unit reaches a maximum of c. 25 m in thickness, and comprises centimetre-bedded, silicified, felsic volcaniclastic tuffs interlayered with sub-concordant layers of black hydrothermal vein chert and overlying pebble to cobble conglomerate with rounded clasts of a variety of volcanic rocks and chert (Brasier et al., 2005). Along strike to the north, the bedded chert forms a series of lenses bridged by thin zones of silicified basalt, interpreted to reflect chert accumulation in depressions in the surface topography of the underlying basalt (Van Kranendonk and Pirajno, 2004). Individual bedded chert lenses are each underlain by a set of weakly radiating, blue-black hydrothermal chert veins that cut up through the underlying basalt for a distance of up to 750 m

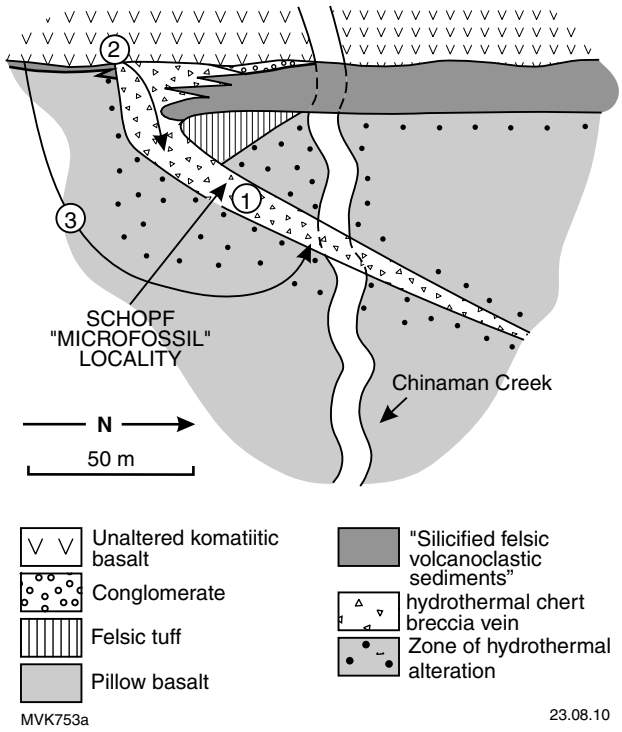

Figure 57. Simplified geological map of the Schopf locality at Chinaman Creek (Excursion Locality 6.2). 1, 2 and 3 represent different possible pathways for microbes to be entrained into hydrothermal breccia vein (from Van Kranendonk, 2007).

(Fig. 58; Van Kranendonk and Pirajno, 2004; Brasier et al., 2005; Van Kranendonk, 2006). None of these veins penetrate into the overlying basalt, indicating that their formation coincided with deposition of the bedded sedimentary rocks (cf. Van Kranendonk and Pirajno, 2004). Similar sets of syndepositional hydrothermal chert veins occur immediately beneath each of the other bedded chert units throughout the higher parts of the Apex Basalt (Fig. 58), indicating a repeated process of hydrothermal circulation between volcanic flow events.

Black chert in the bedded chert unit is demonstrably replaces fine-grained clastic sediment, as traces of ripple-laminated cross bedding are locally preserved in the chert and more massive chert layers locally cut across bedding. Elsewhere, centimetre-bedded blue-black and white-layered chert of primary depositional origin forms mounds over the outlets of the largest hydrothermal chert feeder veins in the footwall, and passes gradually along strike into, and interfingers with, centimetre-bedded felsic volcaniclastic tuffs (Fig. 59a; Van Kranendonk, 2006).

Chert feeder veins have sharp intrusive contacts with the country rocks and commonly show internal breccia textures generated by multiple phases of silica veining (Fig. 59b). The tops of the veins are characterized by breccias that consist of angular fragments of the host rock that have jigsaw puzzle fit in a network of black silica veins (Fig. 59c), very similar to the textures observed at the base of the Marble Bar Chert at the previous stop. The veins themselves are composed of several phases of intrusive silica that change colour from very dark blue-black, through shades of blue-grey, to white. Each successive chert phase cut through the previous generation, spalled off pieces of the older phases, and milled them to various degrees of roundness.

The larger chert veins commonly contain fragments of bedded chert and tuff, derived from the silicified bedded 'chert' unit overlying the veins, to depths of up to 750 m below the paleosurface (point 'A' in Fig. 58). With increasing depth in the vein, the downward-entrained fragments become more rounded, indicating a higher degree of mechanical milling and/or chemical erosion (Fig. 59d; Van Kranendonk, 2006). Such downward entrainment of surface clasts commonly occurs as a result of episodic infill of voids left by phreatomagmatic explosions created when rising gas dissolved in hot fluids from degassing magma chambers mixes with cold groundwater in fluidized breccia pipes, such as occurs in many types of vents and diatremes (e.g. Lorenz, 1986). An alternative origin is entrainment of the fragments through vigorous downward convection during hydrothermal fluid flow in these veins, by analogy with sites of downward fluid flow that occur near episodic gas vents in the Pacific Ocean off Cascadia (Tryon et al., 1999).

Both the bedded chert lenses and associated sets of radiating hydrothermal chert–barite veins are bounded by conjugate sets of listric normal growth faults in the underlying volcanics that contain the thickest chert veins (Fig. 58). Some of the growth faults were long-lived structures, such as those bounding the central lens of the Apex Chert that offset the underlying Marble Bar Chert Member and felsic volcanic rocks of the Duffer Formation with a progressively greater amount of displacement down section — from zero metres in the Apex Chert, to 150 m in the Marble Bar Chert Member, to 350 m in the upper volcanic part of the Duffer Formation (Fig. 58).

The chert breccia vein that hosts the putative microfossils strikes at a low angle to well-bedded cherts higher up, cuts through a thin lens of unsilicified felsic tuff underlying the chert, and contains several fragments of the tuff together with earlier silica phases in a silica matrix that displays macroscopic brecciation, or pseudo-clastic texture (Fig. 59b). Close inspection of the brecciated texture shows that it is the result of multiple injection of various intrusive chert phases, the colour of which progressively changes from very dark blue-black through various shades of blue-grey, to white (Van Kranendonk, 2006). Each successive phase of silica cut through and brecciated the previous phase, producing a range in roundness of fragments of the older phases. The resultant intrusive chert breccia has a broad textural similarity with poorly sorted, coarse, clastic sedimentary rocks, but can be differentiated on the basis of having a matrix of intrusive silica and generally angular clasts formed due to near-instantaneous, explosive degassing of hydrothermal fluids (phreatomagmatic explosion).

Brasier et al. (2002) described hydrothermal minerals from the veins and altered basaltic host rocks beneath the bedded chert-tuff unit, including barite, alunite–jarosite,

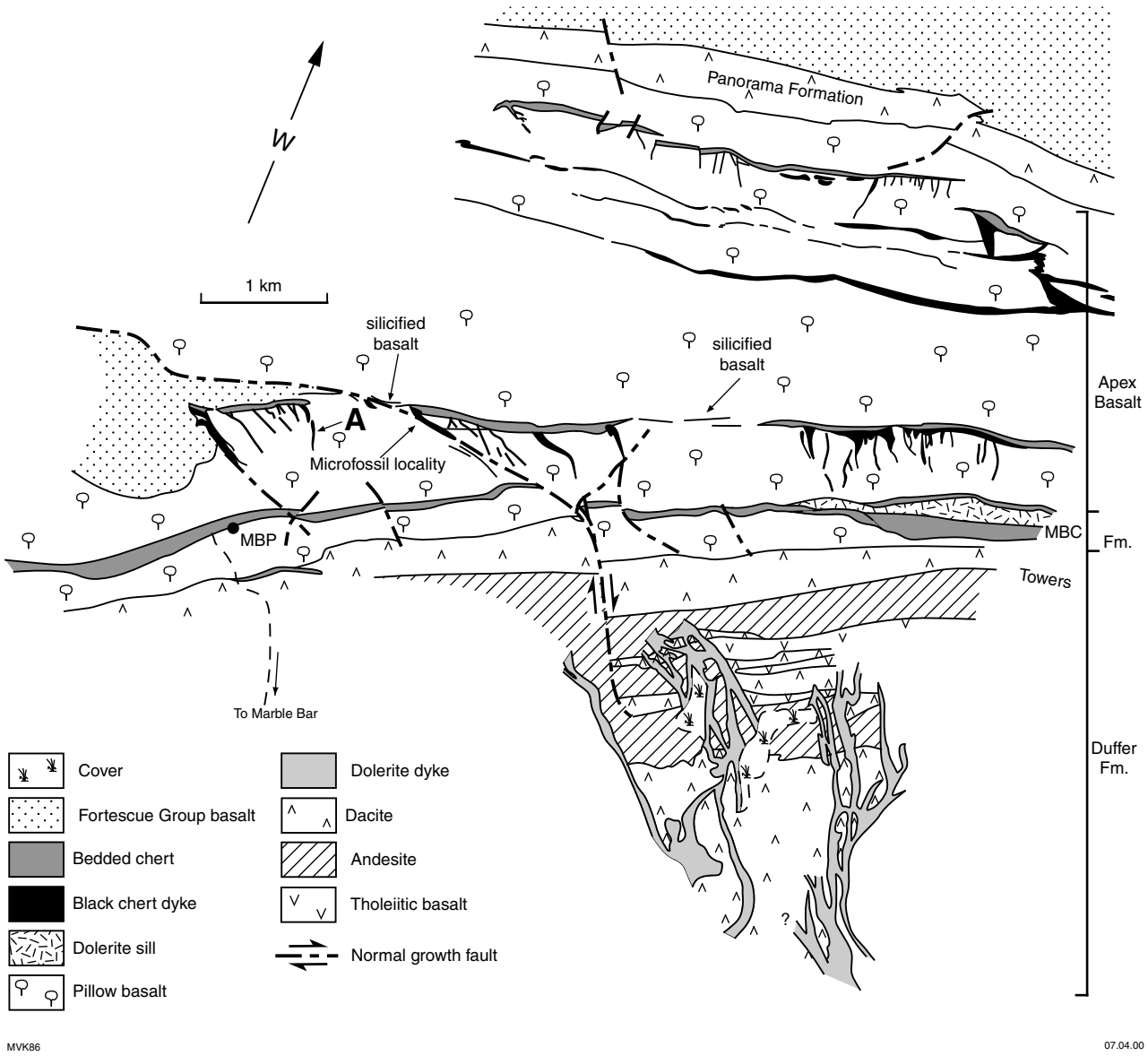

Figure 58. Geological map of part of the Marble Bar greenstone belt west of Marble Bar, showing the location of the Schopf locality. 'A' marks the point where surface clasts of bedded chert occur deep in a hydrothermal chert vein. MBP = Marble Bar Pool.

Al- and K-rich phyllosilicates from hydrothermally altered feldspars, and trace amounts of native metals (Fe, Ni, Cu, Zn, Sn). This mineral assemblage is similar to that associated with hydrothermal alteration that was active during Cenozoic arc volcanism in Antarctica (Willan and Armstrong, 2002), and can be used to deduce relatively high hydrothermal temperatures of alteration (c. 250–350˚C). The distribution of the bedded chert as a series of lenses on hydrothermally altered basalt, combined with evidence that lenses of bedded chert were fed by swarms of hydrothermal feeder veins within an otherwise continuous sequence of pillow basalts, suggests chert deposition within a submarine hot spring environment (Van Kranendonk and Pirajno, 2004). The chert veins that underlie the northernmost chert lens of the 'microfossil'-bearing Apex chert in Figure 58 occur above a dolerite sill that splits apart the Marble Bar Chert Member. Such sills are common throughout the volcanic stratigraphy of the Warrawoona Group and are interpreted here to be the heat source that drove hydrothermal circulation in the overlying host rocks.

Brasier et al. (2002) pointed out that the mode of occurrence of the putative microfossils in a silica breccia vein, together with the much more complicated structures of many of the 'microfossils', indicated that they were unlikely to be of biogenic origin, a conclusion supported by experimental work on inorganic structures formed from mixing of fluids (Garcia-Ruiz et al., 2003).

However, detailed analysis of the putative microfossils using laser-Raman analysis of kerogen supports a biogenic origin (Schopf et al., 2002), although these data were not enough to convince the sceptics since it has been

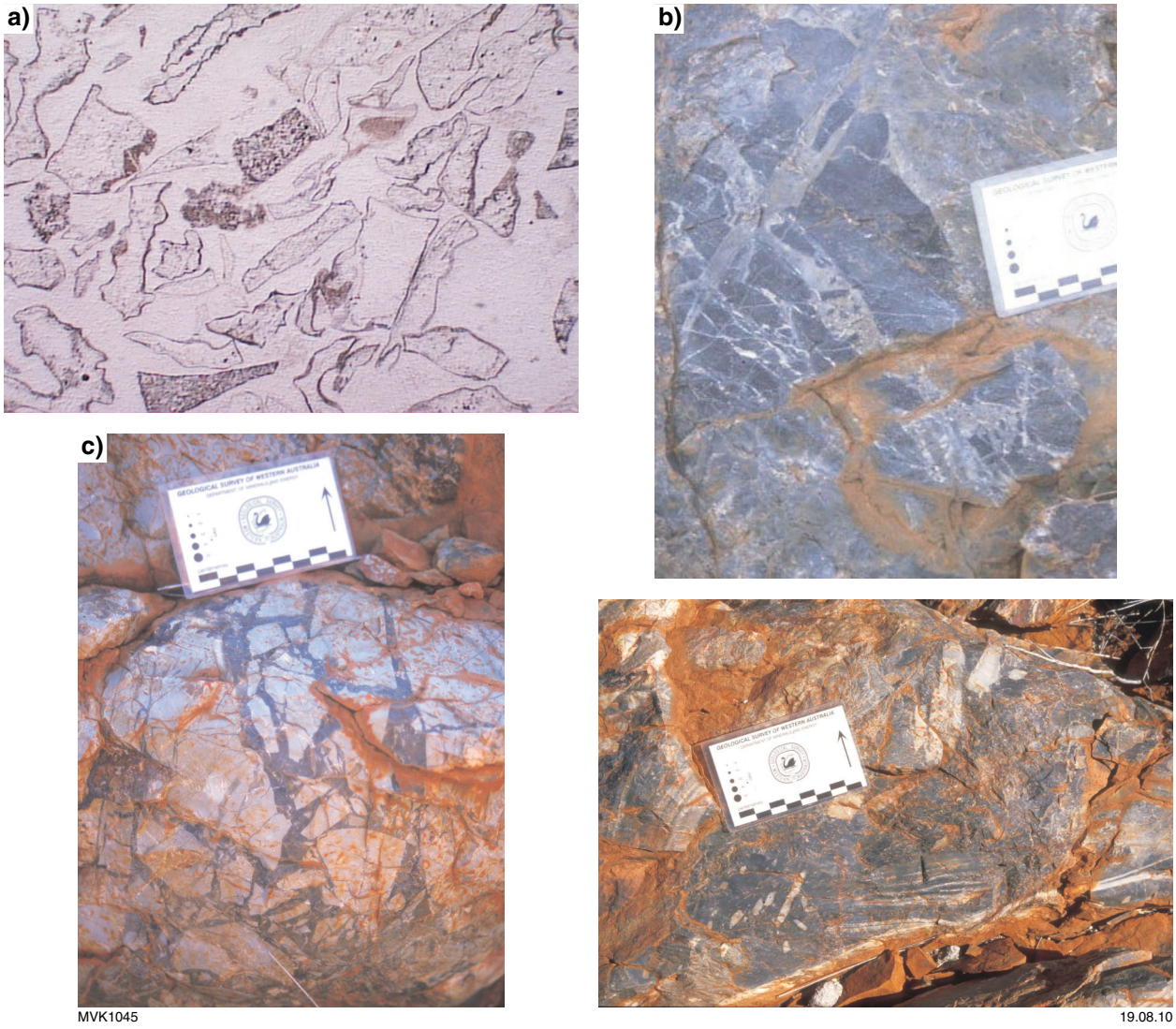

Figure 59. Features of the Schopf locality at Chinaman Creek (Excursion Locality 6.2): a) photomicrograph (plane-polarized light) of the unsilicified felsic tuff beneath bedded chert (width of view = 2.5 cm); b) hydrothermal chert breccia vein near the microfossil sample locality, showing the formation of 'clasts' through multiple generations of hydrothermal brecciation; c) breccia with jigsaw puzzle fit of pieces of the host rock, surrounded by hydrothermal vein chert, from the top of the chert vein where it meets bedded chert; d) thermally eroded fragments of bedded chert from the paleosurface, entrained well down within a hydrothermal chert vein (point 'A' on Fig. 58).

suggested that such values may also be obtained through inorganic processes such as Fischer–Tropsch synthesis (Brasier et al., 2004). Nevertheless, it should be noted that '…Fischer–Tropsch distribution of the light alkanes has never been observed in natural gases, including volcanic and hydrothermal gases. Instead, the distribution of light alkanes in terrestrial gases is very similar to those obtained in experiments on thermal decomposition … of kerogen' (Taran and Giggenbach, 2003, p. 72). In order to counter claims that the microfossils were artifacts of crystal growth processes, Schopf et al. (2007) showed that quartz crystals grew across the kerogenous microstructrures and did not affect their shape, further supporting a biogenic origin.

If some of the putative microfossils prove to be of biogenic origin, as argued by Schopf et al. (2002, 2007), then there are three ways that they may have been incorporated into the silica breccia vein (Fig. 57; Van Kranendonk, 2007). One is that the organisms inhabited the veins themselves during relatively cool periods, as is known to occur in some modern environments (① on Fig. 57; e.g. Onstott et al., 1998). Another possible mechanism is through downward entrainment of surface organisms in a fluidized gas-solid and/or vigorously convecting hydrothermal system (② on Fig. 57). Alternatively, microbes may have been transported into the veins from their habitat within the host pillow basalts by circulating hydrothermal fluids (③ on Fig. 57).

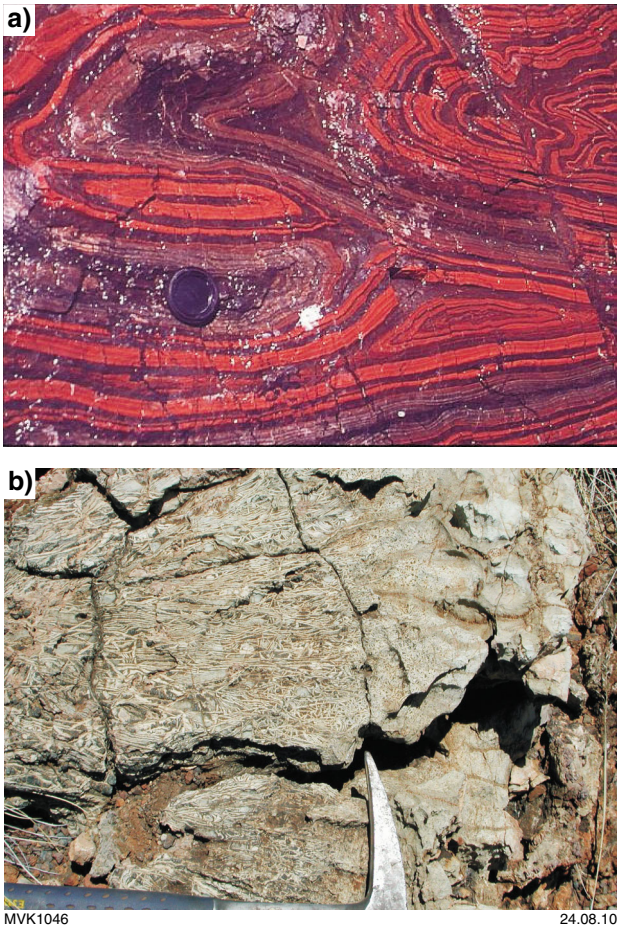

Figure 60. Outcrop features of the geology at Coppin Gap (Excursion Locality 6.3): a) sheath fold in c. 3 Ga banded iron-formation of the Cleaverville Formation; b) olivine spinifex texture in c. 3.35 Ga komatiite of the Euro Basalt.

Locality 6.3: Coppin Gap; Mesoarchean BIF and komatiite (Zone 51K, 200258E 7687994N)

Head back out from Marble Bar Pool onto the sealed road and return to town, first turning left at the T-junction, then right at the next T-junction. Drive through town for 870 m, past the Government offices on your left. At the Ironclad Hotel,set your odometer to 0.0 and continue east, out of town, towards Port Hedland. After 35 km along the main highway, turn right onto a dirt road (Zone 50K, 795546E 7681344N). Crossing the Talga Talga River, proceed for ~15.2 km and turn right onto another dirt road (Zone 50K 810276E 7683740N).Proceed along this road for ~12 km and take the turn left onto the track that leads to Coppin Gap and the Spinifex Ridge Moly Mines project (Zone 51K 197167E 7682451N). Follow this road for 6.3 km, keeping to the right, and park in the gravel car park at the entrance to Coppin Gap.

The spectacular Coppin Gap is a deep river valley that cuts through a ridge of c. 3.0 Ga banded iron-formation belonging to the Cleaverville Formation of the De Grey Supergroup, a thick succession of dominantly sedimentary rocks that unconformably overlies the Pilbara Supergroup (Van Kranendonk et al., 2007a). The rocks here have been strongly deformed into tight folds (including sheath folds; Fig. 60a) within the core of a tight syncline between the Muccan Granitic Complex to the north, and the Mount Edgar Granitic Complex to the south, the northern part of which we drove through to get here.

Back at the car park, if you walk up onto the white rubbly outcrops on the eastern side, you will see extremely well preserved, but completely carbonate-altered, komatiites of the c. 3.35 Ga Euro Basalt of the Kelly Group (Pilbara Supergroup; Fig. 60b). Individual komatiite flows may be recognized by changes in size and orientation of the olivine spinifex texture.

Return to the Marble Bar–Port Hedland Road and turn right. Proceed north along the highway for 60 km and turn left onto a dirt road (Zone 50K 745217E 7706795N). Continue down this track for 42 km. Where the track splits, take the left-hand fork towards Panorama Homestead. As the next two stops are of major geological significance, their precise location is not given in detail.

Day 7: North Pole Dome — c. 3500 Ma depositional environments, and early life

The North Pole Dome is a structural dome of little-deformed, dominantly mafic volcanic rocks of the Warrawoona Group, Strelley Pool Formation, and Kelly Group around a central nucleus occupied by the 3459 ± 18 Ma North Pole Monzogranite (Fig. 61; age from Thorpe et al., 1992a). Younging directions from pillows and graded bedding in volcaniclastic rocks indicate that all the rocks young away from the core of the dome in a radial pattern, although this pattern is slightly disrupted in the western half of the dome by the Antarctic Fault, a curviplanar, post-Fortescue Group structure with west-side-down displacement (Van Kranendonk, 2000). The dip of strata increases outwards from the core of the dome, from gentle dips of 40° to dips of 80°at the outer edges of the dome where remnants of younger rocks of the De Grey Supergroup and Fortescue Group are preserved (Van Kranendonk, 1999). The rocks have been metamorphosed to prehnite–pumpellyite to lower greenschist facies, although a lower amphibolite facies contact metamorphic aureole is developed around the North Pole Monzogranite.

The majority of the North Pole Dome is underlain by pillowed mafic volcanic rocks that vary from dominantly tholeiitic with N-MORB REE profiles, to some komatiitic basalts immediately overlying chert horizons at places throughout the succession. The stratigraphy of the greenstones has been modified since publication of the North Shaw 1:100 000 sheet with the oldest unit as an unnamed and undated metabasalt that surrounds the North Pole Monzogranite at the core of the dome. These metabasalts are thought to represent the lower parts of the Coonterunah Subgroup. Overlying this are two chert ± barite horizons interbedded with pillowed basalts and dolerite, collectively referred to as the Dresser Formation. Two Pb–Pb model ages of c. 3490 Ma on galena in syngenetic barite were previously cited as the age of the formation (Thorpe et al., 1992b), but recent SHRIMP U–Pb zircon dating of a felsic volcaniclastic sandstone from the top of the lowermost chert unit of the formation has yielded a maximum depositional age of 3481 ± 2 Ma, which is interpreted to closely represent the age of deposition of the unit (Van Kranendonk et al., 2008). The stratiform chert–barite units were fed by a set of chert–barite dykes that were emplaced within, and immediately above, listric normal growth faults that were active during deposition of the cherts, as seen at Locality 7.3 (Nijman et al., 1998; Van Kranendonk and Pirajno, 2004; Van Kranendonk, 2006; Van Kranendonk et al., 2008).

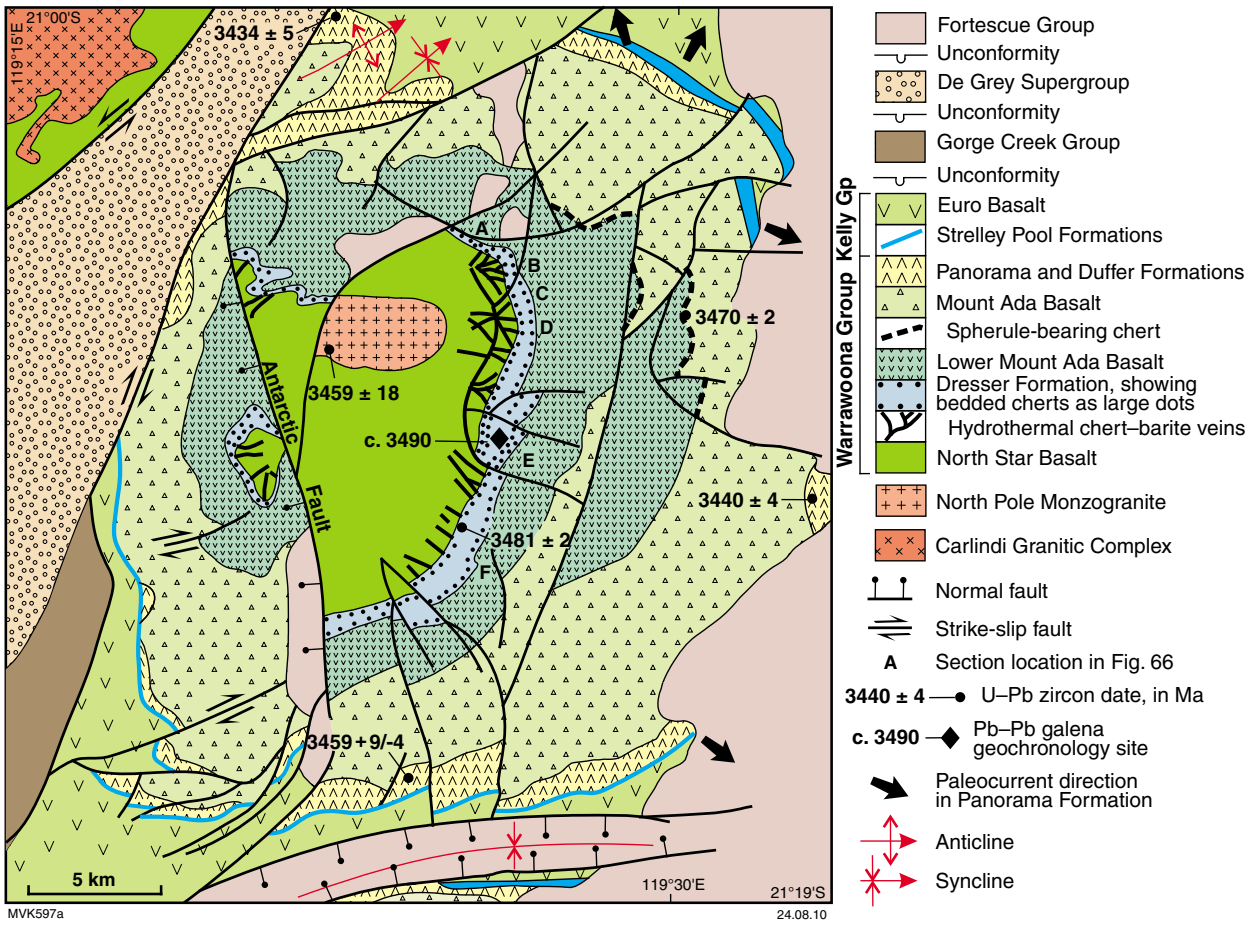

Figure 61. Geological map of the North Pole Dome, showing geochronological data.

Above the Dresser Formation lies a thick succession of mafic volcanic rocks, at least part of which belongs to the Mount Ada Basalt. This includes a thin unit of felsic sandstone and layered blue, grey, and red chert known as the Antarctic Creek Member (Van Kranendonk, 1999, 2000), and known to contain impact-generated spherules. This unit has yielded a conventional U–Pb zircon date of 3470 ± 2 Ma (Byerly et al., 2002), although this may represent the age of the target rock rather than the age of the impact event itself. Overlying this are up to 1.3 km of felsic volcanic and volcaniclastic rocks of the Duffer and Panorama Formations, including up to 150 m of the Marble Bar Chert Member in the far southeastern corner of the dome. A sample of massive rhyolite from the lower part of the felsic volcanic rocks in the southern part of the belt has been dated at 3458 ± 2 Ma, the same age as the North Pole Monzogranite (Thorpe et al., 1992a). A sample of bedded tuff with local pumice layers from the upper part of the volcaniclastic apron of the Panorama volcano in the northwestern part of the dome returned a SHRIMP U–Pb zircon date of 3434 ± 5 Ma (Nelson, 2000; Van Kranendonk, 2000).

Disconformably overlying the Panorama Formation is the Strelley Pool Formation, with its distinctive conical stromatolites (e.g. Lowe, 1983; Hoffman et al., 1999; Van Kranendonk et al., 2003). In the northeastern part of the dome, the formation lies on the underlying rocks across an angular unconformity and contains a basal unit of cobble conglomerate and quartz sandstone up to 1 km thick. Overlying the Strelley Pool Formation is the Euro Basalt, a thick succession of interbedded high-Mg and tholeiitic basalts and chert that reaches a maximum total thickness of 9.4 km in the southwestern extension of the North Pole Dome.

Locality 7.1: Earth's oldest stromatolites in the c. 3480 Ma Dresser Formation, North Pole Dome

Note: This locality of major geological significance and lies within a protected State Geological Reserve. Hammering and sample collection are not permitted.

The hill before you is composed predominantly of bedded grey and white chert of the c. 3480 Ma Dresser Formation, which dips towards you at 34° to the east. Bedding is broadly warped on east-northeasterly plunging axes, but apart from this and despite their great antiquity, the rocks have not been affected by penetrative deformation. A variety of macroscopic stromatolites can be seen at this locality, including wrinkly laminated mats, broad domes, columnar forms, and coniform varieties (Fig. 62; Walter et al., 1980; Buick et al., 1981; Walter, 1983; Van Kranendonk, 2006; Van Kranendonk et al., 2008). For 30 years, these stromatolites have been accepted as some of the best evidence of early life on Earth, although Lowe (1994) suggested that the domical morphology of the best known of the Dresser Formation stromatolites (cover of Schopf, 1983) was the result of faulting.

Silicified carbonate rocks immediately underlying the stromatolitic mats display well preserved ripples, cross-bedding, and local desiccation cracks, indicative of shallow water to periodically exposed conditions (Fig. 63a–c). Within the rippled sandstone, radiating splays of former diagenetic crystals can be observed, up to 2 cm in diameter (Fig. 63d). Buick and Dunlop (1990) suggested that the original material in these rosettes was gypsum. However, the original material of thse crystals has been dissolved or replaced by later materials, including hydrothermal aragonite with colloform banding at one locality. These later minerals are interpreted to represent the topmost, lowest-temperature part of the hydrothermal system affecting the whole of the formation, as described for localities 7.2 – 7.4 below (Van Kranendonk et al., 2008). Also visible here are diagnetic barite crystals that grew in what was still wet sedimentary bedding in carbonates and microbial laminates (Fig. 63e). Later veins of coarsely crystalline barite + silica cut through the bedded rocks, including the diagenetic rosettes.

The majority of these stromatolites are defined by wrinkly laminated material, either within millimetre-layered grey and white cherts, or very finely laminated black and red-weathering rocks. Diamond drilling beneath the weathered surface layers has shown that, whereas the cherts derive from bedded carbonate protoliths at depth (Fig. 64), the red and black laminates represent the weathered products of fresh, laminated pyrite preserved at depth, which itself represents a hydrothermal replacement of primary carbonate (Fig. 65; Van Kranendonk et al., 2008).

Several morphological traits of stromatolites indicate they are primary features that formed *during* sediment accumulation (see also Van Kranendonk, 2006). Most important of these is that irregularly laminated, wrinkly mat material is interbedded with cross-laminated clastic sediment, providing evidence that deformation was not responsible for the development of the finely laminated material or of its wrinkly texture; this observation counters the model proposed by Lowe (1994).

Additional morphological evidence for biogenicity comes from the observation of interference between two independent processes, as highlighted in Figure 62e. At this locality, it is possible to recognize the purely physical geological process of sediment transport by flowing water in the form of ripples. The second, independent, process is represented by a small dome that interferes with the ripple (arrow on Fig. 62e). This dome forms part of a larger coniform stromatolite and reflects an independent biological processes to that represented by the purely physical process that formed the ripple.

Locality 7.2: Dresser Formation 'primary' carbonate

At this locality, the lower chert unit of the Dresser Formation is only 5 m thick, exposed in a cliff on one side of a creek. Primary, bedded carbonate at the top of the cliff section has trace element geochemical signatures indicating deposition from normal seawater (Van Kranendonk et al., 2003). These carbonates have

Figure 62. **Stromatolites of the Dresser Formation at Excursion Locality 7.1: a) wrinkly-laminated microbial mat with overlying broad, domical stromatolites; b) broad, low-amplitude domical form, with wrinkly lamination; c) small columnar form, with wrinkly lamination; d) coniform stromatolites, lying immediately on rippled carbonate sandstone; e) cross-sectional view of wrinkly laminated stromatolite, with overlying rippled carbonate sandstone that is interfered with by a small domical stromatolite (arrow).**

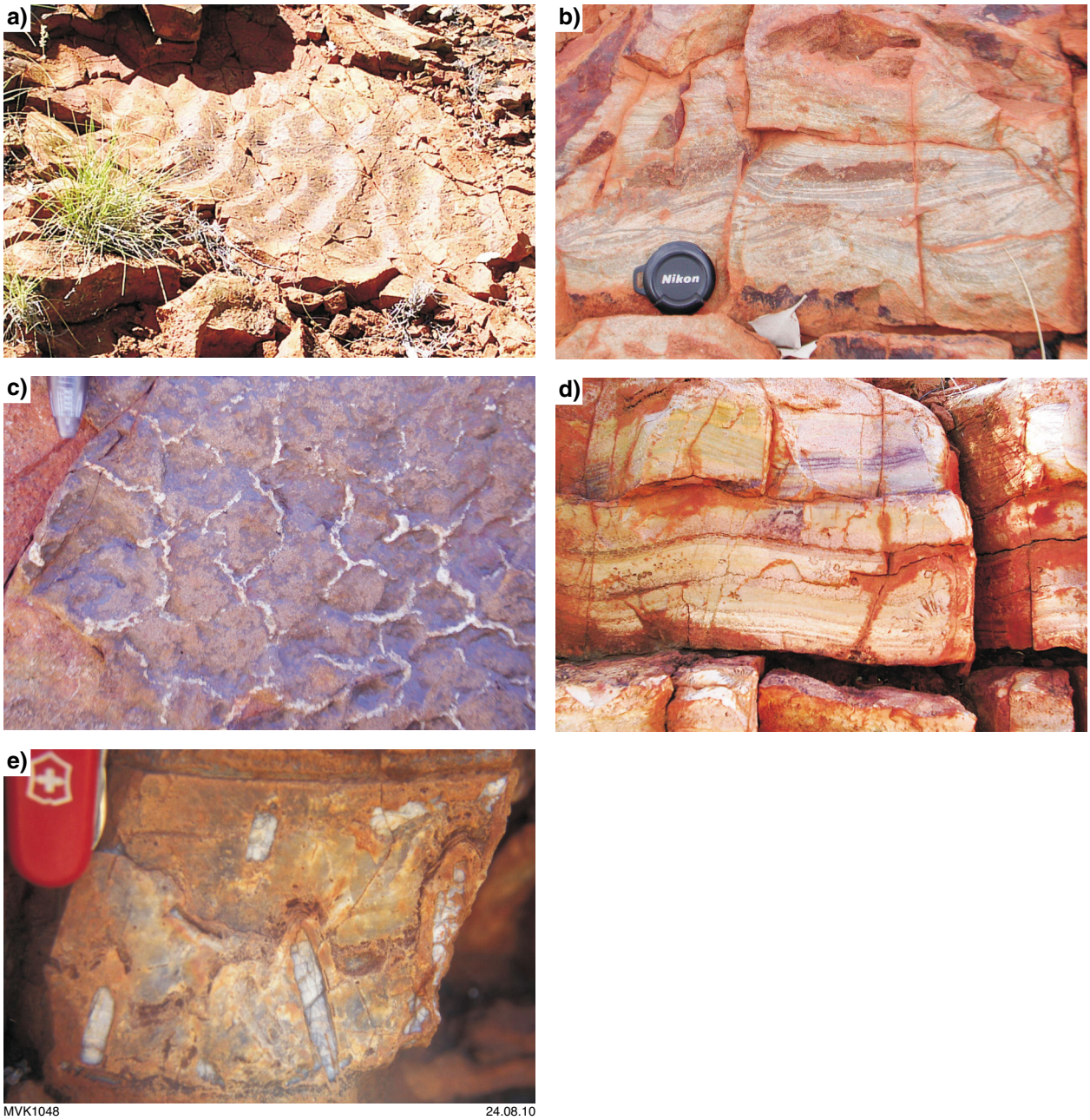

Figure 63. Features of the Dresser Formation at Excursion Locality 7.1: a) bedding-plane view of rippled carbonate sandstone; b) cross-sectional view of rippled carbonate sandstone, immediately underlying microbial mat; c) bedding surface with desiccation cracks; d) bedded carbonate with radiating crystal splays; e) diagenetic barite crystals, which grew in unlithified (wet) carbonate sediment and microbial mat.

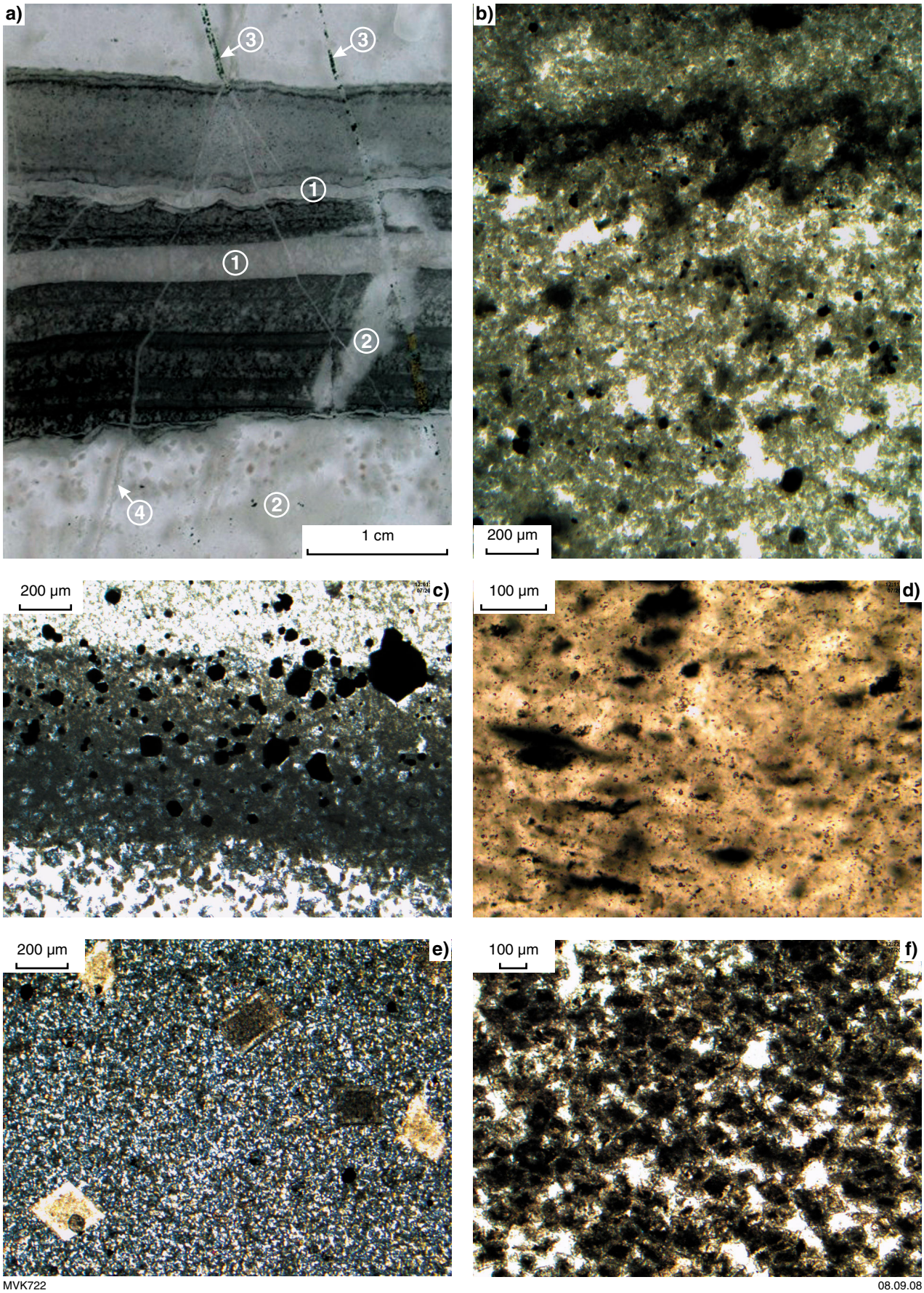
a)
3
3
1
1
2
4
2
1 cm
b)
200 µm
200 µm
c)
100 µm
d)
200 µm
e)
100 µm
f)
MVK722
08.09.08

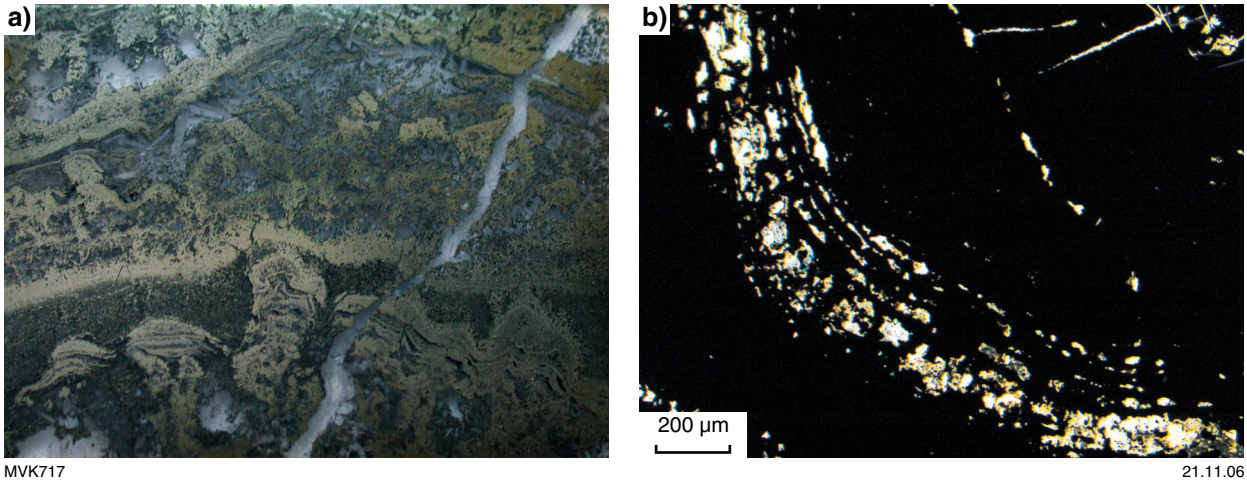

Figure 65. Features of wrinkly laminated material, as seen in PDP drillcore through the Dresser Formation: a) whole thin section view (plane-polarized light) of centimetre-scale stromatolites with wrinkly lamination completely replaced by hydrothermal pyrite (yellow) and barite (white); b) close-up view of the laminated pyrite in a), in cross-polarized light, showing relict carbonate between pyritic laminae. (From Van Kranendonk et al., 2008.)

been partly replaced by spherical radiating crystal fans (now filled by aragonite) and by light green silica in layers alternating with the carbonate (Fig. 67a). Although these green silica layers may represent original chemical precipitates, thin section petrography reveals it is more likely that they represent a hydrothermal replacement feature developed preferentially along ?more porous beds of the carbonate.

Conformably overlying the carbonates are wrinkly black laminates (Fig. 67b) similar to the stromatolites of the last locality, and correlated stratigraphically with them (Fig. 66). The stromatolitic laminates at this locality are directly overlain by basalt with large, undeformed pillows. The low strain of both the underlying and overlying rocks suggests that this is a primary depositional contact, whereas the relative thinness of the chert unit here compared with the last and next stops, suggests that this was horst block during deposition of the chert unit.

Figure 64. (facing page) Features of Dresser Formation carbonate from PDP drillcore: a) whole thin section view of bedded micritic carbonate (dark grey bands) cut by three phases of silica alteration (1–3); b) close-up thin section view of bedded micritic carbonate, showing kerogen-lined stylolite separating two beds and fenestral fabric in lower bed; c) close-up thin section view of bedded micritic carbonate, showing diagenetic pyrite (black euhedral); d) close-up thin section view of bedded micritic carbonate containing detrital clasts of organic material; e) photomicrograph (cross-polarized light) of silica-altered carbonate with zoned carbonate rhombs; f) thin section view of partly silicified carbonate, consisting of euhedral carbonate rhombs interspersed with chert (white patches). (From Van Kranendonk et al., 2008.)

In the creek bed below the cliff, highly altered basalts of the footwall are cut by black chert hydrothermal veins.

Locality 7.3: Dresser Formation, barite mound and diamictite

In a groundbreaking paper, Nijman et al. (1998) showed that the Dresser Formation was deposited during growth faulting and exhalations of sulfate- and silica-rich hydrothermal fluids. This model was further developed by Van Kranendonk (2006) who proposed that deposition was in a much more dynamic environment than previously supposed, within a low-eruptive felsic caldera setting (Fig. 68). Part of the evidence for this change of view from the previous model of deposition in quiet, shallow water lagoonal conditions (Groves et al., 1981; Buick and Dunlop, 1990) is evident at this locality.

Here, a cross-section through the chert–barite unit of the Dresser Formation is exposed. Most of the unit near the entrance to the gully consists of of gently dipping grey and white layered cherts. However, immediately along strike of the bedded cherts, deeper into the gully, is a massive block of coarsely crystalline barite and wrinkly laminate that is oriented at a high angle to the bedded cherts, which occurs together with numerous other large, subrounded to angular blocks in a coarse breccia (Fig. 69). The breccia and the bedded cherts along strike are overlain by more layered grey and white chert, the bedding of which indicates recovery from steep dips back to shallow dips, upsection. Higher up, this unit is overlain by a metre-thick unit of coarse diamictite with clasts of barite, wrinkly laminated rocks, and other lithologies (Fig. 70a). All of these rocks are cut by a 2-m wide, vertical vein of coarsely crystalline barite. Across the gully, a thick barite veins occupies a syndepositional growth fault that separates bedded cherts

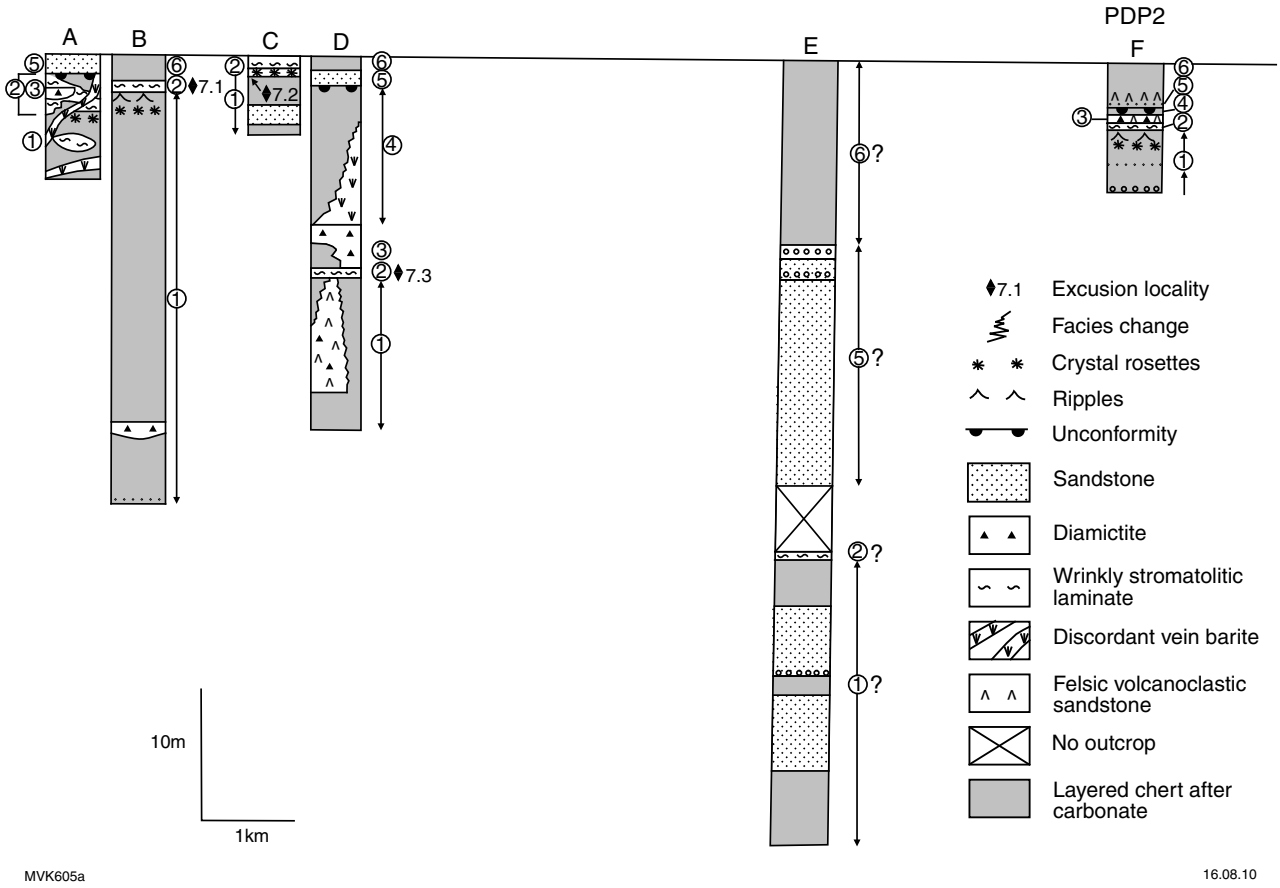

Figure 66. Stratigraphic columns through the lower, main Dresser Formation chert, showing variations in stratigraphic thickness of six identified units along strike from north to south (A–F; see Figure 61 for locations); circled numbers identify lithostratigraphic members. (From Van Kranendonk et al., 2008.)

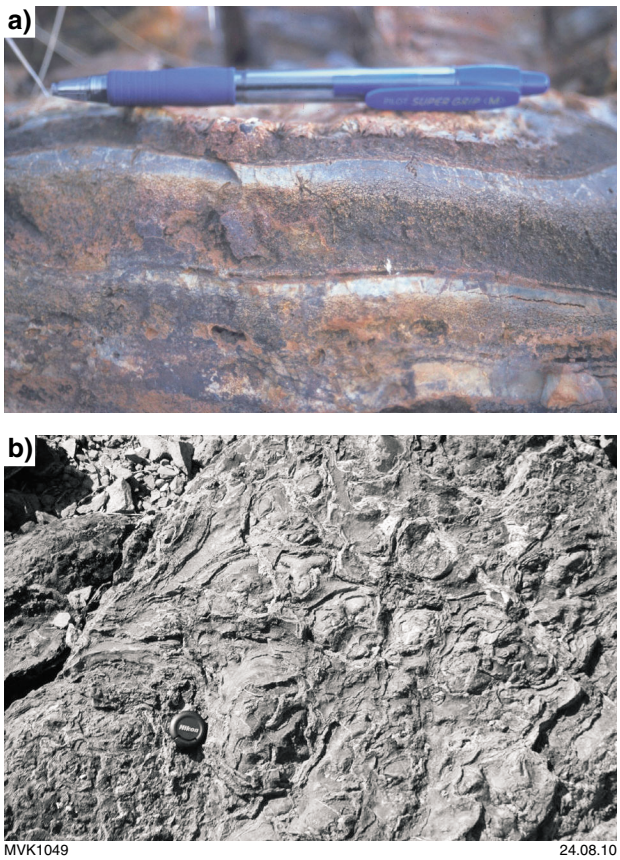

Figure 67. Features of the Dresser Formation at Excursion Locality 7.2: a) 'zebra rock' of 'primary' bedded carbonate and secondary pale green chert. Note radiating diagenetic crystal splays just beneath pen, and the flocculated lower contacts and sharp upper contacts of the green chert layers; b) bedding-plane view of wrinkly laminated stromatolite overlying the carbonate 'zebra rock'.

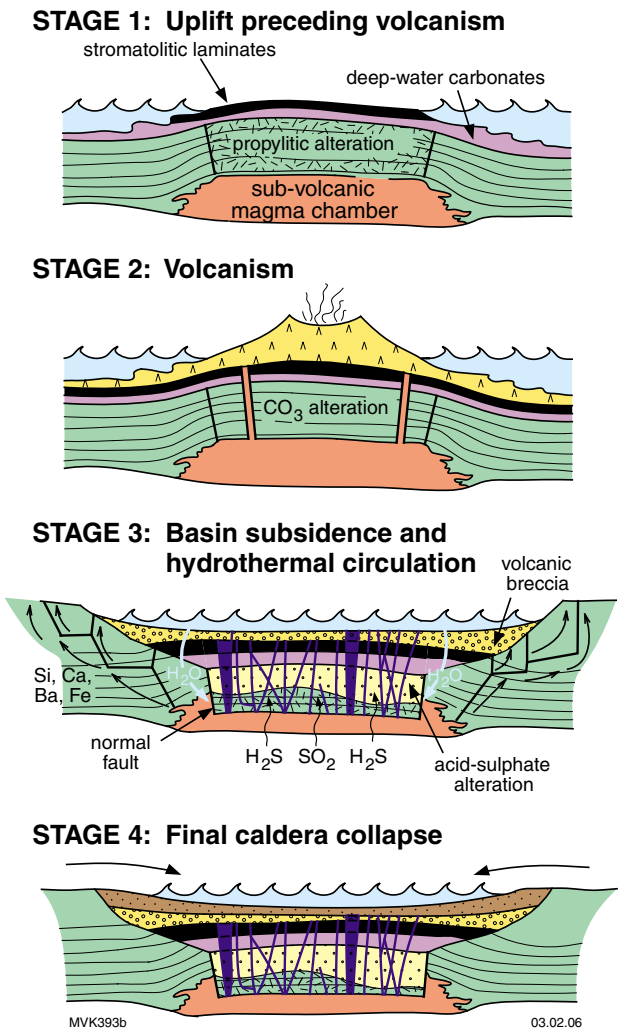

Figure 68. Geological model of formation of the Dresser Formation within a volcanic caldera. (From Van Kranendonk et al., 2008.)

of the Dresser Formation from altered basalts of the footwall (Fig. 70b,c). Along the eastern margin of the vein, drag folds of the bedded cherts can be seen, indicating Dresser Formation-down displacement across this vein-occupied fault.

Locality 7.4: Barite veins and acid sulfate hydrothermal alteration of footwall pillow basalts, Dresser mining centre (Zone 50K, 752740E 7659555N)

Retrace your route back out to the main track, past Panorama Honmestead. Turn left and head south for 8 km, noticing the large hydrothermal chert veins running up the hillside to the base of the Dresser Formation on the hills on the left hand side. Follow the track where it swings to the left into the abandoned Dresser Mine, where 129 505 t of barite were mined between 1970 and 1990. Drive past the ore stockpile and the ruined sorter apparatus, and up the deeply eroded track on the right, driving as far as possible towards pit 1.

This locality is the larger of two Dresser mining pits (Fig. 71); the smaller pit to the east is located in a 15–20 m wide, subvertical barite vein intersecting highly altered pillowed basalts. At this locality, climb up the track towards a notch in the high hill to the east. Here, a zoned chert–barite vein cuts through perfectly preserved, but pervasively altered, moderately east-dipping pillow basalts (Fig. 72). Pillows near the base of the bedded chert are entirely white, in contrast to the generally green-weathering nature of less altered pillow basalts immediately above the Dresser Formation, and are composed entirely of kaolinite — a style of alteration consistent with high-sulfidation epithermal systems (Van Kranendonk and Pirajno, 2004; Van Kranendonk, 2006). Relict vesicles in the basalts are filled by white silic. This alteration is typical of footwall basaltic rocks beneath the areas most strongly affected by hydrothermal veining associated with the Dresser Formation, and corresponds to the zone of advanced argillic alteration common in subaerial epithermal systems at temperatures of c. 150°C (Fig. 73). Zones of sericitic alteration and propylitic alteration have also been recognized in the footwall basalts beneath the Dresser Formation, consistent with this model. Hydrothermal alteration was caused by mixing of circulating groundwater with H_2S derived from the magmatic vapour plume, which was sourced from an unexposed synvolcanic felsic intrusion that generated H_2SO_4, resulting in acid sulfate alteration of the shallow level footwall (shown schematically in Fig. 74; Van Kranendonk, 2006). Downward penetration of meteoric water was probably facilitated by episodic growth faulting associated with felsic volcanic eruptive events within the inferred caldera setting. This activity was repeated numerous times, resulting in the many crosscutting relationships seen between footwall silica–barite veins.

Locality 7.5: Impact breccia bed with spherules; the 3470 Ma Antarctic Creek Member of the Mount Ada Basalt, Warrawoona Group (Zone 50K, 759646E 7660901N)

Return north up the Dresser haul road, and turn right onto a small track (Zone 50K, 750893E 7667063N), heading out towards Panorama homestead. Continue along this track past the homestead and cross Miralga Creek, up onto the east bank of the river, ~5.8 km. Follow the track south for a further 7.6 km to the point where the track swings sharply west to cross a creek (Zone 50K, 759261E 7661007N). Rather than continue to follow the track, head across the flat ground to the southeast towards a low ridge ~450 m away.

Lowe and Byerly (1986) reported millimetre- to submillimetre-scale silicified spherules containing quench-crystallization and glass-devitrification textures from sandstone within the Antarctic Creek Member. Byerly

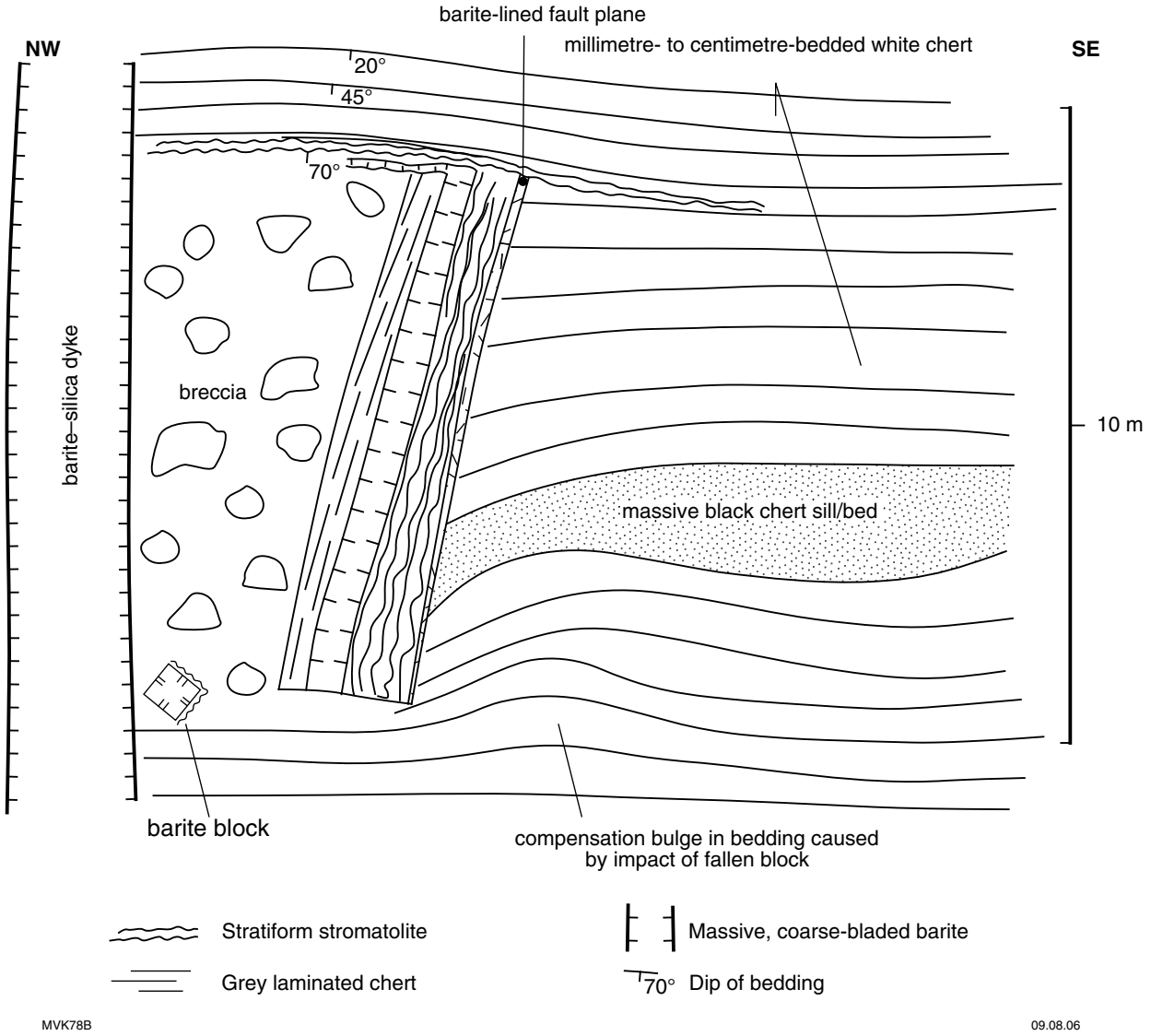

Figure 69. Diagrammatic sketch of the barite breccia at Excursion Locality 7.3.

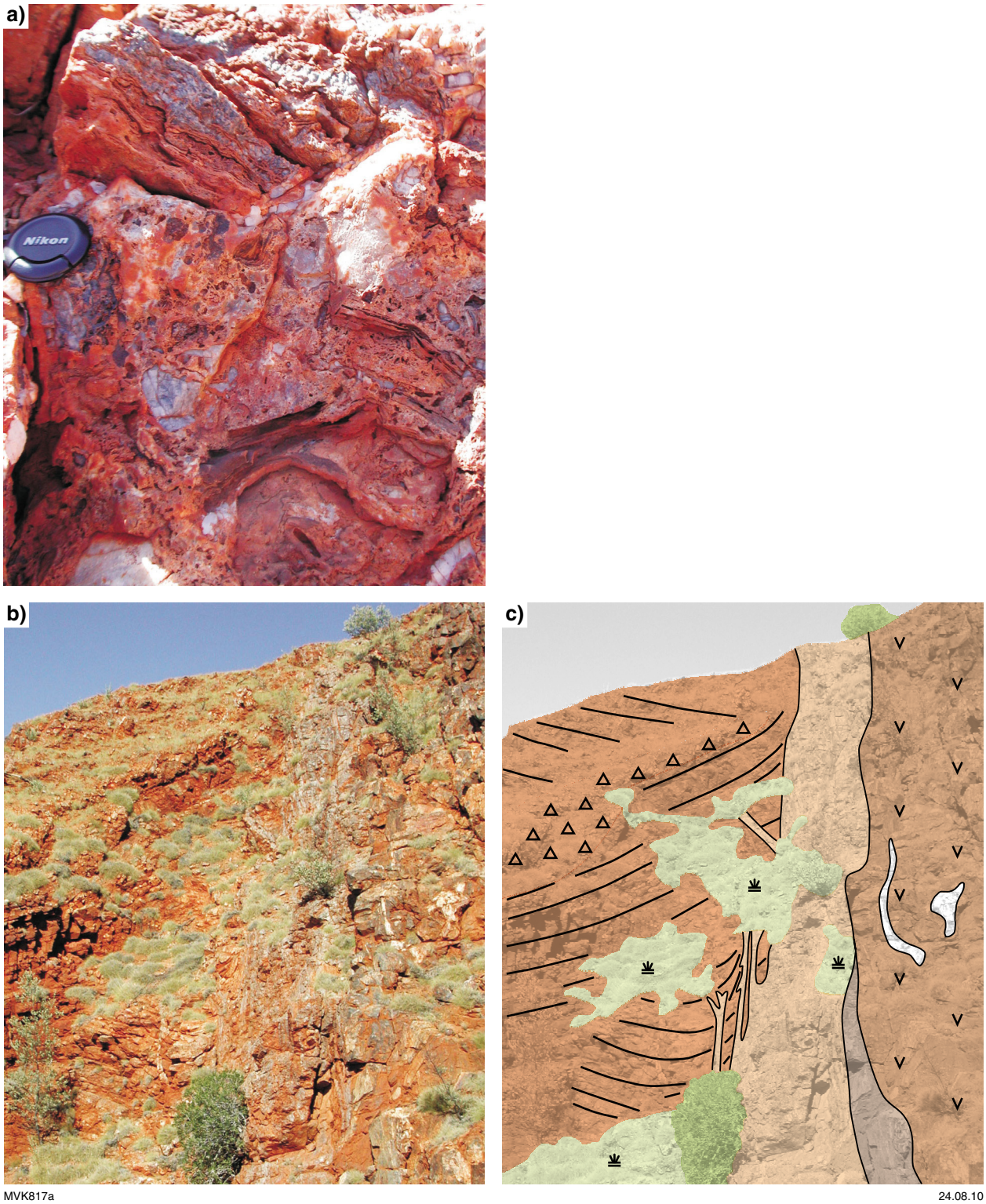

Figure 70. Outcrop features of the barite breccia at Excursion Locality 7.3: a) diamictite with stromatolite and barite clasts; b–c) view (b) and interpretative sketch (c), looking south, of the south gully wall, showing a wide, subvertical barite vein that occupies a syn-depositional fault that separates bedded cherts (left) from uplifted, footwall volcanic rocks (right). Note the rotated bedding of blocks of bedded chert and the drag folds of the bedded cherts against the barite vein (from Van Kranendonk et al., 2008).

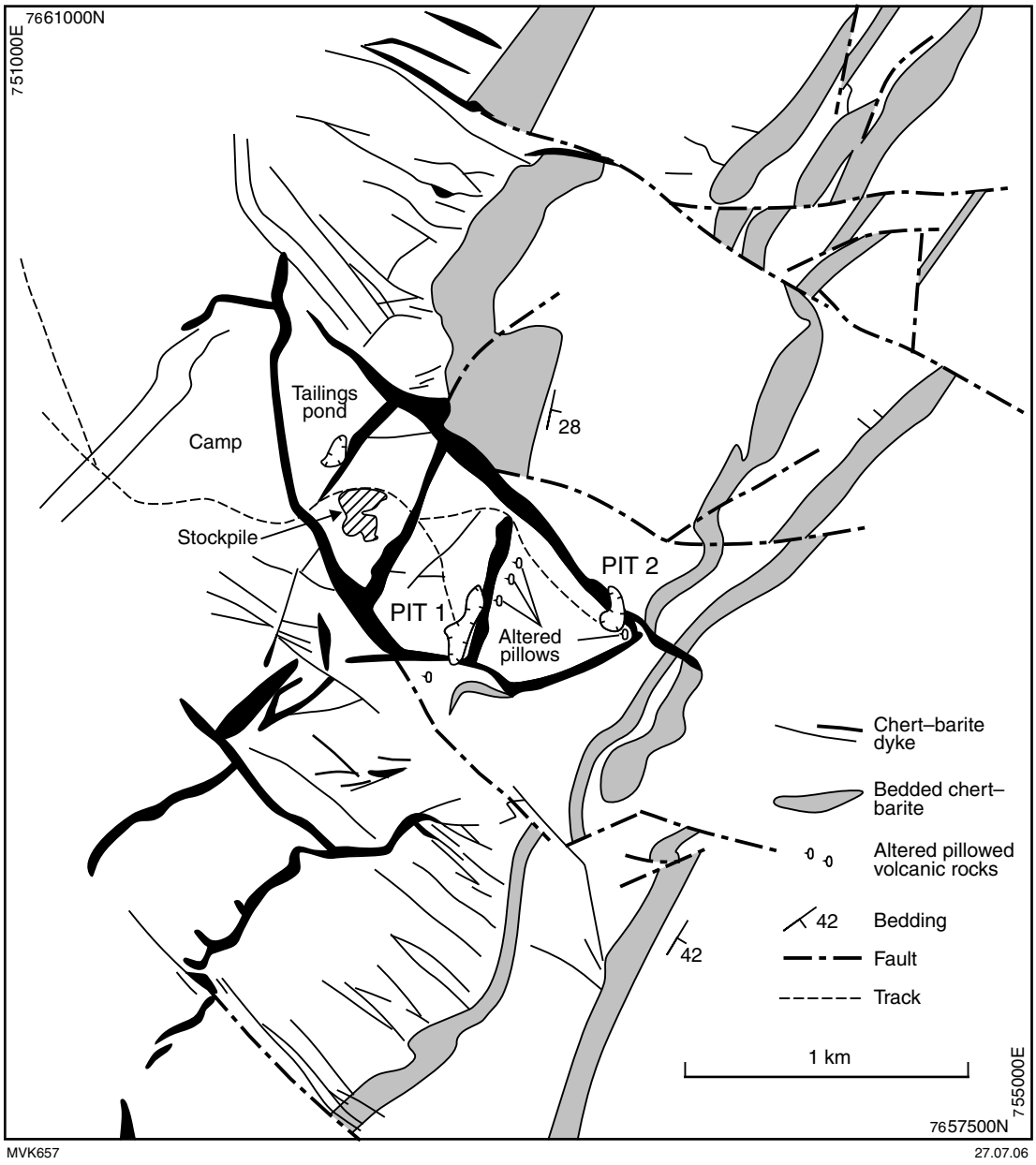

Figure 71. Geological map of the Dresser Mine area.

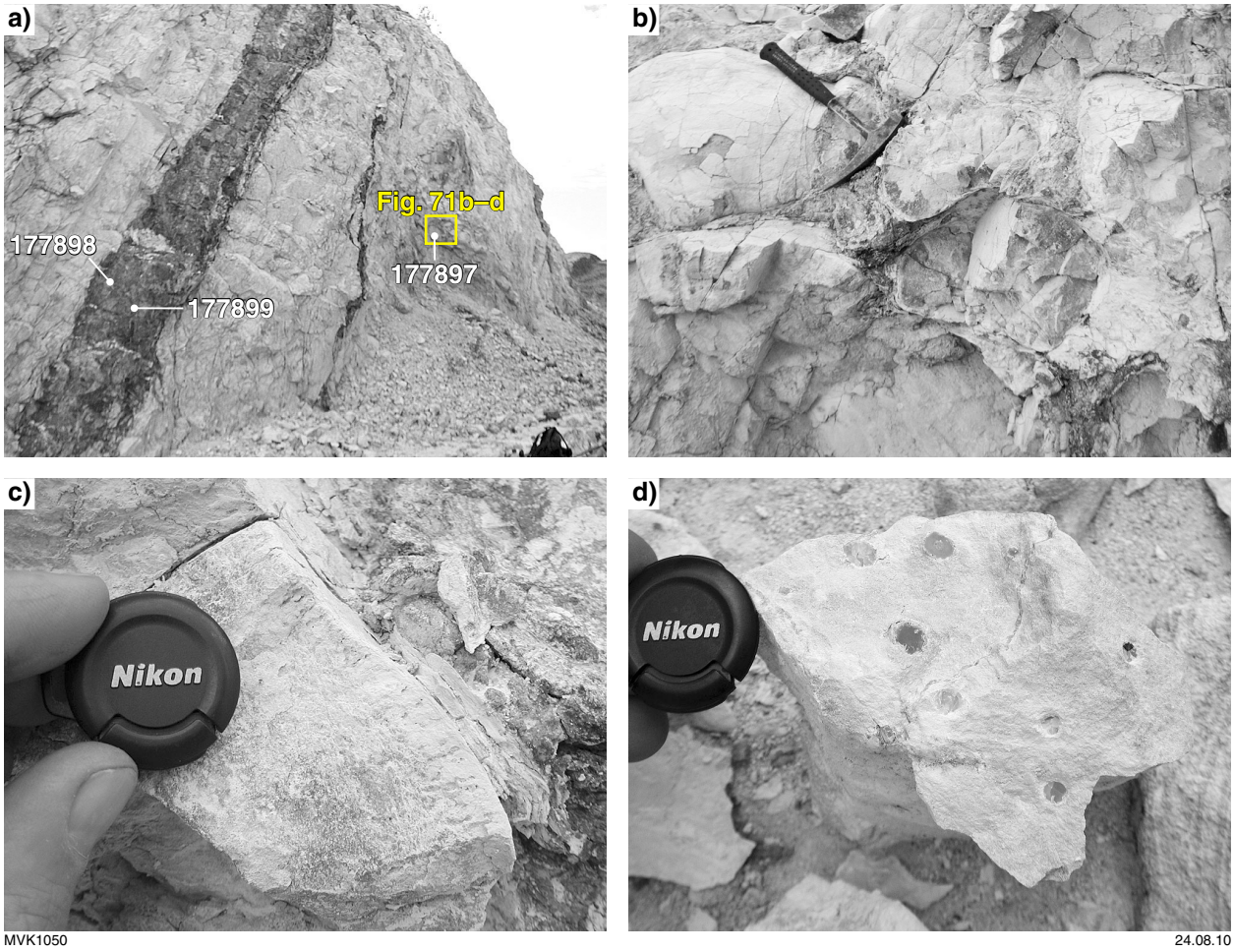

Figure 72. Outcrop features of hydrothermally-altered pillow basalts at Excursion Locality 7.4: a) zoned chert–barite vein cutting through white, hydrothermally-altered footwall pillow basalts immediately beneath the Dresser Formation; b) close-up of hydrothermally-altered pillows, showing their undeformed, primary shapes; c) detail of altered pillow rim, showing marginal vesicles; d) close-up of altered pillow core, showing quartz-filled amygdale (from Van Kranendonk and Pirajno, 2004).

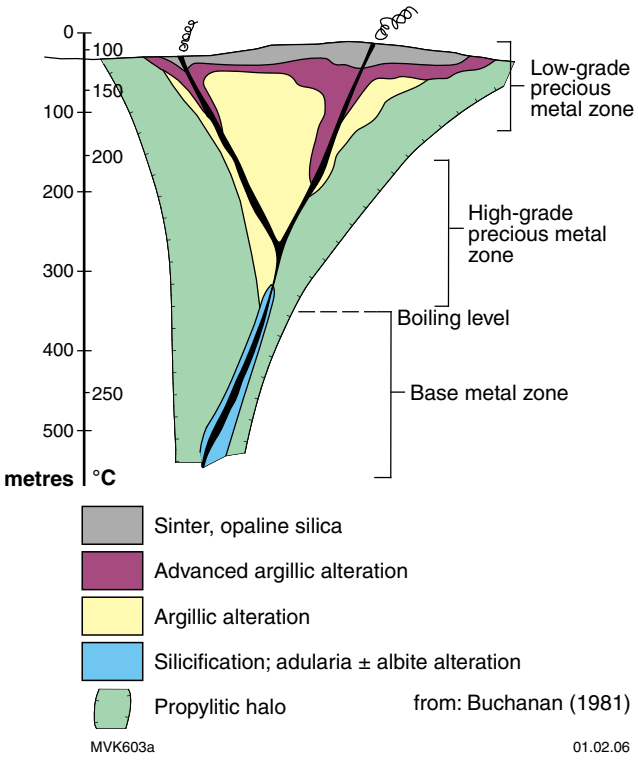

Figure 73. Schematic model of alteration zones associated with epithermal hydrothermal systems (from Van Kranendonk and Pirajno, 2004).

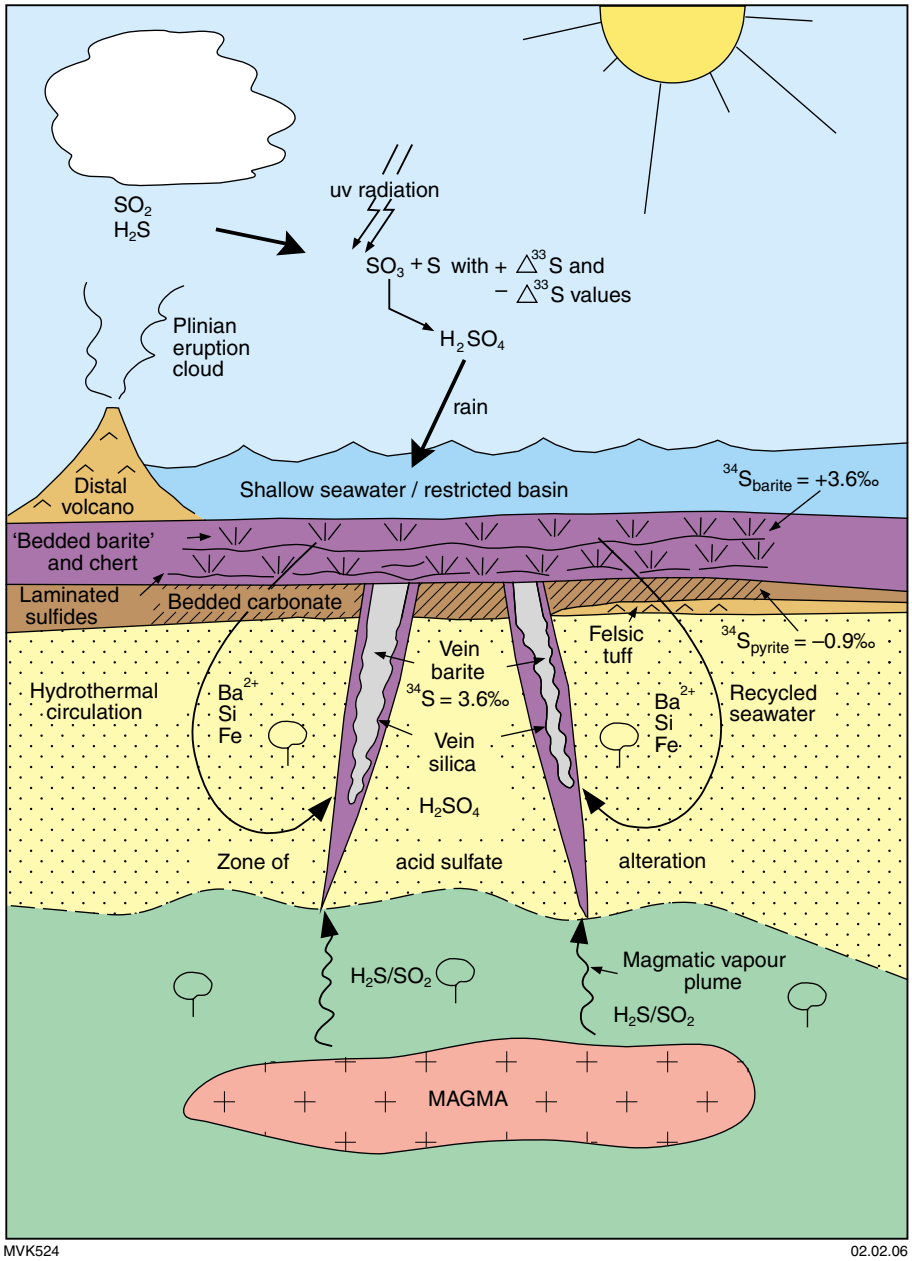

Figure 74. Model of deposition of the Dresser Formation within an active volcanic caldera affected by hydrothermal fluid circulation. Downward circulating seawater is heated and interacts with reducing fluids and volatiles from a degassing magma chamber. These fluids leach Ba, Si, and Fe from footwall basalt, mix with seawater containing dissolved sulfate, and are then expelled to the surface along synvolcanic growth faults, where they precipitate silica, barite, and pyrite (from Van Kranendonk, 2006).

et al. (2002) report a $^{207}Pb/^{206}Pb$ date of 3470.1 ± 1.9 Ma for euhedral zircons derived from the spherule-bearing unit, which is within error of the age of the Mount Ada Basalt and coeval Duffer Formation (3474–3463 Ma; Van Kranendonk et al., 2002). Of the thirty 50–100 μm zircons extracted from 2 kg of rock, 2 grains yielded ages of c. 3510 Ma, suggesting that some of the clastic material was derived from older components of the Warrawoona Group (Coonterunah Subgroup; Buick et al., 1995; Van Kranendonk et al., 2002, 2006). Byerly et al. (2002) correlated the spherule-bearing unit with a similar S_1 unit in the Hoogenoeg Formation, Barberton Greenstone belt, Kaapvaal Craton, South Africa, which yielded a $^{207}Pb/^{206}Pb$ zircon date of 3470.4 ± 2.3 Ma.

Lowe and Byerly (1986) identified spherule-bearing chert and arenite for 1 km along strike, whereas Glikson et al. (2004) was able to extend this to about 15 km along strike in the northeastern part of the North Pole dome (Fig. 61). Spherules mostly 0.10 – 0.75 mm in diameter and consituting <10%, but locally higher proportions, occur within at least two beds of 15–50 cm-thick, current-deposited arenite. Spherules are. Irregular particles, compound spherules, dumbbell shaped particles, and broken spherules are present. Spherules within chert retain high to very high sphericity. In the arenites, the silicified, partly broken, corroded and matrix-resorbed state of scattered spherules makes their identification more difficult.

Lowe and Byerly's (1986) spherule-bearing chert–arenite unit at the type locality (Zone 50K 759685E 7663583N) consists of c.14 m thick, massive to finely laminated chert. The unit comprises up to three horizons of interbanded chert, recrystallized feldspathic arenite with mm-scale chert fragments, and gritstone–intraclast conglomerate consisting of recrystallized arenite grains and mm-scale to several cm-scale, mostly layer-oriented, chert fragments in siliceous matrix. Submillimetre, poorly to moderately well-preserved spherules are scattered within the matrix of the arenite, gritstone, and intraclast conglomerate, and are found as stratiform bands and lenses within the chert. Microkrystite spherules may occur within both chert fragments and in the matrix of the same arenite/microconglomerate units, attesting to multiple spherule deposition stages.

Lowe and Byerly (1986) and Byerly et al. (2002) documented quench-like spinifex textures, crosscutting crystallites, and fan-shaped radiating devitrification features replaced by quartz, mica, and iron oxide. Textures include fibro-radial, ex-centroradial, dendritic, lath-like crystallites, thin tabular crystals, micro-spinifex textures, and barred crystallites — correlated with quench plagioclase, pyroxene, and olivine (figure 3 in Lowe and Byerly, 1986). Other components of the spherule-bearing arenites include altered lithic fragments, many of which contain microlite and lath-like pseudomorphs in matrices of chert, sericite, and minor chlorite. Lowe and Byerly (1986) identified little or no volcanic detritus in the arenite/chert units. Glikson et al. (2004) observed both: 1) lithic microlitic to microporphyritic particles of possible to likely volcanic origin; and 2) distinct, highly spherical spherules with quench and devitrification textures, coexisting within the same arenite samples.

Day 8: Stromatolitic carbonates at the Trendall locality

Locality 8.1: Trendall locality of the c. 3.35 Ga Strelley Pool Formation

The c. 3.35 Ga Strelley Pool Formation (Lowe, 1980; Van Kranendonk et al., 2007a; Hickman, 2008) is a widespread unit across the East Pilbara Terrane, deposited on rocks of the Warrawoona Group across a subaerial erosional unconformity (Buick et al., 1995; Van Kranendonk, 2006). The formation consists of three members: 1) a basal, coarse clastic member; 2) a middle member of laminated and stromatolitic carbonates, with common evaporitic crystal splays; and 3) an upper unit of coarse clastic sedimentary rocks.

Coniform stromatolites are widespread in the Strelley Pool Formation across most of the 220 km breadth of the East Pilbara Terrane (Fig. 75). These have been described in detail by several authors, who support a biogenic interpretation (Lowe, 1980; Hofmann et al., 1999; Van Kranendonk, 2000; Van Kranendonk et al., 2003; Allwood et al., 2006). Conversely, Lowe (1994) and Lindsay et al. (2005) have suggested that coniform structures in the Strelley Pool Chert are abiogenic. Lowe (1994) suggested abiogenic formation of coniform structures through evaporitic precipitation of mineral crusts, whereas Lindsay et al. (2005) concluded that, because 'Laminations within the stromatolitic structures are conspicuously isopachous and comparable with abiotic structures formed by direct precipitation of carbonate… stromatolite structures described from the Strelley Pool Formation are abiotic features deposited by direct precipitation from hydrothermal solutions that were modified by ocean floor currents.' The biogenicity of Strelley Pool Formation stromatolites is discussed in more detail below and is a major focus of discussion at this locality.

Regional setting

Three geological settings have been posed for the carbonates of the Strelley Pool Formation: 1) a shallow marine, evaporative basin (Lowe, 1980, 1983, 1994; Buick et al., 1995; Van Kranendonk, 2000, 2006); 2) a shallow, open marine environment (Hofmann et al., 1999; Van Kranendonk et al., 2003; Allwood et al., 2006); 3) a hydrothermal setting (Lindsay et al., 2005), in which carbonates were deposited from hydrothermal solutions sourced from veins preserved locally in the footwall, based on ideas first presented in Van Kranendonk et al. (2001).

A characteristic feature of the Strelley Pool Formation is that it can be traced in good exposure for tens of kilometers along strike within greenstone belts, it is recognized in all greenstone belts across the terrane, and it contains a recognizable and internally consistent stratigraphy in

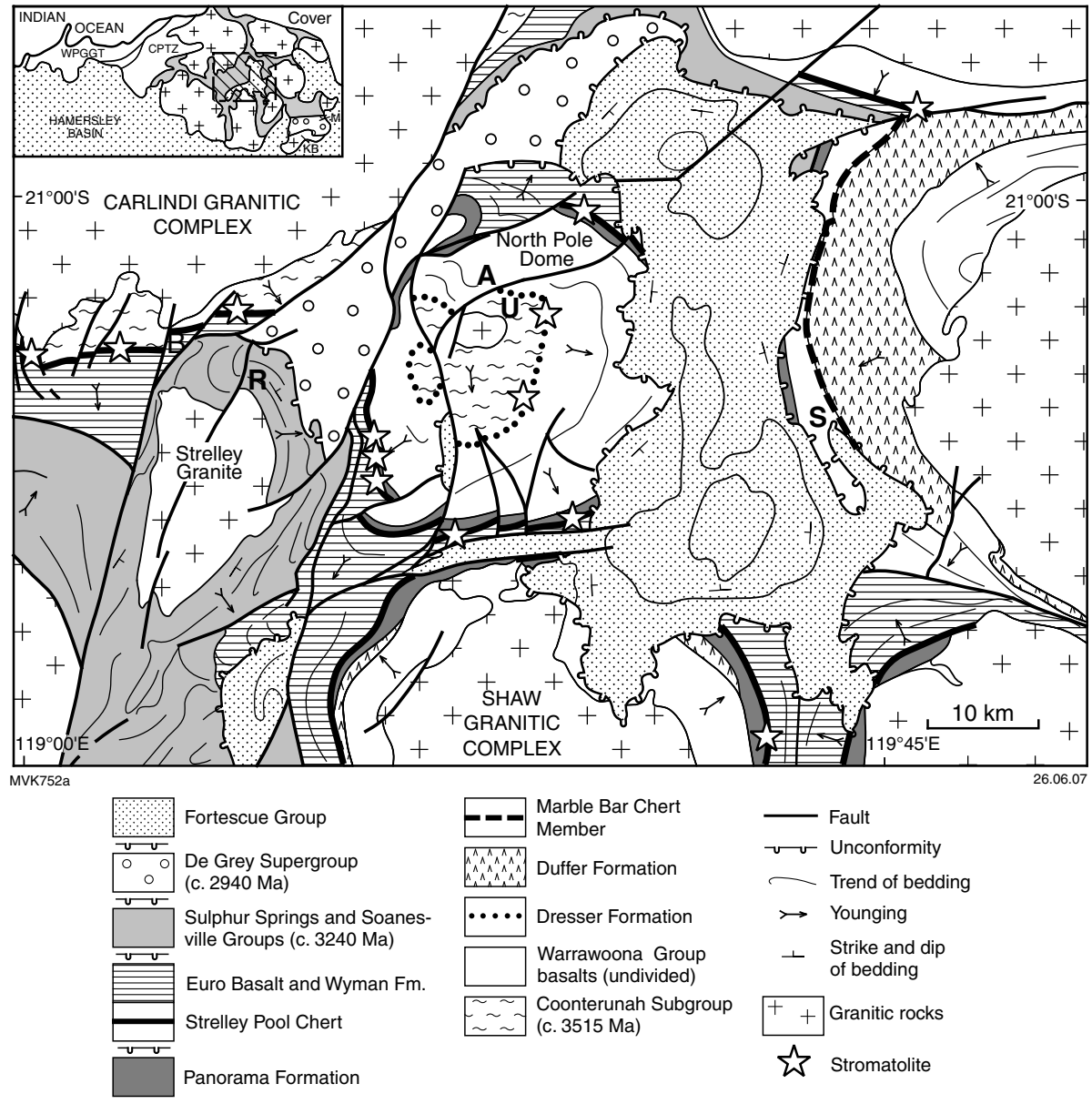

Figure 75. Geological map of the major part of the East Pilbara Terrane, showing the distribution of fossil stromatolite sites. Putative microfossil sites: A = Awramik locality; B = Banerjee locality (ichnofossils); R = Rasmussen locality; S = Schopf locality; U = Ueno locality (from Van Kranendonk, 2010).

most of the belts across the EPT. The only real change within this unit across strike is the thickness of the lower clastic member, which varies from 1 m of boulder and pebble conglomerate to 1000 m of quartz-rich sandstone, reflecting local changes in depositional environments for this member, from fluviatile to rocky shoreline and tide-dominated beach conditions (Lowe, 1983; Buick et al., 1995; Van Kranendonk, 2000, 2004; Allwood et al., 2006). The widespread and consistent distribution of the carbonate lithofacies argues strongly against a hydrothermal setting of deposition, as these latter deposits occur within fault-bounded, active volcanic terrains and are characteristically highly variable in thickness and composition along strike lengths of 1–10 km. Further evidence against a hydrothermal setting was provided by Van Kranendonk et al. (2003) in the form of trace element geochemical data on the carbonates, which demonstrated that they were precipitated from normal seawater, and not from hydrothermal solutions.

It is now clear from detailed studies that the Strelley Pool Formation was deposited through a basin deepening event prior to the onset of submarine basaltic volcanism. The setting was transitional from a locally rocky shoreline to tide-dominated beach setting, through shallow marine conditions that included one or more periods of evaporative conditions and subaerial exposure, followed by basin collapse and deeper marine conditions. Geochemical and geochronological data from the conformably overlying Euro Basalt indicates that the

Strelley Pool Formation – Kelley Group succession can be related to the arrival (uplift and erosion) and eruption (basin deepening and pillow basalt) of a mantle plume at 3.35 Ga (Van Kranendonk and Pirajno, 2004; Smithies et al., 2005b; Van Kranendonk et al., 2007b).

Geology of the Trendall locality

The Trendall locality is one of the principal localities in support of ancient life on early Earth and represents a key locality for understanding the geological setting of ancient stromatolites. A detailed map of the outcrop is presented in Figure 76. At this locality, the formation lies across an unconformity on pyrophyllite-altered, schistose metabasalt of the Mount Ada Basalt and consists of three distinct members: 1) a lower member of black and red, layered chert boulders that pass along strike into a 1–2 m thick unit of chert-pebble conglomerate; 2) a middle member of planar and stromatolitic carbonate laminites, and coarse evaporitic crystal splays; 3) an unconformably overlying upper unit of coarse- to fine-grained clastic sedimentary rocks. All members of the formation are transected by a younger suite of zoned black chert and white quartz veins that extend up to the top of the formation but not into the conformably overlying, vesicular pillow basalts of the Euro Basalt (Van Kranendonk, 2006, 2010). .

Basal clastic member

Widely spaced boulders of laminated black and red chert line the base of the formation at the Trendall locality and pass along strike to the south into 1–2 m of jasper chert pebble conglomerate (Fig. 77a). Boulders are encrusted by the overlying carbonate member. Chert boulders and pebbles in this basal member are derived from units of layered red and black chert within the Mount Ada Basalt, visible at several localities along strike and across strike, downsection to the south. Indeed, stromatolitic carbonates of the middle member of the formation onlap Mount Ada cherts at a locality c. 4.5 km along strike to the north, across a double unconformity (Fig. 78). The boulder beds have been interpreted to represent the deposits on a rocky shoreline at the transition from a subaerial environment of erosion to shallow water deposition (Allwood et al., 2006).

Middle carbonate member

Laminated carbonates

The dominant lithology of the middle carbonate member of the Strelley Pool Formation is planar-bedded, millimetre-scale carbonate laminite. Planar laminite passes along strike into a texturally identical rock with a variety of structures formed by the growth of stromatolites (Hofmann et al., 1999; Van Kranendonk et al., 2003; Allwood et al., 2006). Detailed mapping shows that stromatolite forms vary along strike over distances of 1–1000 m (Allwood et al., 2006). In this outcrop, the largest and most complex stromatolites define three, stacked, offset biostromes (Fig. 76) that dip to the north at up to 15º from bedding, and pass along strike into planar-bedded carbonate laminite.

The dominant stromatolite morphology is stacked, generally slightly elliptical cones that locally display isopachous lamination (Fig. 77b–d). Coniform stromatolites initiate locally from a flat generation surface and form structures that extend upsection for anywhere from a few centimetres up to a metre in height. Individual bedding planes may contain many cones of similar dimension, or of varied size (Fig. 79a). Cross-sectional views show that, whereas the stromatolites are generally symmetrical, others are asymmetrical, with consistently longer northern limbs than southern limbs (Fig. 77d; Hofmann et al., 1999), suggesting growth on a local paleoslope of 15° dip. Conical stromatolites are characteristically elliptical in plan view, and elongate down the dip of bedding; this is not as a result of tectonic strain, but reflects the original shape of the stromatolites and possibly a preferred direction of growth under flowing (tidal) water (Fig. 79a). Some coniform types show incipient branching and may form structures up to 35 cm high (Fig. 79b). Others develop columnar branches off one side of the cone shape (Fig. 79c).

A second stromatolite morphology in carbonate laminites consists of rounded, branching columns (Fig. 79d). Locally, these form isolated structures, but the majority of these types form on the flanks of large domical stromatolites with a maximum amplitude of 25 cm and a maximum height upsection of 1.2 m. Up to 10 small lateral branches have been observed on the flanks of the largest conical forms.

Closer inspection of laminations shows that stromatolite forms display a variety of layering relationships, including onlap of sediment along the sides of coniform stromatolites (Fig. 80a; Van Kranendonk et al., 2003), and growth of coniform stromatolites within, and contemporaneous with (i.e. along strike of), sedimentary rocks deposited from ocean currents (Fig. 80b). These features show that the rocks are not abiogenic precipitates 'modified by ocean currents', as suggested by Lindsay et al. (2005), but rather are structures that formed *during* accumulation of carbonate sedimentary material affected by currents.

The interaction between stromatolite growth and water currents is seen most dramatically in Figure 81, which shows a steep-sided coniform stromatolite that displays continuous growth upwards from fine to moderately laminated carbonates at the base, thorough an 8-cm thick bed of flat-pebble conglomerate, into finely laminated carbonates. This unequivocally demonstrates that coniform stromatolites are not precipitates from solutions of either evaporitic or hydrothermal origin and must have formed as a result of living microbial activity.

The same conclusion may be reached for small, domical-columnar stromatolites higher in the middle carbonate unit, where the rocks have been almost completely silicified and bedding is developed at a finer scale. These rocks contain several horizons with centimeter-high domical-columnar stromatolites defined by rusty red- and yellow-weathering laminates that are associated with crescent-shaped, wind-blown ripples (Fig. 82a–c; Van Kranendonk, 2007). Although these domical-columnar forms display

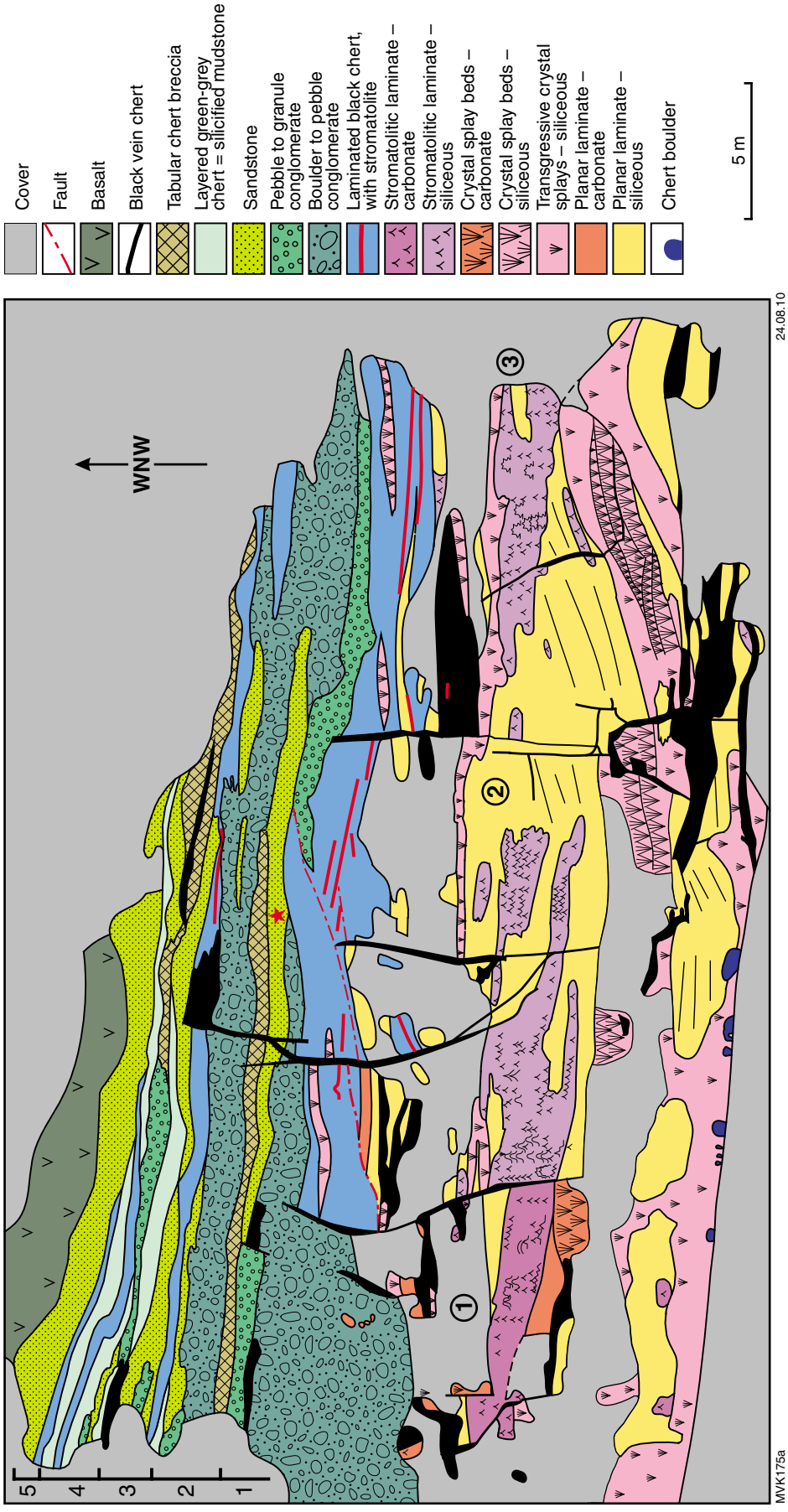

Figure 76. Geological map of the Trendall locality at Excursion Locality 8.1. Numbers in upper left denote fining-up sedimentary cycles, interpreted as receding fans (from Van Kranendonk, 2007).

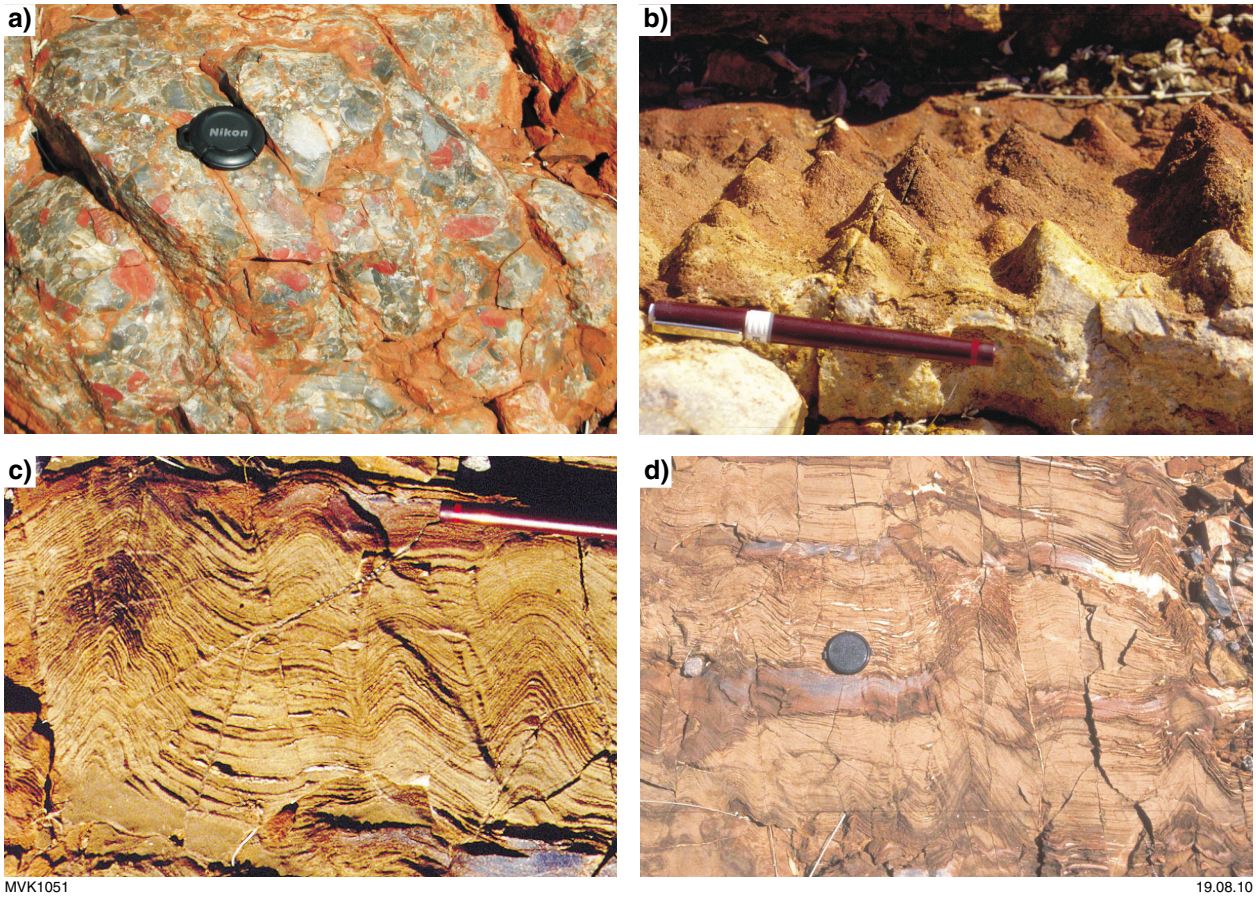

Figure 77. Outcrop features of the Trendall locality at Excursion Locality 8.1: a) basal chert-pebble conglomerate; b) oblique bedding-plane view of coniform stromatolites; c) cross-sectional view of well-laminated dolostone with variable stromatolite forms and isopachous lamination; d) cross-sectional view of large, columnar coniform stromatolites with asymmetrical limbs.

broadly isopachous laminations at outcrop scale, thin section observations show that these stromatolites feature steep-sided growth walls that truncate laminae, internal discordancies of laminae, and growth termination by influx of clastic sediment (Fig. 82d). These morphological features demonstrate dynamic growth within a changing environment and support a biogenic origin for these structures.

In areas where the rocks have not been completely silicified and 'primary' carbonate is preserved (quotations are used because the carbonate is, in fact, diagenetic), laminae are defined by couplets of light-brown siderite/dolomite and dark brown-weathering, heavily silicified carbonate, dominated by polygonal microquartz. In one area, repeated cyclical bundles of 7–11 carbonate-chert couplets are present, with each bundle capped by a slightly thicker dark-brown lamina (Fig. 83). Although the cause of this cyclical bundling is unknown, the scale of the bundling suggests that the couplets represent annual winter–summer cycles, and that a possible cause of the bundling is climatic effects due to varying insolation associated with the sunspot cycle, which operates on an 11-year cycle (e.g. Foukal, 2003).

Radiating crystal splays

A prominent feature of the Strelley Pool Formation in many localities is the widespread development of weakly upward-radiating crystal fans. Together with desiccation cracks and wind-blown ripples, the presence of crystal fans indicate periods of exposure during accumulation of the carbonate member (Van Kranendonk et al., 2003; Allwood et al., 2006; Van Kranendonk, 2010). Significantly, stromatolite abundance is locally directly affected by the formation of crystal fan beds, with the latter forming a cap on the large biostromes at this locality (Fig. 76), above which stromatolite growth is much less abundant and has a different morphology (small, domical forms above vs. large, coniform varieties below). These observations suggest marine precipitation of carbonate rocks under (at least) periodically evaporative conditions.

Two textural types of straight to weakly radiating vertical crystal splays have been recognized. One type grew across planar-bedded and stromatolitic laminites, such as those that occur throughout the lower part of the outcrop and those about halfway up the succession in the northern part of the outcrop (Fig. 84a). A second type includes the

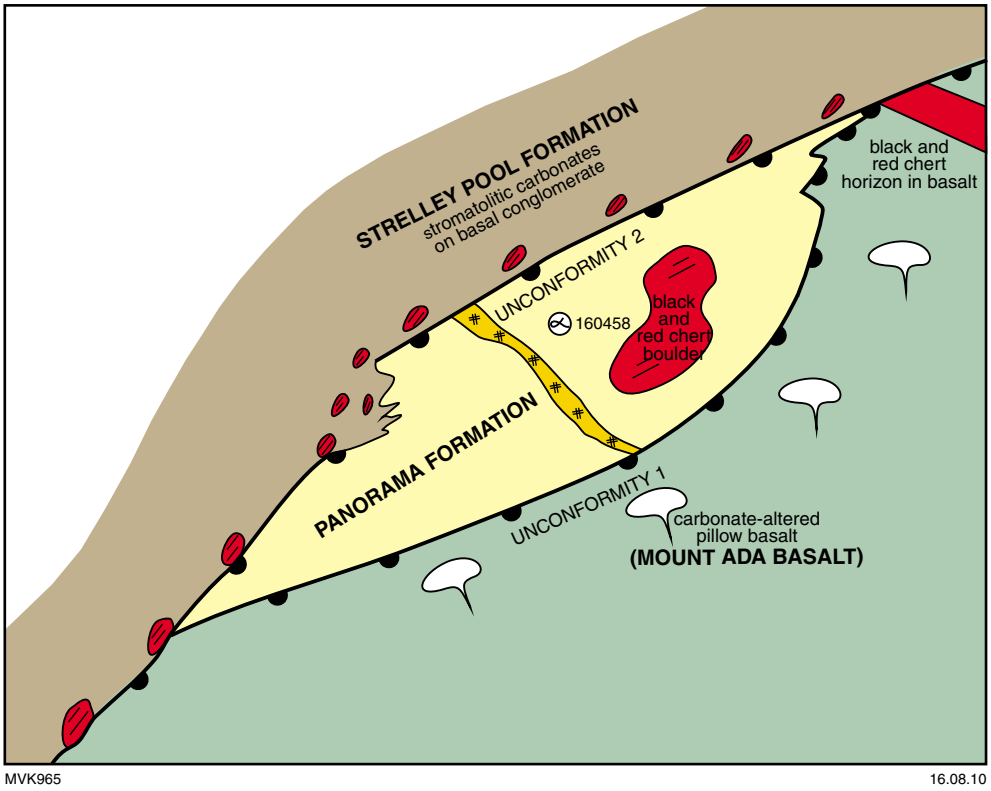

Figure 78. Geological sketch map from north of the Shaw River, showing unconformable relationships between the Strelley Pool Formation, Panorama Formation felsic volcaniclastic rocks, and carbonate-altered, pillowed metabasalt (Mount Ada Basalt); note the presence of jaspilitic chert boulders in the upper two units and the onlap of the Strelley Pool Formation on the layered chert of the Mount Ada Basalt. α symbol denotes location of geochronology sample 160458, dated as $\leq$3447 ± 12 Ma.

largest crystal splays, ≥50 cm long, in which no trace of bedding is evident (Fig. 84b). These include the coarse crystal splays in carbonate immediately adjacent to the black chert-pebble vein that separates carbonate from siliceous laminites in the southern part of the outcrop. Also included in this category are up to five sharply bounded 'beds' of radiating crystal splays, 30 cm thick, that define a broad dome in the northern, more silicified part of the outcrop (Figs 76, 84c). The development of these massive crystal splays is associated with termination of stromatolite growth, as shown, for example by a 20–80 cm thick, massive layer of radiating crystal splays that overlies the main stromatolitic unit. More specific evidence of this was observed at a smaller scale in a nearby outcrop, where a set of radiating crystals grew on top of a single stromatolite column and terminated its growth (Fig. 84d). This is used to argue that episodes of crystal splay growth represent periods of subaerial exposure. Although the original mineral species forming the crystal splays is unknown due to diagenetic carbonate alteration and silicification, preserved cross-sections of some large silicified crystals are pseudo-hexagonal (Fig. 84e).

It is important to emphasize that the crystal splays are unrelated to the development of stromatolitic morphology. The varieties of stromatolite morphology are all observed away from crystal splays and are outlined by the millimeter-scale laminites that, elsewhere in the outcrop, are overgrown by the crystal splays.

Upper clastic member

The upper clastic sedimentary member can be divided into five fining-up successions, interpreted as a series of receding alluvial fans (Fig. 76). A basal conglomerate is very coarse grained, with subrounded boulders up to 40 cm in diameter. Blocks of layered and massive blue-black chert dominate, but boulders of dark brown carbonate — some with stromatolites — are locally common, and fragments of komatiitic basalt were observed 250 m along strike to the south. The basal conglomerate fills a 6.2-m deep channel bounded by normal faults that are lined by veins of black chert extending partway up into, but terminating within, the conglomerate. The presence of vein chert along the channel-forming faults and the abundance of black chert clasts in the conglomerate suggest that at least some of the black chert veining was synchronous with accumulation of the formation.

In one of the coarse sandy layers partway up in the member, stromatolitic mats have been observed, manifest

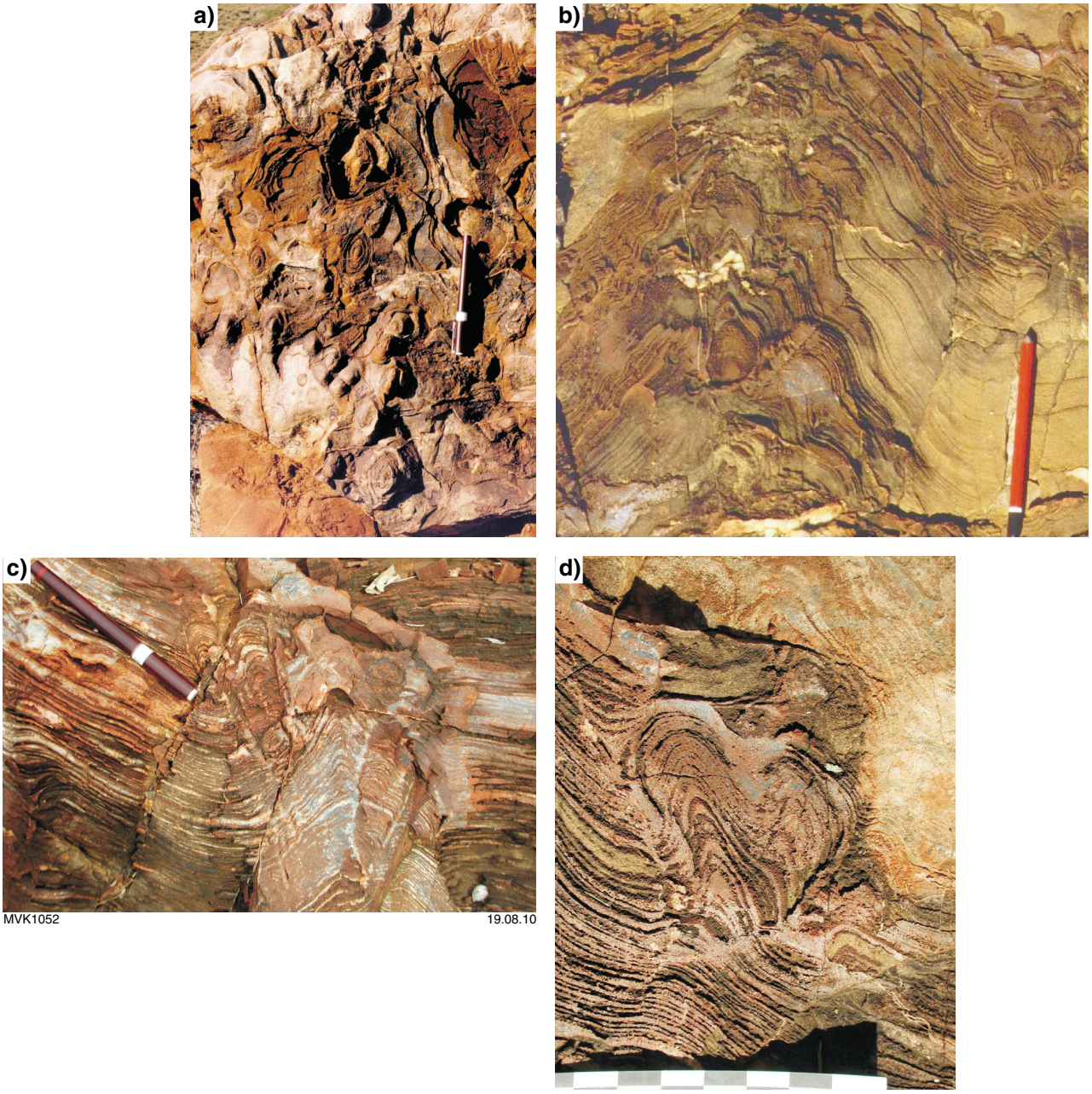

Figure 79. Stromatolites of the Trendall locality at Excursion Locality 8.1: a) bedding-plane view of coniform stromatolites of different sizes, all showing parallel elongation; b) large, incipiently branching coniform stromatolite with branched columnar form on upper right flank; c) coniform stromatolites with branched offshoots on upper left flank; d) close-up of upper right part of b), showing branched columnar stromatolite ('Mickey Mouse ears'; scale in centimetres).

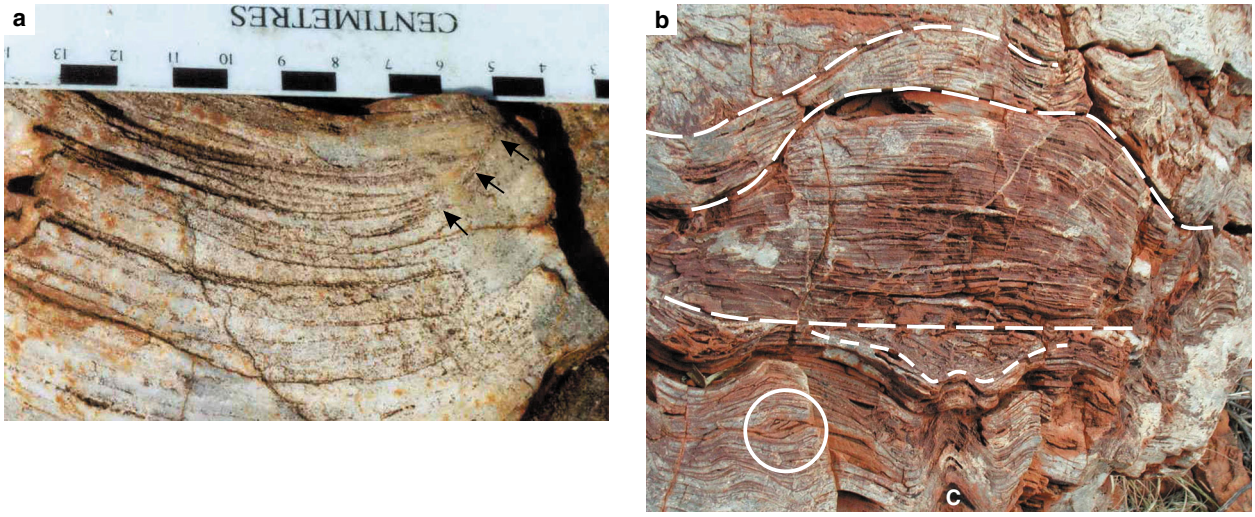

MVK756 05.02.09

Figure 80. Bedding features of (silicified) carbonates at the Trendall locality: a) detailed, cross-sectional outcrop view of the flank area of a coniform stromatolite, showing onlap of carbonate beds against stromatolite flank (arrows; from Van Kranendonk et al., 2003); b) cross-sectional outcrop view of silicified carbonates, showing coniform stromatolite ('c' at bottom middle) growing within rippled carbonate sediment (circle) and overlain by flat-pebble conglomerate (above short-dash line) that terminated stromatolite growth. Overlying laminated sediment displays high amplitude, symmetrical swale, the geometry of which suggests microbial binding of clastic sediment under high-energy conditions (from Van Kranendonk, 2007).

MVK757 22.02.07

Figure 81. Steep-sided coniform stromatolite of the Strelley Pool Formation, which passes up from finely bedded carbonate at the base, through a layer of flat-pebble conglomerate, into finely bedded carbonate at the top. Arrows point to coniform peak of the stromatolite in the uppermost carbonate (from Van Kranendonk, 2007).

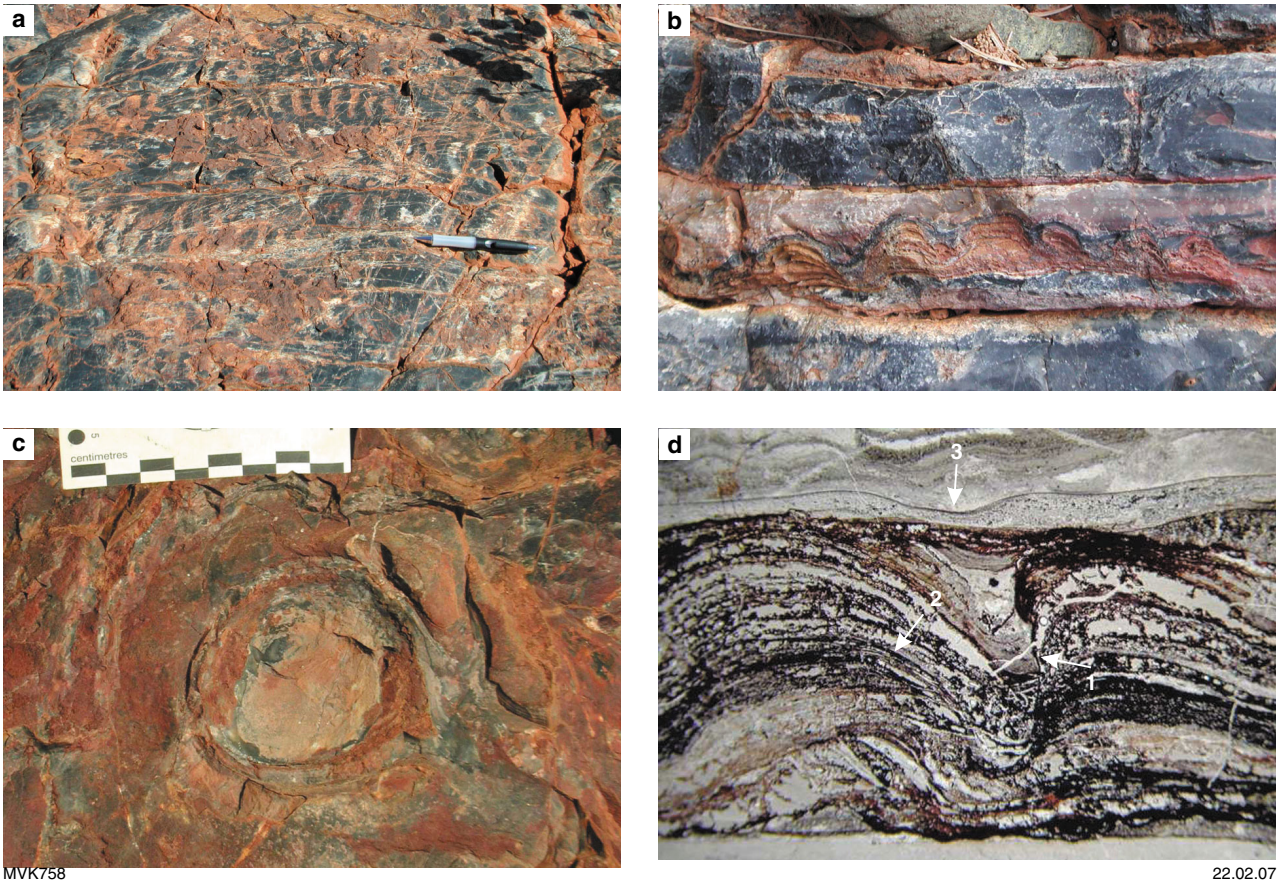

Figure 82. Features of the upper part of the carbonate member of the Strelley Pool Formation: a) small, crescent-shaped, wind-blown ripples in silicified carbonate; b) cross-sectional outcrop view of centimetre-high, domical-columnar stromatolites in silicified carbonate (represented as red lines on Fig. 76); c) plan view of surface outcrop, with small domical-columnar stromatolites in silicified carbonate; d) cross-sectional thin section view of centimetre-high, domical-columnar stromatolites, showing: steep-sided growth walls that truncate growth laminae (arrow 1), internal discordancies of laminae (arrow 2), and growth termination by influx of clastic sediment (arrow 3) (from Van Kranendonk, 2007).

Figure 83. Detail of laminated carbonate, showing cyclical bundling of 7–11 dark–light dolomite couplets (from the stromatolite shown in Figure 79b).

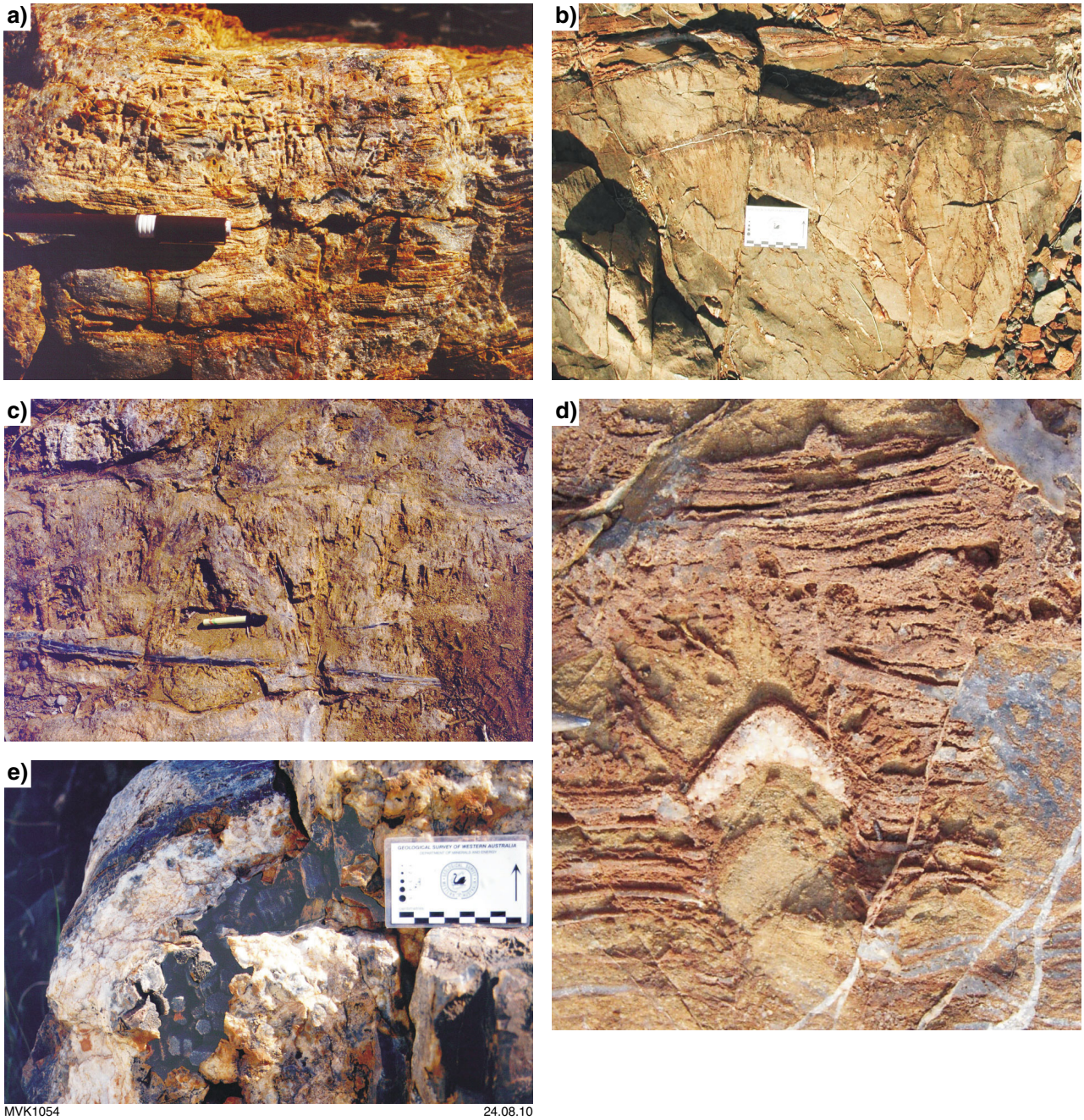

Figure 84. Features of radiating crystal splays in the Strelley Pool Formation: a) weakly radiating crystals cutting bedding in silicified carbonate; b) large, weakly radiating crystal fans in dolomite; c) large sets of radiating crystal fans in silicified carbonate; d) small coniform stromatolite capped by radiating splay of crystals; e) cross-sectional view of pseudo-hexagonal crystals now completely silicified.

as 2–5 mm thick layers of blue-black chert (Fig. 85a; thick red lines on Fig. 76). In thin section, the mats show good preservation of wavy laminite structure, and contain clots of organic material and gas bubbles suggestive of decayed organic matter (Fig. 85b–d). It is not known how widespread or common these stromatolites are in the clastic succession, but they are at least locally prevalent.

Trough cross-bedding in sandstone and imbricate clasts from a conglomerate in this member indicate a paleocurrent direction towards 132°, or towards the core of the North Pole Dome when bedding is rotated back to the horizontal. Significantly, this is opposite to the paleocurrent data from the underlying volcaniclastic rocks of the Panorama Formation, which are everywhere oriented pointing away from the centre of the North Pole Dome (DiMarco and Lowe, 1989). This suggests that the dome formed a topographic high during Panorama felsic volcanism, but then collapsed and was a depocentre during subsequent events.

Hydrothermal veins

A suite of black chert veins transects the outcrop and displays a variety of textures. Whereas some are massive black chert, others are zoned with a white quartz core, in places with euhedral quartz crystals (Fig. 86). Other zoned veins have massive, black, chert margins and a core of pebble breccia derived through phreatomagmatic brecciation and thermal rounding of host rocks. One massive sill displays a pseudo-conglomeratic breccia texture derived from nearly in situ breakup of the country rock during chert intrusion (phreatic brecciation). Such black veins are common throughout the Pilbara Supergroup, but absent from rocks <3.2 Ga — what does this tell us about ocean/atmosphere conditions and/or tectonic processes in this type of terrain?

This is the end of the fieldtrip. From this locality, we will follow our route back out to the Marble Bar – Port Hedland highway, turn left and drive to Port Hedland for the flight back to Perth.

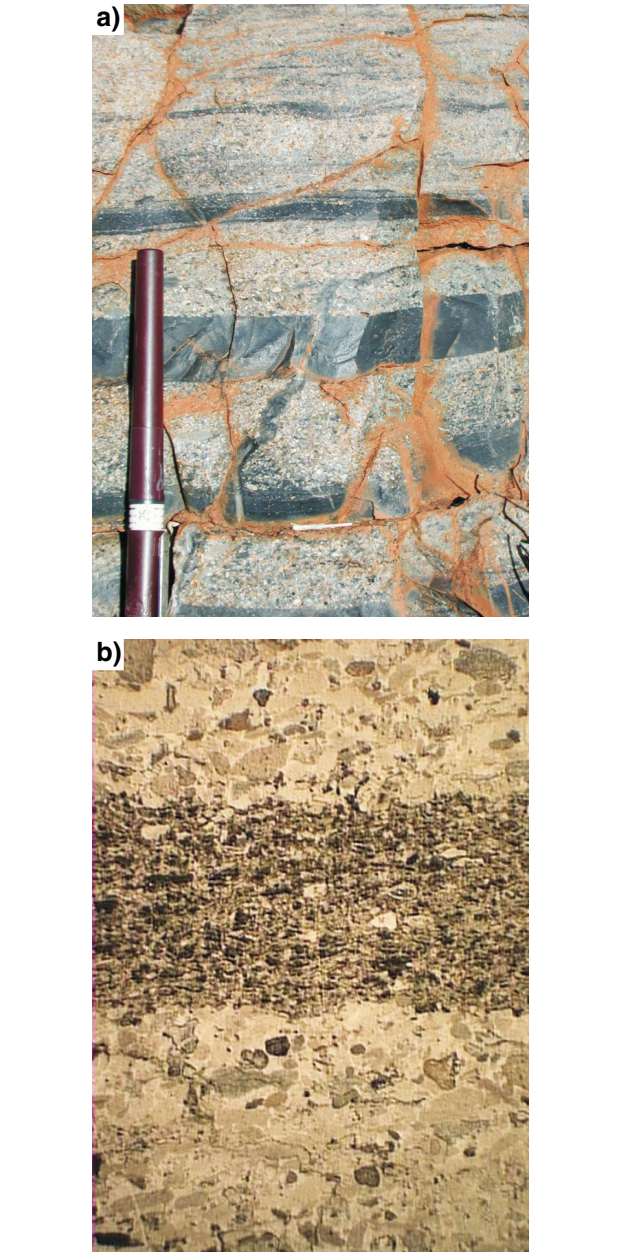

Figure 85. Features of silicified microbial mats in sandstone from the upper clastic member of the Strelley Pool Formation at the Trendall locality: a) general appearance of mats in silicified sandstone with transecting black chert vein; b) whole thin section view (plane-polarized light) of microbial mat in sandstone, showing clotted texture of kerogen and scattered sand grains (width of view = 2 cm; c) detailed photomicrograph (plane-polarized light) of clotted kerogen texture and silica-filled fenestrae (width of view = 1 mm).

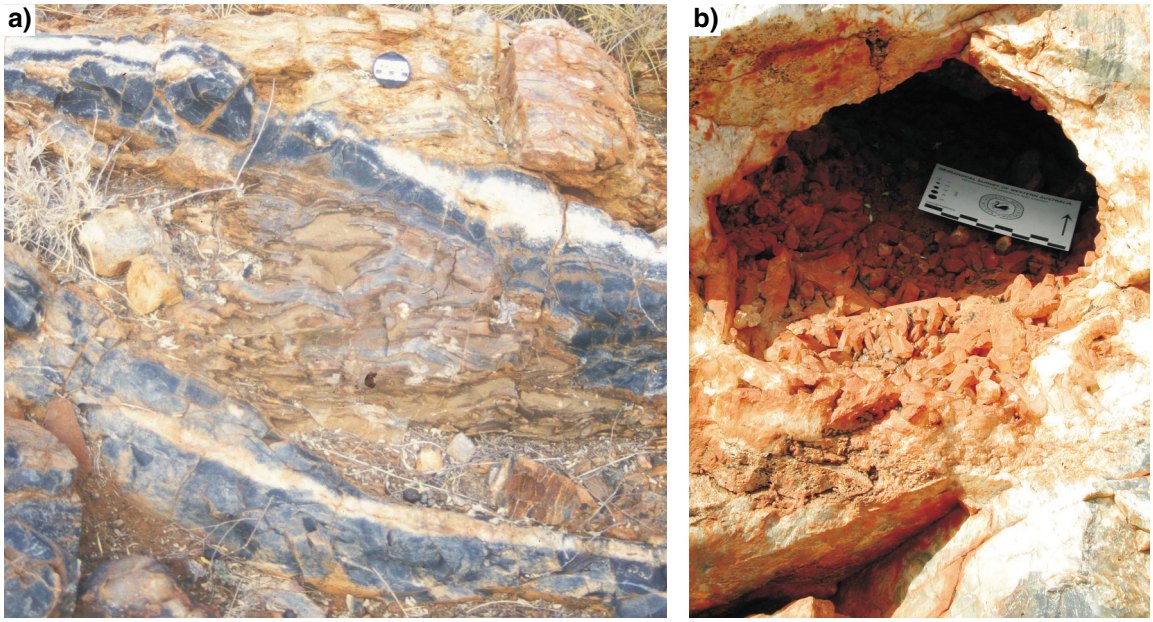

Figure 86. Hydrothermal quartz veins at the Trendall locality: a) zoned hydrothermal silica veins cutting dolomite, with black chert margins and white quartz cores. Note how fingers of silicification emanate out from the veins parallel to bedding in the dolomite; b) open central zone of hydrothermal quartz vein, lined with euhedral quartz crystals (coated with iron oxides).

References

Abouchami, W, Boher, M, Michard, A and Albarede, F 1990, A major 2.1 Ga event of mafic magmatism in West Africa: An early stage of crustal accretion: Journal of Geophysical Research, v. 95, p. 17 605–17 629.

Allen, RL 1988, False pyroclastic textures in altered silicic lavas, with implications for volcanic-associated mineralization: Economic Geology, v. 83, p. 1424–1446.

Allwood, AC, Walter, MR, Kamber, BS, Marshall, CP and Burch, IW 2006, Stromatolite reef from the Early Archaean era of Australia: Nature, v. 441, p. 714–717.

Anbar, AD, Duan, Y, Lyons, TW, Arnold, GL, Kendall, B, Creaser, RA, Kaufman, AJ, Gordon, GW, Scott, C, Garvin, J and Buick, R 2007, A whiff of oxygen before the Great Oxidation Event?: Science, v. 317, p. 1903–1906.

Arndt, NT, Nelson, DR, Compston, W, Trendall, AF and Thorne, AM 1991, The age of the Fortescue Group, Hamersley Basin, Western Australia, from microprobe zircon U–Pb results: Australian Journal of Earth Sciences, v. 38, p. 261–181.

Awramik, SM and Buchheim, HP 2009, A giant, Late Archean lake system: The Meetheena Member (Tumbiana Formation; Fortescue Group), Western Australia: Precambrian Research, v. 174, p. 215–240.

Banerjee, NR, Simonnetti, A, Furnes, H, Muehlenbachs, K, Staudigel, H, Heaman, L and Van Kranendonk, MJ 2007, Direct dating of Archean microbial ichnofossils: Geology, v. 35, p. 487–490.

Barley, ME, Pickard, AL and Sylvester, PJ 1997, Emplacement of a large igneous province as a possible cause of banded iron formation 2.45 billion years ago: Nature, v. 385, p. 55–58.

Bekker, A, Kaufman, AJ, Karhu, JA and Eriksson, KA 2005, Evidence for Paleoproterozoic cap carbonates in North America: Precambrian Research, v. 137, p. 167–206.

Beukes, NJ, Klein, C, Kaufman, AJ and Hayes, JM 1990, Carbonate petrography, kerogen distribution, and carbon and oxygen isotope variations in an early Proterozoic transition from limestone to iron-formation deposition, Transvaal Supergroup, South Africa: Economic Geology, v. 85, p. 663–690.

Blake, TS 1993, Late Archaean crustal extension, sedimentary basin formation, flood basalt volcanism and continental rifting: the Nullagine and Mount Jope Supersequences, Western Australia: Precambrian Research, v. 60, p. 185–241.

Blake, TS 2001, Cyclic continental mafic tuff and flood basalt volcanism in the Late Archaean Nullagine and Mount Jope Supersequences in the eastern Pilbara, Western Australia: Precambrian Research, v. 107, p. 139–177.

Blake, TS and Barley, ME 1992, Tectonic evolution of the Late Archaean to early Proterozoic Mount Bruce megasequence set, Western Australia: Tectonics, v. 11, p. 1415–1425.

Blake, TS, Buick, R, Brown, SJA and Barley, ME 2004, Geochronology of a Late Archaean flood basalt province in the Pilbara Craton, Australia: constraints on basin evolution, volcanic and sedimentary accumulation, and continental drift rates: Precambrian Research, v. 133, p. 143–173.

Bodorkos, S and Sandiford, M 2006, Thermal and mechanical controls on the evolution of Archean crustal deformation: examples from Western Australia, *in* Archean Geodynamics and Environments *edited by* K Benn, J-M Mareschal, and K Condie: American Geophysical Union, Geophysical Monograph Series 164, p. 131–147.

Bolhar, R and Van Kranendonk, MJ 2007, A non-marine depositional setting for the northern Fortescue Group, Pilbara Craton, inferred from trace element geochemistry of stromatolitic carbonates: Precambrian Research, v. 155, p. 229–250.

Brasier, MD, Green, OR, Jephcoat, AP, Kleppe, AK, Van Kranendonk, MJ, Lindsay, JF, Steele, A and Grassineau, N 2002, Questioning the evidence for Earth's oldest fossils: Nature, v. 416, p. 76–81.

Brasier, MD, Green, OR, Lindsay, JF, McLoughlin, N, Steele, A and Stokes, C 2005, Critical testing of Earth's oldest putative fossil assemblage from the ~3.5 Ga Apex chert, Chinaman Creek, Western Australia: Precambrian Research, v. 140, p. 55–102.

Brasier, MD, Green, OR, Lindsay, JF and Steele, A 2004, Earth's oldest (~3.5 Ga) fossils and the 'Early Eden hypothesis': Questioning the evidence: Origins of life and evolution of the Biosphere, v. 34, p. 257–269.

Brauhart, C 1999, Regional alteration systems associated with Archean volcanogenic massive sulphide deposits at Panorama, Pilbara, Western Australia: The University of Western Australia, Perth, PhD thesis (unpublished).

Brocks, JJ, Logan, GA, Buick, R and Summons, RE 1999, Archean molecular fossils and the early rise of Eukaryotes: Science, v. 285, p. 1033–1036.

Brocks, JJ, Buick, R, Logan, GA and Summons, RE 2003a, Composition and syngenicity of molecular fossils from the 2.78 to 2.45 billion-year-old Mount Bruce Supergroup, Pilbara Craton, Western Australia: Geochimica et Cosmochimica Acta, v. 67, p. 4289–4319.

Brocks, JJ, Buick, R, Summons, RE and Logan, GA 2003b, A reconstruction of Archean biological diversity based on molecular fossils from the 2.78 to 2.45 billion-year-old Mount Bruce Supergroup, Hamersley basin, Western Australia: Geochimica et Cosmochimica Acta, v. 67, p. 4321–4335.

Buggisch, W, Joachimski, MM, Lehnert, O, Bergstrom, SM, Repetski, JE and Webers, GF 2010, Did intense volcanism trigger the Ordovician icehouse?: Geology, v. 38, p. 327–330.

Buick, R 1984, Carbonaceous filaments from North Pole, Western Australia: are they fossil bacteria in Archean stromatolites?: Precambrian Research, v. 24, p. 157–172.

Buick, R 1988, Carbonaceous filaments from North Pole, Western Australia: are they fossil bacteria in Archean stromatolites? a reply: Precambrian Research, v. 39, p. 311–317.

Buick, R 1992, The antiquity of oxygenic photosynthesis — evidence from stromatolites in sulfate-deficient Archean lakes: Science, v. 255, p. 74–77.

Buick, R and Barnes, KR 1984, Cherts in the Warrawoona Group: Early Archaean silicified sediments deposited in shallow-water environments, *in* Archaean and Proterozoic Basins of the Pilbara, Western Australia: Evolution and Mineralization Potential *edited by* JR Muhling, DI Groves, and TS Blake: University of Western Australia, The Geology Department and University Extension, Publication 9, p. 37–53.

Buick, R and Dunlop, J 1990, Evaporitic sediments of early Archaean age from the Warrawoona Group, North Pole, Western Australia: Sedimentology, v. 37, p. 247–277.

Buick, R, Brauhart, CW, Morant, P, Thornett, JR, Maniw, JG, Archibald, NJ, Doepel, MG, Fletcher, IR, Pickard, AL, Smith, JB, Barley, ME, McNaughton, NJ and Groves, DI 2002, Geochronology and stratigraphic relationships of the Sulphur Springs Group and Strelley Granite: a temporally distinct igneous province in the Archaean Pilbara Craton, Australia. Precambrian Research, v. 114, p. 87–120.

Buick, R, Dunlop, JSR and Groves, DI 1981, Stromatolite recognition in ancient rocks: an appraisal of irregular laminated structures in an early Archaean chert–barite unit from North Pole, Western Australia: Alcheringa, v. 5, p. 161–181.

Buick, R, Thornett, JR, McNaughton, NJ, Smith, JB, Barley, ME and Savage, M 1995, Record of emergent continental crust ~3.5 billion years ago in the Pilbara Craton of Australia: Nature, v. 375, p. 574–577.

Byerly, GR, Lowe, DR, Wooden, JL and Xie, X 2002, An Archean impact layer from the Pilbara and Kaapvaal cratons: Science, v. 297, p. 1325–1327.

Cannon, WF, Schulz, KJ, Horton, JW Jr and Kring, DA 2010, The Sudbury impact layer in the Paleoproterozoic iron ranges of northern Michigan, USA: Geological Society of America, Bulletin, v. 122, p. 50–75.

Catling, DC, Zahnle, KJ and McKay, CP 2001, Biogenic methane, hydrogen escape, and the irreversible oxidation of early Earth: Science, v. 293, p. 839–843.

Cawood, PA and Tyler, IM 2004, Assembling and reactivating the Proterozoic Capricorn orogen: lithotectonic elements , orogenies, and significance: Precambrian Research, v. 128, p. 201–218.

Chivas, AR, Torgersen, T and Polach, HA 1990, Growth rates and Holocene development of stromatolites from Shark Bay, Western Australia: Australian Journal of Earth Sciences, v. 37, p. 113–121.

Condie, KC, O'Neill, C and Aster, RC 2009, Evidence and implications for a widespread magmatic shutdown for 250 My on Earth: Earth and Planetary Science Letters, v. 282, p. 294–298.

Corfu, F and Andrews, AJ 1986, A U–Pb age for mineralized Nipissing diabase, Gowganda, Ontario: Canadian Journal of Earth Sciences, v. 23, p. 107–109.

Cornell, DH, Schütte, SS and Eglington, BL 1996, The Ongeluk basaltic andesite formation in Griqualand West, South Africa: submarine alteration in a 2222 Ma Proterozoic sea: Precambrian Research, v. 79, p. 101–123.

Czaja, AD, Johnson, CM, Beard, BL, Eigenbrode, JL, Freeman, KH and Yamaguchi, KE 2010, Iron and carbon isotope evidence for ecosystem and environmental diversity in the ~2.7 to 2.5 Ga Hamersley Province, Western Australia: Earth and Planetary Science Letters, v. 292, p. 170–180.

Davy, R 1991, Mineralogy and chemical composition of a core from the Weeli Wolli Formation in the Hamersley Basin: Geological Survey of Western Australia, Record 1991/6, 103p.

Davy, R and Hickman, AH 1988, The transition between the Hamersley and Fortescue groups as evidenced in a drill core: Geological Survey of Western Australia, Report 23 Professional Papers, p. 85–97.

DiMarco, MJ and Lowe, DR 1989, Stratigraphy and sedimentology of an Early Archean felsic volcanic sequence, eastern Pilbara Block, Western Australia, with special reference to the Duffer Formation and implications for crustal evolution: Precambrian Research, v. 44, p. 147–169.

Duck, LJ, Glikson, M, Golding, SD and Webb, RE 2007, Microbial remains and other carbonaceous forms form the 3.24 Ga Sulphur Springs black smoker deposit, Western Australia: Precambrian Research, v. 154, p. 205–220.

Eigenbrode, JL, Freeman, KH and Summons, RE 2008, Methylhopane biomarker hydrocarbons in Hamersley Province sediments provide evidence for Neoarchean aerobiosis: Earth and Planetary Science Letters, v. 273, p. 323–331.

Evans, DAD, Sircombe, K, Wingate, MTD, Doyle, M, McCarthy, M, Pidgeon, RT and van Niekerk, HS 2003, Revised geochronology of magmatism in the western Capricorn Orogen at 1805–1785 Ma: diachroneity of the Pilbara–Yilgarn collision: Australian Journal of Earth Sciences, v. 50, p. 853–864.

Foukal, P 2003, Can slow variations in solar luminosity provide missing link between Sun and climate?: Eos, v. 84 (22), p. 205–208.

Furnes, H, Banerjee, NR, Staudigel, H, Muehlenbachs, K, de Wit, M and Van Kranendonk, MJ 2007, Comparing petrographic signatures of bioalteration in recent to Mesoarchean pillow lavas: Tracing subsurface life in oceanic igneous rocks: Precambrian Research, v. 158, p. 156–176.

Garcia-Ruiz JM, Hyde, ST, Carnerup, AM, Christy, AG, Van Kranendonk, MJ and Welham, NJ 2003, Self-assembled silica–carbonate structures and detection of ancient microfossils: Science, v. 302, p. 1194–1197.

Garret, P 1970, Phanerozoic stromatolites: noncompetitive ecological restriction by grazing and burrowing organisms: Science, v. 169, p. 171–173.

Garvin, J, Buick, R, Anbar, AD, Arnold, GL and Kaufman, AJ 2009, Isotopic evidence for an aerobic nitrogen cycle in the latest Archean: Science, v. 323, p. 1045–1048.

Glikson, AY, Allen, C and Vickers, J 2004, Multiple 3.47-Ga-old asteroid impact fallout units, Pilbara Craton, Western Australia: Earth and Planetary Science Letters, v. 21, p. 383–396.

Glikson, M, Duck, LJ, Golding, SD, Hofmann, A, Bolhar, R, Webb, R, Baiano, JCF and Sly, LI 2008, Microbial remains in some earliest Earth rocks: Comparison with a potential modern analogue: Precambrian Research, v. 164, p. 187–200.

Green, MG, Sylvester, PJ and Buick, R 2000, Growth and recycling of early Archaean continental crust: geochemical evidence from the Coonterunah and Warrawoona Groups, Pilbara Craton, Australia: Tectonophysics, v. 322, p. 69–88.

Grey, K and Thorne, AM 1985, Biostratigraphic significance of stromatolites in upward shallowing sequences of the early Proterozoic Duck Creek Dolomite, Western Australia: Precambrian Research, v. 29, p. 183–206.

Griffin, WL and O'Reilly, SY 2007, The earliest subcontinental lithospheric mantle, *in* Earth's Oldest Rocks *edited by* MJ Van Kranendonk, RH Smithies, and V Bennett: Elsevier, Amsterdam, Developments in Precambrian Geology 15, p. 1013–1036.

Groves, DI, Dunlop, JSR and Buick, R 1981, An early habitat of life: Scientific American, v. 245, p. 64–73.

Hall, CE, Powell, CM and Bryant, J 2001, Basin setting and age of the Late Paleoproterozoic Capricorn Formation, Western Australia: Australian Journal of Earth Sciences, v. 48, p. 731–744.

Hassler, SW and Simonson, BM 2001, The sedimentary record of extraterrestrial impacts in deep-shelf environments: Evidence from the early Precambrian: The Journal of Geology, v. 109, p. 1–19.

Hassler, SW, Simonson, BW, Sumner, DY and Murphy, M 2005, Neoarchaean spherule layers in the Fortescue and Hamersley groups: Stratigraphic and depositional implications of re-correlation: Australian Journal of Earth Sciences, v. 52, p. 759–771.

Hickman, AH 1983, Geology of the Pilbara Block and its environs: Geological Survey of Western Australia, Bulletin 127, 268p.

Hickman, AH 1984, Archaean diapirism in the Pilbara Block, Western Australia, *in* Precambrian Tectonics Illustrated *edited by* A Kröner and RE Greiling: Schweizerbarts'che Verlagsbuchhandlung, Stuttgart, p. 113–127.

Hickman, AH 2004, Two contrasting granite–greenstones terranes in the Pilbara Craton, Australia: evidence for vertical *and* horizontal tectonic regimes prior to 2900 Ma: Precambrian Research, v. 131, p. 153–172.

Hickman, AH 2008, Regional review of the 3426–3350 Ma Strelley Pool Formation, Pilbara Craton, Western Australia: Geological Survey of Western Australia, Record 2008/15, 27p.

Hickman, AH and de Laeter, JR 1977, The depositional environment and age of a shale within the Hardey Sandstone of the Fortescue Group: Geological Survey of Western Australia, Annual Report 1976, p. 62–68.

Hickman, AH and Van Kranendonk, MJ 2004, Diapiric processes in the formation of Archaean continental crust, East Pilbara Granite-Greenstone Terrane, Australia, *in* The Precambrian Earth: Tempos and Events *edited by* PG Eriksson, W Altermann, DR Nelson, WU Mueller, and O Catuneau: Elsevier, Amsterdam, Developments in Precambrian Geology 12, p. 54–75.

Hoffman, P 1976, Stromatolite morphogenesis in Shark Bay, Western Australia, *in* Stromatolites *edited by* MR Walter: Elsevier, Amsterdam, Developments in Sedimentology, v. 20, p. 261–271.

Hofmann, HJ, Grey, K, Hickman, AH and Thorpe, R 1999, Origin of 3.45 Ga coniform stromatolites in the Warrawoona Group, Western Australia: Geological Society of America, Bulletin, v. 111, p. 1256–1262.

Holland, HD 1994, Early Proterozoic atmospheric change, *in* Early Life on earth *edited by* S Bengston: Nobel Symposium, v. 84, p. 237–244.

Holland, HD 2002, Volcanic gases, black smokers, and the Great Oxidation Event: Geochimica et Cosmochimica Acta, v. 66, p. 3811–3826.

Horwitz, RC 1982, Geological history of the Early Proterozoic Paraburdoo Hinge Zone, Western Australia: Precambrian Research, v. 19, p. 191–200.

Huston, DL, Brauhart, CW, Dreiberg, SL, Davidson, GJ and Groves, DI 2001, Metal leaching and inorganic sulphate reduction in volcanic-hosted massive sulphide mineral systems: Evidence from the paleo-Archean Panorama district, Western Australia: Geology, v. 29, p. 687–690.

Jahn, B-M and Simonson, MB 1995, Carbonate Pb–Pb ages of the Wittenoom Formation and Carawine Dolomite, Hamersley Basin, Western Australia (with implications for their correlation with the Transvaal Dolomite of South Africa): Precambrian Research, v. 72, p. 247–261.

Jost, H, Chemale Jr, F, Dussin, IA, Tassinari, CCG and Martins, R 2010, A U–Pb zircon Paleoproterozoic age for the metasedimentary host rocks and gold mineralization of the Crixás greenstone belt, Goiás, Central Brazil: Ore Geology Reviews, v. 37, p. 127–139.

Kirschvink, JL, Gaidos, EJ, Bertani, LE, Beukes, NJ, Gutzmer, J, Maepa, LN and Steinberger, RE 2000, Paleoproterozoic snowball Earth: Extreme climatic and geochemical global change and its biological consequences: Proceedings of the National Academy of Sciences, v. 97, p. 1400–1405.

Knoll, AH and Barghoorn, ES 1976, A Gunflint-type microbiota from the Duck Creek Dolomite, Western Australia: Origins of Life and Evolution of Biospheres, v. 7, p. 417–423.

Knoll, AH, Strother, PK and Rossi, S 1988, Distribution and diagenesis of microfossils from the Lower Proterozoic Duck Creek Dolomite, Western Australia: Precambrian Research, v. 38, p. 257–279.

Krapež, B 1996, Sequence stratigraphic concepts applied to the identification of basin-filling rhythms in Precambrian successions: Australian Journal of Earth Sciences, v. 43, p. 355–380.

Krapež, B 1999, Stratigraphic record of an Atlantic-type global tectonic cycle in the Paleoproterozoic Ashburton Province of Western Australia: Australian Journal of Earth Sciences, v. 46, p. 71–87.

Krapež, B, Barley, ME and Pickard, AL 2003, Hydrothermal and resedimented origins of the precursor sediments to banded iron formation: sedimentological evidence from the Early Paleoproterozoic Brockman Supersequence of Western Australia: Sedimentology, v. 50, p. 979–1011.

Krapež, B and McNaughton, NJ 1999, SHRIMP zircon U–Pb age and tectonic significance of the Paleoproterozoic Boolaloo Granodiorite in the Ashburton Province, Western Australia: Australian Journal of Earth Sciences, v. 46, p. 283–287.

Lambert, I, Donnelly, T, Dunlop, J and Groves, D 1978, Stable isotopic compositions of early Archaean sulphate deposits of probable evaporitic and volcanogenic origins: Nature, v. 276, p. 808–811.

Lepot, K, Benzerara, K, Brown, Jr, GE and Philippot, P 2008, Microbially influenced formation of 2,724-million-year-old stromatolites: Nature Geoscience, v. 1, p. 118–121.

Lepot, K, Benzerara, K, Rividi, N, Cotte, M, Brown, Jr, GE and Philippot, P 2009, Organic matter heterogeneities on 2.72 Ga stromatolites: Alteration versus preservation by sulfur incorporation: Geochimica et Cosmochimica Acta, v. 73, p. 6579–6599.

Lindsay, JF and Brasier, MD 2002, Did global tectonics drive early biosphere evolution? Carbon isotope record from 2.6 to 1.9 Ga carbonates of Western Australia: Precambrian Research, v. 114, p. 1–34.

Lindsay, JF, Brasier, MD, McLoughlin, N, Green, OR, Fogel, M, Steele, A and Mertzman, SA 2005, The problem of deep carbon — an Archaean paradox: Precambrian Research, v. 143, p. 1–22.

Logan, BW 1961, Cryptozoon and associate stromatolites from the Recent Shark Bay, Western Australia: Journal of Geology, v. 69, p. 517–533.

Logan, BW, Hoffman, P and Gebelein, CD 1974, Algal mats, cryptalgal fabrics and structures, Hamelin Pool, Western Australia, *in* Evolution and diagenesis of Quaternary carbonate sequences, Shark Bay, Western Australia: American Association of Petroleum Geology, Memoir 22, p. 140–194.

Lorenz, V 1986, On the growth of maars and diatremes and its relevance to the formation of tuff rings: Bulletin of Volcanology, v. 48, p. 265–274.

Lowe, DR 1980, Stromatolites 3,400-Myr old from the Archaean of Western Australia: Nature, v. 284, p. 441–443.

Lowe, DR 1983, Restricted shallow-water sedimentation of Early Archaean stromatolitic and evaporitic strata of the Strelley Pool Chert, Pilbara Block, Western Australia: Precambrian Research, v. 19, p. 239–283.

Lowe, DR 1994, Abiological origin of described stromatolites older than 3.2 Ga: Geology, v. 22, p. 387–390.

Lowe, DR and Byerly, GR 1986, Early Archaean silicate spherules of probable impact origin, South Africa and Western Australia: Geology, v. 14, p. 83–86.

Marshall, CP, Love, GD, Snape, CE, Hill, AC, Allwood, AC, Walter, MR, Van Kranendonk, MJ, Bowden, SA, Sylva, SP and Summons, RE 2007, Structural characterization of kerogen in 3.4 Ga Archaean cherts from the Pilbara Craton, Western Australia: Precambrian Research, v. 155, p. 1–23.

Martin, DM 1999, Depositional setting and implications of Paleoproterozoic glaciomarine sedimentation in the Hamersley Province, Western Australia: Geological Society of America, Bulletin, v. 111, p. 189–203.

Martin, DM and Morris, P in press, Tectonic setting and regional implications of c. 2.2 Ga mafic magmatism in the southern Hamersley province, Western Australia: Australian Journal of Earth Sciences.

Martin, DM and Thorne, AM 2004, Tectonic setting and basin evolution of the Bangemall Supergroup in the northwest Capricorn Orogen: Precambrian Research, v. 128, p. 385–409.

Martin, DM, Li, ZX, Nemchin, AA and Powell, CM 1998, A pre-2.2 Ga age for giant hematite ores of the Hamersley province, Australia: Economic Geology, v. 93, p. 1084–1090.

Martin, DM, Powell, CM and George, AD 2000, Stratigraphic architecture and evolution of the early Paleoproterozoic McGrath Trough, Western Australia: Precambrian Research, v. 99, p. 33–64.

McCollom, TM 2003, Formation of meteorite hydrocarbons from thermal decomposition of siderite ($FeCO_3$): Geochimica et Cosmochimica Acta, v. 67, p. 311–317.

McConchie, D 1987, The geology and geochemistry of the Joffre and Whaleback Shale members of the Brockman Iron Formation, Western Australia, *in* Precambrian iron formations *edited by* PWU Appel, and GL LaBerge: Theophrastus Publications, SA, Athens, p. 541–597.

Melezhik, VA, Fallick, AE, Hanski, EJ, Kump, LR, Lepland, A, Prave, AR and Strauss, H 2005, Emergence of the aerobic biosphere during the Archean–Proterozoic transition: Challenges of future research: GSA Today, v. 15, p. 4–11.

Müller, SG, Krapež, B, Barley, ME and Fletcher, IR 2005a, Giant iron-ore deposits of the Hamersley province related to the breakup of Paleoproterozoic Australia: New insights from in situ SHRIMP dating of baddeleyite from mafic intrusions: Geology, v. 33, p. 577–580.

Müller, SG, Krapež, B, Bekker, A and Barley, ME 2005b, A Palaeoproterozoic (~2030 Ma) syn-rift carbonate platform from the Ashburton Province, Western Australia: global significance of $\delta^{13}C$ enriched carbonates from the Wooly Dolomite, *in* The tectonic evolution and volcanism of the Lower Wyloo Group, Ashburton Province, with timing implications for giant-ore deposits of the Hamersley Province, Western Australia: The University of Western Australia, Perth, PhD thesis (unpublished).

Myers, JS 1993, Precambrian history of the West Australian Craton and adjacent orogens: Annual review of Earth and Planetary Sciences, v. 21, p. 453–485.

Nelson, DR 2000, Compilation of geochronology data, 1999: Geological Survey of Western Australia, Record 2000/2, 251p.

Nelson, DR 2004a, 169084: ferruginous sandstone, Miringee Well; Geochronology Record 43: Geological Survey of Western Australia, 5p.

Nelson, DR 2004b, 169081: pebbly sandstone, Meteorite Bore; Geochronology Record 116: Geological Survey of Western Australia, 4p.

Nelson, DR 2004c, 169082: sandstone, Meteorite Bore; Geochronology dataset 42: Geological Survey of Western Australia, 4p.

Nelson, DR 2004d, 148922: crystal-vitric tuff, Koonong Pool; Geochronology dataset 249: Geological Survey of Western Australia, 4p.

Nijman, W and de Vries, ST 2004, Early Archaean crustal collapse structures and sedimentary basin dynamics, *in* The Precambrian Earth: Tempos and Events *edited by* PG Eriksson, W Altermann, DR Nelson,WU Mueller, and O Catuneau: Elsevier, Amsterdam, Developments in Precambrian Geology 12, p. 139–154.

Nijman, W, de Bruijne, KCH and Valkering, ME 1998, Growth fault control of Early Archaean cherts, barite mounds and chert–barite veins, North Pole Dome, Eastern Pilbara, Western Australia: Precambrian Research, v. 88, p. 25–52.

Noble, SR and Lightfoot, PC 1992, U–Pb baddelyite ages of the Kerns and Triangle Mountain intrusions, Nipissing Diabase, Ontario: Canadian Journal of Earth Sciences, v. 29, p. 1424–1429.

Onstott, TC, Phelps, TJ, Colwell, FS, Ringelberg, D, White, DC and Boone, DR 1998, Observations pertaining to the origin and ecology of microorganisms recovered from the deep subsurface of Taylorsville Basin, Virginia: Geomicrobiology, v. 15, p. 353–385.

Packer, BM 1990, Sedimentology, paleontology, and stable-isotope geochemistry of selected formations in the 2.7-billion-year-old Fortescue Group, Western Australia: University of California at Los Angeles, Los Angeles, PhD thesis (unpublished).

Papineau, D, Mojzsis, SJ and Schmitt, AK 2007, Multiple sulphur isotopes from Paleoproterozoic Huronian interglacial sediments and the rise of atmospheric oxygen: Earth and Planetary Science Letters, v. 255, p. 188–212.

Partridge, MA, Golding, SD, Baublys, KA and Young, E 2008, Pyrite paragenesis and multiple sulphur isotope distribution in late Archean and early Paleoproterozoic Hamersley Basin sediments: Earth and Planetary Science Letters, v. 272, p. 41–49.

Pavlov, AA, Hurtgen, MT, Kasting, JF and Arthur, MA 2003, Methane-rich Proterozoic atmosphere?: Geology, v. 31, p. 87–90.

Pavlov, AA, Kasting, JF, Eigenbrode, JL and Freeman, KH 2001, Organic haze in Earth's early atmosphere: Source of low-^{13}C Late Archean kerogens?: Geology, v. 29, p. 1003–1006.

Pecoits, E, Gingras, MK, Barley, ME, Kappler, A, Posth, NR and Konhauser, KO 2009, Petrography and geochemistry of the Dales Gorge banded iron formation: Paragenetic sequence, source and implications for paleo-ocean chemistry: Precambrian Research, v. 172, p. 163–187.

Philippot, P, Van Zuilen, M, Lepot, K, Thomazo, C, Farquhar, J and Van Kranendonk, M 2007, Early Archean microorganisms preferred elemental sulphur, not sulphate: Science, v. 317, p. 1534–1537.

Pickard, AL 2002, SHRIMP U–Pb zircon ages of tuffaceous mudrocks in the Brockman Iron Formation of the Hamersley Range, Western Australia: Australian Journal of Earth Sciences, v. 49, p. 3491–3507.

Pickard, AL, Barley, ME and Krapež, B 2004, Deep-marine depositional setting of banded iron formation: sedimentological evidence from interbedded clastic sedimentary rocks in the early Paleoproterozoic Dales Gorge Member of Western Australia: Sedimentary Geology, v. 170, p. 37–62.

Pirajno, F, Hocking, RM, Reddy, SM and Jones, AM 2009, A review of the geology and geodynamic evolution of he Paleoproterozoic Earaheedy Basin, Western Australia: Earth-Science Reviews, v. 94, p. 39–77.

Playford, PE 1990, Geology of the Shark Bay artea, Western Australia, *in* Research in Shark Bay *edited by* PF Berry, SD Bradshaw, and BR Wilson: Western Australian Museum, p. 13–31.

Playford, PE and Cockbain, AE 1976, Modern algal stromatolites at Hamelin Pool, a hypersaline barred basin in Shark Bay, Western Australia, *in* Stromatolites *edited by* MR Walter: Elsevier, Amsterdam, Developments in Sedimentology 20, p. 389–411.

Powell, CMcA and Horwitz, RC 1994, Late Archean and early Proterozoic tectonics and basin formation of the Hamersley Ranges: 12th Australian Geological Convention, Perth, Geological Society of Australia, Excursion Guidebook 4, 57p.

Rasmussen, B 2000, Filamentous microfossils in a 3,235-million-year-old volcanogenic massive sulphide deposit: Nature, v. 405, p. 676–679.

Rasmussen, B, Blake, TS and Fletcher, IR 2005b, U–Pb zircon age constraints on the Hamersley spherule beds: Evidence for a single 2.63 Ga Jeerinah–Carawine impact ejecta layer: Geology, v. 33, p. 725–728.

Rasmussen, B, Blake, TS, Fletcher, IR and Kilburn, MR 2009, Evidence for microbial life in synsedimentary cavities from 2.75 Ga terrestrial environments: Geology, v. 37, p. 423–426.

Rasmussen, B, Fletcher, IR, Brocks, JJ and Kilburn, MR 2008, Reassessing the first appearance of eukaryotes and cyanobacteria: Nature, v. 455, p. 1101–1104.

Rasmussen, B, Fletcher, IR and Muhling, JR 2007. In situ U–Pb dating and element mapping of three generations of monazite: Unravelling cryptic tectonothermal events in low-grade terranes: Geochimica et Cosmochimica Acta, v. 71, p. 670–690.

Rasmussen, B, Fletcher, IR and Sheppard, S 2005a, Isotopic dating of a low-grade metamorphic front during orogenesis: Geology, v. 33, p. 773–776.

Rasmussen, B and Koeberl, C 2004, Iridium anomalies and shocked quartz in a Late Archean spherule layer from the Pilbara craton: New evidence for a major asteroid impact at 2.63 Ga: Geology, v. 32, p. 1029–1032.

Reid, RP, James, NP, Macintyre, IG, Dupraz, CP and Burne, RV 2003, Shark Bay Stromatolites: microfabrics and reinterpretation of origins: Facies, v. 49, p. 299–324.

Sakuri, R, Ito, M, Ueno, Y, Kitajima, K and Maruyama, S 2005, Facies architecture and sequence-stratigraphic features of the Tumbiana

Formation in the Pilbara Craton, northwestern Australia: Implications for depositional environments of oxygenic stromatolites during the Late Archean: Precambrian Research, v. 138, p. 255–273.

Sandiford, M, Van Kranendonk, MJ and Bodorkos, S 2004, Conductive incubation and the origin of dome-and-keel structure in Archean granite–greenstone terrains: a model based on the eastern Pilbara Craton, Western Australia: Tectonics, v. 23, TC1009, doi: 10.1029/2002TC001452.

Schopf, JW 1993, Microfossils of the Early Archaean Apex Chert: new evidence of the antiquity of life: Science, v. 260, p. 640–646.

Schopf, JW, Kudryavtsev, AB, Agresti, DG, Wdowiak, TJ and Czaja, AD 2002, Laser-Raman imagery of Earth's earliest fossils: Nature, v. 416, p. 73–76.

Schopf, JW, Kudryavtsev, AB, Czaja, AD and Tripathi, AB 2007, Evidence of Archean life: Stromatolites and microfossils: Precambrian Research, v. 158, p. 141–155.

Schopf, JW and Walter, MR 1983, Archean microfossils: new evidence of ancient microbes, *in* Earth's earliest biosphere *edited by* JW Schopf: Princeton University Press, Princeton, p. 214–239.

Seymour, DB, Thorne, AM and Blight, DB 1988, Wyloo, Western Australia (2nd edition): Geological Survey of Western Australia, 1:250 000 Geological Series Explanatory Notes, 36p.

Shen, Y, Buick, R and Canfield, DE 2001, Isotopic evidence for microbial sulphate reduction in the early Archaean era: Nature, v. 410, p. 77–81.

Simonson, BM 1992, Geological evidence for a strewn field of impact spherules in the early Precambrian Hamersley Basin of Western Australia: Geological Society of America, Bulletin, v. 104, p. 829–839.

Simonson, BW and Hassler, SW 1997, Revised correlations in the early Precambrian Hamersley Basin based on a horizon of resedimented impact spherules: Australian Journal of Earth Sciences, v. 44, p. 37–48.

Sircombe, K 2003, Age of the Mt Boggola volcanic succession and further geochronological constraint on the Ashburton Basin, Western Australia: Australian Journal of Earth Sciences, v. 50, p. 967–974.

Slack, JF and Cannon WF 2010, Extraterrestrial demise of banded iron formations 1.85 billion years ago: Geology, v. 37, p. 1011–1014.

Smith, JB, Barley, ME, Groves, DI, Krapež, B, McNaughton, NJ, Bickle, MJ and Chapman, HJ 1998, The Sholl Shear Zone, West Pilbara: evidence for a domain boundary structure from integrated tectonic analyses, SHRIMP U–Pb dating and isotopic and geochemical data of granitoids: Precambrian Research, v. 88, p. 143–171.

Smith, RE, Pedrix, JL and Parks, TC 1982, Burial metamorphism in the Hamersley Basin, Western Australia: Journal of Petrology, v. 23, p. 75–102.

Smithies, RH, Champion, DC and Sun, S–S 2004, Evidence for early LILE-enriched mantle source region: diverse magmas from the c. 2.95 – 3.0 Ga Mallina Basin, Pilbara Craton, NW Australia: Journal of Petrology, v. 45, p. 1515–1537.

Smithies, RH, Champion, DC and Van Kranendonk, MJ 2007a, The oldest well-preserved volcanic rocks on Earth: geochemical clues to the early evolution of the Pilbara Supergroup and implications for the growth of a Paleoarchean continent, *in* Earth's Oldest Rocks *edited by* MJ Van Kranendonk, RH Smithies, and V Bennet: Elsevier, Amsterdam, Developments in Precambrian Geology 15, p. 339–367.

Smithies, RH, Champion, DC, Van Kranendonk, MJ, Howard, HM and Hickman, AH 2005a, Modern-style subduction processes in the Mesoarchaean: geochemical evidence from the 3.12 Ga Whundo intraoceanic arc: Earth and Planetary Science Letters, v. 231, p. 221–237.

Smithies, RH, Van Kranendonk, MJ and Champion, DC 2005b, It started with a plume — early Archaean basaltic proto-continental crust: Earth and Planetary Science Letters, v. 238, p. 284–297.

Smithies, RH, Van Kranendonk, MJ and Champion, DC 2007b, The Mesoarchaean emergence of modern style subduction, *in* Island Arcs: Past and Present *edited by* S Maruyama and M Santosh; Gondwana Research, v. 11, p. 50–68.

Strik, GMHA 2004, Paleomagnetism of late Archaean flood basalt terrains: implications for early Earth geodynamics and geomagnetism: Geological Ultraiectina, v. 242, Mededelingen van de Faculteit Geowetenschappen, Universiteit Utrecht, 160p.

Strik, GMHA, Blake, TS, Zegers, TE, White, SH and Langereis, CG 2003, Paleomagnetism of flood basalts in the Pilbara Craton, Western Australia: Late Archaean continental drift and the oldest known reversal of the geomagnetic field: Journal of Geophysical Research, v. 108, No. B12, 2551, doi:10.1029/2003JB002475.

Sun, S-S and McDonough, WF 1989, Chemical and isotopic systematics of oceanic basalts: implications for mantle compositions and processes: Geololgical Society, Special Publication 42, p. 3131–3145.

Takehara, M, Komure, M, Kiyokawa, S, Horie, K and Yokoyama, K 2010, Detrital zircon SHRIMP U–Pb age of 2.3 Ga diamictites of the Meteorite Bore Member in south Pilbara, Western Australia: Geological Survey of Western Australia, 5th International Archean Symposium, Abstracts volume, in press.

Taran, YA and Giggenbach, WF 2003, Geochemistry of light hydrocarbons in subduction-related volcanic and hydrothermal fluids, *in* Volcanic, geothermal, and ore-forming fluids: rulers and witnesses of processes within the Earth, *edited by* SF Simmons and I Graham; Society of Economic Geologists, Special Publication 10, p. 61–74.

Taylor, D, Dalstra, HJ, Harding, AE, Broadbent, GC and Barley, ME 2001, Genesis of high-grade hematite orebodies of the Hamersley Province, Western Australia: Economic Geology, v. 96, p. 837–873.

Taylor, SR and McLennan, SM 1985, The continental crust: its composition and evolution: Blackwell Scientific Publications, Oxford, 312p.

Thorne, AM 1990, Ashburton Basin, *in* Geology and mineral resources of Western Australia: Geological Survey of Western Australia, Memoir 3, p. 210–219.

Thorne, AM and Seymour, DB 1991, Geology of the Ashburton Basin: Geological Survey of Western Australia, Bulletin 139, 141p.

Thorne, AM and Tyler, IM 1996, Roy Hill, WA Sheet 50-12: Geological Survey of Western Australia, 1:250 000 Geological Series.

Thorne, AM, Tyler, IM and Blight, DF 1995, Rocklea, WA Sheet 2352: Geological Survey of Western Australia, 1:100 000 Geological Series.

Thorpe, RA, Hickman, AH, Davis, DW, Mortensen, JK and Trendall, AF 1992a, U–Pb zircon geochronology of Archaean felsic units in the Marble Bar region, Pilbara Craton, Western Australia: Precambrian Research, v. 56, p. 169–189.

Thorpe, RI, Hickman, AH, Davis, DW, Mortensen, JK and Trendall, AF 1992b, Constraints to models for Archaean lead evolution from precise U–Pb geochronology from the Marble Bar region, Pilbara Craton, Western Australia, *in* The Archaean: Terrains, processes and metallogeny *edited by* JE Glover and S Ho: The University of Western Australia, Geology Department and University Extension, Publication 22, p. 395–408.

Trendall, AF 1979, A revision of the Mount Bruce Supergroup: Geological Survey of Western Australia, Annual Report 1978, p. 63–71.

Trendall, AF 1981, The Lower Proterozoic Meteorite Bore Member, Hamersley Basin, Western Australia, *in* Earth's Pre-Pleistocene glacial record *edited by* MJ Hambrey and WB Harland: Cambridge University Press, Cambridge, p. 555–557.

Trendall, AF 1990, Hamersley Basin, *in* Geology and mineral resources of Western Australia: Geological Survey of Western Australia, Memoir 3, p. 163–190.

Trendall, AF and Blockley, JG 1970, The iron formations of the Precambrian Hamersley Group, Western Australia: Geological Survey of Western Australia, Bulletin 119, 366p.

Trendall, AF, Compston, W, Nelson, DR, de Laeter, JR and Bennett, VC 2004, SHRIMP zircon ages constraining the depositional chronology of the Hamersley Group, Western Australia: Australian Journal of Earth Sciences, v. 51, p. 621–644.

Trendall, AF, Nelson, DR, de Laeter, JR and Hassler, SW 1998, Precise zircon U–Pb ages from the Marra Mamba Iron Formation and Wittenoom Formation, Hamersley Group, Western Australia: Australian Journal of Earth Sciences, v. 45, p. 137–142.

Tryon, MD, Brown, KM, Torres, ME, Tréhu, AM, McManus, J and Collier, RW 1999, Measurements of transience and downward fluid flow near episodic methane gas vents, Hydrate Ridge, Cascadia: Geology, v 27, p. 1075–1078.

Tyler, IM and Thorne, AM 1990, The northern margin of the Capricorn Orogen, Western Australia — an example of an Early Proterozoic collision zone: Journal of Structural Geology, v. 12, p. 685–701.

Ueno, Y, Yoshioka, H, Maruyama, S and Isozaki, Y 2004, Carbon isotopes and petrography in ~3.5 Ga hydrothermal silica dykes in the North Pole area, Western Australia: Geochimica et Cosmochimica Acta, v. 68, p. 573–589.

Van Kranendonk, MJ 1999, North Shaw, WA Sheet 2755: Geological Survey of Western Australia, 1:100 000 Geological Series.

Van Kranendonk, MJ 2000, Geology of the North Shaw 1:100 000 sheet: Geological Survey of Western Australia, 1:100 000 Geological Series Explanatory Notes, 86p.

Van Kranendonk, MJ 2004, Coongan, WA Sheet 2856: Geological Survey of Western Australia, 1:100 000 Geological Series.

Van Kranendonk, MJ 2006, Volcanic degassing, hydrothermal circulation and the flourishing of early life on Earth: new evidence from the Warrawoona Group, Pilbara Craton, Western Australia: Earth Science Reviews, v. 74, p. 197–240.

Van Kranendonk, MJ 2007, A review of the evidence for putative Paleoarchean life in the Pilbara Craton, *in* Earth's Oldest Rocks *edited by* MJ Van Kranendonk, RH Smithies, and V Bennet: Elsevier, Amsterdam, Developments in Precambrian Geology 15, p. 855–896.

Van Kranendonk, MJ 2010, Stromatolite morphology as an indicator of biogenicity for Earth's oldest fossils from the 3.5 – 3.4 Ga Pilbara Craton, Western Australia, *in* Advances in Stromatolite Geobiology *edited by* J Reitner, N-V Queric, and G Arp: Springer, Germany, Lecture Notes in Earth Sciences, v. 131, 200p.

Van Kranendonk, MJ and Pirajno, F 2004, Geological setting and geochemistry of metabasalts and alteration zones associated with hydrothermal chert ± barite deposits in the c. 3.45 Ga Warrawoona Group, Pilbara Craton, Australia: Geochemistry: Exploration, Environment, Analysis, v. 4, p. 253–278.

Van Kranendonk, MJ, Bleeker, W and Ketchum, J 2006, Phreatomagmatic boulder conglomerates at the fracture propagation tip of the 2.77 Ga Black Range dolerite dyke, Pilbara Craton, Western Australia: Australian Journal of Earth Sciences, v. 53, p. 617–630.

Van Kranendonk, MJ, Collins, WJ, Hickman, AH and Pawley, MJ 2004, Critical tests of vertical vs horizontal tectonic models for the Archaean East Pilbara granite–greenstone terrane, Pilbara Craton, Western Australia. Precambrian Research, v. 131, p. 173–211.

Van Kranendonk, MJ, Hickman, A and Smithies, RH 2007b, The East Pilbara Terrane of the Pilbara Craton, Western Australia: Formation of a continental nucleus through repeated mantle plume magmatism, *in* Earth's Oldest Rocks *edited by* MJ Van Kranendonk, RH Smithies, and V Bennet: Elsevier, Amsterdam, Developments in Precambrian Geology 15, p. 307–337.

Van Kranendonk, MJ, Hickman, AH, Smithies, RH, Nelson, DN and Pike, G 2002, Geology and tectonic evolution of the Archaean North Pilbara terrain, Pilbara Craton, Western Australia: Economic Geology, v. 97, p. 695–732.

Van Kranendonk, MJ, Hickman, AH, Williams, IR and Nijman, W 2001, Archaean geology of the East Pilbara Granite–Greenstone Terrane, Western Australia — a field guide: Geological Survey of Western Australia, Record 2001/9, 134p.

Van Kranendonk, MJ, Philippot, P, Lepot, K, Bodorkos, S and Pirajno, F 2008, Geological setting of Earth's oldest fossils in the c. 3.5 Ga Dresser Formation, Pilbara Craton, Western Australia: Precambrian Research, v. 167, p. 93–124.

Van Kranendonk, MJ, Smithies, RH, Hickman, AH and Champion, DC 2007a, Secular tectonic evolution of Archaean continental crust: interplay between horizontal and vertical processes in the formation of the Pilbara Craton, Australia: Terra Nova, v. 19, p. 1–38.

Van Kranendonk, MJ, Smithies, RH, Hickman, AH, Wingate, MTD and Bodorkos, S 2010, Evidence for Mesoarchean (~3.2 Ga) rifting of the Pilbara Craton: The missing link in an early Precambrian Wilson cycle: Precambrian Research, v. 177, p. 145–161.

Van Kranendonk, MJ, Webb, GE and Kamber, BS 2003, Geological and trace element evidence for a marine sedimentary environment of deposition and biogenicity of 3.45 Ga stromatolitic carbonates in the Pilbara Craton, and support for a reducing Archean ocean: Geobiology, v. 1, p. 91–108.

Vearncombe, S, Vearncombe, JR and Barley, ME 1998, Fault and stratigraphic controls on volcanogenic massive sulphide deposits in the Strelley Belt, Pilbara Craton, Western Australia: Precambrian Research, v. 88, p. 67–82.

Walter, MR 1983, Archean stromatolites: evidence of the Earth's oldest benthos, *in* Earth's earliest biosphere *edited by* JW Schopf: Princeton University Press, Princeton, p. 187–213.

Walter, MR, Buick, R and Dunlop, JSR 1980, Stromatolites, 3,400–3,500 Myr old from the North Pole area, Western Australia: Nature, v. 284, p. 443–445.

Wang, Z, Wilde, SA and Wan, J 2010, Tectonic setting and significance of 2.3 – 2.1 Ga magmatic events in the Trans-North China Orogen: New constraints from the Yanmenguan mafic–ultramafic intrusion in the Hengshan–Wutai–Fuping area: Precambrian Research, v. 178, p. 27–42.

Wilhelmij, HR and Dunlop, JSR 1984, A genetic stratigraphic investigation of the Gorge Creek Group in the Pilgangoora syncline, *in* Archaean and Proterozoic Basins of the Pilbara, Western Australia *edited by* JR Muhling, DI Groves, and TS Blake: Evolution and Mineralisation Potential: University of Western Australia, Geology Department and University Extension, v. 9, p. 68–88.

Willan, RC and Armstrong, DC 2002, Successive geothermal, volcanic-hydrothermal and contact-metasomatic events in Cenozoic volcanic-arc basalts, South Shetland Islands, Antarctica: Geological Magazine, v. 139, p. 209–231.

Wilson, JP, Fischer, WW, Johnston, DT, Knoll, AH, Grotzinger, JP, Walter, MR, McNaughton, NJ, Simon, M, Abelson, J, Schrag, DP, Summons, R, Alwood, A, Andres, M, Gammon, C, Garvin, J, Rashby S, Schweizer, M and Watters, WA 2010, Geobiology of the late Paleoproterozoic Duck Creek Formation, Western Australia: Precambrian Research, v. 179, p. 135–149.

Wingate, MTD 1999, Ion microprobe baddeleyite and zircon ages for Late Archaean mafic dykes of the Pilbara Craton, Western Australia: Australian Journal of Earth Sciences, v. 46, p. 493–500.

Woodhead, JD, Hergt, JM and Simonson, BM 1998, Isotopic dating of an Archean bolide impact horizon, Hamersley Basin, Western Australia: Geology, v. 26, p. 47–50.

Zhao, G, Wilde, SA, Sun, M, Li, S, Li, X and Zhang, J 2008, SHRIMP U–Pb zircon ages of granitoid rocks in the Lülian Complex: Implications for the accretion and evolution of the Trans-North China Orogen: Precambrian Research, v. 160, p. 213–226.

RECORD 2010/21

Three and a half billion years of life on earth: a transect back into deep time

Van Kranendonk

This Record is published in digital format (PDF) and is available online at <www.dmp.wa.gov.au/GSWApublications>.
Laser-printed copies can be ordered from the Information Centre for the cost of printing and binding.

Further details of geological products produced by the Geological Survey of Western Australia can be obtained by contacting:

Information Centre
Department of Mines and Petroleum
100 Plain Street
EAST PERTH WESTERN AUSTRALIA 6004
Phone: (08) 9222 3459 Fax: (08) 9222 3444
www.dmp.wa.gov.au/GSWApublications